SYNTHESIS AND DESIGN OF THIOPHENE MATERIALS: EFFECTS OF RING FUSION AND METAL COORDINATION

A Dissertation
Submitted to the Graduate Faculty
of the
North Dakota State University
of Agriculture and Applied Science

By

Kristine Louise Konkol

In Partial Fulfillment of the Requirements
for the Degree of
DOCTOR OF PHILOSOPHY

Major Department:
Chemistry and Biochemistry

May 2019

Fargo, North Dakota

North Dakota State University
Graduate School

Title

Synthesis and Design of Thiophene Materials: Effects of Ring Fusion and Metal Coordination

By

Kristine Louise Konkol

The Supervisory Committee certifies that this ***disquisition*** complies with North Dakota State University's regulations and meets the accepted standards for the degree of

DOCTOR OF PHILOSOPHY

SUPERVISORY COMMITTEE:

Dr. Seth C. Rasmussen
Chair

Dr. Pinjing Zhao

Dr. Gregory Cook

Dr. Erik Hobbie

Approved:

7-1-2019
Date

Dr. Gregory Cook
Department Chair

ABSTRACT

Conjugated organic materials comprise a field of materials chemistry focused on the development of semiconducting organic plastics, popular applications of which are plastic solar cells and display technologies. One of the reasons these materials have gained so much attention is that their optical and electronic properties can be tuned through engineering at the molecular level. Thiophene, an aromatic heterocycle, is a popular building block in the synthesis of many conjugated materials, prized for both the ease in which it can be synthetically functionalized and its ability to form highly conductive and low band gap materials.

The Rasmussen group has previously reported on the generation of two classes of materials, the inorganic metal thiophenedithiolenes and the fused-ring heterocycle unit thieno[3,4-*b*]pyrazine (TP), both of which have applications in conducting materials. In an effort to expand upon the applicability and versatility of these materials, a series of interconnected projects were performed to further tune their optical, electronic, and physical (e.g. solubility) properties. This involved synthetic molecular design, including judicious consideration of structure-function relationships, and characterization of the resulting materials. Highlights include a sterics vs. electronics consideration of the catalyzed hydrodebromination of the molecular building-block 2,3,5-tribromothiophene, variation of the coordinating metal in thiophenedithiolenes to tune the optics and electronics, and characterization of the effects of ring-fusion on TP-based terthienyl homopolymers. Additionally, a new application of the TP monomer was found, whereby it was successfully incorporated as a bridging ligand into a multi-metallic Ru(II) supramolecular assembly, which demonstrated good metal-metal communication.

ACKNOWLEDGEMENTS

Most importantly, I would like to thank my advisor, Professor Seth Rasmussen, for his guidance, support, and excellent conversation over my graduate studies. His door was always open to discuss anything and everything, whether chemistry, books, or world events. In particular, I would like to thank him for his support and encouragement with chemical history research. Although not part of this thesis, his invitation for me to co-author the chapter An Ancient Cleanser: Soap Production and Use in Antiquity in the ACS Symposium Series book *Chemical Technology in Antiquity* was a special highlight of my time in graduate school. I would also like to thank the rest of my committee, Dr. Greg Cook, Dr. Pinjing Zhao, and Dr. Erik Hobbie for help throughout my graduate career. Also thank you Greg Oswald for your continuous support of my teaching over the years and general goodwill, and Amy Kain for her assistance.

A special thanks to all the former and current Rasmussen group members, both graduate and undergraduate, for all their support and excellent times that were had throughout our years together. Although there are too many to name them all, a special thanks to Eric Uzelac, Trent Anderson, Mike Mulholland, Ryan Schwiderski, Casey McCausland, Evan Culver and Wyatt Wilcox.

I would like to thank my family, who were there to talk during both the good and bad times, and never lost faith in my ability to finish this long journey and persevere to my PhD.

Finally, I would like to thank all the members of the D&D/Savage Worlds/ Game Night group: especially Erik Janssen, Jesse Joyce, and Andrew Kalbach for organizing our weekly adventures over the course six years. So many people have helped me throughout this process, for which I am truly grateful. And yes, I finally finished!

TABLE OF CONTENTS

LIST OF TABLES

LIST OF FIGURES

LIST OF SCHEMES

CHAPTER 1. INTRODUCTION

1.1. Conjugated Materials

Conjugated materials combine the optical and electronic properties of classical inorganic semiconductors with many of the desirable properties of plastics (processability, flexibility, and low production costs).[1] These materials find wide usage in organic photovoltaics (OPVs), organic light emitting diodes (OLEDs), organic field-effect transistors (OFETs), sensors, and electrochromic devices.[2-19] Polyacetylene, the simplest example of a conjugated polymer, has alternating single and double bonds (average bond order ≈ 1.5), where conjugation arises from the delocalization of the π-electrons (overlap of *p*-orbitals) across the molecular backbone (overlap of *p*-orbitals) (Figure 1.1).

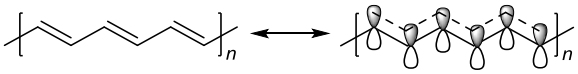

Figure 1.1. Polyacetylene with *p*-orbitals shown

In the case of conjugated materials containing heteroatoms (e.g. thiophene, pyrrole, aniline), non-bonding electrons occupying *p*-orbitals within the plane of the π-system can participate in conjugation as well (Figure 1.2).[1]

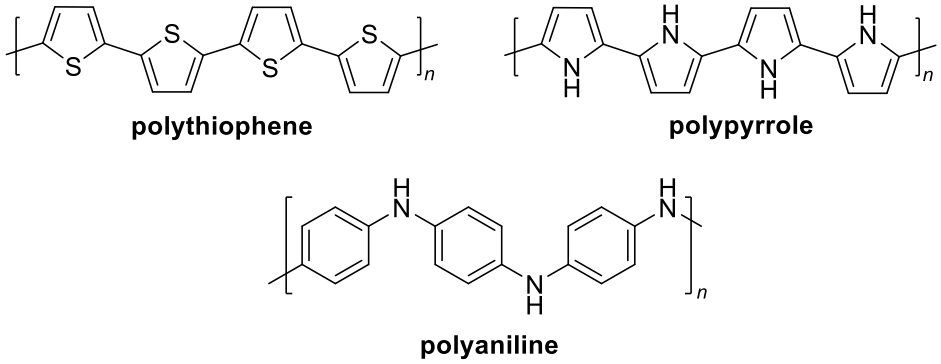

Figure 1.2. Conjugated polymers containing heteroatoms: polythiophene, polypyrrole, and polyaniline

All conjugated polymers (CPs) will exhibit conductivity as long as the electron delocalization is not compromised by factors that limit the orbital overlap such as torsional strain and molecular geometry.[1] Polyacetylene, the simplest conjugated polymer, has been shown to demonstrate conductivities as high as 120,000-170,000 S cm^{-1} in the doped state.[20] To put this in perspective, the most electronically conductive metals exhibit conductivity on the same order of magnitude as highly-structured polyacetylene, such as silver (630,100 S cm^{-1}), copper (595,900 S cm^{-1}), and gold (451,700 S cm^{-1}).[21] These conjugated materials are commonly referred to as *synthetic metals*, a term first coined Herbert N. McCoy in 1911[22,23] and later popularized by Alfred R. Ubbelohde who began using the term in reference to intercalated graphites as soon as 1969.[21,24-25] This term has come to describe materials that are produced from non-metallic components but are conductive like metals.

Although CPs are often viewed as quite modern materials, studies of these materials date to the early 19th century. The majority of modern conjugated materials are produced by either various transition-metal cross-coupling methods, including Stille, Suzuki, Kumada, and Negishi,[26-28] or direct arylation polymerization (DArP), which involves C-H bond activation.[29,30] However, oxidative polymerization was the dominant method of synthesis in the early history of CPs. As shown in Figure 1.3,[31] electron-rich monomers polymerize anodically via chemical or electrochemical oxidation of the π-system, forming the radical cation intermediate, with the localization of the unpaired electron occurring at the α-position for heterocycles (e.g. thiophene, furan, pyrrole). Thus, coupling of the radical cations occurs predominantly through the α-position, which is followed by deprotonation to give the neutral α,α'-dimer. Chain propagation is continued through a step-growth process involving the oxidation, coupling, and deprotonation steps.

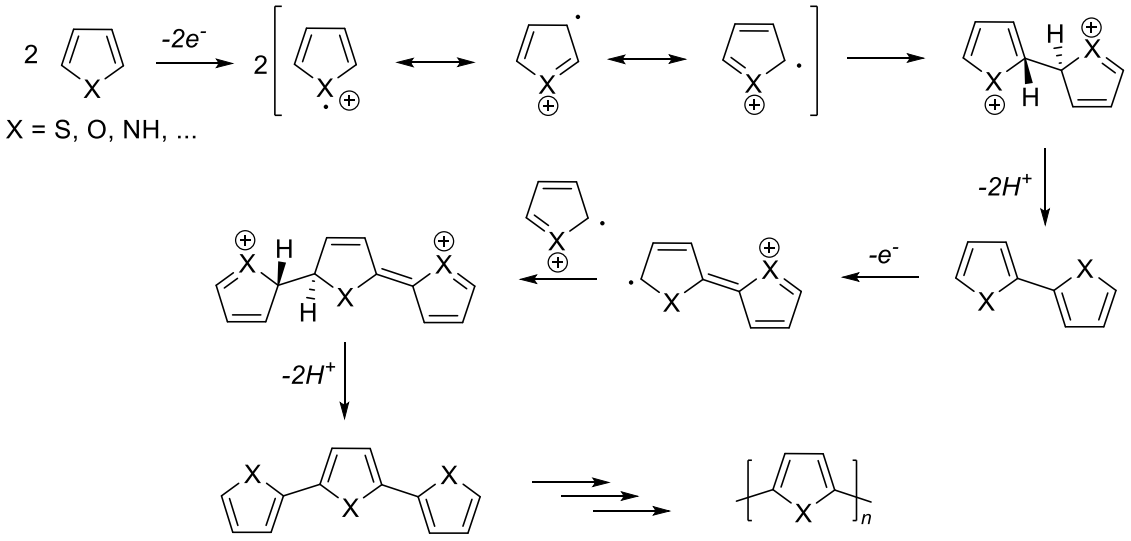

Figure 1.3. 5-membered heterocycle oxidative polymerization

Conjugated polymers in their oxidized form are referred to as p-doped, in analogy to p-doped semiconductors, because the oxidation of organic CPs generates both positive charge character (i.e. holes) and an increase in p-type character (Figure 1.4).[31,32] Counterions are simultaneously incorporated into the polymer to balance the charge – the source of which can be either anions generated in the redox process if the doping is accomplished via an oxidation agent or anions from the supporting electrolyte if the doped species is formed through an electrochemical oxidation. Some polymers, in contrast, can undergo n-doping via reduction, although this is a rarer process.

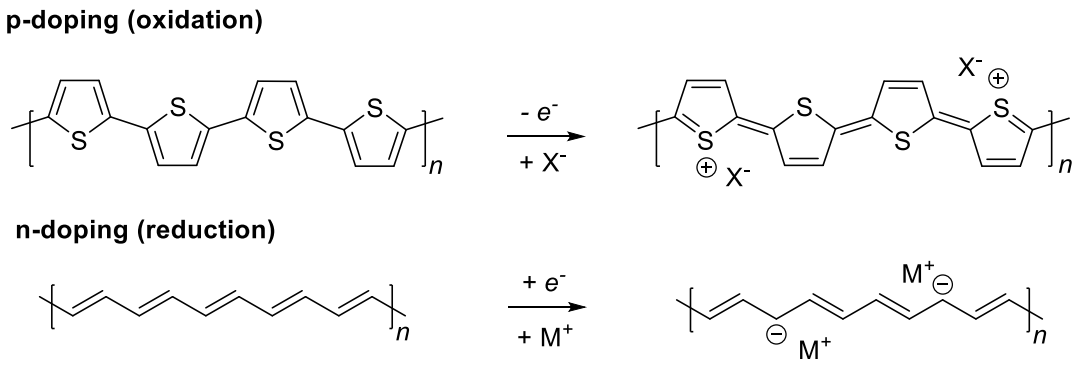

Figure 1.4. p- and n-doping of conjugated polymers

1.2. History of Conjugated Polymers

1.2.1. Polyaniline

There are four key conjugated polymers (polyaniline, polypyrrole, polyacetylene, and polythiophene) that are of historical significance to the field. Polyaniline, also referred to at times as *emeraldine* and *aniline black*, was the earliest conjugated polymer to be discovered.[31] In 1834 F. Ferdinand Runge was the first to report a species consistent with our modern understanding of polyaniline, although the discovery of polyaniline was primarily dependent on the discovery of aniline itself. Various researchers reported the discovery of aniline starting in 1826 with Otto Unverdorben reporting the isolation of an oil from the dry distillation of indigo, which he named *crystallin*. F. Ferdinand Runge (1834, *kyanol)*. Carl Julius Fritzche (1840, *anilin*) and Nikolai Zinin (1842, *benzidam*) also reported similar materials, but it wasn't until 1843 that August Wilhelm Hofmann conclusively proved that all of these substances were the same species, which came to be known as *aniline*.[31,33-35] However, the long-chain polymeric nature of polyaniline was not recognized until the early 1900s, and our modern understanding of the concept of the macromolecule was not introduced until the 1920s by Hermann Staudinger. It wasn't until the mid-1960s that Rene Buvet and Marcel Jozefowicz made the first detailed characterization of the electronic properties of polyaniline, with early conductivities ranging from 10^{-5} to 10 S cm^{-1}.[31,36]

1.2.2. Polypyrrole

Polypyrrole has a long history dating back to the early 20th century, and holds the distinction for being both the first organic polymer reported to exhibit significant conductivity and the first conjugated polymer to be prepared as a plastic film.[37,38] Angelo Angeli (1915) was the first to prepare a black precipitate which he named *pyrrole black* from the treatment of pyrrole with hydrogen peroxide in acetic acid.[31,37] Riccardo Ciusa began investigating the

thermal polymerization of tetraiodopyrrole in 1921, producing a black material with a graphitic appearance, although only the appearance and elemental composition characterization of these materials was reported.[31,37] Beginning in 1959, Donald Weiss modified Ciusa's conditions to form polypyrrole that contained adsorbed molecular iodine, which assisted in the oxidation of the polypyrrole. The presence of the oxidant iodine, and in its absence oxygen, facilitated the oxidation of the polymer through p-doping. Measurement of the polypyrrole conductivity (0.005-0.09 S cm^{-1}) represented the highest known conductivity for an organic polymer at the time.[31,37] In the late 1960s, scientists at the University of Parma reported the formation via electrolysis of a laminar film of polypyrrole (7.54 S cm^{-1}),[31,37,39] and later efforts by Arthur F. Diaz at IBM reported conductivities of 10-100 S cm^{-1} for electropolymerized polypyrrole films.[31,40,41]

1.2.3. Polyacetylene

Polyacetylene is probably the most historically well-known conjugated polymer, but its discovery is more recent. Polymerization of acetylene dates to 1866 when the French chemist Pierre Eugène Marcellin Berthelot formed a cross-linked three-dimensional material later referred to as *cuprene*.[42] However, this was not a conjugated polymer, and it wasn't until 1955 that the Italian chemist Giulio Natta reported the successful generation of polyacetylene using organometallic catalysts of group 4-8 transition metals, later refinements reporting catalysts consisting of triethylaluminium (Et_3Al) and titanium alkoxides.[31,35] In 1967 a Korean scientist Hyung Chick Pyun visiting the Ikeda research lab where Hideki Shirakawa was assisting added an 1000 excess of catalyst to produce ragged pieces of polyacetylene film. This high catalyst content accelerated the rate of polymerization to the point that the acetylene polymerized at the air-solvent interface or the vessel walls to give silvery films, a fascinating difference from the typical black precipitates observed previously.[31,42] Conductivities for both the film and powder

were similar, on the order of 10^{-9} -10^{-4} S cm^{-1}.[31,43] Shirakawa would go on to collaborate with Alan G. MacDiarmid and Alan J. Heeger on doped polyacetylene films, eventually reporting conductivities as high as 560 S cm^{-1},[44] and the three would go on to win the 2000 Nobel Prize in Chemistry for their work on *the discovery and development of electrically conductive polymers*, although others had reported on conducting polymers pre-dating their work by over a decade.[31]

1.2.4. Polythiophene

Polythiophene is the final of the four historically significant conjugated polymers discussed above, its history only dating back a few decades. Multiple groups reported the preparation and characterization of polythiophene near-simultaneously, the first of which was Takakazu Yamamoto in January 1980, using single equivalents of 2,5-dibromothiophene and magnesium in a catalytic cross-coupling with $NiCl_2$.[45] Conductivities of 5.3 x 10^{-11} S cm^{-1} for the purified polymer and 3.4 x10^{-4} S cm^{-1} for the polymer doped with I_2 were measured. Polythiophene was first electropolymerized in late 1980 in Russia by Afanas'ev and coworkers who reported oxidized polythiophene films balanced by BF_4^- counterions with conductivities of 10^{-3} S cm^{-1}.[31] However, the better known Diaz and coworkers would expand their electrochemical polypyrrole work to other cyclic molecules, including thiophenes and phenylenes, and publish much on this subject.[46-49] In 1982, Gérard Tourillon and Francis Garnier reported the generation of highly-pure polythiophene-ClO_4 films with conductivities of 10-100 S cm^{-1}.[50] The high conductivities, along with other properties would make polythiophene and its derivatives one of the most-studied conjugated polymers of the 21st century. Conjugated polymers continue to be an important area of research, with over 800 articles being published on the subject in 2018.[51]

1.3. Conjugation and Band Gap

1.3.1. Band Gap

Band gap (E_g) is one of the critical parameters that determines the optical and electronic properties of conjugated polymers, such as energy of absorption, conductivity, and luminescence color.[1] The E_g is a solid-state property of a material that is defined as the energetic separation between the filled valence band and the empty conduction band. This gap is analogous to the energy difference between the highest occupied molecular orbital and lowest unoccupied molecular orbital (HOMO-LUMO) gap for molecular species in the solution state.[1,52]

Band gap is defined in units of electron volts (eV), and the size of the E_g determines how a material is classified conductively.[1,52] Conductors (E_g = 0 eV), such as metallic species, have no gap and thus electrons can move freely throughout the material. Insulators (E_g > 2.0 eV) have a large gap and electrons have difficulty being excited into the higher energy conduction band at reasonable temperatures. Semiconductors ($E_g \geq$ 0-2.0 eV) possess the capability of having induced conductivity because electrons can be excited from the filled valence band into the conduction band leaving behind partially filled bands that allows for the flow of electrons. As the E_g increases it requires more energy to thermally or photophysically excite electrons from the valence band into the conduction band, resulting in materials that have lowered conductivities. Within CPs, semiconducting materials are also often separated in definition into *low band gap* (E_g < 1.5 eV) and *reduced band gap* (E_g = 1.5-2.0 eV) materials.[1,53]

1.3.2. Molecular Orbitals and Interactions

While bulk metallic materials feature true band-like energy structure, molecular systems such as CPs have bands which are derived from the combination of molecular orbitals (MOs). To get mixing of orbitals, there needs to be both an energy match and a spatial match between

orbitals. Provided spatial overlap exists, the atomic orbitals (AOs) which make up MOs of similar energy can mix and hybridize, forming new orbital pairs in conjugated systems.[1] These new orbital pairs are non-degenerate, meaning that one orbital is slightly stabilized (lowered) and one is slightly destabilized (raised). As a result of this, the molecule's HOMO is destabilized and the LUMO is stabilized. As discussed previously, conjugated systems feature extended *p*-orbital overlap which leads to greater π-conjugation of the material backbone and delocalization of electrons. This π-conjugation leads to a molecular structure that has narrowly spaced energy levels.

The conjugation length of the system is determined by the number of monomer units that contribute to the overall delocalization of electrons throughout the material.[1,11,52] Figure 1.5 shows how the band structure changes as the conjugation length of a material increases. As the number of monomers increases, the analogous MOs mix with each other to form corresponding non-degenerate MOs that are now higher and lower in energy than the parent MOs. As the conjugation increases, there is continued mixing of the orbitals creating a network of MOs of similar energy; whereas the number of MOs increases, the spacing between the MOs continues to decrease. This results in a large number of MOs that are so close in energy that they become energetically indistinguishable from one another. Upon formation of this bulk solid-state material the MOs blend to form the filled π valence band and the empty π* conduction band. The space between the bands is then the band gap of the bulk material.[1,11,52] The top edge of the valence band can be viewed as analogous to a HOMO, and the bottom edge of the conduction band can be viewed as analogous to a LUMO. However, this narrowing of the energetic gap as the conjugation length increases does have a limit, as the length of the polymer approaches the limit of electron delocalization. For example, the effective limit of electron delocalization for

polythiophene is 24 units,[54,55] and thus any polymer beyond that length will not show significant reduction in E_g.

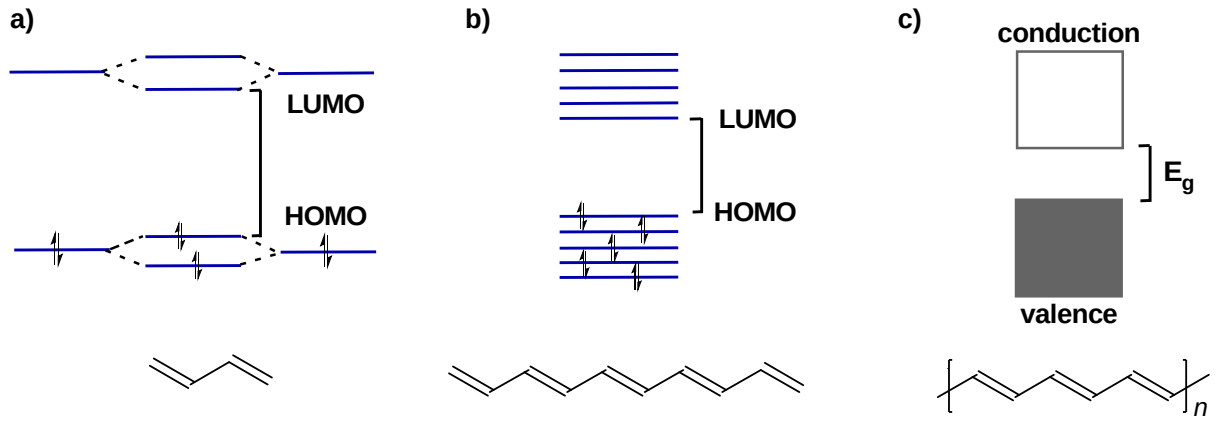

Figure 1.5. Simplified molecular orbital structure of (a) a short oligomer in solution, (b) a longer oligomer in solution, and (c) the band structure of a polymer in the solid state

While individual oligomers or polymers in solution will still feature a HOMO and a LUMO due to discrete MOs, the solid state allows π-electrons to delocalize across molecules as the CP transitions from a coil-like configuration to its planar form in the solid state. This enhanced delocalization is a result of both the increase in molecular planarity and π-stacking, an intermolecular interaction between aromatic species. Benzene is one example of an electron-rich aromatic molecule that exhibits π-stacking (Figure 1.6).

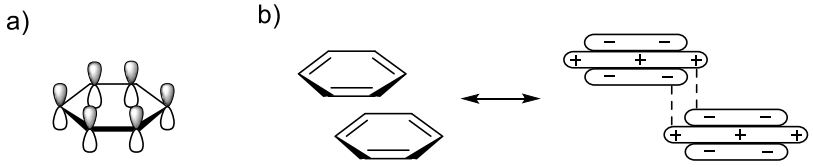

Figure 1.6. (a) Benzene π-system *p*-orbitals (b) benzene molecules results in off-center parallel packing due to the π-stacking

π-Stacking often manifests through a quadrupolar (distribution of charge consisting of four equal monopoles) attraction between the electron rich π-system and the electron-poor sp^2 C-H plane in the molecular backbone. The π-stacking interaction enhances the electron

delocalization because the quadrupole distorts the π-system's electric field and thus provides a stabilizing effect. Where the π-system sandwiches the molecular backbone, the π-stacked units in these configurations exhibit close molecular contacts, allowing for "hopping" of electrons and holes from one localized state to another via electron transfer. This hopping is also the way in which charge carriers migrate across molecular boundaries, giving conjugated materials their conductivity. In the case of two electron-rich aromatics such as benzene, face centered packing is disfavored because there is an electrostatic repulsion, and thus off-center parallel packing is favored due to π-stacking (edge-to-face interactions are also possible).[56,57]

1.3.3. Determination of Gap

The HOMO-LUMO gap and E_g are commonly determined by optical or electrochemical experimental methods.[1] Electrochemical techniques such as cyclic voltammetry (CV) provide an accurate measurement of the potential (voltage) at which electrons begin to be removed or added to the molecule's frontier orbitals by determining the material's onset of oxidation (loss of electrons) and reduction (gain of electrons). For example, the onset of oxidation (a tangential line extrapolated to the slope of the peak in reference to the baseline is used as this onset, Figure 1.7) indicates the energy at which an electron can be removed from the molecule's HOMO, and the onset of reduction indicates the energy at which an electron can be added to the molecule's LUMO. These potentials are referenced to an internal standard, for example the oxidation couple of ferrocene Fc/Fc^+ (-5.1 eV from E_{vac}), which is necessary to convert a potential value referenced to a standard, to a linear energy value in eV versus vacuum.[58] The onset potential values can be converted to E_{HOMO} and E_{LUMO} by Equations 1.1 and 1.2.

$$E_{HOMO} = - (E_{[\text{onset ox vs. } Fc/Fc^+]} + 5.1)\ \text{eV} \qquad \text{(Equation 1.1)}$$

$$E_{LUMO} = - (E_{[\text{onset red vs. } Fc/Fc^+]} + 5.1)\ \text{eV} \qquad \text{(Equation 1.2)}$$

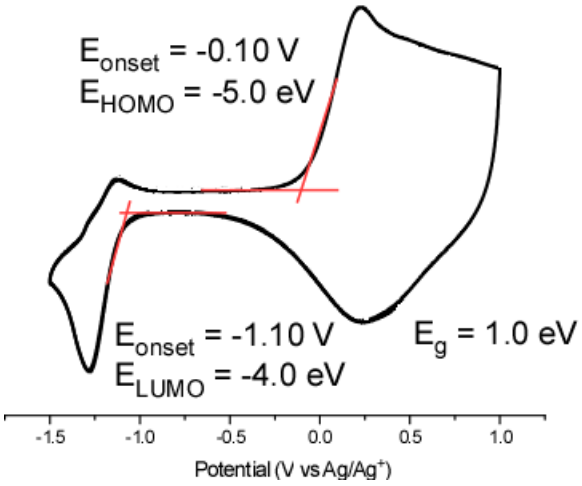

Figure 1.7. Determination of electrochemical band gap via the onsets of oxidation and reduction

Although electrochemical methods provide accurate oxidation and reduction potentials of the materials, they are not a direct measurement of the HOMO and LUMO themselves. Instead, the energies of the ionized levels can be directly probed by photoelectron spectroscopy techniques such as UV or inverse photoelectron spectroscopy, however, the accessibility of these techniques is quite limited and thus indirect methods such as CV are frequently employed.[59] The limiting factor of electrochemical measurement is that both the potentials of oxidation and reduction must lay within the solvent window, otherwise an electrochemical measurement of the gap cannot be obtained.

A more accurate way to measure the band gap or HOMO-LUMO gap is through solid-state absorption spectroscopy of a film. Although solution-state optical measurements are a quick way to determine an approximate value, solid-state is a more accurate method to determine optical band gaps and a more accurate method overall because in solution interchain coupling is limited. By extrapolating the onset of the lowest energy transition in reference to the baseline, a rough estimate of the E_g can be made.[1] The onset of the lowest energy transition corresponds to a wavelength that represents the difference between the edges of the valence and conduction band

energies. The wavelength's energy can then be converted to a potential via a conversion factor of 1240 nm = 1 eV. However, the formally accepted measurement of band gap is to graph the low-energy side of the absorption band as a Tauc plot of hν vs. $(A \times h\nu)^2$ and the linear portion is extrapolated to the baseline, where A is the absorbance and hν is the photon energy in eV (Figure 1.8).[60] The limitation of the optical determination of E_g or HOMO-LUMO gap is that this method gives no information on the oxidation or reduction potentials, and only the gap is determined.

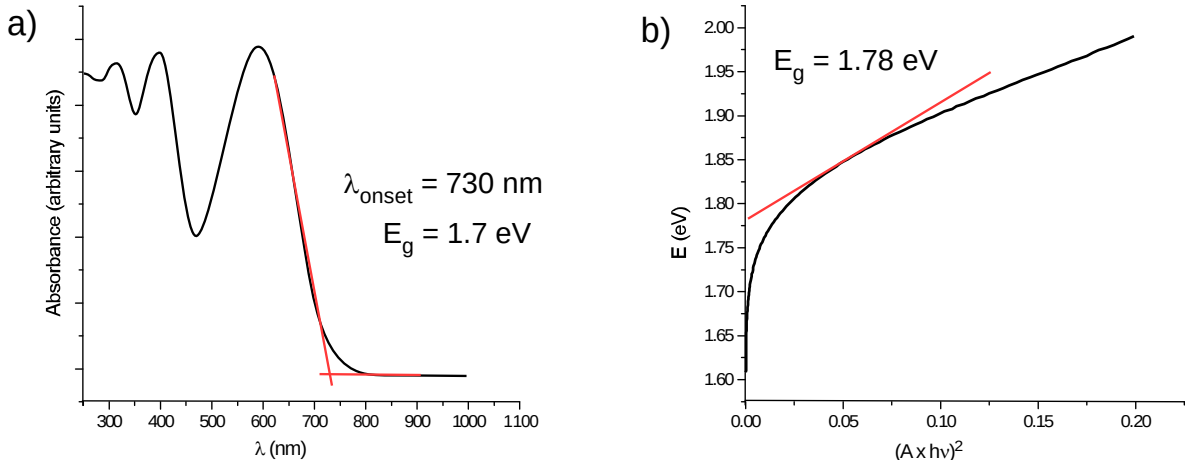

Figure 1.8. Determination of (a) optical band gap via absorption onset and (b) Tauc plot method

1.4. Structure-Function Relationships

Structure-function relationships have to do with how changing the structure of a conjugated material can affect the function of its corresponding properties. Common structure-function relationships to consider when thinking about these materials include bond length alternation, molecular planarity, aromaticity, and heteroatom effects.

1.4.1. Bond Length Alternation

The control and tuning of energy gaps are of great interest to materials chemists, given how instrumental the band gap is in determining a material's optical and electronic properties. Bond length alternation (the difference in length of adjacent bonds) across the π-system has one

of the largest effects on the magnitude of the band gap, with E_g lowering with reduced alternation. This is because lower degrees of bond length alternation lead to better electron delocalization across a molecule's π-system and less localization of charge.[1,56] For example in Figure 1.9, compare polyacetylene (alternating single and double bonds, where the average bond = 1.5 units) to a hypothetical polymer of alternating single and triple bonds (where the average bond = 2 units). The alkene will have a lower band gap than the alkyne because it has less bond length alternation.

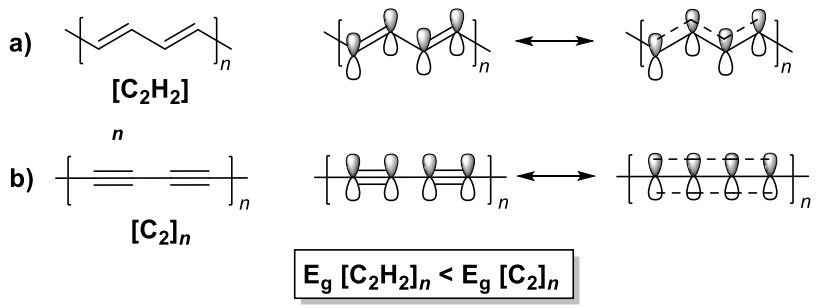

Figure 1.9. (a) alternating single and double bonds (bond = 1.5 units) (b) alternating single and triple bonds (bond = 2 units) [E_g (a) < E_g (b)]

1.4.2. Planarity

Molecular planarity also is a factor that contributes to band gap, as increased backbone planarity results in a lower band gap. This is because the conjugation length along the backbone can be reduced by torsional strain. Significant deviations from planarity (i.e. > 40° between units), which disturb the *p*-orbital overlap, result in a significant increase in band gap and decreased conjugation.[1] Steric interactions affect the band gap of the material, causing deviations from the plane.

The two most common causes of deviations in planarity are β-hydrogen interactions amongst neighboring aromatic units and side chain interactions. Bond rotation due to β-hydrogen

repulsion is mostly an issue for six-membered aryl polymers (e.g. benzene) and less so for five-membered systems (e.g. thiophene).

Most unfunctionalized CPs are completely insoluble due to strong π-stacking, and thus functionalization via side chain addition is required to increase solubility. However, while increasing the side chains enhances the solubility, it can also intensify the steric interactions via repulsion from side chains with the polymer backbone and neighboring side chains, causing an increase in E_g. This is demonstrated in Figure 1.10, where *regioregular* poly-3-heyxylthiophene (rr-P3HT, 98% head-to-tail (HT) arrangement) only has a lone pair interaction between the sulfur lone pair and the side-chain (E_g = ~1.8 eV). However, *regiorandom* poly-3-hexylthiophene (P3HT, 70-80% head-to-tail (HT) arrangement), can have more interactions, such as significant side-chain interactions, and thus has a larger band gap (E_g = 2.0 eV). Of the three coupling modes: HH, HT, and TT (tail-to-tail), it is the case of the HT coupling that the overall chain interactions are most minimized thus leading to limited rotation and reduction of steric interactions.[61]

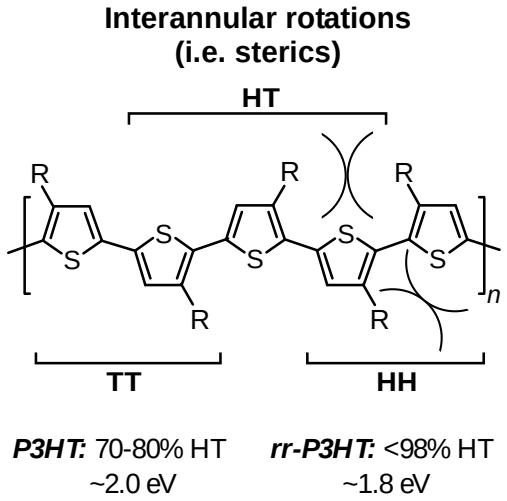

Figure 1.10. Steric interactions and resulting bandgap of *regiorandom*-P3HT and *regioregular*-P3HT

1.4.3. Heteroatom Effects

The presence of a heteroatom (a non-carbon in the cyclic ring) can also affect the band gap of the material. The electronic effect of the heteroatom is thought to strongly correlate with its electron affinity, with the higher the electron affinity of a heteroatom corresponding to a lower E_g in its material. For example, sulfur (200 KJ/mol) has a larger electron affinity than nitrogen (7 KJ/mol), and thus polythiophene (E_g = 2.0 eV) has a smaller band gap than polypyrrole (E_g = 3.0 eV).[62] Figure 1.11 shows some common conjugated organic polymers, both with and without heteroatoms, and their corresponding band gaps.

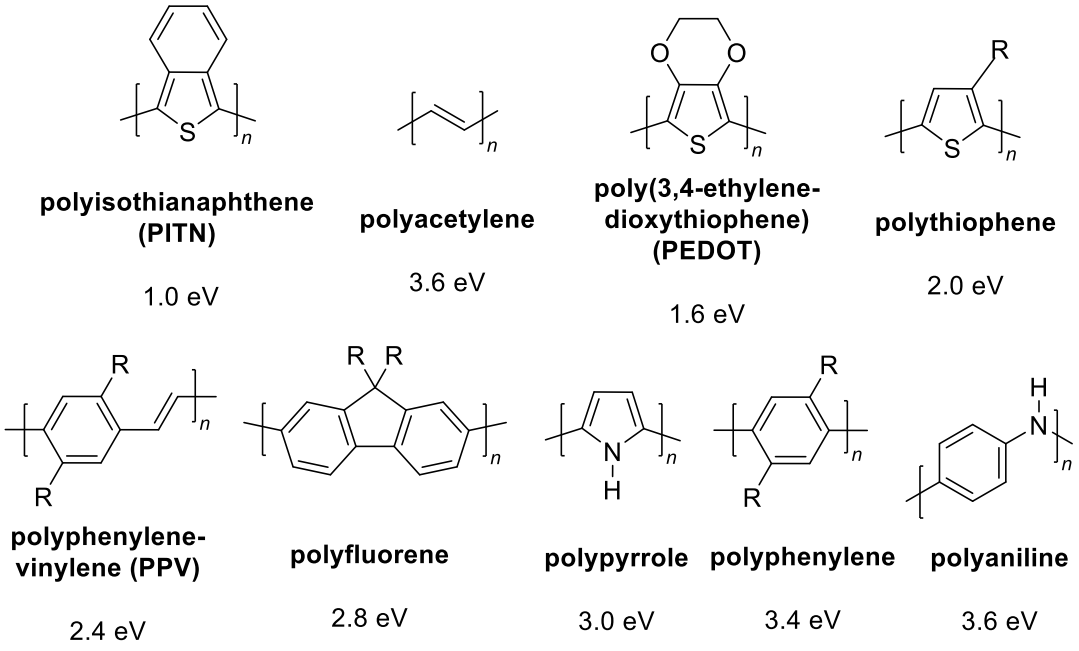

Figure 1.11. Band gaps of common organic conjugated polymers

1.4.4. Monomer Aromaticity

In terms of monomer aromaticity, it is believed that the aromaticity determines the confinement potential of the π-electrons within the monomer.[1] Aromaticity provides an internal stabilization to the molecule, but can result in electron trapping within the ring, which can give rise to less electron delocalization across the chain. The delocalization length along the backbone

is reduced as the confinement within the ring increases, which results in larger E_g values. For example, benzene (aromaticity = 25.0 KJ mol^{-1}) has a greater relative aromaticity than thiophene (aromaticity = 20.3 KJ mol^{-1}), and thus has less electron delocalization along the chain, and a larger band gap in polyphenylene vs. polythiophene.[62,63]

However, a caveat exists when it comes to structure-function relationships, which is that all structure-function relationships do not exist in isolation from one another.[1] This means that these structure-function relationships are difficult to separate. For example, when considering aromaticity, one must also consider sterics, or also keep planarity effects in mind when considering conjugation length. These structure-function relationships have an impact when it comes to the design and tuning of conjugated materials.

1.5. Molecular Engineering

To reduce band gap by molecular tuning, two popular approaches have emerged: enhancing the polymer's quinoidal form and utilizing the donor-acceptor (D-A) approach.[1] The quinoidal form is a non-degenerate resonance structure of a conjugated material which also has an aromatic form (Figure 1.12). The non-degenerate resonance states contribute significantly to a material's E_g, with the extent to which each resonance state contributes to the observed ground state determining the band gap of the material. The more one can maximize the quinoidal structure of the ground state, the smaller the band gap that results.[62] For example, in the non-degenerate states of polythiophene, the aromatic form has an E_g of 2.0 eV and the quinoid form has a much reduced calculated E_g of 0.47 eV.[1] The preferred resonance of polythiophene is the lower energy aromatic state (Figure 1.12) and this is representative of the true ground state of polythiophene, but the quinoidal resonance form displays a significantly lower band gap, a result of the combined destabilization of the HOMO and stabilization of the LUMO energy levels. A

common approach to reduce the band gap of a system is through the structural modifications of the material to increase its quinoidal character. This is commonly performed through the incorporation of fused rings to the monomer backbone in polymers and end-capping to favor the quinoid form in oligomers.[1]

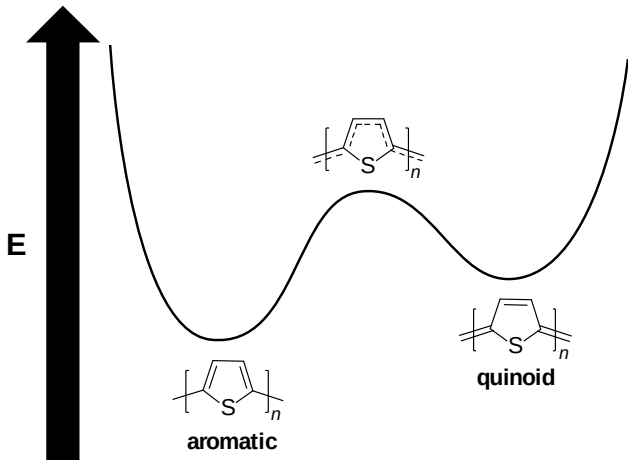

Figure 1.12. Aromatic and quinoidal resonance forms of polythiophene

The donor-acceptor (D-A) approach is the second main method of molecular engineering, which is based on the alternation of electron-rich donor (D) and electron-poor acceptor (A) species.[1,62] First reported by Havinga and coworkers in 1992, the foundations of the D-A theory are based on their research with polysquarains and polycroconains.[52] In this theory it was proposed that the donor species would be associated with the polymer's HOMO and the acceptor with the polymer's LUMO. Combining these effects in a polymer featuring strong donor and acceptor units, an overall reduction in band gap can occur.[62,64,65] Figure 1.13 shows energy schemes for the D-A model showing different dimer combinations.

It was later shown that the simple D-A model is more complex than initially proposed, where many species previously categorized as either donors or acceptors can act as both, which have been termed *ambipolar* units for units that can act as both the donor and the acceptor. The Rasmussen group has shown that for certain fused-ring D-A polymers, the HOMO does not lie

solely on the monomer as previously thought, instead being delocalized along the polymer backbone, with the LUMO being mostly confined to the acceptor.[66] This can also explain why the LUMO of D-A polymers tends to not change much in energy (Figure 1.13).

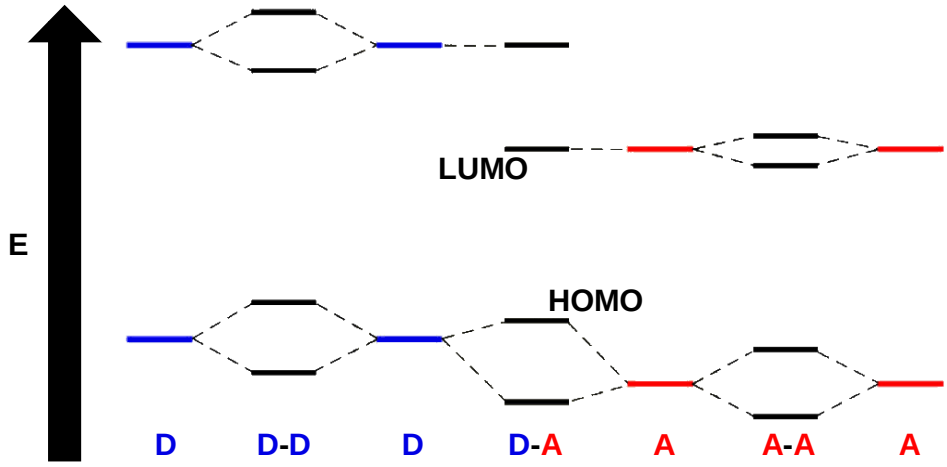

Figure 1.13. Conventional hybridization energy diagram to give symmetric (D-D or A-A) or hybrid (D-A) dimeric units

In the case of the ambipolar unit thieno[3,4-*b*]pyrazine (TP, Figure 1.14),[1] which was classically perceived as an acceptor in D-A systems, when combined with various classical donor units (e.g. EDOT [3,4-ethylenedioxythiophene], thiophene), the TP is oftentimes the stronger donor of the two. Because of this, instead of a destabilization of the HOMO which would be the expectation of the combination of TP with an electron rich donor, this combination of the stronger donor TP with a classical donor unit reduces the donor character of the polymer backbone, resulting in a stabilized HOMO and an increase in E_g.[67]

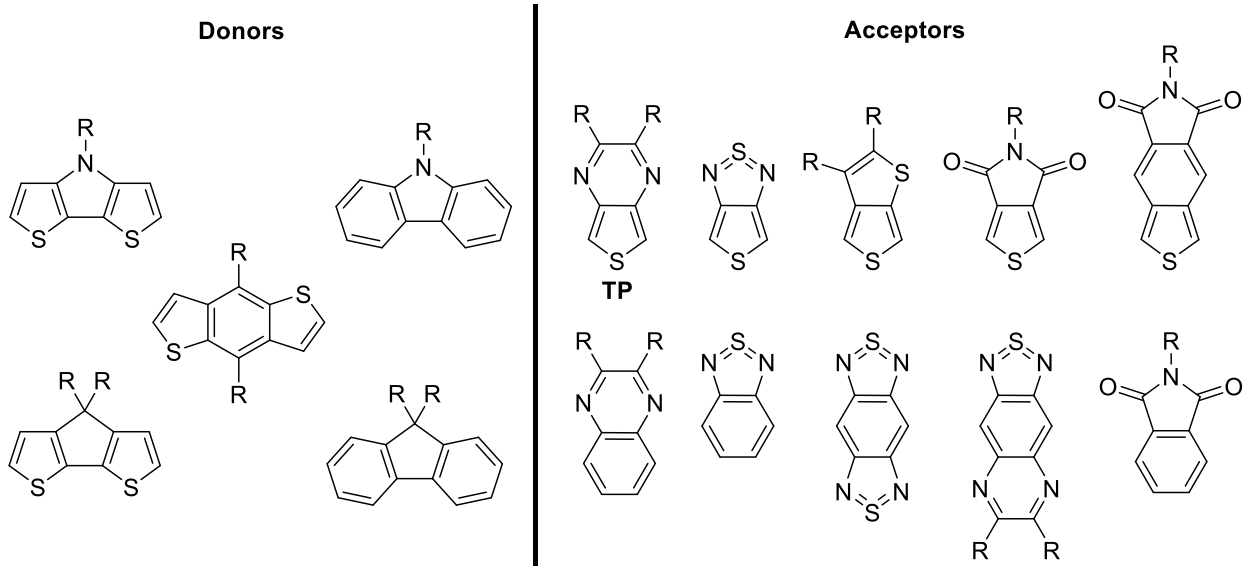

Figure 1.14. Common fused-ring donors and acceptors applied to D-A frameworks

1.6. Fused-Ring Systems

The incorporation of fused-ring systems into conjugated materials is a common method employed to both enhance the polymer's quinoidal form and provide the electronics needed for D-A polymers. Highly aromatic units such as benzene can be fused to a heterocyclic monomer, which can limit aromaticity in the fused heterocycle to preserve its own aromaticity. Other heterocycles are often incorporated into fused-ring systems to provide electron-rich or electron-poor units for D-A polymers (Figure 1.14).[1] Fused-ring systems also have the advantages of enhancing planarity and greater π-electron surface area. The first of which enhances orbital overlap and the second enhances interchain interactions and π-stacking.

1.7. Thiophene in Conjugated Materials

1.7.1. Thiophene Introduction

Thiophene has become one of the most widely-used building blocks in the field of conjugated materials, possessing many advantages over other aromatic systems.[1-3,8,62] It is produced as a by-product in the petroleum refining process (ca ~3% crude petroleum),[68] and

more commonly, synthesized through high-temperature reactions of hydrocarbons and sulfur dioxide.[69] The thiophene unit is less aromatic than benzene (therefore smaller band gap in the homopolymer), it is more oxidatively stable than furan (which has ring-opening issues), and more resistant to basic attack than pyrrole.

Oligo- and polythiophenes are the simplest forms of thiophene materials, and among the most investigated. The discovery that conjugated oligomers and polymers could be used as the active component in organic electronic devices caused an explosion in the development of new materials. The reasons for why this development focused on thiophene are two-fold.[2] First, thiophene chemistry is well-established and has been under development for a long time, with thiophenes being ideal building-blocks in transition metal-catalyzed cross coupling reactions (Kumada, Stille, Suzuki, Negishi, Ullmann). These reactions provide an enormous potential of structural variations which allow for a wide range of tuning of the electronic properties. Second, these thiophene-based materials are popular because of their outstanding physical and chemical properties, including high stability in the conducting and semiconducting states. These thiophene materials can be readily characterized by many methods, with unique optical, electronic, redox, charge transport and self-assembly processes. Also, the high polarizability of the sulfur atom in the thiophene ring causes a stabilization in the conjugation chain and excellent charge transport properties.

1.7.2. Oligo- and Polythiophenes

In five-membered heterocyclic rings such as thiophene, coupling can occur at the α- or β-positions. Some degree of α-β coupling probably occurs, however the longer conjugation lengths are a result of the more favored α-coupling. If the β-positions are blocked, such as through ring-

fusion, then coupling can only occur at the open α-positions and a more homogeneous polymer is formed.[2]

Since the first report of polythiophene in 1980 as a one-dimensional linear conjugated system, many thiophene-based polymers have been synthesized, including smaller oligothiophenes as monomers for corresponding thiophene polymers.[45-50] One of the most prevalent thiophene polymers is P3HT, an electron-donor, with a HOMO of -5.2 eV and LUMO of -3.2 eV (E_g = 2.0 eV).[70] P3HT is often paired with the n-type organic semiconductor phenyl-C_{61}-butyric acid methyl ester (PCBM) in bulk heterojunction (BHJ) solar cells to give power conversion efficiencies (PCEs) greater than 5% (Figure 1.15a).[71]

Poly(3,4-ethyelenedioxythiophene) (PEDOT) is another common polythiophene, advantages of which include being an electron-rich material that is stable in the oxidized state and optically transparent. Films of PEDOT are typically doped with polystyrene sulfonate (PSS) to balance ionic charges in the system, forming the PEDOT:PSS macromolecular salt (Figure 1.15b).[2] P3HT and PEDOT:PSS are applied as hole-transport components in OLEDs and flexible OPVs, primary examples of commercially-produced CP systems.[2]

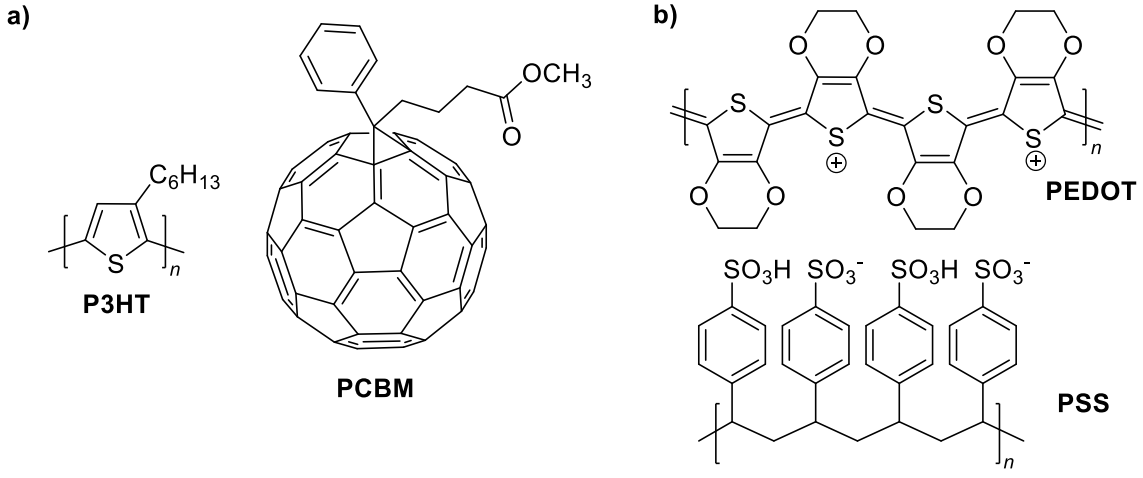

Figure 1.15. (a) P3HT and PCBM (b) PEDOT:PSS system

In comparison to polythiophenes, oligothiophenes have controllable conjugation length, which allows for both tuning of the optical and electronic properties and use as modeling the behavior of their corresponding polymers. The peripheral units of oligothiophenes can also be readily functionalized, allowing the conjugated core to be applied to many different types of chemistry. Functionalized oligothiophenes have been incorporated into pendant groups grafted onto polymer backbones, utilized surface-active groups such as thiols and phosphines, attached biologically active groups such as amino acids, been dye-functionalized for use in dye-sensitized solar cells (DSSCs), and been synthesized containing redox active groups (e.g. ferrocene and ruthenium polypyridyl chelating complexes), to name a few of the many types of modifications that can be done to them.[2]

1.7.3. Fused-ring Thiophenes

Fused-ring thiophenes are important building blocks in conjugated materials. As discussed previously, in comparison to 'normal' thiophene units, fused-ring thiophenes exhibit more rigid structures and an extended π-conjugation. This also provides for flat π-systems with excellent charge transport capabilities and unique electronic features, especially the enhancement of the quinoidal character in the ground state.[2] There are two categories of fused-ring thiophenes: those that contain moieties fused at the *b*-face or *d*-face and those that contain moieties fused at the *c*-face (Figure 1.16).

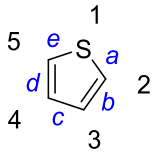

Figure 1.16. Positions and faces of the thiophene heterocycle

Thieno[3,2-*b*]thiophene (TT) is the simplest example of a fused-ring thiophene, where fusion occurs at the *b*-face of the molecule. In comparison to simple 2,2'-bithiophene, TT

exhibits limited torsional deviations from the plane (Figure 1.17). This rigidity both enhances planarity and suppresses non-radiative emission pathways from the excited state, which encourages fluorescence.[72]

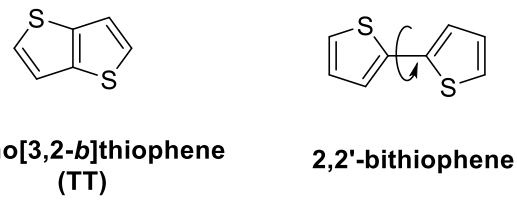

thieno[3,2-*b*]thiophene (TT) **2,2'-bithiophene**

Figure 1.17. Structures of thieno[3,2-*b*]thiophene and 2,2'-bithiophene with torsional rotation

Poly(isothianapthene) (PITN) was the first fused thiophene-based polymeric material, reported by Wudl et al. in 1984 (Figure 1.11).[73] In this case, fusion occurs on the *c*-face of the molecule. The fusion of the benzene ring to the thiophene increases the quinoidal character in the electronic ground state, and PITN exhibits a band gap of ~1.0 eV, a significant decrease from unfused polythiophene (2.0 eV). More soluble alkyl- and alkoxy-substituted PITNs have also been reported, with similar band gaps to parent PITN.[2] If two pendant thiophene groups are added to the PITN core, such as for 1,3-bis(2-thienyl)benzo[*c*]thiophene (Figure 1.18), when the molecule is electropolymerized, it exhibits a band gap of 1.6 eV between that of PITN and polythiophene.[2] However, in poly(benzo[*c*]thiophene) systems, such as PITN, there is a steric hinderance between the benzo-H and thiophene-S atoms of adjacent thiophene rings, which creates a significant twist (~39°) and results in reduced π-conjugation in the polymeric backbone.[2]

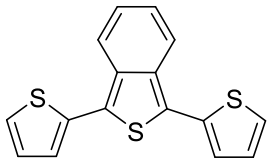

1,3-bis(2-dithienyl)benzo[*c*]thiophene

Figure 1.18. Structure of 1,3-bis(2-thienyl)benzo[*c*]thiophene, an analogue of the parent PITN

This issue with steric hinderance can be overcome in two ways, either integration of a spacer unit such as thiophene, or substitution of the C-H group with nitrogen, diminishing the hinderance (torsion angle 3.5°).[2] This lowering of the torsional strain is shown in Figure 1.19.

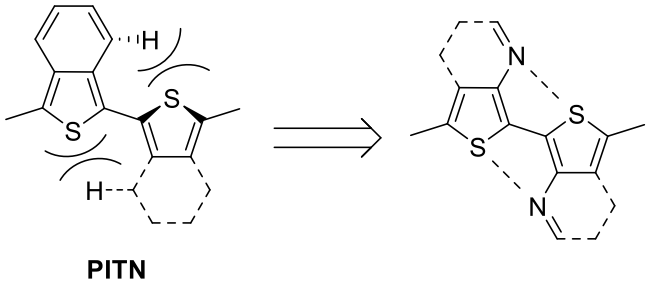

Figure 1.19. Substitution of C-H group in PITN with nitrogen

Heteroaromatic fused-ring monomers like thieno[3,4-*b*]pyrazine (TP, Figure 1.14) have become important building blocks in the construction of low E_g polymers, and the Rasmussen group has published extensively on the TP unit in the preceding two decades.[58,74-80]

1.7.4. Thiophene in Inorganic Materials

Besides being incorporated into purely organic conjugated materials, thiophenes have also found use in inorganic hybrid materials.[81] Thiophene can be incorporated into bulk composite materials such as perovskites and nanocomposites.[83,83] Additionally, the reverse can occur where metals are incorporated into conjugated organic materials themselves such as oligo- and polymers, dendrimers, macrocycles, and catenane-type structures.[81] The arrangement of the metal and the conjugated backbone occurs in three different categories. Figure 1.20 shows a general diagram and representative examples of all three types of linkages.

In Type I materials, the metal is tethered to the backbone by a flexible, non-conjugated linker such as an alkyl chain, where the polymer acts as a conductive support and the electronic, optical, and chemical properties of the metal group behaves similarly to those of the untethered complex.

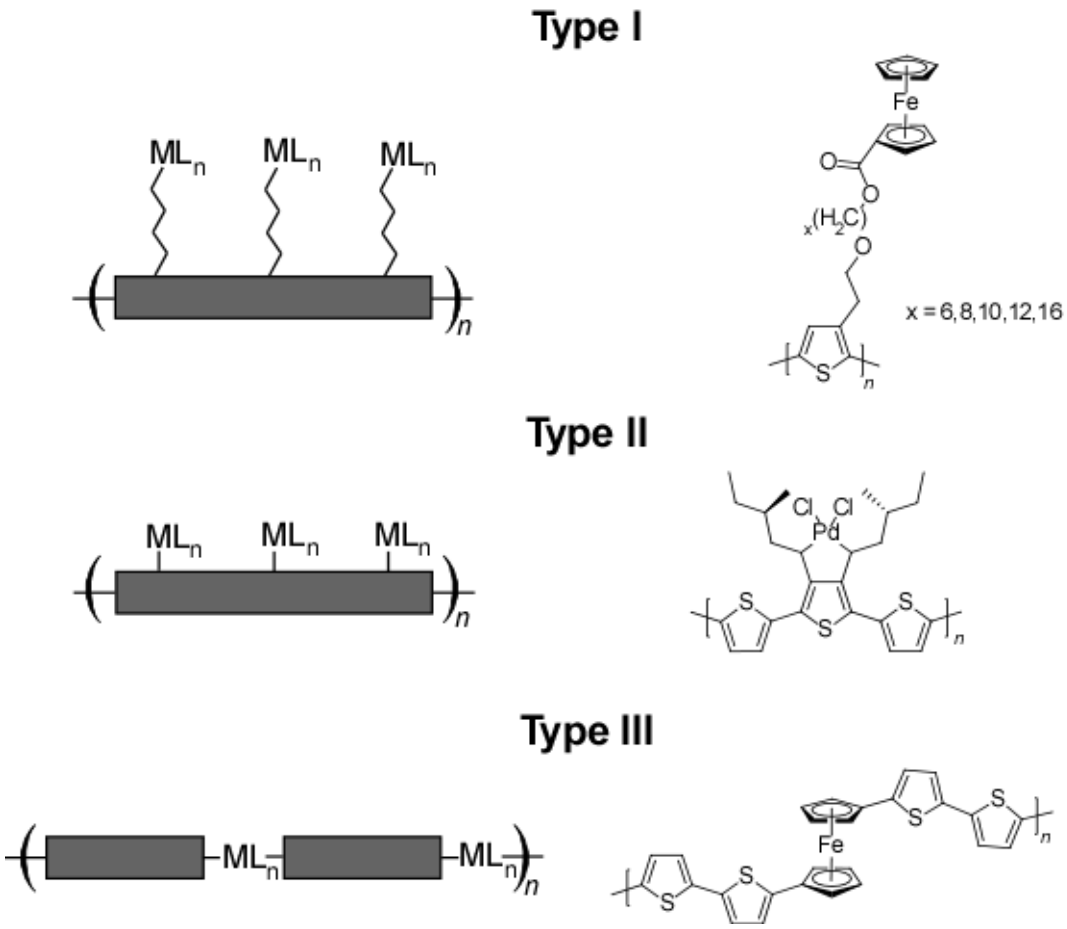

Figure 1.20. Examples of metal containing conjugated polymers of Type I, II, and II

In Type II materials, the metal and the backbone are electronically coupled to one another, and the metal and the polymer may influence the properties of one another. Since many metal groups and π-conjugated backbones are redox-active, this can afford systems in which the properties of the metal and backbone can be electrochemically tuned. In Type III materials, the metal is located directly in the conjugated backbone. Although there is a perturbation that exists because of the introduction of the metal into the organic material, strong electronic interactions between the organic bridge and the metal group are still possible, which means it can participate in d-π mixing.[84] Incorporating metals into the CP would have a couple of advantages. First, metal substitution could potentially provide conductive polymers with increased solubility and

stability. Second, by coupling the electrochemical and photochemical properties of the metal systems with the conductive properties of the polymers, the produced materials could display characteristics of both parent systems and potentially be capable of long-range electron transfer.

Thiophenedithiolenes (TDTs) are one class of inorganic complexes that can fall into both Type II and Type III categories of materials, depending if the transition metal is pendant or incorporated into the polymer backbone. In TDTs, the electronically delocalized core is coordinated to at least one bidentate thiolate ligand, and the central metal consists of a variety of transition metals, such as cobalt, nickel, or copper.[81,85] Capable of vivid redox behavior, TDTs often have optical absorbances in the near infrared (NIR) region of the electromagnetic spectrum. This makes these materials attractive for applications in NIR photodetectors, along with conducting and magnetic materials.[81] Figure 1.21 shows an example of a metal thiophenedithiolene of the Type II variety that has been electropolymerized through the *tert*-thiophene backbone.[86]

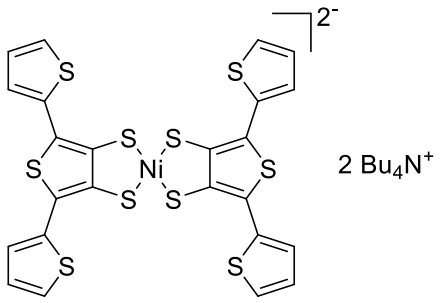

Figure 1.21. Metal dithiolene complex that has been electropolymerized

1.8. Research Goals

Conjugated organic small molecules and polymers have been applied to semiconducting materials for applications in renewable energy devices such as organic solar cells and conductive plastics. The overall goal of this work is to gain improved understanding of structure-function

relationships through the synthesis and characterization of certain thiophene-based materials, in particular how material design can allow for tuning of the optical and electronic properties.

Synthesis of functionalized thiophenes is often the basis of many conducting materials, and the basic chemistry of this synthesis is often overlooked. The first project will focus on an interesting discussion of the catalytic hydrodebromination of functionalized 2,3,5-tribromothiophene, a common precursor in the synthesis of functionalized thiophene materials.

Regarding TDTs, much work has already been completed on how by changing the structure of the organic ligands that surround the dithiolene core, one can tune the optical and electronic properties of the materials. Instead, we wanted to examine how changing the central transition metal affects the properties, and how these properties can be tuned through different modifications.

Ample background has already been presented about the importance of conjugated polymers in materials chemistry, particularly fused-ring species such as thieno[3,4-*b*]pyrazine. Looking at the structure of the TP unit, it was determined that there were promising possibilities for the use of the TP moiety as a bridging ligand in supramolecular assemblies for improved M-M communication. If successful, this would provide the first of a completely new family of ligands for application to these materials, since focus on TPs has primarily been engaged in CP materials.

Finally, various synthesis and characterization of small molecules and polymers containing the TP moiety will be presented, along with a discussion of how properties change with structural modification.

1.9. References

1. Rasmussen, S. C. Low Bandgap Polymers. In *Encyclopedia of Polymeric Nanomaterials*; Mullen, K., Ed.; Springer: Berlin, 2013; pp 1-13.
2. Mishra, A.; Ma, C.-Q.; Segura, J. L.; Bauerle, P. In *Handbook of Thiophene-Based Materials: Applications in Organic Electronics and Photonics*; Perepichika, I. F., Perepichka, D. F., Eds.; Wiley: West Sussex, U.K., 2009; Vol 1, pp 1-157.
3. Barbella, G.; Melucci, M. In *Handbook of Thiophene-Based Materials: Applications in Organic Electronics and Photonics*; Perepichika, I. F., Perepichka, D. F., Eds.; Wiley: West Sussex, U.K., 2009; Vol 1, pp 255-292.
4. Christian-Pandaya, H.; Vaidyanathan, S.; Galvin, M. In *Handbook of Conducting Polymers: Conjugated Polymers Processing and Applications*, 3rd ed.; Skotheim, T. A.; Reynolds, J. R., Eds.; CRC Press: Boca Raton, FL, 2007, Chapter 5.
5. Dalton, L. R. In *Handbook of Conducting Polymers: Conjugated Polymers Processing and Applications*, 3rd ed.; Skotheim, T. A.; Reynolds, J. R., Eds.; CRC Press: Boca Raton, FL, 2007, Chapter 6.
6. Mozer, A. J.; Sariciftci, N. S. In *Handbook of Conducting Polymers: Conjugated Polymers Processing and Applications*, 3rd ed.; Skotheim, T. A.; Reynolds, J. R., Eds.; CRC Press: Boca Raton, FL, 2007, Chapter 10.
7. Guiseppi-Elie, A.; Brahim, S.; Wilson, A. M. In *Handbook of Conducting Polymers: Conjugated Polymers Processing and Applications*, 3rd ed.; Skotheim, T. A.; Reynolds, J. R., Eds.; CRC Press: Boca Raton, FL, 2007, Chapter 12.

8. Rasmussen, S. C.; Pomerantz, M. In *Handbook of Conducting Polymers: Theory, Synthesis, Properties, and Characterization*, 3rd ed.; Skotheim, T. A.; Reynolds, J. R., Eds.; CRC Press: Boca Raton, FL, 2007, Chapter 12.

9. Blanchard, P.; Leriche, P.; Frère, P.; Roncali, J. In *Handbook of Conducting Polymers: Theory, Synthesis, Properties, and Characterization*, 3rd ed.; Skotheim, T. A.; Reynolds, J. R., Eds.; CRC Press: Boca Raton, FL, 2007, Chapter 13.

10. Roncali, J. *Chem. Rev.* **1992,** *92* (4), 711-738.

11. Roncali, J. *Chem. Rev.* **1997,** *97* (1), 173-206.

12. Logothetidis, S.; Laskarakis, A. *Euro. Phys. J. Appl, Phys.* **2009**, *46* (1), 12502/1-12502/9.

13. Sekitani, T.; Someya, T. *Adv. Mater.* **2010**, *22*, 2228-2246.

14. Allen, K. J. *Proc. IEEE* **2005**, *93* (8), 1394-1399.

15. Beaujuge, P. M.; Reynolds, J. R. *Chem. Rev.* **2010**, *110*, 268-320.

16. Lange, U.; Roznyatovskaya, N. V.; Mirsky, V. M. *Anal. Chim. Acta* **2008**, *614* (1), 1-26.

17. Hu, J.; Liu, S. *Macromolecules* **2010**, *43*, 8315-8330.

18. Thomas, S. W.; Joly, G. D.; Swager, T. M. *Chem. Rev.* **2007**, *107*, 1339-1386.

19. Facchetti, A. *Chem. Mater.* **2011**, *23*, 733-758.

20. Naarmann, H.; Theophilou, N. *Synth. Met.* **1987**, *22*, 1-8.

21. CRC Handbook of Chemistry and Physics, 89th ed.; Lide, D. R., Ed.; CRC Press: Boca Raton, FL, 2008, pp 12-39 – 12-40.

22. Rasmussen, S. C. *Bull. Hist. Chem*. **2016**, 41 (1/2), 64-73.

23. McCoy, H. N. *Science* **1911**, *34*, 138-142.

24. Ubbelohde, A. R. *Proc. Royal Soc. A* **1969**, *309* (1498), 297-311.

25. Murray, J. J.; Ubbelohde, A. R. *Proc. Royal Soc. A* **1969**, *312* (1510), 371-379.

26. Verheyen, L.; Leysen, P.; Van Den Eede, M.-P.; Ceunen, W.; Hardeman, T.; Koeckelberghs, G. *Polymer* **2017**, *108* (2017), 521-546.

27. Babudri, F.; Farinola, G. M.; Naso, F. *J. Mater. Chem.* **2004**, *14*, 11-34.

28. Yamamoto, T. *J. Organomet. Chem.* **2002**, *635*, 195-199.

29. Mercier, L. G.; Leclerc, M. *Acc. Chem. Res.* **2013**, *46*, 1597-1605.

30. Morin, P.-O.; Bura, T.; Leclerc, M. *Mater. Horiz.* **2016**, *3*, 11-20.

31. Rasmussen, S. C. In *Handbook of Conducting Polymers*, 4th ed.; Reynolds, J. R., Thompson, B. C., Skotheim, T. A., Eds.; CRC Press: Boca Raton, FL, 2019, Chapter 1.

32. MacDiarmid, A. G. *Angew. Chem. Int. Ed.* **2001**, *40*, 2581-2590.

33. Rasmussen, S. C. *Substantia* **2017**, *1*, 99-109.

34. Rasmussen, S. C. *Ambix* **2018**, *65* (4), 356-372.

35. Rasmussen, S. C. *Bull. Hist. Chem*. **2014**, 39 (1), 64-72.

36. Rasmussen, S. C. In *Conductive Polymers: Electrical Interactions in Cell Biology and Medicine*; Zhang, Z., Rouabhia, M., Moulton, S. E., Eds.; CRC Press: Boca Raton, FL 2017; pp 1-14.

37. Rasmussen, S. C. *Bull. Hist. Chem*. **2015**, 40 (1), 45-55.

38. Rasmussen, S. C. In *100+ Years of Plastics: Leo Baekeland and Beyond*, ACS Symposium Series 1080; Strom, E. T., Rasmussen, S. C. Eds.; American Chemical Society: Washington, DC 2011.

39. Chierici, L.; Artusi, G. C.; Bocchi, V. *Ann. Chim.* **1968**, *58*, 903-913.

40. Kanzawa, K. K.; Diaz, A. F., Geiss, R. H.; Gill, W. D.; Kwak, J. F.; Logan, J. A.; Rabolt, J. F.; Street, G. B. *J. Chem. Soc. Chem. Commun.* **1979**, (19), 854-855.

41. Diaz, A. F.; Martinez, A.; Kanazawa, K. K.; Salmon, M. *J. Electroanal. Chem.* **1981**, *130*, 181-187.

42. Rasmussen, S. C. *Bull. Hist. Chem.* **2017**, *42* (1), 63-78.

43. Sirakawa, H.; Ito, T.; Ikeda, S. *Makromol. Chem.* **1978**, *179*, 1565-1573.

44. Chiang, C. K.; Park, Y. W.; Heeger, A. J.; Shirakawa, H.; Louis, E. J.; MacDiarmid, A. G. *J. Chem. Phys.* **1978**, *69* (11), 5098-5104.

45. Yamamoto, T.; Sanechika, K.; Yamamoto, A. *J. Polym. Sci. Polym. Lett. Ed.* **1980**, *18*(1), 9-12.

46. Diaz, A. F.; Crowley, J.; Bargon, J.; Gardini, G. P.; Torrance, J. B. *J. Electroanal. Chem.* **1981,** *121*, 355-361.

47. Waltman, R. J.; Bargon, J.; Diaz, A. F. *J. Phys. Chem.* **1983**, *87* (8), 1459-1463.

48. Hernandez, R.; Diaz, A. F.; Waltman, R.; Bargon, J. *J. Phys. Chem.* **1984**, *88* (15), 3353-3357.

49. Waltman, R. J.; Diaz, A. F.; Bargon, J. *J. Phys. Chem.* **1984**, *88* (19), 4343-4346.

50. Tourillon, G.; Garnier, F. *J. Electronanal. Chem.* **1982**, *135* (1), 173-178.

51. SciFinder search. https://scifinder.cas.org/scifinder/view/scifinder/scifinderExplore.jsf (Accessed 1/10/2019).

52. Van Mullekom, H. A. M.; Vekemans, J. A. J. M.; Havinga, E. E.; Meijer, E. W. *Mat. Sci. Eng.* **2001,** *32* (1), 1-40.

53. Rasmussen, S. C.; Evenson, S. J. *Prog. Poly. Sci.* **2013**, *38* (12), 1773-1804.

54. Sumi, N.; Nakanishi, H.; Ueno, S.; Takimiya, K.; Aso, Y.; Otsubo, T. *Bull. Chem. Soc. Jpn.* **2001**, *74*, 979-988.

55. Izumi, T.; Kobashi, K.; Takimiya, K.; Aso, Y.; Otsubo, T. *J. Am. Chem. Soc*. **2003**, *125*(18), 5286-5287.

56. Brédas, J.-L.; Beljonne, D.; Coropceanu, V.; Cornil, J. *Chem. Rev*. **2004**, *104* (11), 4971-5004.

57. Nakano, T. *Poly. J*. **2010**, *42*, 103-123.

58. Rasmussen, S. C.; Schwiderski, R. L.; Mulholland, M. E. *Chem. Commun.* **2011**, *47* (41), 11394-11410.

59. Sworakowski, J. *Synth. Metals* **2018**, *235*, 125-130.

60. Rasmussen, S. C.; Ogawa, K.; Rothstein, S. D. In *Handbook of Organic Electronics and Photonics: Electronic Materials and Devices*; Nalwa, H. S., Ed.; American Scientific Publishers: Stevenson Ranch, CA, 2008; pp 1-50.

61. McCullough, R. D.; Lowe, R. D. *J. Chem. Soc., Chem. Commun.* **1992**, (1), 70-72.

62. Barbella, G.; Melucci, M. In *Handbook of Thiophene-Based Materials: Applications in Organic Electronics and Photonics*; Perepichika, I. F., Perepichka, D. F., Eds.; Wiley: West Sussex, U.K., 2009; Vol 1, pp 341-364.

63. Cary, F. A.; Sunberg, R. J. *Advanced Organic Chemistry Part A: Structure and Mechanisms*, 5th ed.; Springer: New York, NY, 2007; pp 713-760.

64. Bundgaard, E.; Krebs, F. C. *Sol. Energy Mater. Sol. Cells* **2007**, *91*, 954-985.

65. Brèdas, J.-L.; Norton, J. E.; Cornil, J.; Coropceasnu, V. *Acc. Chem. Res.* **2009**, *9* (11), 1691-1699.

66. Mulholland, M. E.; Schwiderski, R. L.; Rasmussen, S. C. *Poly. Bull.* **2012**, *69* (3), 291-301.

67. Wen, L; Heth, C. L.; Rasmussen, S. C. *Phys. Chem. Chem. Phys.* **2014**, *16* (16), 7231-7240.

68. Babich, I. V.; Moulijn, J. A. *Fuel* **2003,** *82*, 607-631.

69. Conary, R. E.; Devaney, L. W.; Ruidisch, L. E.; McCleary, R. F.; Kreuz, K. L. *Ind. Eng. Chem.* **1950**, *42*, 467-471.

70. Khlybich, P. P.; Burkhart, B.; Rudenko, A. E.; Thompson, B. C. *Polymer* **2013**, *54*, 5267-5298.

71. Li, Y. *Acc. Chem. Res.* **2012**, *45* (5), 723-733.

72. Turro, N. J.; Ramamurthy, V.; Scaiano, J. C. Modern Molecular Photochemistry of Organic Molecules; University Science Books: Sausalito, CA; 2010; pp 169-264.

73. Wudl, F.; Kobayashi, M.; Heeger, A. J. *J. Org. Chem.* **1984**, *49*, 3382-3384.

74. Kenning, D. D.; Mitchell, K. A.; Calhoun, T. R.; Funfar, M. R.; Sattler, D. J.; Rasmussen, S. C. *J. Org. Chem*. **2002**, *67* (25), 9073-9076.

75. Wen, L.; Nietfeld, J. P.; Rasmussen, S. C. *J. Org. Chem*. **2008**, *73* (21), 8529-8536.

76. Rasmussen, S. C.; Mulholland, M. E.; Schwiderski, R. L.; Larsen, C. A. *J. Heterocyclic Chem.* **2012**, *49* (3), 479-493.

77. Schwiderski, R. L.; Rasmussen, S. C. *J. Org. Chem*. **2013**, *78* (11), 5453-5462.

78. Mulholland, M. E.; Konkol, K. L.; Anderson, T. E.; Schwiderski, R. L.; Rasmussen, S. C. *Aust. J. Chem.* **2015**, *68* (11), 1759-1766.

79. Konkol, K. L.; Schwiderski, R. L.; Rasmussen, S. C. *Materials* **2016**, *9*, 404.

80. Culver, E. W.; Anderson, T. E.; Lopez Navarrete, J. T.; Ruiz Delgado, M. C.; Rasmussen, S. C. *ACS Macro Lett.* **2018**, *7* (10), 1215-1219.

81. Wolf. M. O. In *Handbook of Thiophene-Based Materials: Applications in Organic Electronics and Photonics*; Perepichika, I. F., Perepichka, D. F., Eds.; Wiley: West Sussex, U.K., 2009; Vol 1, pp 293-319.

82. Mitzi, D. B.; Chondroudis, K.; Kagan, C. R. *Inorg. Chem.* **1999**, *28* (26), 6246-6256.

83. Goward, G. R.; Leroux, F.; Nazar, L. F. *Electrochimica Acta* **1998**, *43* (10-11), 1307-1313.

84. Wolf, M. O. *Adv. Mater.* **2001**, *13* (8), 545-553.

85. Belo, D.; Almeida, M. *Coord. Chem. Rev.* **2010**, *254* (13-14), 1479-1492.

86. Pozo-Gonzalo, C.; Berridge, R.; Skabara, P. J.; Cerrada, E.; Laguna, M.; Coles, S. J.; Hursthouse, M. B. *Chem. Commun.* **2002**, (20), 2408-2409.

CHAPTER 2. CATALYTIC REGIOSELECTIVE HYDRODEBROMINATION OF 2,3,5-TRIBROMOTHIOPHENE

2.1. Introduction

This first project developed from efforts to synthesize 2,3-dialkylthiophenes which could then be incorporated into thiophenedithiolene materials (Chapter 3), to hopefully provide an increase in solubility with the integration of solubilizing chains. However, initial attempts to replicate a synthesis ended up giving results in direct contrast to what was presented in the literature, and this ended up becoming a more complex discussion than had ever been initially imagined.

Halothiophenes, particularly bromothiophenes, are the most common synthetic precursors for the production of functionalized thiophene materials.[1] These have found extensive use as building blocks for the synthesis of materials, natural products, and pharmaceuticals.[2-12] Bromothiophenes are typically prepared from direct bromination of thiophene with *N*-bromosuccinimide (NBS) or Br_2.[13-15] As shown in Scheme 2.1, the electronic differences between the α- and β-positions of the thiophene ring (**2.1**) favor the successive formation of 2-bromothiophene (**2.2**),[16,17] 2,5-dibromothiophene (**2.3**),[18] 2,3,5-tribromothiophene (**2.4**),[19,20] and 2,3,4,5-tetrabromothiophene (**2.5**).[21]

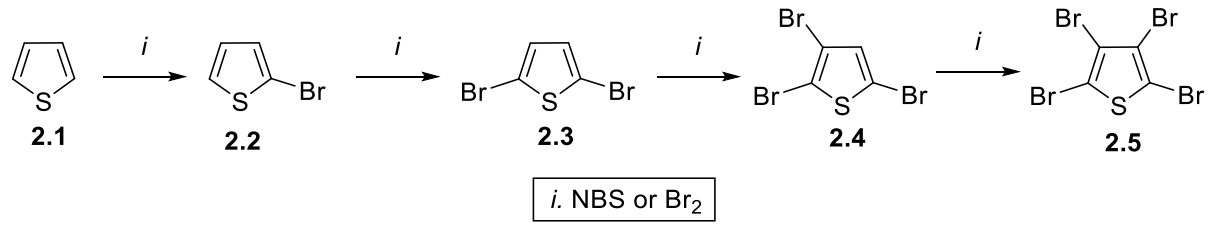

Scheme 2.1. Sequential bromination of thiophene

However, when it comes to the debromination of brominated thiophene species, a different series of brominated thiophenes is formed - again because of the electronic differences

between the α- and β-positions of the thiophene ring, with the bromination/debromination more favored at the α-position. This is usually accomplished using Zn/AcOH or the gentler $NaBH_4$ as the debrominating reagent. As shown in Scheme 2.2, the pathway for the debromination of 2,3,4,5-tetrabromothiophene (**2.5**) is the successive formation of 2,3,4-tribromothiophene (**2.6**),[22,23] 3,4-dibromothiophene (**2.7**),[22,24] 3-bromothiophene (**2.8**),[25] and thiophene (**2.1**).

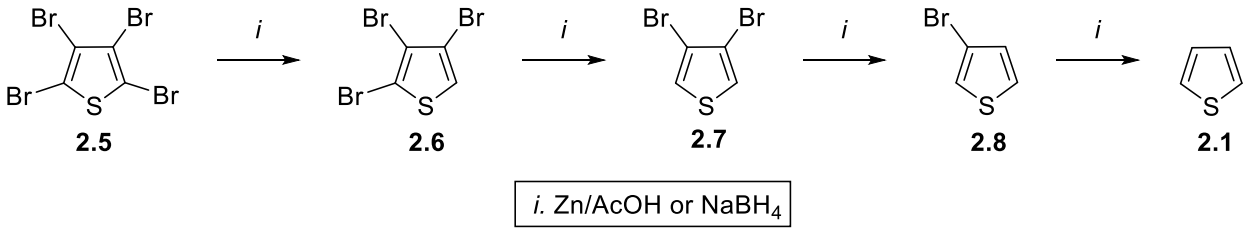

S**cheme 2.2.** Sequential debromination of brominated thiophene

While these synthetic steps are relatively straightforward, the production of bromothiophenes can become more complex when attempting to selectively brominate the less readily accessible β-positions, which requires either blocking of the more reactive α-positions or the removal of unwanted α-bromides following polybromination. This can become even more difficult for the production of asymmetric dibromothiophenes containing both α- and β-bromides.[26-32] The simplest conversion is the selective debromination of **2.4** to give 2,4-dibromothiophene (**2.9**) (Scheme 2.3), which can be done with either butyllithium or $NaBH_4$ (Table 2.1, entries 1 and 2).[27,28,30]

The formation of **2.9** benefits from the fact that the most reactive bromide is being removed in the process and thus the electronics drive selectivity.[32] Such electron preference can be overcome via the use of larger reagents, which has been demonstrated through the use of Grignard reagents (Table 2.1, entry 3) to selectively produce 2,3-dibromothiophene (**2.10**) from **2.4**.[26]

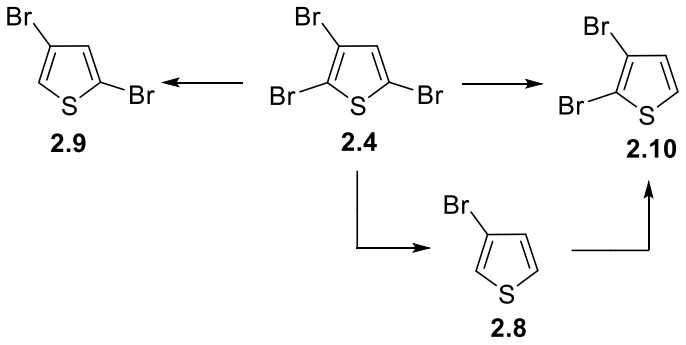

Scheme 2.3. Synthesis of asymmetric dibromothiophenes

Because of steric hindrance between the 3-bromo group and the incoming reagent, reaction at the 2-position is inhibited and thus debromination at the 5-position is preferred. However, both cost and difficulties in preparing the Grignard reagents make it far more common to produce **2.10** from the removal of both α-bromides of **2.4**. This is accomplished using inexpensive reagents to form **2.8**, followed by a single bromination to yield **2.10**.[29]

Table 2.1. Debromination of 2,3,5-tribomothiophene (**2.4**)

entry	reagent	**2.9**[a]	**2.10**[a]
1[b]	BuLi	75	25
2[c]	$NaBH_4$	95	3
3[d]	MeMgBr	18	82
4[c,e]	$Pd(PPh_3)_4/NaBH_4$	6	92

[a]Values given are ratios of products **2.9** and **2.10**. [b]References 27 and 28. [c]Reference 30. [d]Reference 26. [e]Reference 22.

It was reported by Hor and co-workers beginning in 1996 that the combination of the use of a stoichiometric amount of the debrominating/reducing agent $NaBH_4$ and a sterically bulky Pd catalyst could successfully produce the asymmetric species **2.10**, which eliminates the use of the previously necessary Grignard reagents.[22,30] Two reports presented this approach and cited both 100% conversion and high selectivity of for **2.10** over the electronically favored **2.9** (ca.

15:1, Table 2.1, entry 4). This approach of using sterically bulky Pd catalysts to overcome the thiophene electronics was then successfully applied to regioselective cross-coupling by the Rasmussen group in 2008.[31] Extending the methods of Hor and co-workers to cross-coupling reactions of **2.4**, the application of the sterically bulky catalyst $Pd(dppf)Cl_2$ (dppf = 1,1′-bis(diphenylphosphino)ferrocene) disfavored oxidative addition at the electronically favored 2-position to allow selective coupling of a variety of arylzinc chlorides at the 5-position. The selectivity observed in all cases was ca. 10:1.[31] The bulk of work presented in this chapter was previously published in *Organometallics*.[32]

2.2. Results and Discussion

2.2.1. Initial Attempts at Synthesis

Using the original synthesis presented Hor and co-workers,[22] we initially attempted to utilize their method of Pd-catalyzed hydrodebromination for the synthesis of asymmetric 2,3-dibromothiophene (**2.10**). However, puzzling and significant inconsistencies in selectivity were observed, and we were unable to replicate their results. Further efforts to replicate the previously reported reaction conditions as close as possible to begin with were complicated by the fact that different reaction conditions are reported between the initial report in 1996[30] and the more detailed paper in 1998.[22]

It is worth noting that although the reaction conditions changed between these two reports ($NaBH_4$ amount, catalyst amount, reaction time), the stated results remain essentially identical with complete conversion and excellent selectivity for **2.10** (Table 2.2, entries 1 and 2). Although the authors were not specific about how the reducing agent $NaBH_4$ was added to the reaction flask, with the published procedure stating that it was “added in small portions” over 1.5

h, two separate methods including both portion-wise addition and the use of a powder addition funnel were attempted to replicate the results.

Table 2.2. Initial results from attempts to reproduce literature procedures[a]

Entry	Method	# of $NaBH_4$ portions	total time (h)	conversion (%)	Products[b] 2.9	2.10	2.8
1[c,d]	unknown	unknown	6	100	6.1	92.5	1.4
2[e]	unknown	unknown	6	100	6	92	1
3	1[f]	5	6	79	48	43	9
4	1[f]	2	6	77	39	55	6
5	1[f]	1	6	99	95	5	0
6	2[g]	40-50	6	46	29	67	4

[a]Constant conditions: **2.4** (20 mmol), $NaBH_4$ (30 mml), and $Pd(PPh_3)_4$ (1 mol%) in 100 mL CH_3CN and heated at 70 °C. [b]Values given are ratios of products. **2.8-2.10**. [c]For entry 1, catalyst load was 5%. [d]Reference 30. [e]Reference 22. [f]Individual powder portions of $NaBH_4$ were added through the side-neck followed by evacuating/backfilling the flask with N_2 over 1.5 h. [g]Small powder portions of $NaBH_4$ were added via the screw of the powder addition funnel over 1.5 h.

The best we were able to do in our initial attempts to reproduce the literature procedure was incomplete conversion (46%) and moderate selectivity for **2.10** (ca. 2.3:1 for **2.10**:**2.9**) (Table 2.2, entry 5). While adding the $NaBH_4$ as slow as possible resulted in slight improvements in selectivity, this was not very practical and any improvement in selectivity was offset by lower conversion. As these initial results seemed inconsistent with the reports of either Hor[22,30] or Rasmussen,[32] it was decided that it was valuable to revisit methods to utilize catalyst sterics to overcome electronic selectivity, with the goal to provide greater understanding concerning the choice of this approach to controlling selectivity in halothiophenes.

Assuming the later conditions[22] to be the more optimized, it was these conditions we

determined to more fully investigate. In comparison to adding the $NaBH_4$ in small portions (Table 2.3, entry 3), the use of a powder addition funnel seemed to increase the conversion of the reaction in later results (Table 2.3, entry 4). Note that this contrasts with the switch between small portions and powder addition funnel reported in Table 2.2 (entries 3 and 6), which could be attributed to further familiarity with the procedure as the reaction was repeatedly replicated. However, neither the percent conversion nor selectivity previously reported by Hor could be obtained in our hands.

Table 2.3. Comparative results from refinement of literature procedures[a]

Entry	$NaBH_4$ (mmol)	catalyst (mol %)	time (h)	conversion (%)	Products[b] 2.9	2.10	2.8
1[c]	20	5	24	100	6.1	92.5	1.4
2[d]	30	1	6	100	6	92	1
3	30[e]	1	6	79	48	43	9
4	30[f]	1	6	85	40	52	8
5	30[f]	1[g]	6	88	40	50	10
6	30[f]	5	6	100	14	66	20

[a]Constant conditions: **2.4** (20 mmol), $NaBH_4$, and $Pd(PPh_3)_4$ in 100 mL of CH_3CN and heated at 70 °C. [b]Values given are ratios of products **2.8-2.10**. [c]Reference 30. [d]Reference 22. [e]Added in small solid aliquots. [f]Added via powder addition funnel. [g]Catalyst synthesized from reference 33.

As the previous reports had not used a commercial catalyst but had synthesized and purified $Pd(PPh_3)_4$ (tetrakis(triphenylphosphine)palladium(0)) in-house, the potential effects of catalyst purity were then investigated. Fresh $Pd(PPh_3)_4$ was synthesized[33] and purified via the same methods reported by Hor and co-workers, after which the conditions given in entry 4 were repeated with the fresh catalyst (Table 2.3, entry 5). As the results comparing a commercial catalyst and freshly synthesized $Pd(PPh_3)_4$ gave nearly identical results, it was concluded that the

catalyst source was not a significant factor in the selectivity issues. Finally, the amount of catalyst was increased to 5 mol %, which did result in complete conversion and an increase in selectivity for the production of **2.10**. However, this selectivity was still well below that previously reported.[30,31]

2.2.2. Background Reaction and Solvent Choice

It was assumed that the lack of reproducibility could be due to an unintentional lack of detail in the published procedure, especially concerning the method of $NaBH_4$ addition, which had already been shown to affect conversion and selectivity in the initial trials (Table 2.3). Attempting to better understand the effect of $NaBH_4$ addition, we then examined noncatalyzed conditions in order to determine the extent of any background reaction. A background reaction is a reaction that is also occurring in the reaction, in this case absent the Pd-catalyst. As shown in Table 2.4, the noncatalyzed debromination of **2.4** was previously reported by Hor and co-workers in DMSO (dimethylsulfoxide).[30] In this polar aprotic solvent, the direct reaction at room temperature is highly facile, with 100 % conversion within 4 h when 2 equiv. of $NaBH_4$ was utilized (Table 2.4, entry 3). This conversion becomes less efficient with lower amounts of $NaBH_4$, with a slight decrease in selectivity. However, as the previously reported catalytic methods used the slightly more polar CH_3CN (acetonitrile) as the solvent, [22,30] it was unclear to what extent the change in solvent may inhibit this background reaction.

To measure this effect of solvent choice, the noncatalyzed debromination of **2.4** in CH_3CN was first carried out at room temperature (Table 2.4, entry 4). The change to CH_3CN gave almost no reaction at room temperature, with only 3% conversion after 7 h. Selectivity for the electronically favored 2-position, however, was complete at these conditions and no reaction was observed at the 5-position. However, when the reaction was carried out at the temperature

given under the reported catalytic conditions (i.e. 70 °C), it was complete within 6 h and showed the expected selectivity for the electronically favored 2-position (entry 5), although a small amount of 5-position product **2.10** was observed. When THF (tetrahydrofuran) was utilized as the solvent in the noncatalyzed conditions, zero conversion was observed at room temperature (Table 2.4, entry 6) and a very small portion at reflux (Table 2.4, entry 7). This small conversion in THF can be attributed to the low solubility of $NaBH_4$ in the solvent, with the solubility of the reducing agent in DMSO > CH_3CN > THF.

Table 2.4. Noncatalyzed debromination of 2,3,5-tribromothiophene (**2.4**)[a]

Entry	solvent	3:$NaBH_4$	temp (°C)	time (h)	conversion (%)	Products[b] 2.9	2.10	2.8
1[c]	DMSO	1:1	rt	24	50	90	1	8
2	DMSO	1:1.5	rt	6	73	93	7	0
3[c]	DMSO	1:2	rt	4	100	95	2.6	2.9
4	CH_3CN	1:1.5	rt	7	3	100	0	0
5	CH_3CN	1:1.5	70	6	99	95	5	0
6	THF	1:1.5	rt	6	0	0	0	0
7	THF	1:1.5	66	6	2	100	0	0

[a]Constant conditions: **2.4** (5 mmol) and $NaBH_4$ in 100 mL of solvent. [b]Values given are ratios of products **2.8-2.10**. [c]Reference 30.

The reactivity of $NaBH_4$ with **2.4** in hot CH_3CN is quite problematic and explains the difficulty in achieving the high selectivity previously reported by Hor and co-workers. [22,30] As selective debromination at the 5-position only occurs when it is mediated by the bulky catalyst, conditions would need to inhibit any background reaction. Nevertheless, as the background reaction readily occurs under the conditions utilized, the only way selectivity could possibly be achieved is if the $NaBH_4$ were added at a rate in which it was immediately consumed in the

catalytic cycle (Scheme 2.4) and not allowed to participate in direct reaction with **2.4**, something that would be almost impossible to control.

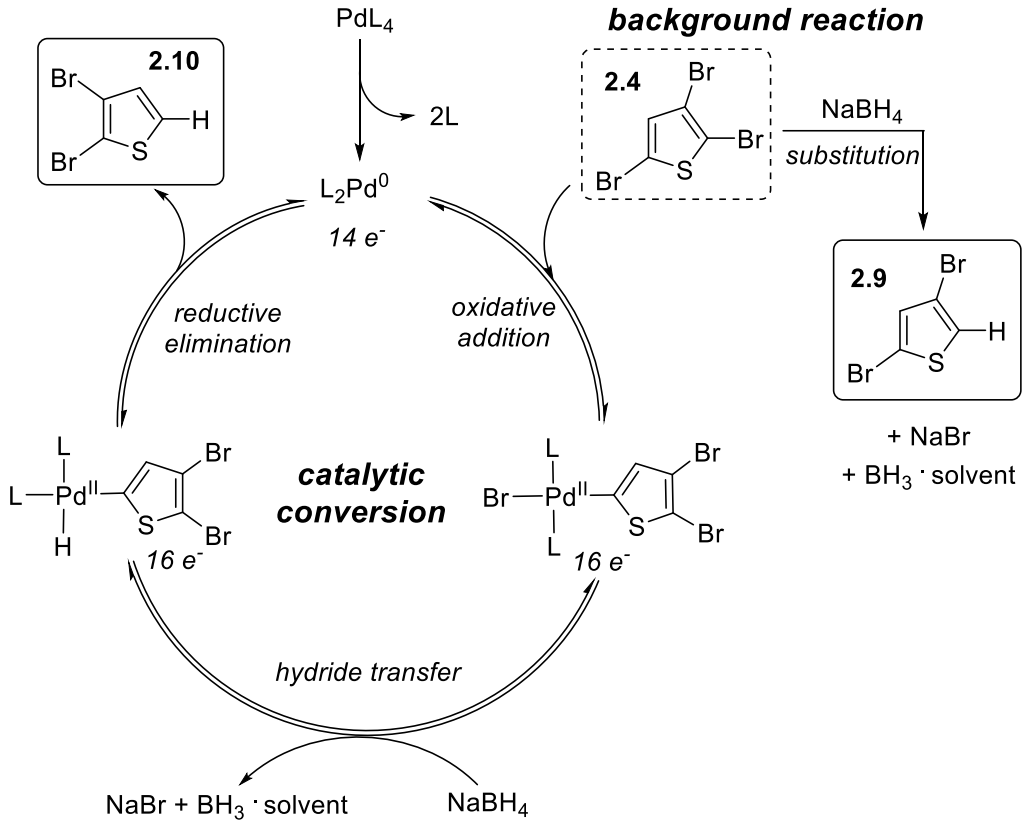

Scheme 2.4. Catalytic cycle and competing background reaction for hydrodebromination of **2.4**

The catalytic cycle proposed below follows the general scheme also seen for Pd-catalyzed cross-coupling reactions. The first step is oxidative addition of the 2,3,5-tribromothiophene **2.4** which adds *trans* to the Pd(0) metal, forming a Pd(II) species. Although not shown, it is possible that the initial active catalyst also contains one or two associated solvent molecules to form a more stable 16- or 18-electron species, instead of the 14-electron PdL_2 species shown. These solvent molecules would then dissociate concurrently with the oxidative addition step.

The second step of the reaction is the hydride transfer, whereby the $NaBH_4$ serves as a hydride source for the exchange of the bromide for hydride ligand. Analogous to transmetallation, the driving force of this hydride transfer can be discussed in terms of Hard-Soft Acid-Base Theory (HSAB).[34] The formation of the favored soft acid (SA) – soft base (SB) (Pd-H) pair and hard acid (HA) – hard base (HB) (Na-Br) pair is both the driving force and the rate limiting step of this catalytic reaction: {Pd-Br (SA-HB) + Na-H (HA-SB) → Pd-H (SA-SB) + Na-Br (HA-HB)}.

The third and final step of this catalytic reaction is the reductive elimination, whereby the *cis*-arranged thiophene and hydride ligands are eliminated and combine in a very favorable process to reform the Pd(0) catalytic species. Again, it is quite possible that solvent molecules re-associate with the active catalytic species to form more stable species.

The rate of catalytic conversion of **2.4** to **2.10** is very important to the success of the reaction, as the background reaction is competing in solution with the catalytic reaction. This would not be an issue for the majority of the catalytic debrominations reported by Hor and co-workers,[22] as the bromide being removed is usually in the electronically favored position and thus the catalytic and background reactions would give the same product. In fact, it is only the example of **2.4** in which this background reaction would demonstrate a role in affecting selectivity. Unfortunately, the selective debromination of the 5-position of **2.4** under these conditions did not seem to be practical.

2.2.3. Attempts to Inhibit the Background Reaction

Coming to this disappointing conclusion, alternate conditions were then investigated in order to find practical methods that would inhibit the background reaction while still allowing efficient and selective conversion of **2.4** to **2.10**. As solvent choice plays a large role in the

background reaction, this was the initial variable considered. The extent of the background reaction is essentially controlled by the solubility of $NaBH_4$ under the particular conditions. As shown in Table 2.4, CH_3CN provides low solubility and thus low reactivity at room temperature but better solubility and higher reactivity at reflux. However, it should be noted that $NaBH_4$ is still not completely soluble in hot CH_3CN, which accounts for its lower reactivity in comparison to DMSO. More polar solvents such as DMF (dimethylformamide) provide good solubility and fall in between CH_3CN and DMSO in terms of facilitating the background reaction. Diethyl ether (Et_2O), on the other hand, showed no solubility or reactivity at either room temperature or reflux temperatures. The closely related THF, however, provided an intermediate solubility between that of CH_3CN and diethyl ether and was thus selected as the primary solvent for further consideration.

In addition to the change in solvent, we determined to use $Pd(dppf)Cl_2$ ([1,1'-bis(diphenylphosphino)ferrocene]dichloropalladium(II)) in place of $Pd(PPh_3)_4$ as the catalyst going forward. This change was inspired by the fact that the bulkier dppf ligand was found to give slightly better steric-mediated selectivity in previous Pd-catalyzed cross-coupling of **2.4**,[31] and thus should provide increased selectivity in these catalytic hydrodebromination conditions as well. In order to keep the methods as simple as possible, initial trials utilized a one-pot method in which all reagents were added collectively at the start (Table 2.5). These initial conditions exhibited reasonable selectivity but poor product conversion, as shown in entry 1.

Presuming that the low conversion was due to limited $NaBH_4$ solubility, we thought that this could be improved via the addition of agents to chelate the sodium cation. This could allow for optimization of the $NaBH_4$ solubility such that conversion is enhanced while still minimizing the background reaction. Crown ethers can strongly bind certain cations (e.g. Na^+), forming

coordination complexes. The addition of various crown ethers, particularly 15-crown-5 $(C_2H_4O)_5$, to $NaBH_4$ solutions seemed too successful at solubilizing the sodium salt, resulting in both increased conversion but decreased selectivity.

Table 2.5. Comparative results from one-pot methods[a]

entry	catalyst (mol %)	$NaBH_4$:TMEDA	time (h)	conversion (%)	Products[b] 2.9	2.10	2.8
1	1	1:0	7	9	19	81	0
2	1	1:1	7	11	17	83	0
3	1	1:1	24	34	29	72	0
4	2.5	1:1	48	33	22	78	0
5	2.5	1:2	24	30	17	83	0

[a]Constant conditions: **2.4** (5 mmol), $NaBH_4$ (1.5 equiv), and $Pd(dppf)Cl_2$ in 100 mL THF at reflux. [b]Values given are ratios of products **2.8**-**2.10**.

Thus, our attention shifted to tetramethylethylenediamine (TMEDA) as a potential additive. The use of TMEDA as an additive in metal-catalyzed $NaBH_4$ reductions has been previously reported,[35] and its addition to $NaBH_4$ solutions appeared qualitatively to give a good level of solubility adjustment. Reactions in THF with TMEDA did show slightly better conversion, along with a slight enhancement in selectivity (Table 2.5, entry 2). Extending the reaction time (Table 2.5, entry 3) resulted in a substantial increase in conversion, although it was still lower than desired, and this was also coupled with a reduction in selectivity. Further increasing the reaction time did not result in further increases in conversion, but increasing the catalyst loading to 2.5 mol % did help counteract the lower selectivity (Table 2.5, entry 4). Increasing both the catalyst load and ratio of TMEDA to $NaBH_4$ did positively affect selectivity, however similar trends in low conversion were observed (Table 2.5, entry 5).

The effects of TMEDA have been previously credited to either stabilization of the resting state of the catalyst via coordination of Pd or assisting the hydride transfer step by coordination of the resulting BH_3.[35] While coordinating the resting state of the catalyst is possible, the addition of the bidentate TMEDA ligand would result in an 18-electron Pd species.[36] This species would significantly inhibit oxidative addition, either by quenching catalytic activity or negatively affecting the corresponding kinetics. Therefore, for TMEDA chelation to occur, dissociation of a third PPh_3 ligand from the catalyst would most likely be necessary in order to maintain catalytic activity. Coordination of the TMEDA to boron is also an option for stabilization, but the fact that these reactions are carried out in coordinating solvents (DMSO, CH_3CN, THF)[37] in molar quantities excess to the TMEDA reagent (ca. 80:1), makes it much more probable that solvent coordination satisfies the electron-deficient BH_3. Consequently, the most likely effect of the TMEDA is simple coordination to the sodium cation of $NaBH_4$, which enhances the solubility of the salt in THF. This is supported by both the enhanced THF solubility of TMEDA/$NaBH_4$ mixtures by visible inspection and the reports of multiple crystal structures exhibiting the chelation of sodium by TMEDA.[38,39]

With the conditions starting to look promising for the one-pot methods, efforts moved to investigation of slow addition methods in order to further optimize the reaction. During the initial investigations outlined in Table 2.2, the catalyst and **2.4** were combined in solvent and the reducing agent was added in small portions as a solid while the reaction mixture was stirred under N_2 at an elevated temperature. However, the one-pot addition methods of $NaBH_4$ required the removal of a septum, which both exposed the reaction to O_2 and introduced loss of solvent via escaping vapor at reflux. These issues could be overcome via the use of a powder addition funnel, but this was found to be impractical due to the small quantities of reducing agent

involved, unless the reaction was carried out on a suitably large scale. Similarly, attempts to add the reducing agent via solution addition funnel were unsuccessful because of the low solubility of $NaBH_4$ in almost all solvents, and when $NaBH_4$ was soluble, the background reaction was predominant (Table 2.4). Accordingly, a reverse approach was taken to limit the amount of **2.4** in solution, rather than attempting to control the amount and reactivity of the $NaBH_4$. By controlling the availability of **2.4** via its slow addition to the reaction mixture, we assumed it should be possible to maintain a concentration near the catalyst concentration, thus limiting transformation via the background reaction. Therefore, reactant **2.4** in 50 mL of THF was added dropwise to the hot reaction mixture (Table 2.6) consisting of the remaining components dissolved in another 50 mL of THF. This maintained the total solvent volume at 100 mL. The slow addition of reactant **2.4** to $NaBH_4$ resulted in significantly large increases in conversion such that complete consumption of **2.4** had occurred within 19-20 h (Table 2.6, entries 1 and 2).

Table 2.6. Effects of slow addition of 2,3,5-tribromothiophene (**2.4**)[a]

entry	precatalyst	add time (h)	total time (h)	conversion (%)	Products[b] 2.9	2.10	2.8
1	$Pd(dppf)Cl_2$	2	20	100	5	31	64
2	$Pd(dppf)Cl_2$	3	19	100	10	34	56
3	$Pd(PPh_3)_4$	1.5	6	100	4	65	31
4	$Pd(PPh_3)_4$	1.5	4	69	10	63	27
5[c]	$Pd(PPh_3)_4$	1.5	6	71	9	76	15

[a]Constant conditions: **2.4** (5 mmol), $NaBH_4$ (1.5 equiv), TMEDA (3 equiv), and catalyst (2.5 mol %) in 100 mL THF at reflux. [b]Values given are ratios of products **2.8**-**2.10**. [c]Only 1 equiv of $NaBH_4$ used.

Regrettably, this positive advance in conversion was coupled with over-debromination, whereby a significant amount of the recovered product (ca. 60%) was the doubly debrominated product 3-bromothiophene (**2.8**).

At this point, the soundness of the earlier decision to move from $Pd(PPh_3)_4$ to the bulkier $Pd(dppf)Cl_2$ was questioned. Although this original decision was due to the enhanced steric-mediated selectivity previously observed for $Pd(dppf)Cl_2$,[31] we realized that the enhanced sterics of this catalyst which helped favor formation of 2,3-dibromothiophene had the unfortunate effect of contributing to a reduction in reaction rate. For example, it is known that increasing ligand sterics negatively affects the rate of oxidative addition.[40-42] Therefore, any benefits in reaction selectivity may not be worth the accompanying cost in terms of reduced reaction rate. To confirm this, the high conversion conditions were repeated with the less sterically bulky $Pd(PPh_3)_4$ catalyst. As shown in Table 2.6 (entry 3), a substantial increase in reaction rate was observed, with the total reaction time reduced by half. In addition, the problem of over-debromination was also significantly reduced and selective debromination of the 5-position to produce **2.10** over the more reactive 2-position was quite high (ca. 16:1).

2.2.4. Final Modifications

In a final attempt to minimize over-debromination and increase the isolated yield of 2,3-dibromothiophene (**2.10**), the reaction time was limited to 4 h (Table 2.6, entry 4). Unfortunately, this negatively affected conversion to a greater extent than reducing over-debromination, confirming that these conditions required the full 6 h to run to completion. Attempts to reduce the amount of $NaBH_4$ to 1 equiv (Table 2.6, entry 5) did help in limiting over-debromination, but also adversely reduced conversion to 71%. This final result was consistent with the initial studies

of the background reaction under optimal conditions (Table 2.4), which revealed that an excess of $NaBH_4$ was necessary to reach complete conversion.

As none of these final modifications (catalyst, time) successfully increased the isolation of **2.10**, the maximum yield observed under the final optimized conditions provided here was limited to only 65% (Table 5, entry 3). However, this does not disqualify additional gains from being possible with further tuning of the reactions. For example, the modest investigation of solvent choice (Table 2.4) could be expanded to mixed-solvent systems, which could allow for both more fine-tuning of the $NaBH_4$ solubility and more limited contributions from the background reaction under the reaction conditions applied. However, we would expect any further gains to be relatively minor at this point.

Although the yield provided by the optimized conditions here (Table 2.6, entry 3) is not as high as was hoped and is substantially lower than that originally reported by Hor and co-workers (Table 2.2, entries 1 and 2),[22,30] the conditions still provide better selectivity than is possible via noncatalytic sterically controlled methods such as the use of Grignard reagents (Table 2.1). In addition, the methods reported here result in the production of very low amounts of 2,4-dibromothiophene (**2.8**), which allows for the purification of the desired isomer 2,3-dibromothiophene (**2.10**). These two isomers are virtually impossible to separate from one another, as they elute similarly on silica gel and exhibit very similar boiling points (210-212 °C for **2.8**;[43] 218.6–219.6 °C for **2.10**).[44] Under the optimized conditions given here, the primary byproduct is 3-bromothiophene (**2.8**, bp = 157-158 °C),[45] which is considerably easier to remove from the desired product.

2.3. Conclusions

These results reconfirm previous reports[30-32,46] that reactivity at the more electronically favored 2-postion of 2,3,5-tribromothiophene can be overcome through the use of sterically bulky catalysts to give selective reaction at the less sterically hindered 5-postion. However, it has been shown that this reaction can really only be successful in the absence of any significant background reaction. The extremely facile background reaction that occurs in the absence of a catalyst when $NaBH_4$ is used as the hydrogen source limits applications of this methodology to the hydrodebromination of heterocycles. As shown in these results, any attempts to restrict the background reaction generally results in low conversion, while conditions that enhance conversion tend to also make the background reaction more favorable.

The final optimized conditions reported here do the best to balance these factors yet still suffer from significant over-debromination, which lowers the yield of the desired product. Fundamentally, the extremely high levels of selectivity previously reported by Hor and co-workers[30,31] are just not practical via the use of $NaBH_4$. It is possible that Hor and co-workers also suspected this, as their later efforts shifted to the use of alcohols as the hydrogen source for such hydrodebrominations.[47] Of the 30 different examples of "selective" catalytic hydrodehalogenation of bromothiophenes and related analogues reported by the groups of Hor and Chelucci,[22,30,35] the example of selective debromination of 2,3,5-tribromothiophene is the *only* case in which the catalytic process and the background reaction would be expected to give different products. Consequently, it is perhaps therefore not surprising that this complicating issue with the facile background reaction had been previously overlooked until our recent examination of it.[32]

2.4. Experimental Methods

Unless otherwise specified, all reactions were carried out under an N_2 atmosphere with reagent grade materials. Diethyl ether and THF were distilled from sodium/benzophenone prior to use. Acetonitrile was dried over calcium hydride and distilled prior to use. Sodium borohydride was stored in a desiccator and used within 1 year of purchase. Palladium catalysts were purchased from Sigma-Aldrich, and $Pd(PPh_3)_4$ was stored at −5 °C in the absence of light. 2,3,5-Tribromothiophene (**2.4**)[20] was synthesized using literature procedures and purified by distillation. ^{1}H NMR spectra were measured on a 400 MHz Varian spectrometer in $CDCl_3$ unless otherwise stated. Percent conversions and product distributions were determined through integration of NMR peaks. All NMR data were referenced to residual solvent peaks, and peak multiplicities are reported as follows: s = singlet, d = doublet, dd = doublet of doublets.

Reaction Conditions for Attempts to Reproduce Literature Methods via Addition of Individual Powder Portions. Tribromothiophene **2.4** (20 mmol) and $Pd(PPh_3)_4$ (1 mol%) were added to a three-neck flask equipped with a condenser. The flask was then evacuated and backfilled three times with N_2, followed by the addition of CH_3CN (100 mL). The reaction was heated to 70 °C with stirring. Powder portions of $NaBH_4$ were then added by removing the septum from one of the flask necks, adding the $NaBH_4$ aliquot and evacuating/backfilling the flask again with N_2. This was continued until all of the $NaBH_4$ (30 mmol) was added within the specified time (1.5 h), after which heating continued for 4.5 h. The reaction was then cooled to room temperature and the solvent removed via rotary evaporation. An aliquot of the crude product was then dissolved in $CDCl_3$ and analyzed by ^{1}H NMR to determine product distribution.

Reaction Conditions for Attempts to Reproduce Literature Methods via Powder Addition Funnel. Tribromothiophene **2.4** (20 mmol) and $Pd(PPh_3)_4$ (1 mol%) were added to a three-neck flask equipped with a condenser and a powder addition funnel. $NaBH_4$ (30 mmol) was added to the addition funnel and everything was evacuated and backfilled three times with N_2. CH_3CN (100 mL) was then added to the flask and the reaction was heated to 70 °C with stirring. Small powder portions of $NaBH_4$ were then added via the screw of the addition funnel over 1.5 h, after which heating continued for 4.5 h. The reaction was then cooled to room temperature and the solvent removed via rotary evaporation. An aliquot of the crude product was then dissolved in $CDCl_3$ and analyzed by ^1H NMR to determine product distribution.

General One-Pot Reaction Conditions. Tribromothiophene **2.4** (5.0 mmol), $NaBH_4$ (7.5 mmol), TMEDA, and $Pd(dppf)Cl_2$ were placed in a flask equipped with a condenser. The flask was then evacuated and back-filled three times with N_2, followed by the addition of THF (100 mL). The reaction mixture was heated to reflux with stirring, and heating was continued for the allotted time. The reaction mixture was then cooled to room temperature and the solvent removed via rotary evaporation. An aliquot of the crude product was then dissolved in $CDCl_3$ and analyzed by ^1H NMR to determine product distribution.

2,3,5-Tribromothiophene (2.4). ^1H NMR: δ 6.89 (s, 1H). ^{13}C NMR: δ 132.3, 113.7, 112.3, 110.8. NMR spectral data agree well with previously reported values.[19]

3-Bromothiophene (2.8). ^1H NMR: δ 7.28 (dd, J = 3.1, 5.1 Hz, 1H), 7.22 (dd, J = 1.4, 3.1 Hz, 1H), 7.01 (dd, J = 1.4, 5.1 Hz, 1H). ^{13}C NMR: δ 130.0, 126.7, 122.8, 110.2. NMR spectral data agree well with previously reported values.[19,31]

2,4-Dibromothiophene (2.9). ^{1}H NMR: δ 7.14 (d, *J* = 1.7 Hz, 1H), 6.96 (d, *J* = 1.7 Hz, 1H). ^{13}C NMR: δ 132.3, 124.8, 113.5, 110.0. NMR spectral data agrees well with previously reported values.[30,32]

2,3-Dibromothiophene (2.10). ^{1}H NMR: δ 7.23 (d, *J* = 6.0 Hz, 1H), 6.91 (d, *J* = 6.0 Hz, 1H). ^{13}C NMR: δ 130.4, 127.2, 114.3, 111.5. NMR spectral data agree well with previously reported values.[30,31,48]

General Reaction Conditions for Non-Catalyzed Background Reactions. Tribromothiophene **2.4** (5 mmol) and $NaBH_4$ were added to a three-neck flask equipped with a condenser. The flask was then evacuated and backfilled three times with N_2, followed by the addition of 100 mL of the chosen solvent (DMSO, CH_3CN, Et_2O, or THF). The reaction was either run at room temperature (ca. 22-24 °C) with stirring or heated at the specified temperature and allowed to react for the specified time. The reaction was then cooled to room temperature (if not already at room temperature) and the solvent removed via rotary evaporation. An aliquot of the crude product was then dissolved in $CDCl_3$ and analyzed by ^{1}H NMR to determine product distribution.

General Reaction Conditions for Slow Addition of Tribromothiophene. $NaBH_4$ (7.5 mmol), TMEDA (15 mmol), and catalyst (2.5 mol %) were placed in a flask equipped with a condenser and an addition funnel that was then evacuated and back-filled three times with N_2, followed by the addition of THF (50 mL). The addition funnel was then charged with **2.4** (5.0 mmol) in 50 mL of THF. The reaction mixture was heated to reflux with stirring and the solution of **2.4** added dropwise over the specified time period. Heating was continued for the allotted time, after which the reaction mixture was cooled to room temperature and the solvent removed

via rotary evaporation. An aliquot of the crude product was then dissolved in $CDCl_3$ and analyzed by ^1H NMR to determine product distribution.

Optimized Reaction Conditions. $NaBH_4$ (7.5 mmol), TMEDA (15 mmol), and catalyst (2.5 mol %) were placed in a flask equipped with a condenser and an addition funnel. The flask was then evacuated and back-filled three times with N_2, followed by the addition of THF (50 mL). The addition funnel was then charged with **2.4** (5.0 mmol) in 50 mL of THF. The reaction mixture was heated to reflux with stirring and the solution of **2.4** added dropwise over 1.5 h. Heating was continued for 4.5 h, after which the reaction mixture was cooled to room temperature and poured into H_2O. This mixture was then extracted with diethyl ether, washed with H_2O, and dried over $MgSO_4$, and the solvent was removed via rotary evaporation. The crude material was then purified by silica gel chromatography (hexanes) to give product **2.10** as a pale oil (60–65% yield).

Determination of Product Distributions. Integration of ^1H NMR was used to determine percent conversion and product distribution. Examples of analysis of incomplete conversion (Figure 2.1) and complete conversion (Figure 2.2) are shown below.

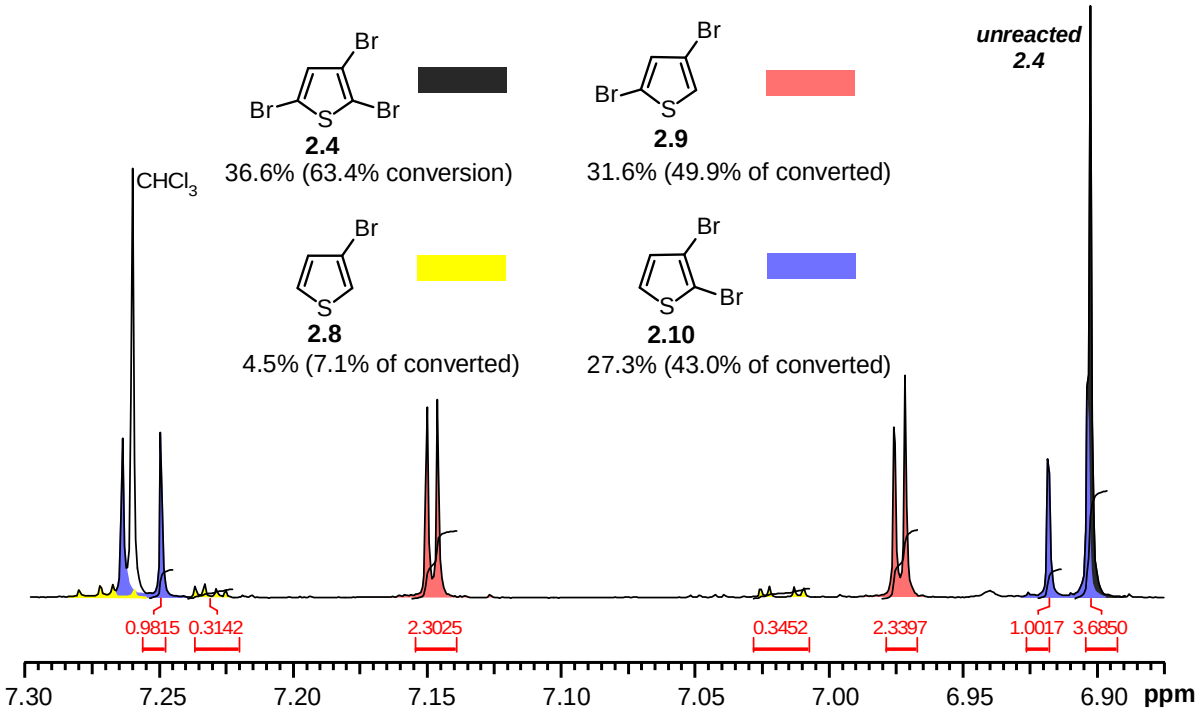

Figure 2.1. Example of determination of products by ^{1}H NMR integration (incomplete conversion)

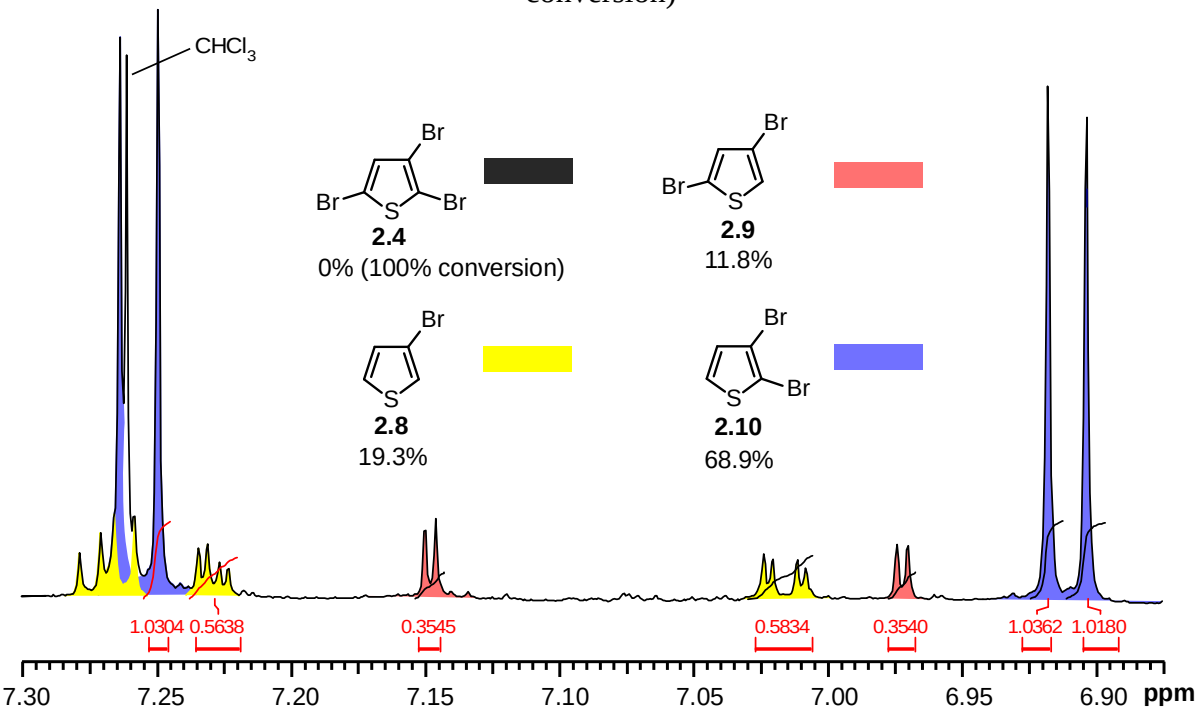

Figure 2.2. Example of determination of products by ^{1}H NMR integration (complete conversion)

2.5. References

1. Gronowitz, S.; Hörnfeldt, A.-B. *Thiophenes*; Elsevier Academic Press: Oxford, UK, 2004.
2. Jeffries-El, M.; McCullough, R. D. In *Handbook of Conducting Polymers: Theory, Synthesis, Properties, and Characterization*, 3rd ed.; Skotheim, T. A.; Reynolds, J. R., Eds.; CRC Press: Boca Raton, FL, 2007, Chapter 9.
3. Kirchmeyer, S.; Reuter, K.; Simpson, J. C. In *Handbook of Conducting Polymers: Theory, Synthesis, Properties, and Characterization*, 3rd ed.; Skotheim, T. A.; Reynolds, J. R., Eds.; CRC Press: Boca Raton, FL, 2007, Chapter 10.
4. Stozing, G. A.; Seshadri, V.; Waller, F. J. In *Handbook of Conducting Polymers: Theory, Synthesis, Properties, and Characterization*, 3rd ed.; Skotheim, T. A.; Reynolds, J. R., Eds.; CRC Press: Boca Raton, FL, 2007, Chapter 11.
5. Rasmussen, S. C.; Pomerantz, M. In *Handbook of Conducting Polymers: Theory, Synthesis, Properties, and Characterization*, 3rd ed.; Skotheim, T. A.; Reynolds, J. R., Eds.; CRC Press: Boca Raton, FL, 2007, Chapter 12.
6. Blanchard, P.; Leriche, P.; Frère, P.; Roncali, J. In *Handbook of Conducting Polymers: Theory, Synthesis, Properties, and Characterization*, 3rd ed.; Skotheim, T. A.; Reynolds, J. R., Eds.; CRC Press: Boca Raton, FL, 2007, Chapter 13.
7. Ewbank, P. C.; Stefan, M. C.; Sauvé, G.; McCullough, R. D. In *Handbook of Thiophene-Based Materials: Applications in Organic Electronics and Photonics*; Perepichika, I. F., Perepichka, D. F., Eds.; Wiley: West Sussex, U.K., 2009; Vol 1, pp 157-217.

8. Skabara, P. J. In *Handbook of Thiophene-Based Materials: Applications in Organic Electronics and Photonics*; Perepichika, I. F., Perepichka, D. F., Eds.; Wiley: West Sussex, U.K., 2009; Vol 1, pp 219-253.

9. Perepichika, I. F.; Perepichka, D. F.; Meng, H. In *Handbook of Thiophene-Based Materials: Applications in Organic Electronics and Photonics*; Perepichika, I. F., Perepichka, D. F., Eds.; Wiley: West Sussex, U.K., 2009; Vol 1, pp 695-756.

10. Invernale, M. A.; Acik, M.; Sotzing, G. A. In *Handbook of Thiophene-Based Materials: Applications in Organic Electronics and Photonics*; Perepichika, I. F., Perepichka, D. F., Eds.; Wiley: West Sussex, U.K., 2009; Vol 1, pp 757-782.

11. Bohlmann, F.; Zdero, C. In *Thiophene and its Derivatives*; Gronowitz, S., Ed.; The Chemistry of Heterocyclic Compounds, series 44 (part 1); Wiley: New York, 1985; pp 261-323.

12. Press, J. B. In *Thiophene and its Derivatives*; Gronowitz, S., Ed.; The Chemistry of Heterocyclic Compounds, series 44 (part 4); Wiley: New York, 1991; pp 397-502.

13. Katritzky, A. R.; Pozharskii, A. F. *Handbook of Heterocyclic Chemistry*, 2nd ed.; Pergamon: Amsterdam, 2000; pp 308-310.

14. Katritzky, A. R.; Taylor, R. *Adv. Heterocycl. Chem.* **1990**, *47*, 1-467.

15. Belen'kii, L. I.; Kim, T. G.; Suslov, I. A.; Chuvylkin, N. D. *Russ. Chem. Bull.* **2005**, *54*, 853-863.

16. Mo, D.; Zhen, S.; Xu, J.; Zhou, W.; Lu, B.; Zhang, G.; Wang, Z.; Zhang, S.; Feng, Z. *Synth. Met.* **2014**, 198, 19-30.

17. Keegstra, M. A.; Brandsma, L. *Synthesis* **1988**, 1988, 890-891.

18. Liu, X.; Li, L.; Sun, J.; Yan, Y.; Shu, X.; Liu, B.; Sha, W.; Feng, H.; Sun, S.; Zhu, J. *Inorg. Chem*. **2012**, *51*, 188-192.

19. Heinrich, A. C. J.; Thiedemann, B.; Gates, P. J.; Staubitz, A. *Org. Lett.* **2013**, *15*, 4666-4669.

20. Brandsma, L.; Verkruijsse, H. D. *Synth. Commun.* **1988**, *18*, 1763-1764.

21. Chen, X.; Liu, B.; Zou, Y.; Tang, W.; Li, Y.; Xiao, D. *RSC Adv.* **2012**, *2*, 7439-7448.

22. Xie, Y.; Wu, B.-M.; Xue, F.; Ng, S.-C.; Mak, T. C. W.; Hor, T. S. A. *Organometallics* **1998**, 17, 3988-3995.

23. Bratt, J.; Iddon, B.; Mack, A. G.; Suschitzky, H.; Taylor, J. A.; Wakefield, B. J. *J. Chem. Soc., Perkin Trans. I* **1980**, 2, 648-656.

24. Tietz, J. I.; Seed, A. J.; Sampson, P. *Org. Lett.* **2012**, *14* (19), 5058-5061.

25. Gronowitz, S.; Hailberg, A.; Glennow, C. *J. Heterocyclic Chem.* **1980**, *17* (1), 171-174.

26. Steinkopf, W.; Jacob, H.; Penz, H. *Justus Liebigs Ann. Chem.* **1934**, 512, 136-164.

27. Lawesson, S.-O. *Ark. Kemi* **1957**, 11, 317-324.

28. Ladd, D. L.; Harrsch, P. B.; Kruse, L. I. *J. Org. Chem.* **1988**, 53, 417-420.

29. Gronowitz, S.; Zhang, Y.; Hörnfeldt, A.-B. *Acta Chem. Scand.* **1992**, 46, 654-660.

30. Xie, Y.; Ng, S.-C.; Hor, T. S. A.; Chan, H. S. O. *J. Chem. Research (S)* **1996**, 150-151.

31. Amb, C. M.; Rasmussen, S. C. *Eur. J. Org. Chem.* **2008**, *2008*, 801-804.

32. Konkol, K. L.; Rasmussen, S. C. *Organometallics* **2016**, *35*, 3234-3239.

33. Coulson, D. R. *Inorg. Synth.* **1971**, *13*, 121-124.

34. Atkins, P.; Overton, T.; Rourke, J.; Weller, M.; Armstrong, F. Shriver and Atkins' Inorganic Chemistry, 5th ed.; Oxford University Press: Oxford, U.K., 2010; pp 138-140.

35. Chelucci, G.; Baldino, S.; Ruiu, A. *J. Org. Chem.* **2012**, *77*, 9921-9925.

36. Rasmussen, S. C. *ChemTexts* **2015**, *1*, 10.1-10.9.

37. Diaz-Torres, R.; Alvarez, S. *Dalton Trans.* **2011**, *40*, 10742-17050.

38. Baker, D. R.; Clegg, W.; Horsburgh, L.; Mulvey, R. E. *Organometallics* **1994**, *13*, 4170-4172.

39. Barker, J.; Barnett, N. D. R.; Barr, D.; CIegg, W.;Muhey, R. E.; O'Neil, P. A. *Angew. Chem., Int. Ed. Engl.* **1993**, *32*, 1366-1368.

40. Shaw, B. L.; Stainbank, R. E. *J. Chem. Soc., Dalton Trans.* **1972**, 223-228.

41. Brunker, T. J.; Blank, N. F.; Moncarz, J. R.; Scriban, C.; Anderson, B. J.; Glueck, D. S.; Zakharov, L. N.;Golen, J. A.; Sommer, R. D.; Incarvito, C. D.; Rheingold, A. L. *Organometallics* **2005**, *24*, 2730-2746.

42. Barrios-Landeros, F.; Carrow, B. P.; Hartwig, J. F. *J. Am. Chem. Soc.* **2009**, *131*, 8141-8154.

43. Bellenghi, M.; Carrara, G.; Fava, F.; Ginoulhiac, E.; Martinuzzi, C.; Vecchi, A.; Weitnauer, G. *Gazz. Chim. Ital.* **1952**, *82*, 773-807.

44. Steinkopf, W.; Kohler, W. *Justus Liebigs Ann. Chem.* **1937**, *532*, 250-282.

45. Steinkopf, W.; Jacob, H.; Penz, H. *Justus Liebigs Ann. Chem.* **1934**, *512*, 136-164.

46. Xie, Y.; Ng, S. C.; Wu, B.-M.; Xue, F.; Mak, T. C. W.; Hor, T. S. A. *J. Organomet. Chem.* **1997**, *531*, 175-181.

47. Xie, Y.; Tan, G. K.; Yan, Y. K.; Vittal, J. J.; Ng, S. C.; Hor, T. S.A. *J. Chem. Soc., Dalton Trans.* **1999**, 773-779.

48. Antolini, L.; Goldoni, F.; Iarossi, D.; Mucci, A.; Schenetti, L. *J. Chem. Soc., Perkin Trans. 1* **1997**, 1957-1982.

CHAPTER 3. TUNING THE OPTICAL, ELECTRONIC, AND SOLUBILITY PROPERTIES OF METAL THIOPHENEDITHIOLENES

3.1. Introduction

Since their initial independent reports by Schrauzer[1] and Grey[2] in 1962, metal dithiolenes (MDs) have generated significant interest in the subsequent decades because of their rich electronic and magnetic attributes. Such attributes, coupled with their bulk solid-state packing abilities, have led to desirable material properties including metal conductivity and superconductivity, ferromagnetism, ambipolar charge transport, non-linear optical response, and catalytic water splitting.[3-13] Accordingly, they have been widely studied as building blocks for crystalline molecular materials. These complexes are often intensely colored and display numerous reversible electron transfer processes. Applications of MDs include conducting and magnetic materials, dyes, non-linear optical materials, catalysis, and electroactive substrates in olefin separation methods.

A metal dithiolene consists of a metal center coordinated to at least one bidentate thiolate ligand conjugated by a carbon-carbon double bond. Figure 3.1 illustrates some examples of MDs reported in the literature.[1,10,14,15] These complexes can exist as either homoleptic (all ligands are identical) or heteroleptic complexes with one to three dithiolate ligands complexing the central metal. The identity of the central transition metal varies widely, some of the most popular include Ni, Pt, Pd, Fe, Au, Co, and Cu. The geometry of the metal dithiolene is dependent on the central metal, and a diversity of metal dithiolene molecular geometries are possible including 4-coordinate tetrahedral and square-planar and 6-coordinate octahedral complexes.[3-13]

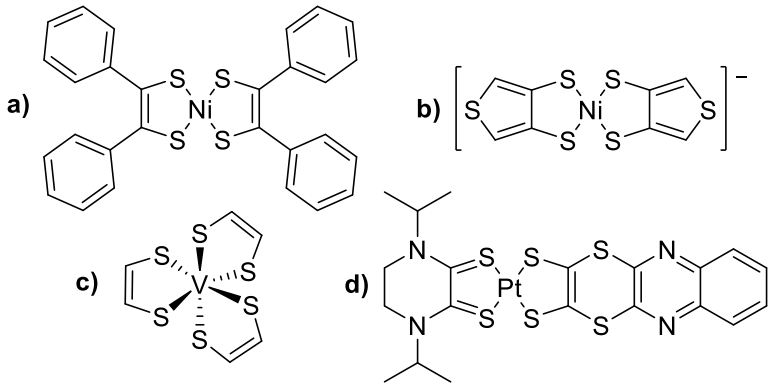

Figure 3.1. Representative examples including (a) the first reported literature example of a dithiolene,[1] (b) fused-ring anionic thiophene-dithiolene with fusion at the *c*-face,[10] (c) vanadium dithiolene with D_{3h} symmetry,[14] and (d) heteroleptic platinum dithiolene complex[15]

The broad interest in dithiolene complexes is partly related to the "non-innocent" character of the dithiolene ligands.[16,17]A ligand is innocent if it allows the unambiguous determination of the oxidation state of the central metal atom,[18] thus in the MD systems since there is a strong mixing of the ligand and metal contributions to the frontier orbitals, the ligand is an active partner in the reactivity and redox properties of the complex.[12] Figure 3.2 illustrates how the loss of an electron can occur either on the metal or the dithiolene ligand. In fact, the ligand is capable to bind a variety of metals as ene-1,2-ditholate dianion, as monoanion thioketone-radical resonance hybrid, and as neutral dithioketone.[13]

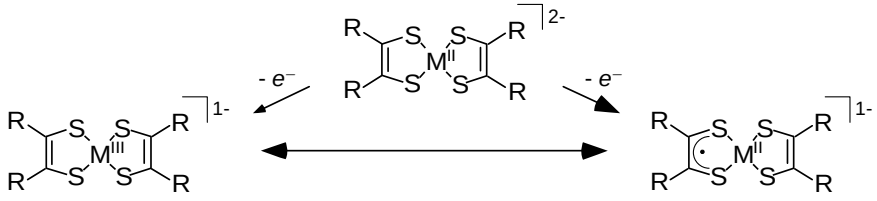

Figure 3.2. Potential oxidation of non-innocent dithiolene complexes

The stability of the neutral or charged dithiolene species, as a consequence of its redox properties, is greatly influenced by the choice and the substituents on the dithiolene ligands. A variety of air-stable cationic, anionic, and neutral complexes have been described in the

literature, as metal dithiolenes have been shown to exhibit one-, two-, and even three-reverseible one-electron redox processes that can be explained by Equation 3.1.[3-13,19,20]

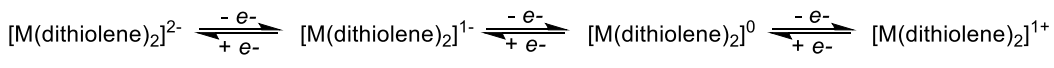

(Equation 3.1)

Of special interest are mononuclear anionic $[Y^+][M(dithiolene)_2]$ or neutral $M(dithiolene)_2$ [$Y = Bu_4N^+$, NMP^+; M = Ni, Pd, Pt, Au…] complexes that are of square-planar geometry, as these are particularly adapted to stacking, thus providing conductive materials.[6,12] Additionally, the ability to delocalize electrons from the metal to the ligands is one of the most desirable properties of metal dithiolenes, and this can be exploited by tuning the ligands similarly to other types of conjugated materials to afford varying optical and electronic properties. By fusing an aromatic ring to the dithiolene core, one can enhance the electron delocalization onto the rings via increased molecular planarity and enhanced orbital overlap, common themes in conjugated materials. Examples of fused-ring dithiolenes include benzene,[21,22] pyridine,[23] and thiophene,[24,25] among other heterocycles.[3-13]

In 2009, the Rasmussen group reported a π-extended nickel thiophene dithiolene that coupled a pendant aryl group to the 5-position of the thiophene ring,[26] with the possibility of combining the characteristics of metal dithiolenes and oligothiophenes in these materials. The regioselective cross-coupling developed by Amb and Rasmussen led to the thiophene-extended Ni(II) complex **3.4** as illustrated in Scheme 3.1,[27] and the first in a new family of π-extended metal dithiolenes.[28.29] The first step of the synthesis involves the palladium-catalyzed regioselective cross-coupling of 2,3,5-tribromothiophene to form the polybrominated species **3.2**, using the sterics of the bulky catalyst to encourage coupling at the less electronically favorable 2-position, similar chemistry of which was discussed previously (Chapter 2).

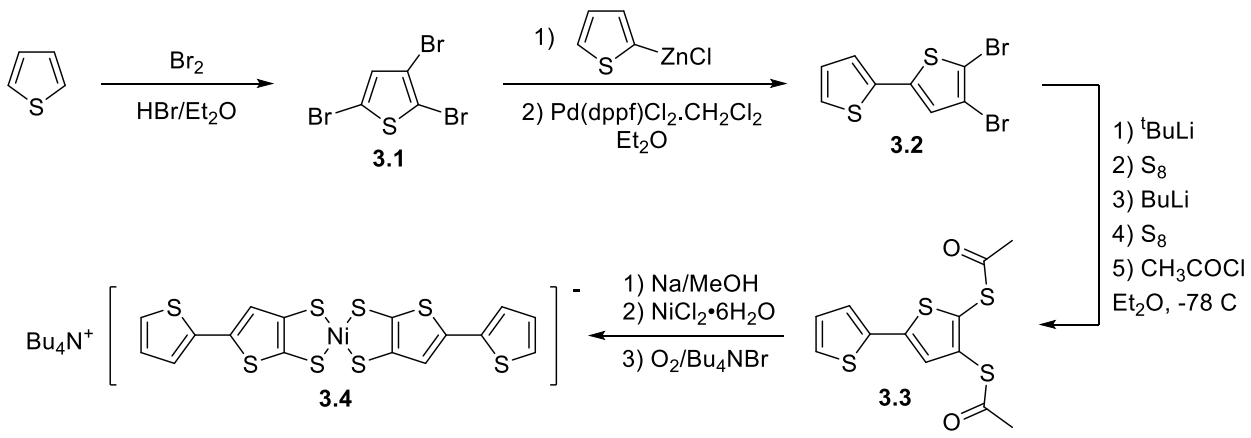

Scheme 3.1. Synthesis of π-extended nickel thiophenedithiolene[27]

The protected dithiolate **3.3** is then formed, with careful selection of reagent order to avoid halogen-dance.[30] Using sodium methoxide to remove the acetate groups, the disodium salt of the nickel complex is formed, and air oxidation resulted in the monosodium anion, which was finally precipitated as the salt **3.4** by the addition of the tetra-*N*-butylammonium bromide. The choice of counterion affects the solubility and intermolecular interactions of the resulting complex, with the alkyl cation assisting in solubilizing the complex in a variety of organic solvents. Other cations, in particular the planar aromatic cation *N*-methylpyridinium, can form materials with close-packing arrangements and semiconducting behavior in the metal dithiolenes.[27-29]

The optical properties of this species (**3.4**) included a strong absorbance in the near-infrared (NIR) region of the spectrum, which is assigned as an intervalence charge transfer (IVCT) band (Figure 3.3). As discussed earlier, the ligands of MDs are non-innocent and mixed-valent, meaning the oxidation state of each ligand is unclear.[16-18] The IVCT is an electron transition that involves electron transfer from one dithiolene ligand to another $[L\bullet\text{-}Ni^{II}\text{-}L]^{-} \rightarrow [L\text{-}Ni^{II}\text{-}L\bullet]^{-}$.

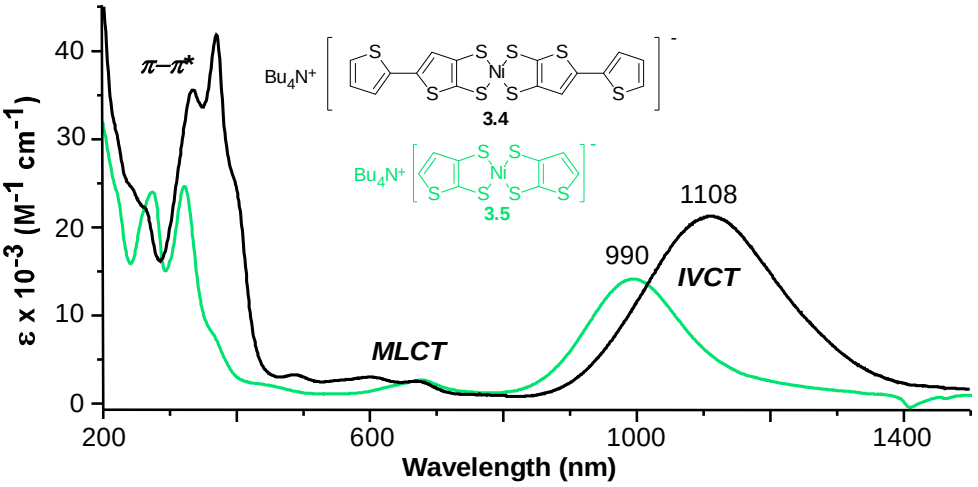

Figure 3.3. Absorption spectra of π-extended nickel thiophenedithiolene **3.4** and parent thiopehenedithiolene **3.5**

The singly occupied molecular orbital (SOMO) can play an important role in this charge transfer, whereby a paired electron is excited from the filled SOMO-1 energy level to the singly occupied SOMO, which results in an unpaired electron on the opposing ligand as shown in Figure 3.4. Therefore, the oxidation state of each ligand is instantaneously switched. The metal mediates communication between the dithiolene ligands, and thus the IVCT too. However, the coordinating metal contributes only to the SOMO, and not the SOMO-1. Therefore, the metal mediates the inter-ligand communication through the interruption of conjugation in the SOMO-1, which must be overcome by low-energy NIR radiation. The IVCT transition is thus distinct from a normal π→π* transition. Both the parent (**3.5**) and the π-extended (**3.4**) species exhibit this IVCT transition, along with higher energy π→π* transitions (Figure 3.2). As would be expected, as the conjugation path is extended, there is a red-shift in absorbance (bathochromic shift *ca.* 118 nm). The unique NIR absorption proved to be a more compelling material property to devote attention to than the magnetic properties that first attracted the Rasmussen group to these materials. Since such a low energy absorbance is unique among thiophene materials, the π-extended dithiolene unit has potential as a donor unit in donor-acceptor polymeric frameworks to

utilize a larger portion of the solar spectrum, valuable in photovoltaic applications. The characteristics of rich electrochemistry, good-solid state intermolecular contacts, and attainable semiconducting properties make thiophenedithiolenes attractive for materials applications.

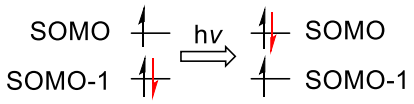

Figure 3.4. Interpretation of the IVCT transition upon photon absorption in $[Y^+][Ni(dithiolene)_2]$ complexes

Of special interest is the ability to tune the optical and electronic properties of these materials. The Rasmussen group has already reported how changing the π-extended aryl group (phenyl),[28] adding functionalizing groups (hexyloxy, bromine, acetyl),[28] and replacing the fused thiophene with the more electron deficient thiazole affects these properties,[29] but little effort has been put forth on considering the identity of the transition metal. The requirement to make planar dithiolenes is a transition metal that arranges the ligands in a square-planar geometry. Nickel(II), a d^8 transition metal, is often chosen because it is cost efficient and easy to work with, but there are other transition metals that can afford square-planar geometry (Pt(II), Pd(II), Au(III), Co(II) etc.). Characterization of how the properties of these π-extended thiophenedithiolenes change with changing transition metals could potentially be applied as general trends to the dithiolene class of materials as a whole and used in the selective tuning and design of these materials. Additionally, when examining this materials class, it was realized that the parent metal-dithiolenes (Figure 3.5) have been incompletely characterized.

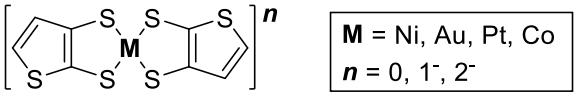

Figure 3.5. Representation of parent metal thiophenedithiolene with thiophene fused at the *b*-face

Table 3.1. Literature data for known parent metal thiophenedithiolenes with thiophene fused at the *b*-face

Entry	Metal	Charge (*n*)	λ_{max} (nm)[b]	ε (M^{-1} cm^{-1})	Reference
1	Ni	0	*nr*	*nr*	25
2	Ni	1-	672 989	*nr*	24,31[c]
4	Au	0	*nr*	*nr*	24,32
5	Au	1-	540 857	*nr*	24[c]
6	Pt	0	*nr*	*nr*	33
7	Pt	2-	990 1912	*nr*	33[c]
8	Co	0	*nr*	*nr*	33
9	Co	2-	581 795 1912	*nr*	33[c]

[a]*np* = not reported. [b]In CH_3CN. [c]Includes electrochemical data.

As seen in Table 3.1, all of the neutral species of Ni, Au, Pt, and Co have been reported, but because of solubility issues none of the optical or electrochemical properties of these species have been characterized, and at best crystal data is reported. The more processible monanionic (Ni, Au) and dianionic (Pt, Co) charged species report optical absorbances and electrochemical data, and sometimes the crystal structures, but no molar absorptivity values are provided, which makes direct comparison difficult. Of special interest is the complete characterization of Co and Pt dianionic species, in which an extremely low-energy transition is reported for both species (1912 nm).[33] Belo et. al reports that the Co and Pt complexes can only be obtained in the

dianionic state, as the monoanionic state is unstable, and can be easily oxidized to neutral insoluble material.[33] They based this on the instability of these species on their inability to get a crystal structure for the monoanions. On further examination of this, the authors actually report a similar transition for six completely different structures with absorbances within *ca.* 7 nm (1908-1915 nm) of each other, including the *b*- and *c*-face fused octahedral Cu(I) analogues. However, as this is the only absorption data provided in the literature for any of these species, full characterization would provide answers to this interesting observation.

Additionally, it is difficult to make direct comparisons between the monoanions and dianions, as the charge of the complex will affect the charge transfer transitions. Furthermore, the palladium thiophenedithiolene complex has never been reported, including either isomer of thiophene fused at the *b*-face or the *c*-face, although it feasibly should have square-planar geometry and be able to be synthesized in the dianionic, monoanionic and neutral forms. The complete family of the parent and π-extended square-planar metal thiophenedithiolenes with varying transition metals will be synthesized and characterized.

One of the possible applications of these species is incorporation into larger oligomeric or polymeric architectures, but solubility can sometimes be an issue. The solution-processible forms of the dithiolenes are in salt form, but it would be especially worthwhile to be able to utilize solution-processible neutral species.[3-13] Incorporation of additional solubilizing chains should hopefully overcome this issue. Overall, in the following sections the synthesis of new metal thiophenedithiolenes will be discussed, along with structural modifications to increase solubility and incorporation of these architectures into polymeric materials.

3.2. Transition Metal Substitution in Thiophenedithiolenes

3.2.1. Synthesis of π-extended metal thiophenedithiolenes

To produce a family of metal thiophene dithiolenes, the synthesis involved production of the protected dithiolate ligand **3.3** which was previously reported,[26] then complexation with the appropriate metal salt. Finally, depending on the desired oxidation state of the species, it was oxidized in the presence of an oxidizing agent (O_2 or I_2) and then the salt was formed by precipitating the species in the presence of a planar *N*-methylpyridine iodide or alkyl tetra-*N*-butylammonium bromide as the cation source. Usually, the NMP^+ cation was preferred for attempts to grow-single crystals for crystal structures, and Bu_4N^+ for general characterization testing. This is because the complexes pack in a planar close-packing arrangement with these π-extended species, as previously reported for the nickel analogue.[26] Scheme 3.2 illustrates this synthesis. The platinum monoanion **3.6** was synthesized in good yield, however it was found that air was not a strong enough oxidant so a 1 mol of I_2 was mixed with the complex, and finally a color change was observed to form dark green crystals. Since the gold source, $KAuCl_4$ is already Au(III), no oxidation of the final complex was needed to produce the monoanion **3.7**. The palladium salt **3.8** was formed similar to the platinum, however the material itself seemed quite insoluble in comparison to other dithiolene analogues, and this species also exhibited interesting optical and electronic properties that will be discussed later. Additionally, the HRMS of this species showed a repeating fragment of increasing molecular weight, which appeared like a polymeric species fragmenting into increasingly smaller fragments. For this reason, the structure of **3.8** is tentatively assigned right now. Cobalt(II), a d^7 transition metal, has demonstrated square-planar geometry in metallic complexes.[34] Both the monoanion and dianion were synthesized, in an attempt to compare to properties to known dianion complexes (Table 3.1).

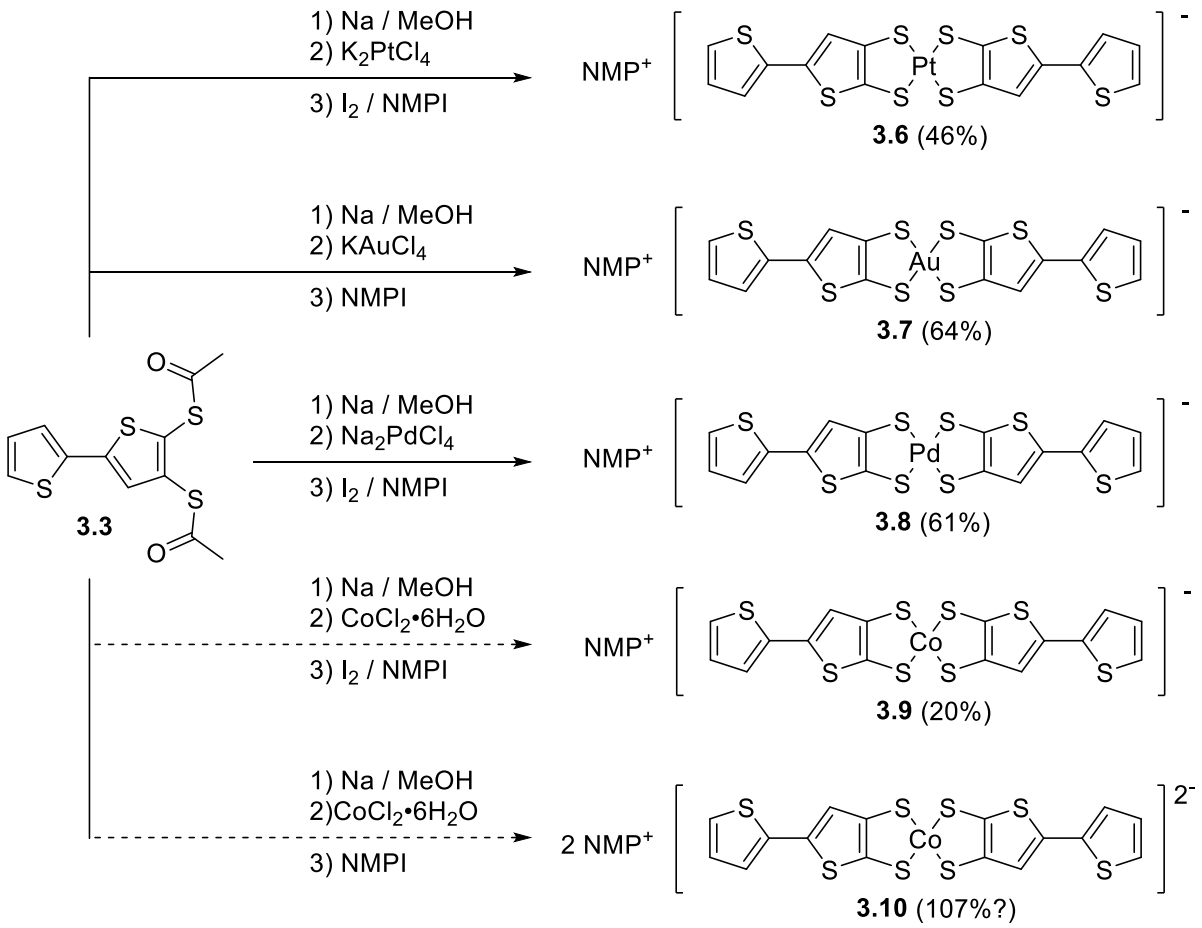

Scheme 3.2. Synthesis of π-extended metal thiophenedithiolenes

Based on initial color-change observations, it was concluded the monoanion was easily formed, however part of the issue with dianion formation seemed to be that it was partially oxidizing during the workup, from O_2 in the air. Additionally, a higher than 100% yield (*ca.* 107%) was calculated for the dianion **3.10**, so it was concluded that **3.10** was probably a mixture of **3.9** and **3.10**, and therefore impure.

The parent thiophenedithiolenes **3.12-3.16** were synthesized in an essentially identical manner to their π-extended analogues, just substituting the protected thiolate ligand **3.11**, which was prepared according to published literature procedures.[24,35,36] Yields for the Pt, Au, and Pd species are all good (47-76%). Again, the monoanionic Co species **3.15** had a lower yield (15%)

for the parent species, just like its π-extended analogue **3.9** (20%). Observationally, it seemed like the Co species didn't form a precipitate as easily as the other analogues. Additionally, it was concluded that the parent dianionic Co complex **3.16** was probably at least partially a mixture of the Co(2-) and Co(1-) species, or maybe even some neutral species too, both by colorimetric observations and high calculated yield. However, elemental analysis will need to be performed to confirm this conclusion.

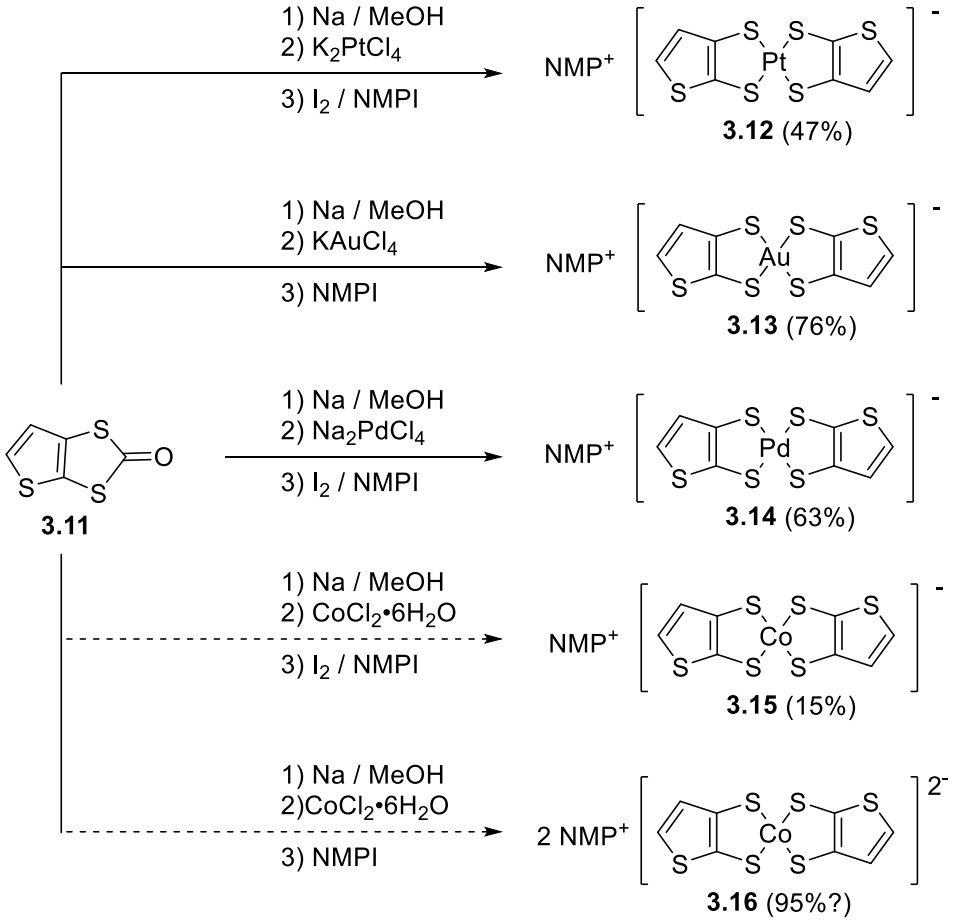

Scheme 3.3. Synthesis of parent protected ligand

3.2.2. Optical properties of metal thiophenedithiolenes

Absorption spectra for compounds **3.6-3.9** and **3.12-3.15** were obtained and the observed λ_{max}, assigned transitions, and collected ε data are tabulated in Table 3.2.

Table 3.2. Absorption data for metal thiophenedithiolenes **3.6-3.9** and **3.12-3.15**[a]

Compound	Metal	λ_{max} (nm)	Assigned transition	ε (M^{-1} cm^{-1})
3.6	Pt	232	π→π*	28000
		353	π→π*	17000
		1104	IVCT	11000
3.7	Au	254	π→π*	47000
		303	π→π*	50000
		389	π→π*	34000
		~1100	d-d?	<100
3.8	Pd	258	π→π*	19000
		308	π→π*	19000
		361	π→π*	17000
		1407	IVCT	7100
3.9	Co	250	π→π*	
		351	π→π*	
		454	π→π*?	
			No IVCT	
3.12	Pt	232	π→π*	
		982	IVCT	
3.13	Au	254	π→π*	67000
		293	π→π*	36000
			d-d?	
3.14	Pd	247	π→π*	
		302	π→π*	
		506	LMCT	
3.15	Co	245	π→π*	
		497	LMCT	

[a]In CH_3CN.

Representative spectrums for the π-extended thiophenedithiolenes are illustrated in Figure 3.6. The π-extended monanionic platinum species **3.6** exhibits two high energy π→π* transitions, and a lower energy transition assigned as an IVCT, the result of an electron transfer from one radical dithiolene ligand to another (which could also be described as electronic transition form an electron-rich site to an electron-deficient site). Additionally, **3.6** shows vibrational shoulders in the IVCT transition (Figure 3.6), a result of electronic transitions between the different vibrational energy levels possible for each electronic state.

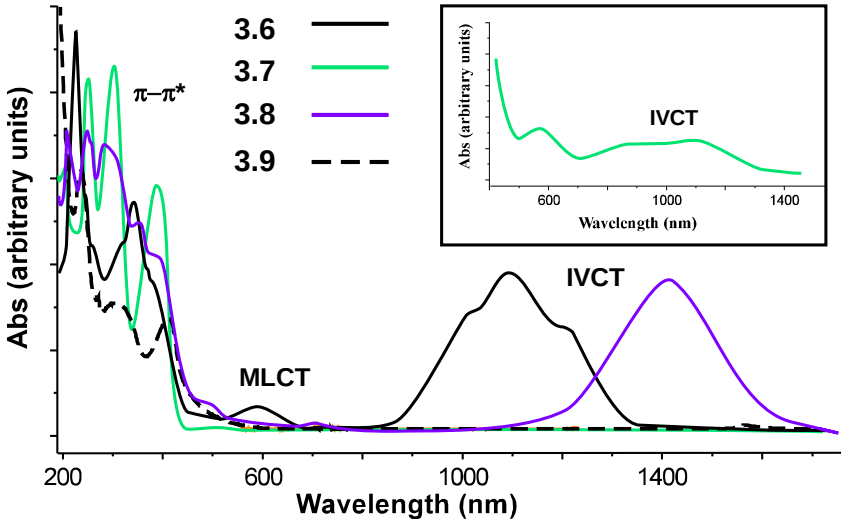

Figure 3.6. UV-vis-NIR spectra for π-extended metal thiophenedithiolenes **3.6**-**3.9**

The presence of this IVCT transition provides confidence that species **3.6** is indeed the monoanion. This is because with oxidation from the dianion to the monoanion, the complex loses an electron, potentially on the ligand. Although because of the "non-innocent" character of the dithiolene ligands, it is impossible to definitively say if this loss occurs on the ligand or the central metal. However, if no oxidation occurred, there would likely be no or minimal oxidation of the dithiolene ligand, which means that no IVCT transition would be observed. Instead of excitation being between a partially filled SOMO and SOMO-1, the MO would be a fully filled HOMO, which could then excite an electron to the LUMO in a CT transition. The act of

oxidizing the complex, which occurs for all species but Au(1-) **3.7** and Co(2-) **3.10**, in a respect 'primes' the species for IVCT. Figure 3.7 attempts to illustrate this situation, and Table 3.3 lists the expected ligand/metal charge distributions and observed transitions. The information in Table 3.3 was correlated from observed literature transitions for dithiolene species. However, if the dithiolene species was fully oxidized to the neutral form, an IVCT transition would still expect to be observed as there would be a transition from one radical oxidized ligand to another (Figure 3.8). Additionally, because neutral species would be uncharged, it would quite likely be insoluble, which would make it difficult to characterize and of limited use.

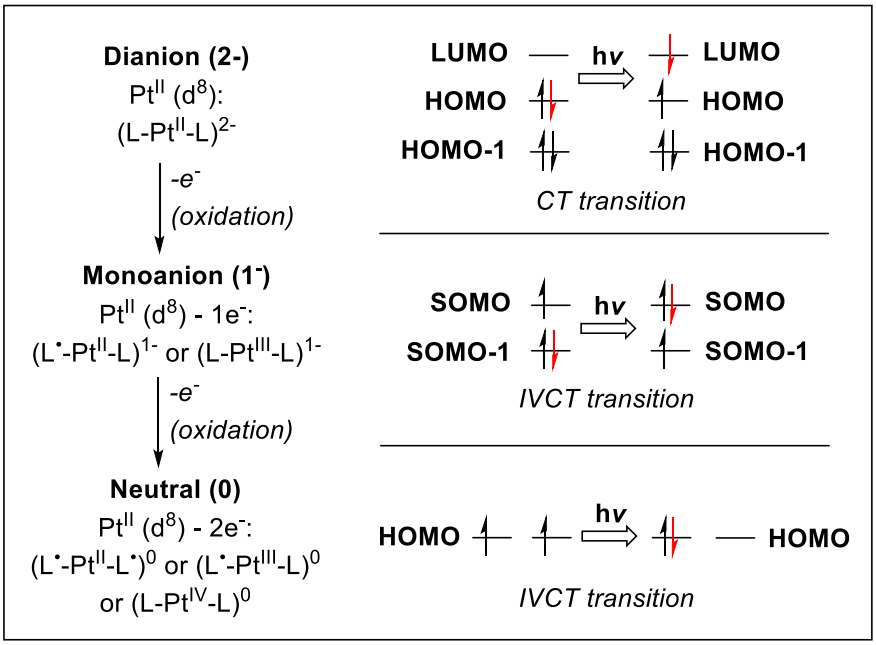

Figure 3.7. Oxidation of dianion to monoanion in Pt complex, and appearance of IVCT

The gold complex **3.7** exhibits several high energy π→π* transitions. As the Au(III) naturally forms the monoanion, it would be d^8 and anticipated to have a filled HOMO. However, at high concentrations a very faint transition is observed (inset, Figure 3.6). This is most likely the result of disfavored d→d transitions, as the monoanionic gold species would not be expected to exhibit an IVCT.[39]

Table 3.3. Expected charge arrangement and anticipated visible transitions for the dianionic, monoanionic, and neutral species

Metal	dianion	monoanion	neutral
nickel[13]	$[L\text{-}Ni^{II}\text{-}L]^{2-}$	$[L\bullet\text{-}Ni^{II}\text{-}L]^{1-}$	$[L\bullet\text{-}Ni^{II}\text{-}L\bullet]^{0}$
	No IVCT	*IVCT*	*IVCT*
platinum[13]	$[L\text{-}Pt^{II}\text{-}L]^{2-}$	$[L\bullet\text{-}Pt^{II}\text{-}L]^{1-}$	$[L\bullet\text{-}Pt^{II}\text{-}L\bullet]^{0}$
	No IVCT	*IVCT*	*IVCT*
palladium[13]	$[L\text{-}Pd^{II}\text{-}L]^{2-}$	$[L\bullet\text{-}Pd^{II}\text{-}L]^{1-}$	$[L\bullet\text{-}Pd^{II}\text{-}L\bullet]^{0}$
	No IVCT	*IVCT*	*IVCT*
gold[39]		$[L\bullet\text{-}Au^{III}\text{-}L]^{1-}$	$[L\bullet\text{-}Au^{III}\text{-}L\bullet]^{0}$
		No IVCT (d-d)	*IVCT*
cobalt	d^7	d^7	d^7
	$[L\text{-}Co^{II}\text{-}L]^{2-}$	$[L\bullet\text{-}Co^{II}\text{-}L]^{1-}$	$[L\bullet\text{-}Co^{II}\text{-}L\bullet]^{0}$
	paramagnetic	*diamagnetic*	*paramagnetic*
	No IVCT	*IVCT*	*IVCT*

The palladium species **3.8** would be expected to exhibit similar absorption properties as the nickel and platinum dithiolene species because they are in the same group in the periodic table. However, species **3.8** shows a significant red-shift to lower energy from the palladium and nickel complexes (*ca.* ~300 nm). There are a couple of reasons why such a red shift is observed. First, there is something occurring in the palladium species that causes such an abrupt shift, although this is not yet understood. The other option is that the proposed structure **3.8** in Scheme 3.2 is not the actual species synthesized. Usually such a shift in absorption would be attributed to an increase in conjugation, at least in organic materials. Coupled with the fact that there was evidence of multiple fragmented species in the HRMS, maybe some sort of dimerization/coupling occurred in the synthesis. A search of the literature of known similar palladium dithiolenes provided no insight into this unexpected optical property.

The cobalt complex **3.9** showed high energy π→π* transitions, and no NIR absorption in the spectrum. When a high concentration spectrum was taken for the cobalt species, no obvious IVCT/d→d transitions were observed. The question is whether one would actually expect to observe a strong NIR IVCT transition for the Co(1-)/Co(0) species. Because unlike the Ni(II)/Pt(II)/Pd(II), the cobalt is a d^7 and the monoanion would be paramagnetic already. By the previous stated reasoning, the cobalt(1-)/neutral species should show some IVCT character because oxidation does form the radical ligand. However, no NIR absorption is observed (Figure 3.6), which supports that the soluble portion of **3.9** is the cobalt(2-) species **3.10**.

For the known literature parent compound data (Table 3.1), the authors did state that the parent cobalt(1-) species was unstable and unable to be isolated.[33] Maybe this species was partially oxidized during the workup but instead prefers the dianionic state. Additionally, the lowest energy absorption for **3.9** (λ_{max} = 454 nm) seems a little red-shifted and of weaker intensity than a π→π* transition, so possibly this is a MLCT transition.

The parent dithiolene species **3.12-3.15** exhibit very similar trends to the π-extended species discussed above, representative spectrums of which are shown in Figure 3.8.
The platinum species **3.12** exhibits a strong IVCT transition in the NIR, blue-shifted (*ca.* 122 nm) form the π-extended species **3.6**, a result of less conjugation over the backbone. This is similar to the nickel species previously reported.[27] The gold species **3.13** again shows a faint d→d transition at high concentrations, like the π-extended. In place of a strong NIR absorption the parent palladium species **3.14** exhibits a blue-shift in the lowest energy absorbance (*ca.* 476 nm) from the platinum species, which is assigned as a LMCT. HRMS supports the isolation of proposed structure **3.14** (Scheme 3.3), but since no crystal structure was able to be obtained and elemental analysis has not yet been performed on these species, it is difficult to definitively

confirm its structure. Another possibility is that like the cobalt, the parent palladium species is actually the Pd(2-) species, and the monoanion is unstable. This would follow the anticipated optical trends in Table 3.3, where no NIR absorption is observed. However, investigation is still needed to determine why the parent palladium complex shows such different optical properties to both its π-extended analogue and other parent dithiolenes. The cobalt species **3.15** shows similar optical properties to **3.14**, in which they both exhibit a lowest-energy LMCT transition. Additionally, the parent cobalt species **3.15** matches the π-extended cobalt species **3.9** in that neither exhibits a NIR transition, which provides support that the characterized species **3.9**/**3.15** are the dianions **3.10**/**3.16**.

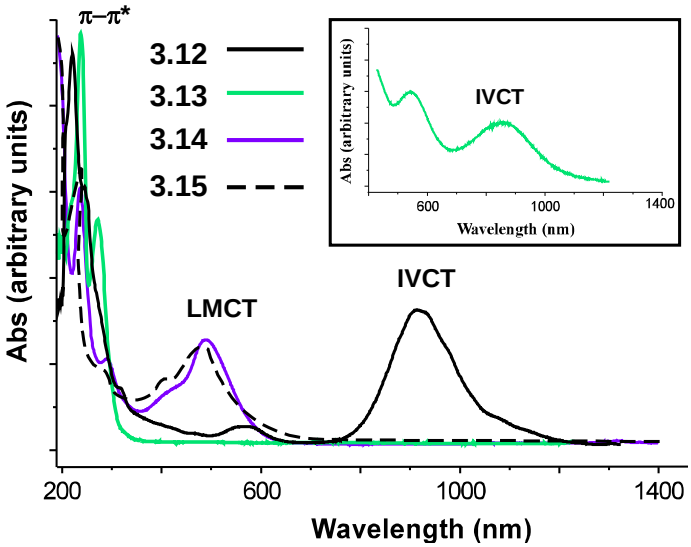

Figure 3.8. UV-vis-NIR spectra for parent metal thiophenedithiolenes **3.12-3.15**

Finally, since some optical properties of the parent dithiolene species have already been reported (Table 3.1), a few comparisons can be made. Absorptions from the literature for gold monoanion **3.13** (550, 857 nm)[24] match well for the very faint d→d transitions observed in Figure 3.7. Only the dianionic species for platinum (990, 1912 nm) and cobalt (581, 795, 1912 nm) are reported.[33] The observed absorbance for the platinum species **3.12** matches well with the

reported absorbance (difference *ca.* 8 nm). The reported literature absorbances for cobalt do not match the observations that no NIR absorbance exists for **3.15**,[33] although maybe the authors are instead observing a faint d→d that we did not experimentally observe. It is possible that the cobalt solution was still not concentrated enough to observe the absorbance, or that in the correct anionic state the intensity of this transition would be higher. Since no molar absorptivity data is given, it is hard to make a definitive conclusion. Finally, regarding the absorptions reported at 1912 nm,[33] it would be fair to say that these are suspect. This could potentially be an effect of poor background subtraction by the instrument, as the solvent acetonitrile does exhibit an intense absorbance at ~1910 nm.

3.2.3. Electrochemical properties of metal thiophenedithiolenes

Cyclic voltammetry was performed for all synthesized species, to characterize the electronic properties. Table 3.4 tabulates the collected data for the π-extended metal thiophenedithiolenes **3.6-3.9** and includes the previously reported nickel species **3.4** for comparison.[26] The nickel, gold and palladium species exhibit a quasi-reversible couple near -1 V, assigned to the 2-/1- redox states.

Table 3.4. Electrochemical data for π-extended metal thiophenedithiolenes **3.6-3.9**[a]

compound	$E_{1/2}^{2-/1-}$ (V)	ΔE (mV)	$E_{1/2}^{1-/0}$ (V)	ΔE (mV)	$E_{pa}^{0/n+}$ (mV)
3.4	-1.00	70	-0.27	60	700
3.6	-1.38	150	-0.35	210	730
3.7	-1.67	260	-0.47[b]	910	900
3.8	-1.29	190	-0.74	230	990
3.9	-1.72	140	-0.26	90	860

[a]All potentials versus Fc/Fc^+ in 0.1 M $TBAPF_6$ in DMF. [b]Potentially irreversible.

The platinum and cobalt species exhibit two quasi-reversible couples near -1 to -1.7 V, assigned to the 2-/1- redox state and potentially the 3-/2- redox state. Or, since these species can also form cations in the redox process, it would be more correct to say that the three quasi-reversible couples observed for the Pt and Co are instead the 2-/1-, 1-/0, and 0/1+ redox states, as it does seem improbable that one could reduce the platinum species beyond the dianion. Figure 3.9 shows the cyclic voltammogram (CV) for the π-extended platinum species **3.6**. In comparison to the parent species **3.12-3.15** (Table 3.4), the π-extended species also exhibit an additional peak at high potential that is attributed to the oxidation of the peripheral thiophenes that are not present in the parent species ($E_{pa}^{0/n+}$). This oxidation increases on the order of Ni < Pt < Co < Au < Pd, but all values are within 290 mV of each other.

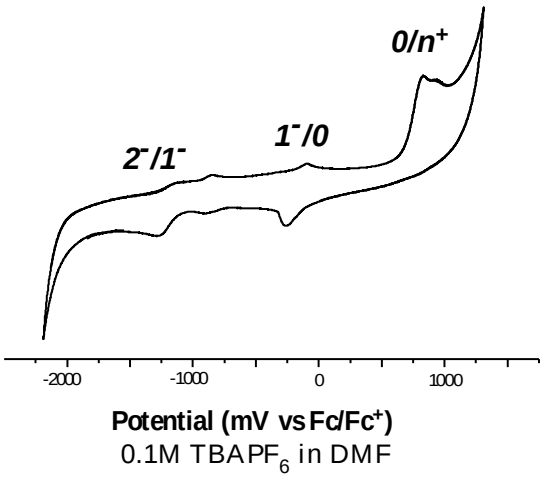

Figure 3.9. Representative example of CV of π-extended platinum complex **3.6**

There are two couples observed for the parent species (Table 3.5), which are assigned to the 2-/1- and 1-/0 redox states. For most, this correlates to a 2-/1- couple around -1 V and a 1-/0 couple around -0.2 V. The parent gold species **3.13** is significantly easier to reduce, with a 2-/1- couple at $E_{1/2}$ = -0.51 V and the 1-/0 couple a positive 0.10 V, a shift of ca. +0.60-0.30 V from the nickel, platinum, and cobalt species.

Table 3.5. Electrochemical data for parent metal thiophenedithiolenes **3.12-3.15**[a]

compound	$E_{1/2}^{2-/1-}$ (V)	ΔE (mV)	$E_{1/2}^{1-/0}$ (V)	ΔE (mV)
3.5	-1.10	70	-0.21	80
3.12	-1.03	50	-0.22	130
3.13	-0.51	220	0.10	160
3.14	-1.76	80	-1.38	260
3.15	-1.37	170	-0.14	420[b]

[a]All potentials versus Fc/Fc^+ in 0.1 M $TBAPF_6$ in DMF. [b]Potentially irreversible.

The CV of **3.13** is shown in Figure 3.10. The parent palladium species **3.14** is much harder to reduce, with shift of ~ -1 V for both the 2-/1- and 1-/0 couples. The choice of metal does affect the energy for both the π-extended and parent complexes, which offers opportunities to tune the electronics at a molecular level.

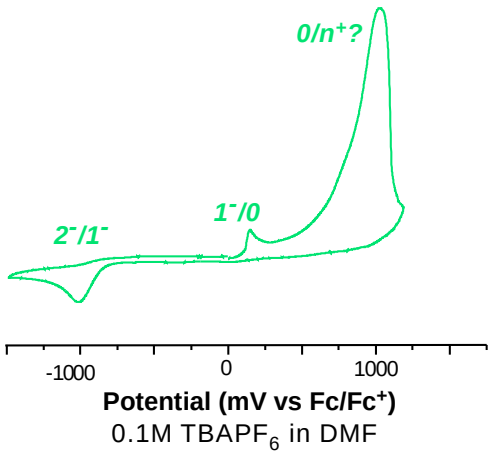

Figure 3.10. Representative example of CV of parent gold complex **3.13**

3.2.4. Other characterization of metal thiophenedithiolenes

Attempts to grow single crystals for x-ray crystallography unsuccessful for all species **3.6-3.9** and **3.12-3.15**. This is disappointing because it would potentially answer some of the questions that persist about the palladium and cobalt species. However, crystal structures have

been reported for many parent and π-extended analogues.[24,25,32,33] This supports that all the parent dithiolenes are square-planar (n = 0, 1-, 2-) and so are the nickel π-extended analogue[26] and other nickel π-extended nickel dithiolenes reported by the Rasmussen group.[28,29]

One common characterization technique for metal dithiolenes is spectroelectrochemistry, where optical absorbances are recorded while the species is held at oxidizing and reducing potentials.[37,38] However, there were instrumentation limitations that prevented this from being successful. It would be expected that as the monoanion is reduced to the dianion, the IVCT transition should disappear. The reverse has been observed for a dianionic nickel dithiolene bearing two terthiophene ligands: as the species is oxidized (0 to +800 mV), an absorbance appears (*ca.* 914 nm) that correlates to the IVCT transition. Additionally, the higher energy portion of the spectrum changes profile with the disappearance of some peaks and appearance of new ones (*ca.* 404-527 nm).[38]

3.2.5. Reevaluation of metal thiophenedithiolenes assignments

Both the parent and the π-extended platinum species showed good agreement in trends, and the optical properties (e.g. presence of IVCT transition) support a monoanionic Pt(1-) assignment for the complexes. The optical and electronic properties of the gold species support that Au(1-) complexes were synthesized, with a weak d→d transition in place of an IVCT. The lack of an IVCT for the supposedly monoanionic cobalt species is concerning. Taking into consideration the synthetic color observations, the optical properties, and the electronic characterization, it would be more correct to say that the synthesized species is likely in majority the Co(2-) dianionic species (or even potentially the neutral, Co(0), which could correlate the general insolubility issues with this complex), with some Co(1-) complex present. For the palladium species, the parent optical properties show more support towards a Pd(2-) assignment.

More characterization is needed to make a definitive conclusion (e.g. elemental analysis, crystal structure). The π-extended palladium species shows an interesting extreme red-shift in the optical properties, which could indicate some sort of conjugation extension, although it does support some sort Pd(1-) π-extended species. In summation, the optical and electronic properties of this family of metal thiophenedithiolenes were successfully tuned by variation of the core metal.

3.3. Creating More Soluble Thiophenedithiolenes

3.3.1. More soluble counterions

One of the greater challenges with metal dithiolenes is the solubility of the materials. Oftentimes, the salt is what provides solubility in solution, but this is not possible for neutral metal dithiolenes, which are often observed to be insoluble species that once formed have little application.[3-13,33] Additionally, even the choice of counterion can affect the solubility of the salts. For example, oftentimes the planar *N*-methylpyridinium species is selected, because it tends to crystallize well in the solid state. But it also participates in π-stacking in the solid state.[26] This intermolecular interaction seems to also influence the solution state properties, with a general observational trend in solubility to be that bulkier counterions tend to break up these interactions and make more soluble complexes. Species **3.17** was synthesized using the asymmetric bulky counterion source trioctylammonium bromide (Figure 3.11), using the synthetic methodologies illustrated in Scheme 3.1.

Qualitatively, solubility increases as the size of the counterion increases ($CH_3(C_8H_{17})N^+$ > Bu_4N^+ > Et_4N^+ > NMP^+). Table 3.6 lists some general solubility observations for nickel thiophene dithiolene species analogous to **3.17**. Dithiolenes tend to be soluble in solvents of intermediate polarity, and insoluble/mostly insoluble in non-polar/less polar (e.g. hexanes, Et_2O) and highly polar (e.g. water) solvents.

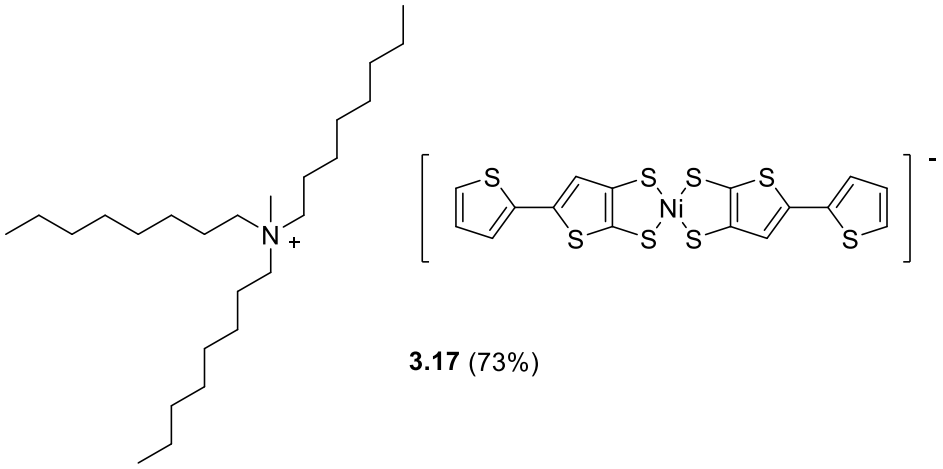

3.17 (73%)

Figure 3.11. More soluble dithiolene complex **3.17** with bulky methyl trioctylammonium cation

Table 3.6. Solubility of π-extended nickel complexes based on cation

Cation	Solubility
NMP$^+$	acetone. DMF, CH_3CN, CH_2Cl_2, $CHCl_3$
Bu_4N^+	acetone. DMF, CH_3CN, CH_2Cl_2, $CHCl_3$
Et_4N^+	acetone. DMF, CH_3CN, CH_2Cl_2, $CHCl_3$
$CH_3(C_8H_{17})N^+$	CH_2Cl_2 - 8 mg/mL $CHCl_3$ – 11 mg/mL chlorobenzene – 9 mg/mL

3.3.2. Addition of solubilizing chains

The neutral nickel thiophenedithiolene parent (analogue to **3.5**) and π-extended (analogue to **3.4/3.17**) were synthesized, but proved to be completely insoluble, which is not unexpected. In an effort to overcome issues of solubility in both the charged and neutral species, it was hypothesized that incorporating alkyl chains onto the pendant thiophene unit should increase solubility (in less polar solvents), similar to organic conjugated materials. Thus, the ligands would have to be redesigned beginning with thiophene, as efforts to affix functionalizing groups to the thiolate protected species **3.3** would in most cases prematurely affect the protecting acetyl

groups. Initial efforts involved the formation of 2-bromo-3-alkylthiophenes **3.19** (Scheme 3.4). However, all efforts to utilize the bulky palladium catalyst to mediate stereoselective Negishi cross-coupling to form **3.20** proved unsuccessful. This is likely because of the alkyl chain hinders the aryl zinc chloride sufficiently that it is unable to undergo transmetallation with the also sterically hindered palladium catalytic species. Shortening the alkyl chain from decyl to hexyl also proved unsuccessful.

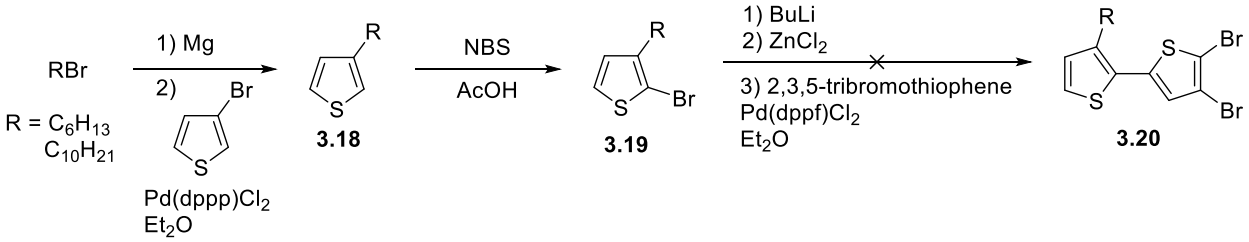

Scheme 3.4. Attempted synthesis of alkylated polybromothiophene **3.20**

Thereafter, instead of functionalizing the 3-position, the unencumbered α-position on the pendant thiophene ring was functionalized with a decyl chain **3.21** (Scheme 3.5). This should provide increased solubility to the charged complexes but removes any possibility of extending the conjugation path or even polymerizing these species. Following already developed chemistry earlier reported by the Rasmussen group,[26,27] the thiolate-protected decyl species **3.23** was synthesized. Efforts to form the monoanionic nickel species **3.24** seemed to have failed, as the resulting material was insoluble in CH_3CN (which seemed counterintuitive from the above reasoning) and possibly the neutral species. However, the formation of **3.24** was not extensively investigated, with only three reactions attempted, and future investigations might be able to solve this issue.

The final synthetic modification attempted was to affix two alkyl chains on each pendant thiophene, with the reasoning being that more solubilizing chains should increase the overall solubility (Scheme 3.6).

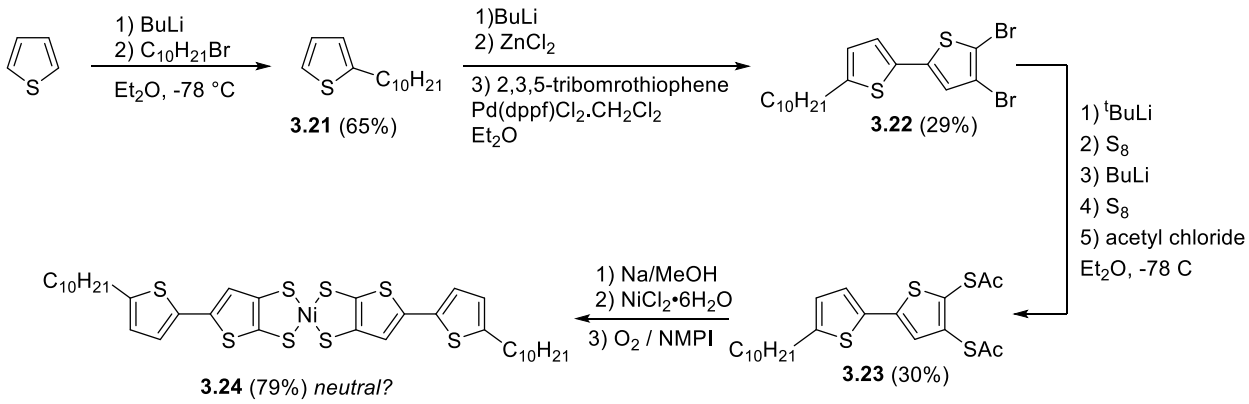

Scheme 3.5. Synthesis of the decyl-functionalized thiophenedithiolenes **3.24**

To form the 2,3-didecylthiophene **3.26**, a Grignard reaction was performed using 2-bromo-3-decylthiophene **3.25**. Attempts to directly form **3.26** from 2,3-dibromothiophene proved unsuccessful via Grignard reaction, and the only successful way to form **3.26** was found to be the successive alkylation of 3-bromothiophene to form 3-decylthiophene, followed by bromination of alkylated thiophene (**3.25**) and alkylation of brominated thiophene (**3.26**). Species **3.26** was then successfully cross-coupled with 2,3,5-tribromothiophene to form **3.28** in 22% yield. However, the thiolate-protected species **3.29** was unrealized. Again, there is room for improvement in this synthesis (e.g. yield of **3.28**, formation of **3.29**) and future investigations might be able to overcome some of the synthetic issues.

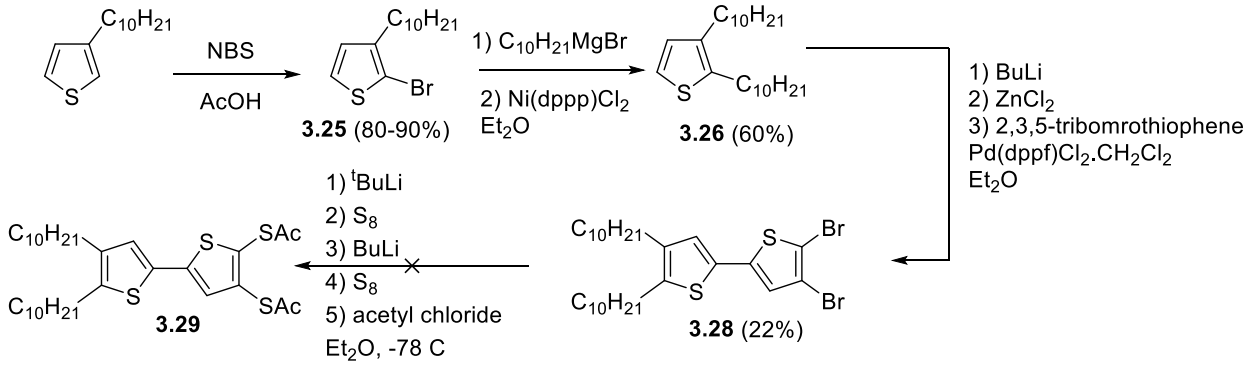

Scheme 3.6. Attempted synthesis of protected thiolate **3.29**

3.4. Polymerization of Thiophenedithiolenes

3.4.1. Synthesis of polymers

In 2009, Amb and Rasmussen reported the homopolymerization of π-extended nickel thiophenedithiolene via electropolymerization of the film. To make more processible materials, brominated nickel dithiolenes (**3.31, 3.33**) were co-polymerized with the boroester of the dioctylfluorene monomer (**3.30**)[40] via Suzuki cross-coupling (Scheme 3.7). Fluorene was chosen because it has two solubilizing chains, in the hope that this would afford enough solubility to the materials. However, the formed materials were essentially completely insoluble, with precipitation during the polymerization reactions visible within 24 h.

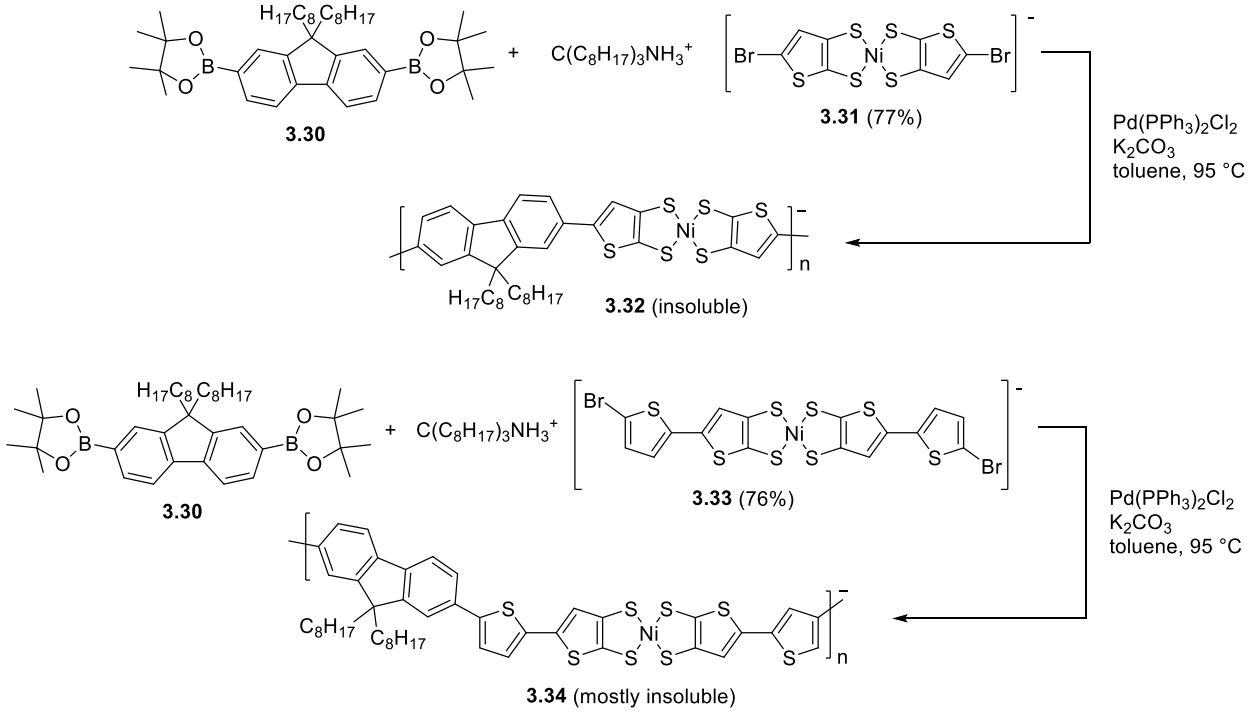

Scheme 3.7. Co-polymerizations of brominated dithiolenes and dioctylfluorene via Suzuki cross-coupling

Although no molecular weight data was collected for these insoluble species, a small amount of the chloroform fraction from the Soxhlet of **3.34** was soluble, and the absorption data is shown in Figure 3.12. The insoluble portion of the polymer was likely higher molecular

weight material. There appears to be a very slight red-shift in the IVCT and a broadening of the region, both indications of polymerization occurring. However, for these metal thiophenedithiolene species to be successfully incorporated into polymeric materials, the solution processability issues need to be overcome.

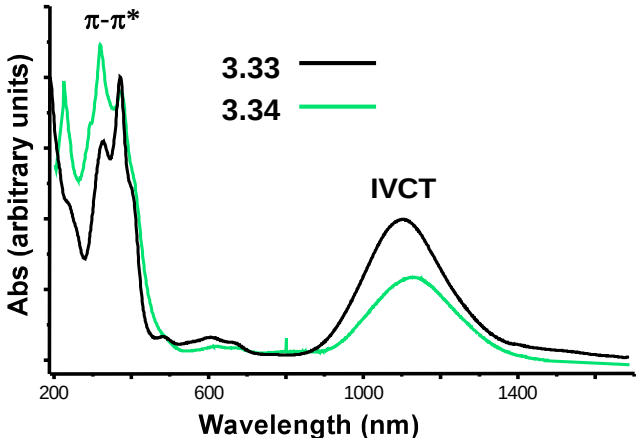

Figure 3.12. Absorption spectrum of copolymer **3.34** compared to monomer **3.33**

3.5. Conclusions

The characterization and tuning of optical and electronic properties of these species proved enlightening, which should assist with current efforts to incorporate metal dithiolenes in NIR photodetectors. Some understanding was gained in tuning the properties by varying the transition metal, but the issues of the palladium and cobalt species need to still be resolved. The incorporation of a bulky asymmetric counterion was found to be quite successful in solving many solubility issues, but true soluble, neutral species have not yet been realized, which would be a necessary benchmark for incorporation of these materials into device applications.

3.6. Experimental Methods

3.6.1. General Methods

Unless otherwise specified, all reactions were carried out under a nitrogen atmosphere with reagent-grade materials. Thieno[2,3-*d*]-1,3-dithiol-2-one (**3.11**),[24,35,36] brominated nickel

thiophenedithiolenes (**3.31, 3.33**),[28] and 9,9-diocyl-2,7- bis(4,4',5,5'-tetramethyl-1,3,2-dioxaborolan-2-yl)-9*H*-fluorene[44] were prepared by published methods. Toluene was distilled from sodium/benzophenone prior to use. Methanol (MeOH) was degassed by freeze−pump−thaw cycles and then backfilled with nitrogen gas. Acetonitrile was distilled over CaH_2 prior to use. DMF was dried over $MgSO_4$, filtered through silica gel, and stored over molecular sieves after bubbling with N_2 to degas. Chromatographic separations were performed using standard column methods with silica gel (230−400 mesh). Electrochemical measurements were performed on a Bioanalytical Systems BAS 100B/W instrument in various solvents using a platinum disk working electrode, a platinum wire counter electrode, and an Ag/Ag^+ reference electrode calibrated to the Fc/Fc^+ redox couple. UV−vis−NIR spectroscopy measurements were taken on a dual-beam-scanning Cary 500 UV−vis−NIR spectrophotometer in matched 1 cm quartz cuvettes.

3.6.2 Synthesis

_N_-methylpyridinium bis(5-(2-thienyl)-2,3-thiophenedithiolato)platinate(1-) (3.6)

Compound **3.3** (0.10 g, 0.32 mmol) was added to a solution of sodium (2.0 g) in 50 mL degassed MeOH and stirred for 1 h, resulting in a clear solution. In a separate flask, K_2PtCl_4 (0.066 g, 0.16 mmol) was added to ~3 mL nitrogen-sparged H_2O, which was then added dropwise to the solution at rt, immediately forming orange solution. The solution was stirred 3 h, filtered, oxidized with I_2, and then *N*-methylpyridinium iodide (0.21 g, 0.96 mmol) was added to form a green precipitate. The solid was filtered and washed with MeOH, H_2O, and Et_2O. Product was recrystallized from CH_3CN to give 55 mg (46%) of a dark green crystalline solid.

_N_-methylpyridinium bis(5-(2-thienyl)-2,3-thiophenedithiolato)aurate(1-) (3.7)

Compound **3.3** (0.10 g, 0.32 mmol) was added to a solution of sodium (2.0 g) in 50 mL degassed MeOH and stirred for 1 h, resulting in a clear solution. In a separate flask, $KAuCl_4$ (0.060 g, 0.16

mmol) was added to ~3 mL nitrogen-sparged H_2O, which was then added dropwise to the solution at rt, immediately forming green solution. The solution was stirred 2 h, filtered, and then *N*-methylpyridinium iodide (0.21 g, 0.96 mmol) was added to form a purple-brown precipitate. The solid was filtered and washed with MeOH, H_2O, and Et_2O. Product was recrystallized from CH_3CN to give 77 mg (64%) of a brown crystalline solid.

***N*-methylpyridinium bis(5-(2-thienyl)-2,3-thiophenedithiolato)palladate(1-) (3.8)**

Compound **3.3** (0.202 g, 1.28 mmol) was added to a solution of sodium (2.0 g) in 50 mL degassed MeOH and stirred for 1 h, resulting in a clear solution. In a separate flask, $PdCl_2$ (0.114 g, 0.642 mmol) and NaCl (0.0750 g, 1.28 mmol) were added to ~3 mL nitrogen-sparged H_2O, which was then added dropwise to the solution at rt, immediately forming red-brown solution. The solution was stirred overnight, filtered, oxidized with I_2, and then *N*-methylpyridinium iodide (0.21 g, 0.96 mmol) was added to form a green precipitate. The solid was filtered and washed with MeOH, H_2O, and Et_2O. Product was recrystallized from CH_3CN to give 259 mg (61%) of a green crystalline solid.

***N*-methylpyridinium bis(5-(2-thienyl)-2,3-thiophenedithiolato)cobaltate(1-) (3.9)**

Attempted synthesis of **3.9**. Compound **3.3** (0.096 g, 0.31 mmol) was added to a solution of sodium (2.0 g) in 50 mL degassed MeOH and stirred for 1 h, resulting in a clear solution. In a separate flask, $CoCl_2 \cdot 6H_2O$ (0.036 g, 0.15 mmol) was added to ~3 mL nitrogen-sparged H_2O, which was then added dropwise to the solution at rt, immediately forming orange solution. The solution was stirred 3 h, filtered, oxidized with I_2, and then *N*-methylpyridinium iodide (0.22 g, 1.0 mmol) was added to form a green precipitate. The solid was filtered and washed with MeOH, H_2O, and Et_2O. Product was recrystallized from CH_3CN to give 18 mg (20%) of a blue-black crystalline solid.

***N*-methylpyridinium bis(5-(2-thienyl)-2,3-thiophenedithiolato)cobaltate(2-) (3.10)**

The oxidation occurred naturally as observed by green color that formed over time in solution. Compound **3.3** (0.10 g, 0.32 mmol) was added to a solution of sodium (2.0 g) in 50 mL degassed MeOH and stirred for 1 h, resulting in a clear solution. In a separate flask, $CoCl_2 \cdot 6H_2O$ (0.038 g, 0.16 mmol) was added to ~3 mL nitrogen-sparged H_2O, which was then added dropwise to the solution at rt, immediately forming purple solution that turned green over time. The solution was stirred 3 h, filtered, and then *N*-methylpyridinium iodide (0.21 g, 0.96 mmol) was added to form a green precipitate. The solid was filtered and washed with MeOH, H_2O, and Et_2O. Product was recrystallized from CH_3CN to give 103 mg (107%?) of a blue-black crystalline solid.

***N*-methylpyridinium bis-(2,3-thiophenedithiolato)platinate(1-) (3.12).** Compound **3.11** (0.10 g, 0.57 mmol) was added to a solution of sodium (2.0 g) in 50 mL degassed MeOH and stirred for 1 h, resulting in a clear solution. In a separate flask, K_2PtCl_4 (0.12 g, 0.28 mmol) was added to ~3 mL nitrogen-sparged H_2O, which was then added dropwise to the solution at rt, immediately forming orange solution. The solution was stirred 2 h, filtered, oxidized with I_2, and then *N*-methylpyridinium iodide (0.25 g, 1.1 mmol) was added to form a green precipitate. The solid was filtered and washed with MeOH, H_2O, and Et_2O. Product was recrystallized from CH_3CN to give 79 mg (47%) of a dark green crystalline solid.

***N*-methylpyridinium bis-(2,3-thiophenedithiolato)aurate(1-) (3.13).** Compound **3.11** (0.10 g, 0.57 mmol) was added to a solution of sodium (2.0 g) in 50 mL degassed MeOH and stirred for 1 h, resulting in a clear solution. In a separate flask, $KAuCl_4$ (0.11 g, 0.28 mmol) was added to ~3 mL nitrogen-sparged H_2O, which was then added dropwise to the solution at rt, immediately forming pink solution. The solution was stirred 2 h, filtered, and then *N*-methylpyridinium iodide (0.25 g, 1.1 mmol) was added to form a red precipitate. The solid was

filtered and washed with MeOH, H_2O, and Et_2O. Product was recrystallized from CH_3CN to give 97 mg (76%) of a red crystalline solid.

***N*-methylpyridinium bis-(2,3-thiophenedithiolato)palladiate(1-) (3.14).** Compound **3.11** (0.075 g, 0.43 mmol) was added to a solution of sodium (2.0 g) in 50 mL degassed MeOH and stirred for 1 h, resulting in a clear solution. In a separate flask, $PdCl_2$ (0.038 g, 0.21 mmol) and NaCl (0.025 g, 0.43 mmol) were added to ~3 mL nitrogen-sparged H_2O, which was then added dropwise to the solution at rt, forming green solution. The solution was stirred 2 h, filtered, oxidized with I_2, and then *N*-methylpyridinium iodide (0.189 g, 0.84 mmol) was added to form a brown precipitate. The solid was filtered and washed with MeOH, H_2O, and Et_2O. Product was recrystallized from CH_3CN to give 66 mg (63%) of a red-brown solid. HRMS = (M^{1-}): calc. 399.7666, expt. 399.7684.

***N*-methylpyridinium bis-(2,3-thiophenedithiolato)cobaltate(1-) (3.15).** Attempted synthesis of **3.15.** Compound **3.11** (0.052 g, 0.30 mmol) was added to a solution of sodium (2.0 g) in 50 mL degassed MeOH and stirred for 1 h, resulting in a clear solution. In a separate flask, $CoCl_2 \cdot 6H_2O$ (0.036 g, 0.15 mmol) was added to ~3 mL nitrogen-sparged H_2O, which was then added dropwise to the solution at rt, immediately forming brown-blue solution. The solution was stirred 2 h, filtered, oxidized with I_2, and then *N*-methylpyridinium iodide (0.13 g, 0.60 mmol) was added to form a blue-black precipitate. The solid was filtered and washed with MeOH, H_2O, and Et_2O. Product was recrystallized from CH_3CN to give 10 mg (15%) of a dark blue-black solid.

***N*-methylpyridinium bis-(2,3-thiophenedithiolato)cobaltate(2-) (3.16).** The oxidation occurred naturally as observed by green-blue color that formed over time in solution. Compound **3.11** (0.050 g, 0.29 mmol) was added to a solution of sodium (2.0 g) in 50 mL degassed MeOH

and stirred for 1 h, resulting in a clear solution. In a separate flask, $CoCl_2 \cdot 6H_2O$ (0.034 g, 0.14 mmol) was added to ~3 mL nitrogen-sparged H_2O, which was then added dropwise to the solution at rt, immediately forming blue solution. The blue-green solution was stirred 2 h, filtered, and then *N*-methylpyridinium iodide (0.19 g, 0.84 mmol) was added to form a blue precipitate. The solid was filtered and washed with MeOH, H_2O, and Et_2O. Product was recrystallized from CH_3CN to give 69 mg (95%) of a dark blue-black solid.

***N*-methyltrioctylammonium bis(5-(2-thienyl)-2,3-thiophenedithiolato)nickelate(1-) (3.17)** Compound **3.3** (0.50 g, 1.59 mmol) was added to a solution of sodium (2.0 g) in 50 mL degassed MeOH and stirred for 1 h, resulting in a clear solution. In a separate flask, $NiCl_2 \cdot 6H_2O$ (0.19 g, 0.79 mmol) was added to ~3 mL nitrogen-sparged H_2O, which was then added dropwise to the solution at rt, immediately forming red solution. The solution was stirred 2 h, filtered, bubbled with O_2, and then methyltrioctylammonium bromide (0.53 g, 2.39 mmol) was added to form a green precipitate. The solid was filtered and washed with MeOH, H_2O, and Et_2O. Product was recrystallized from CH_3CN to give 510 mg (73%) of a dark green crystalline solid.

Poly(bis(2,3-thiophenedithiolato)nickelate(1-)-*alt*-9,9-dioctyl-9H-fluorene) (3.32). To a 50-mL Schlenk tube was added 1.6 M K_2CO_3 in H_2O (0.493 g / 2 mL) and degassed 2 h. Then, **3.30** 9,9-diocyl-2,7- bis(4,4',5,5'-tetramethyl-1,3,2-dioxaborolan-2-yl)-9*H*-fluorene (0.110 g, 0.171 mmol), **3.31** (0.150 g, 0.171 mmol), and $Pd(PPh_3)_2Cl_2$ (0.0060 g, 5 mol%). The tube was then evacuated and backfilled five times with N_2, and then toluene (10 mL) was added and the reaction was heated to 95 °C for 4 days. After 24 h noted that the solution is clear brown, and a dark green precipitate had formed at solvent/N_2 interface. The reaction was then cooled to room temperature, and the product concentrated under vacuum and precipitated in MeOH (100 mL). The crude polymer was purified by Soxhlet extraction with MeOH, acetone, hexanes, and then

$CHCl_3$. Color did not come off with any fraction. The insoluble polymer was a dark-blue solid (227 mg).

Poly(bis(5-(2-thienyl)-2,3-thiophenedithiolato)nickelate(1-)-*alt*-9,9-dioctyl-9H-fluorene) (3.34). To a 50-mL Schlenk tube was added 1.6 M K_2CO_3 in H_2O (0.493 g / 2 mL) and degassed 2 h. Then, **3.30** 9,9-diocyl-2,7- bis(4,4',5,5'-tetramethyl-1,3,2-dioxaborolan-2-yl)-9*H*-fluorene (0.110 g, 0.171 mmol), **3.33** (0.178 g, 0.171 mmol), and $Pd(PPh_3)_2Cl_2$ (0.0060 g, 5 mol%). The tube was then evacuated and backfilled five times with N_2, and then toluene (10 mL) was added and the reaction was heated to 95 °C for 4 days. After 24 h noted that the solution is clear blue-brown, and a dark green precipitate had formed at solvent/N_2 interface. The reaction was then cooled to room temperature, and the product concentrated under vacuum and precipitated in MeOH (100 mL). The crude polymer was purified by Soxhlet extraction with MeOH, acetone, hexanes, and then $CHCl_3$. Color did not come off with any fraction, except a tiny amount with $CHCl_3$. The insoluble polymer was a dark-blue solid (250 mg).

3.7. References

1. Schrauzer, G. N.; Mayweg, V. *J. Am. Chem. Soc.* **1962**, *84*, 3221.
2. Gray, H. B.; Williams, R.; Bernal, I.; Billig, E. *J. Am. Chem. Soc.* **1962**, *84*, 3596.
3. Ouahab, L. *Coord. Chem. Rev*. **1998**, *178-180*, 1501-1531.
4. Robertson, N.; Cronin, L. *Coord. Chem. Rev.* **2002**, *227* (1), 93-127.
5. Stiefel, E. I.; Karlin, K. D., Eds.; Dithiolene Chemistry: Synthesis, Properties, and Applications. In *Progress in Inorganic Chemistry*, Vol. 52, John Wiley & Sons: Hoboken, NJ, 2004.
6. Kato, R. *Chem. Rev.* **2004**, *104*, 5319-5346.
7. Dalgleish, S.; Robertson, N. *Coord. Chem. Rev.* **2010**, *254*, 1549-1558.

8. Belo, D.; Almeida, M. *Coord. Chem. Rev.* **2010**, *254*, 1479-1492.

9. Hine, F. J.; Taylor, A. J.; Garner, C. D. *Coord. Chem. Rev.* **2010**, *254*, 1570-1579.

10. Rasmussen, S. C.; Amb, C. M. Synthesis and Structural Characterization of Thiophene-Functionalized Metal Dithiolenes. In *Chemical Crystallography*; Connelly, B. L., Ed.; Nova Publishers, Hauppage, NY, 2010; pp 69-101.

11. Sproules, S. Tris(dithiolene) chemistry: A Golden Jubilee. In *Progress in Inorganic Chemistry*, Vol. 58*;* Karlin, K. D., Ed.; John Wiley & Sons: Hoboken, NJ, 2014; pp 1-144.

12. Pop, F.; Avarvari, N. *Coord. Chem. Rev.* **2017**, *346*, 20-31.

13. Espa, D.; Pilia, L.; Attar, S.; Salahuddin, A.; Deplano, P. *Inorg. Chim. Acta.* **2018**, *470*, 295-302.

14. Kondo, M.; Minakoshi, S.; Iwata, K.; Shimizu, T.; Matsuzaka, H.; Kamigata, N.; Kitagawa, S. *Chem. Lett.* **1996**, (6), 489-490.

15. Attar, S. S.; Artizzu, F.; Marchio, L.; Espa, D.; Pilia, L.; Casula, M. F.; Serpe, A.; Pizzotti, M.; Orbelli-Biroli, A.; Deplano, P. *Chem. Eur. J.* **2018**, *24*, 10503-10512.

16. Butin, K. P.; Beloglazkina, E. K.; Zyk, N. V. *Russ. Chem. Rev.* **2005**, *74*, 531-553.

17. Eisenberg, R.; Gray, H. B. *Inorg. Chem.* **2011**, *50*, 9741-9751.

18. Jørgensen, K. *Coord. Chem. Rev.* **1966**, *1* (1-2), 164-178.

19. Fourmigué, M. *Acc. Chem. Res.* **2004**, *37* (3), 179-186.

20. Eisenberg, R. *Coord. Chem. Rev.* **2011**, *255*, 825-836.

21. Ray, K.; Weyhermueller, T.; Neese, F.; Wieghardt, K. *Inorg. Chem.* **2005**, *44* (15), 7345-5360.

22. Kambe, T.; Sakamoto, R.; Hoshiko, K.; Takada, K.; Miyachi, M.; Ryu, J.-H.; Sasaki, S.; Kim, J.; Nakazato, K.; Takata, M.; et al. *J. Am. Chem. Soc.* **2013**, *135* (7), 2462-2465.

23. Shibahara, S.; Kitagawa, H.; Kubo, T.; Nakasuji, K. *Inorg. Chem. Commun.* **2007**, *10* (8), 860-862.

24. Belo, D.; Alves, H.; Lopes, E. B.; Duarte, M. T.; Gama, V.; Henriques, R. T.; Almeida, M.; P.-B., A.; Rovira, C.; Veciana, J. *Chem. Eur. J.* **2001**, *7* (2), 511-519.

25. Neves, A. I. S.; Santos, I. C.; Pereira, L. C. J.; Rovira, C.; Ruiz, E.; Belo, D. Almeida, M. *Eur. J. Inorg. Chem.* **2011**, (31), 4807-4815.

26. Amb, C. M.; Rasmussen, S. C. *Synth. Met.* **2009**, *159*, 2390-2393.

27. Amb, C. M.; Rasmussen, S. C. *Eur. J. Org. Chem.* **2008**, 801-804.

28. Amb, C. M.; Heth, C. L.; Evenson, S. J.; Pokhodnya, K. I.; Rasmussen, S. C. *Inorg. Chem.* **2016**, *55* (21), 10978-10989.

29. Uzelac, E. J.; Rasmussen, S. C. *Eur. J. Inorg. Chem.* **2017**, (33), 3878-3883.

30. Schnurch, M.; Spina, M.; Khan, A. F.; Mihovilovic, M. D.; Stanetty, P. *Chem. Soc. Rev.* **2007**, *36*, 1046-1057.

31. Belo, D.; Alves, H.; Rabaca, S.; Pereira, L. C.; Duarte, M. T.; Gama, V.; Henriques, R. T.; Almeida, M.; Ribera, E.; Rovira, C.; et al *Eur. J. Inorg. Chem.* **2001**, (12), 3127-3133.

32. Belo, D.; Alves, H.; Lopes, E. B.; Gama, V.; Henriques, R. T.; Duarte, M. T.; Almeida, M.; Perez-Benitez, A.; Rovira, C.; Vecina, J. *Synth. Met.* **2001**, *120*, 699-702.

33. Belo, D.; Figuiera, M. J.; Mendoca, J.; Santos, I. C.; Almeida, M.; Henriques, R. T.; Duarte, M. T.; Rovira, C.; Veciana, J. *Eur. J. Inorg. Chem.* **2005**, (16), 3337-3345.

34. Cibian, M.; Derossi, S.; Hanan, G. S. *Dalton Trans.* **2011**, *40*, 1038-1040.

35. Perez-Benitez, A.; Tarres, J.; Ribera, E.; Veciana, J.; Rovira, C. *Synthesis* **1999**, (4), 577-579.

36. Miller, G.; Heindel, N. D. *J. Org. Chem.* **1981**, *46* (23), 4751-4753.

37. Geary, E. A. M.; McCall, K. L.; Turner, A.; Murray, P. R.; McInnes, E. J. L.; Jack, L. A.; Yellowlees, L. J.; Robertson, N. *Dalton Trans.* **2008**, (28), 3701-3708.

38. Skabara, P. J.; Pozo-Gonzalo, C.; Lardies Miazza, N.; Laguna, M.; Cerrada, E.; Luquin, As.; Gonzalez, B.; Coles, S. J.; Hursthouse, M. B.; Harrington, R. W.; et al *Dalton Trans.* **2008**, (23), 3070-3079.

39. Ray, K.; Weyhermuller, T.; Gossens, A.; Craje, M. W. J.; Wieghardt, K. *Inorg. Chem.* **2003**, *42*, 4082-4087.

40. Roncali, J. *Macromol. Rapid Commun*. **2007**, *28* (17), 1761-1775.

CHAPTER 4. SYNETHESIS AND POLYMERIZATION OF THIENO[3,4-*b*]PYRAZINE MATERIALS

4.1. Introduction

Organic conjugated polymers (CPs) have received considerable fundamental and technological interest because of their combination of the of the electronic and optical properties of classical inorganic semiconductors with many of the desirable properties of plastics (flexibility and low production costs).[1-4] This has led to the rise of the current field of organic electronics, with substantial effort focused on the development of technological applications such as sensors, electrochromic devices, organic photovoltaics (OPVs), organic light-emitting diodes (OLEDs), and field-effect transistors (FETs).[5-10] Additionally, the flexible, plastic nature of the organic materials used in such electronic devices provides the exciting promise of flexible electronics as a realistic goal.[11-14]

Incorporating organic systems into solar cells is driven by these materials' light weight, solution processability, and cost effectiveness.[6,15-20] OPVs have seen tremendous growth in the previous two decades, especially in terms of efficiency. The power conversion efficiencies (PCEs) – arguably the most important scientific figure of merit for photovoltaics – of current organic device architectures has reached 15% (compared to ~1% in the 1990s).[20] Inorganic technologies (i.e. silicon solar cells), which were first introduced in the 1950s,[21] have long been the economically-viable material of choice because of their high efficiencies (up to PCE = 44%),[18] however organic solar cells have finally reached a reduced cost (this compensates for the lower efficiencies and lifetimes of these systems) that makes them economically feasible.[16]

First reported in 1995,[22] solution-processible bulk-heterojunction (BHJ) solar cells are of exceptional interest to the materials community. Figure 4.1 shows a model of a typical BHJ solar

cell.[20,23] These architectures combine a 'donor' material (e.g. P3HT) with an 'acceptor' material (e.g. $PC_{61}BM$) in an interpenetrating polymer blend. In BHJ solar cells, a disordered blend of the donor and acceptor materials are sandwiched between two electrodes – one of which is transparent.

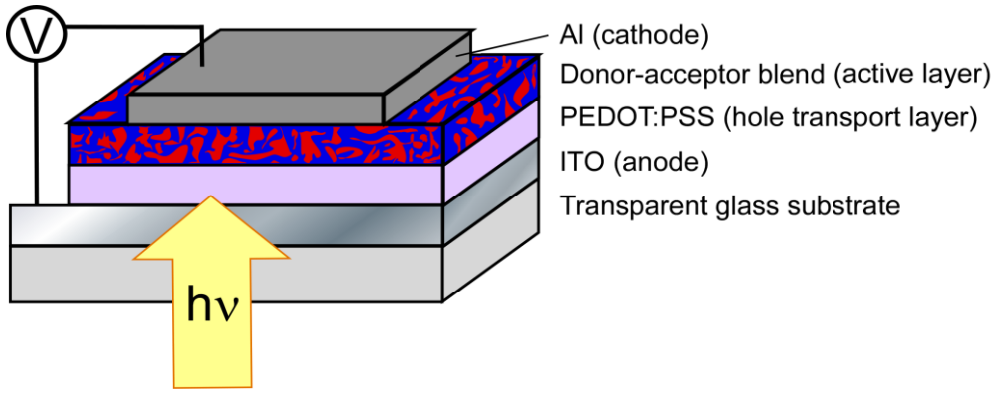

Figure 4.1. Model of a typical BHJ solar cell with the BHJ layer general structure

When a photon of light is absorbed by the electron donor, this leads to the creation of an exciton, a strongly coulombically bound electron [e^-] – hole [h^+] pair (Figure 4.2). If the exciton diffuses to the interface of the donor-acceptor, it dissociates to form a free hole and electron. The electron can only be transferred to the acceptor component if it has a higher electron affinity (i.e. lower-lying LUMO level) than the donor. In contrast, the hole stays within the donor phase because it has a lower ionization potential (i.e. higher-lying HOMO level). The charges then drift through the separate donor and acceptor domains, and then the holes and electrons are collected at the solar cell anode and cathode electrodes, respectively (Figure 4.2). This charge transfer process is an important elementary step in the conversion of light to electricity.[20,23] The harvesting of these charges by the electrodes produces a current in the external circuit, at a specific voltage, the product of which is the power produced by the OPV.

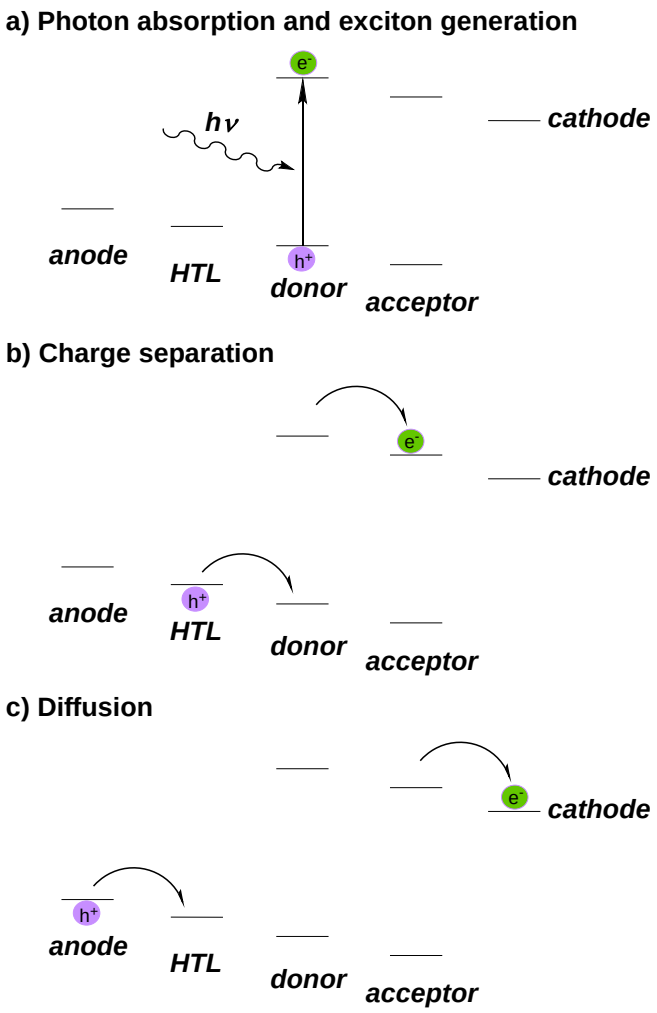

Figure 4.2. Charge generation process in the BHJ

It should be noted that the most recent advances in OPVs are not just limited to the simple BHJ architecture presented above. There are growing numbers of reports utilizing both small molecules and oligomers as donor materials and non-fullerene materials as acceptors.[18-20,23] Additionally, the current record for an OPV device efficiency utilizes a multilayer tandem architecture to achieve a maximum PCE of 17.3%,[24] which is nearly in the range of commercial silicon solar cells (18-22% PCE).[25]

Many of the common applications of organic CPs have to do with the absorption or emission of light, so control of these essential properties is of vital importance. Both properties

are determined by the magnitude of the polymer band gap (E_g), and because of this, significant effort has been given to controlling and tuning the E_g of conjugated materials. Several factors contribute to E_g, including monomer aromaticity, the extent of conjugation, heteroatom effects in heterocyclic systems, and interchain coupling.[2,3,26-28] Additionally, as E_g and frontier orbitals are intrinsically linked, control of the orbital energy levels allows for both tuning of the CPs E_g and their corresponding redox properties. Tuning of the orbital energy levels is also crucial in determining environmental stability, and proper matching of energy levels with other electronic components in device applications and performance.

For control and tuning of the E_g of conjugated materials, much effort has been focused on the goal of producing both *low* band gap (E_g < 1.5 eV) and *reduced* band gap (E_g = 1.5-2.0 eV) conjugated organic materials that can more efficiently absorb solar radiation for applications in solar cell technologies (i.e. OPVs).[2,3,28-37] Thieno[3,4-*b*]pyrazine (TP)[29] is a thiophene-based, fused ring unit comprised of an electron-rich thiophene fused to an electron-poor pyrazine that has become a relatively popular building block for the production of low and reduced band gap conjugated organic materials. As shown in Figure 4.3, TPs owe their low E_g to a combination of the quinoidal character of the TP unit, as well as its strong ambipolar nature. This results in an internal intramolecular charge-transfer (ICT) transition between the partially localized frontier orbitals, from the thiophene-localized HOMO to the more pyrazine-localized LUMO. As a result of this, all TP-based materials exhibit properties of donor-acceptor (D-A) frameworks, even pure TP homopolymers.[40-42] Additionally, though TPs are typically used as acceptors in D-A materials, the ambipolar nature of the TP unit provides significant donor character, which results in a strong contribution to the HOMO energy of copolymeric materials.

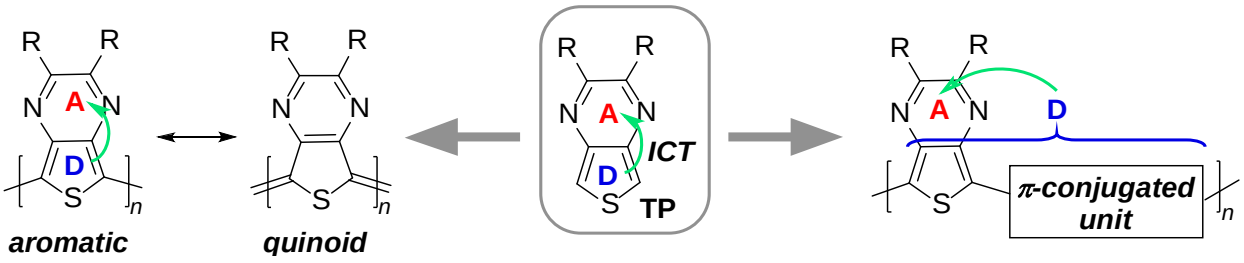

Figure 4.3. Monomeric thieno[3,4-*b*]pyrazine (TP) and TP-based materials

For the majority of traditional TP-based materials, the functionalization of the TP unit is limited typically to 2,3-dialkyl or aryl side chains.[29] More recently, new synthetic methods have been developed that allow for the production of a large group of TP units that feature both electron-donating and electron-withdrawing side chains.[41,43] Several examples have been reported that illustrate the extent to which E_g can be tuned by simple changes in the TP side chains.[30-33,44] While the HOMO levels of TP are affected by the electronics of the side chain, the pyrazine-localized LUMO levels of TP are affected to a far greater extent. This results in an increased HOMO-LUMO gap for donating groups and a decreased gap for withdrawing groups, which is reflected in the absorption profiles. For example, the electron-rich alkyloxy-substituted TP 2,3-dipentoxythieno[3,4-*b*]pyrazine (**4.1a**) features a HOMO destabilized by 1.55 eV, a LUMO destabilized by 2.26 eV, and a reduction in HOMO-LUMO gap of 0.71 eV in comparison to electron-poor cyano substituted analogue 2,3-dicyanothieno[3,4-*b*]pyrazine (**4.1e**).[41] Figure 4.4 shows the HOMO and LUMO energy levels and subsequent gaps for a range of TPs **4.1a-e** featuring electron donating groups (R = OC_5H_{11}, C_6H_{13}, H) and electron withdrawing groups (R = Br, CN).[41] Thus it has been shown that the energy levels in the TP molecules can be effectively and precisely tuned by changing the side chains.

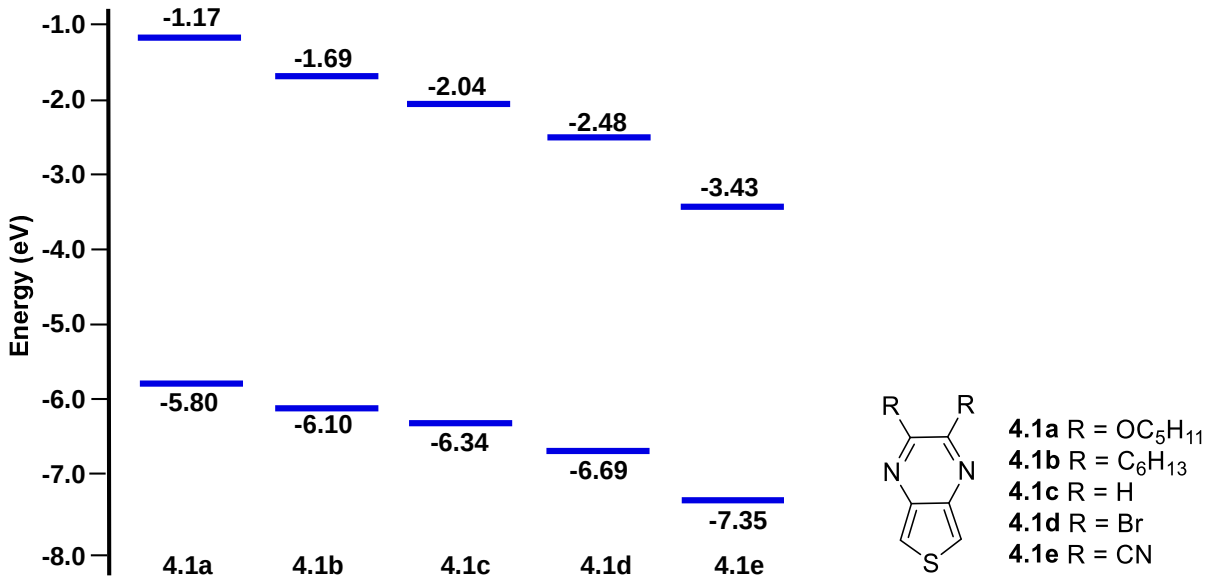

Figure 4.4. Calculated HOMO and LUMO levels for select TPs

The Rasmussen group has previously demonstrated the ability to produce tunable, low E_g materials through the generation of new families of functionalized TPs.[41,45] However, these materials can be hindered by a lack of solubility because they are highly planar systems that exhibit an abundance of π-π interactions, and also a lack of stability due to the somewhat reactive nature of TPs which are susceptible to oxidative polymerization making these monomer units difficult to work with.[2,29] A solution to these issues is the application of TPs in the form of the terthienyl analogue, in which the reactive *α*-positions (5- and 7-positions) of the TP are substituted with 2-thienyl groups (Figure 4.5).

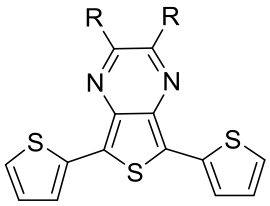

Figure 4.5. Representative example of thieno[3,4-*b*]pyrazine-based terthienyl

The addition of these thienyl groups imparts increased solubility to the monomers. Also, in comparison to conventional TP monomers, the terthienyl analogues undergo oxidation at

much lower potentials, and the increased size and conjugation length of the oligomeric terthienyls results in decreased reactivity, which lowers the chances of losing material through undesirable oxidative coupling processes or decomposition.[30,32,43]

4.2. General TP and TP-based Terthienyl Synthesis

The first initial report of the TP monomer dates to 1957 with the synthesis of 2,3-diphenylthieno[3,4-*b*]pyrazine by Motoyama et al.,[46] however it wasn't until the early 1980's that Outurquin and Paulmier reported the first general route to these compounds.[47,48] Since that time, the basic synthetic pathway of conventional TPs has not really changed, although the methods to generate each of the intermediates has been improved and optimized over the years (Scheme 4.1).[39,41,49,50] The first step of the synthesis involves the bromination of thiophene to yield 2,5-dibromothiophene (**4.2**). The bromine acts to protect these positions for the subsequent nitration at the 3- and 4-positions to generate 2,5-dibromo-3,4-dinitrothiophene (**4.3**). The formation of **4.3** was first reported by Kreis in 1884,[50] in which nitric acid was added to a solution of **4.2** in sulfuric acid. The most recent optimization of this reaction was reported by Rasmussen and coworkers,[50] in which nitric acid is added at a controlled rate to a solution of **4.2** in a mixture of sulfuric and fuming sulfuric acid. In this way, the critical nitrating species NO_2^+ is maximized, while reducing the formation of the byproduct NO^+ that causes decomposition upon reaction with thiophenes This intermediate is then reacted with tin metal in HCl to form the tin salt **4.4**, which is stable and can be stored long-term.[49] Upon neutralization with base, the diamine **4.5** is produced. This neutralization is a requisite step because the exact composition of counterions in the salt **4.4** is variable between reactions, and the mols of **4.5** can be easily calculated. This then allows for typical condensation reactions with various prepared or commercially available α-diones (**4.6**) to form the corresponding TPs. These methods have been

used to produce a wide variety of unfunctionalized, dialkyl, diaryl, and heteroaryl TPs, of which **4.7a-r** in Scheme 4.1 are representative examples.

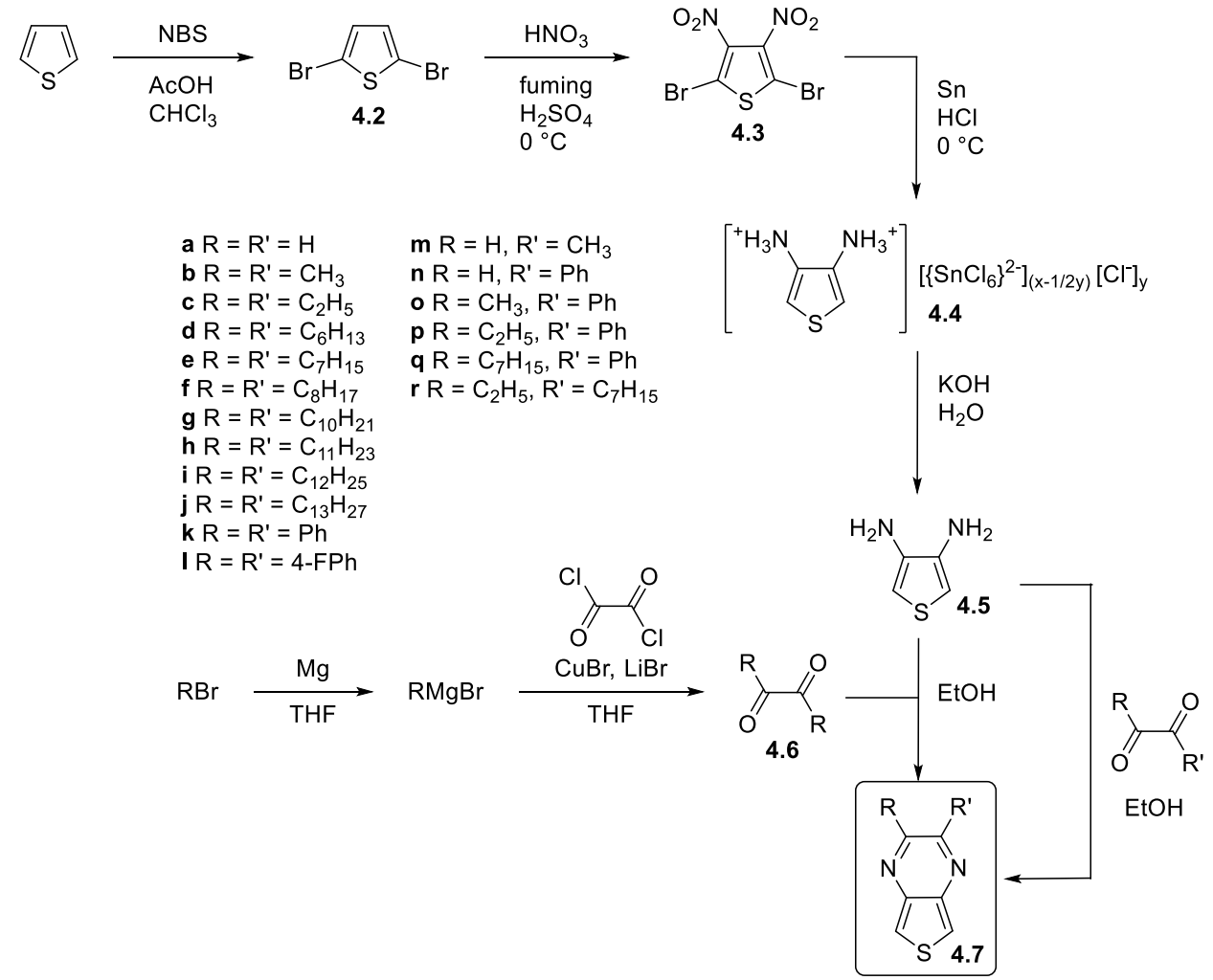

Scheme 4.1. Conventional synthesis of thieno[3,4-*b*]pyrazines via condensation

In comparison to the TP monomers, the TP-based terthienyl oligomers are more modern, with Yamashita and coworkers initially reporting them in 1994.[51,52] The synthetic route for the generation of TP-based terthienyls is shown in Scheme 4.2.[43] The synthetic steps remain the same up to **4.3**, at which point the synthesis deviates and the bromine functionalities of **4.3** are utilized in a Stille coupling reaction with 2-(tributylstannyl)thiophene to generate 3',4'-dinitro-2,2':5',2"-terthiophene (**4.8**).

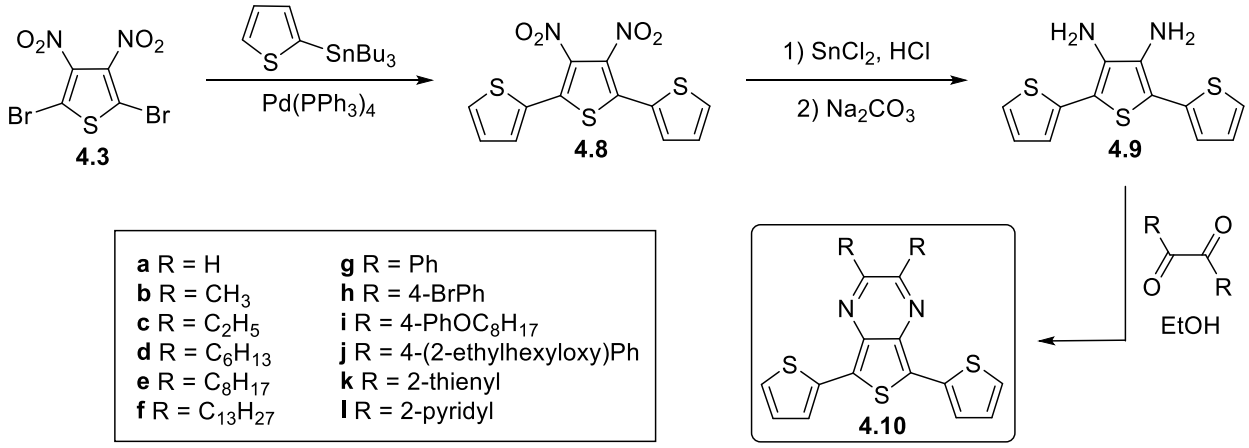

Scheme 4.2. Conventional synthesis of simple thieno[3,4-*b*]pyrazine-based terthienyls via condensation

Next, 3',4'-diamino-2,2':5',2"-terthiophene (**4.9**) is formed from reaction of **4.8** with a tin source in acidic conditions. Although this reaction can be successfully performed with tin metal reagent, it was found that the optimal synthesis uses $SnCl_2$ as the tin source, as this provides the most consistent results and is less affected by the form of the metal (e.g. granules vs. flakes), and the product **4.9** was obtained in yield 80-85%.[35] Also, although an intermediate diamine salt is formed from **4.8**, this can be directly neutralized with base to form **4.9**, as it was observed that this species is stable for a period of several months if stored in cold, dark conditions. It should be highlighted that high purity samples of **4.9** are a golden yellow solid, rather than the other forms commonly reported, and give a high and narrow melting point of 139–141 °C.

Analogous to the TPs, this then allows for typical condensation reactions with various α-diones to generate the corresponding TP-based terthienyls. Methods such as these have been used to produce unfunctionalized, dialkyl, and diaryl TP-based terthienyls, of which **4.10a-l** in Scheme 4.2 are representative examples.[43]

The tunability of both the monomeric TPs and their terthienyl analogues is limited by the stability of the α-diones employed during their synthesis. Although not the focus of this discussion, to include a wider variety of side chains, including electron-donating and electron-withdrawing side chains, the Rasmussen group introduced new methods towards the generation of TPs[41] and TP-based terthienyls to expand upon the families of these materials.[30,43] A TP monomer featuring bromides at the 2- and 3-positions allows for simple substitutions to be performed to access more substituents (e.g. R = OC_5H_{11}, $NHC_{10}H_{21}$, CN).[41] For the TP-based terthienyls, 2,3-ditriflato- and 2,3-bis(bromomethyl)-5,7-bis(2-thienyl)thieno[3,4-*b*]pyrazine were also found to be good precursors to expand upon the functionalization (e.g. R = OC_6H_{13}, $N(CH_2CH_3)_2$, $CH_2OC_6H_{13}$, $CH_2N(CH_2CH_3)_2$).[30,43]

4.3. TP-Fluorene Copolymers

Although several examples have been reported illustrating the extent to which E_g can be tuned by simple changes in the TP side chains,[30-33,44] the majority of these examples have focused on TP homopolymers[31,33,34] and polymerization of TP-based terthienyl precursors.[31,32] However, less work has been published on the application of such tuning to soluble copolymeric D-A materials.[30,31,34] As such, it was determined it would be worthwhile to delve further into the effect of the ambipolar nature of TPs when applied to D-A conjugated polymers. The bulk of work reported in this section has been published as a paper in the *Australian Journal of Chemistry*.[34]

Fluorene (FLO) is an aryl-based system, which is frequently used in the generation of OLEDs due to its charge transport ability and high quantum efficiency.[53,54] Due to its aromatic backbone, fluorene is commonly utilized as an electron-rich 'donor' in D-A frameworks,[55,56] and several TP-fluorene systems have been reported (Figure 4.6).[30,57-74] For these reasons, it serves as

a good co-monomer for comparison of new materials. Comparison of changes in the TP side chain (alkyl vs. alkoxy) and TP monomers with and without thiophene 'spacer' units between the TP and fluorene (TP co-monomer **4.11** vs. TP-based terthienyl co-monomer **4.12**) should allow for discussion of how these affect the material properties of the polymers. Although some view that these 'spacer' units have no effect on properties, it is expected that they will have some role in determining the resultant E_g.[34]

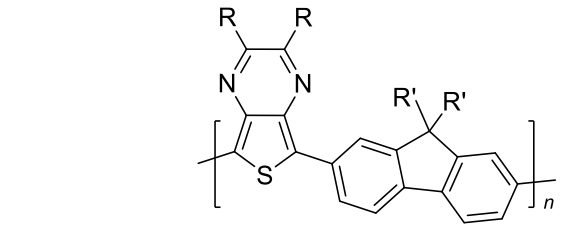

4.11

a R = H, R' = C_6H_{13}
b R = H, R' = $C_{10}H_{21}$
c R = Ph, R' = C_8H_{17}
d R = Ph, R' = $C_{10}H_{21}$
e R = $C_{12}H_{25}$, R' = C_8H_{17}
f R = OC_6H_{13}, R' = C_8H_{17}

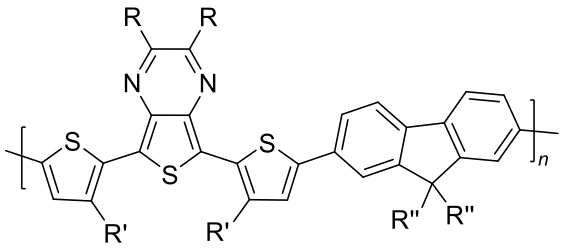

4.12

a R = H, R' = $C_{12}H_{25}$, R" = C_8H_{17}
b R = CH_3, R' = H, R" = C_6H_{13}
c R = CH_3, R' = H, R" = 2•(C_3H_5)C_6H_{12}
d R = C_2H_5, R' = C_6H_{13}, R" = C_8H_{17}
e R = Ph, R' = H, R" = 2•(C_3H_5)C_6H_{12}
f R = Ph, R' = H, R" = C_8H_{17}
g R = Ph, R' = H, R" = $CH_2CH_2OCH_2CH_2OCH_3$
h R = $PhCO_2C(CH_3)_2C_4H_9$, R' = H, R" = C_8H_{17}
i R = R" = C_8H_{17}, R' = H
j R = OC_6H_{13}, R' = H, R" = C_8H_{17}

Figure 4.6. Copolymers of TP-FLO

4.3.1. Synthesis of TP-FLO copolymers

The synthesis of the copolymer **4.12i** containing thiophene spacers was accomplished starting from the TP-based terthienyl **4.10e** as outlined in Scheme 4.3. First, 2,3-dioctyl-5,7-bis(2-thienyl)thieno[3,4-*b*]pyrazine (**4.10e**) was synthesized using the conventional synthetic pathway for TP-based terthienyls in very good yield of 89%. The second step of the reaction involved bromination of the pendant thiophene spacer units, to make 5,7-bis(5-bromo-2-thienyl)-2,3-dioctylthieno[3,4-*b*]pyrazine (**4.14**) using *N*-bromosuccinimide (NBS) as the brominating

reagent in 50:50 v:v mixture of $CH_3COOH:CHCl_3$ (26%). Finally, polymer **4.12i** was generated through Suzuki cross-coupling.[75,76]

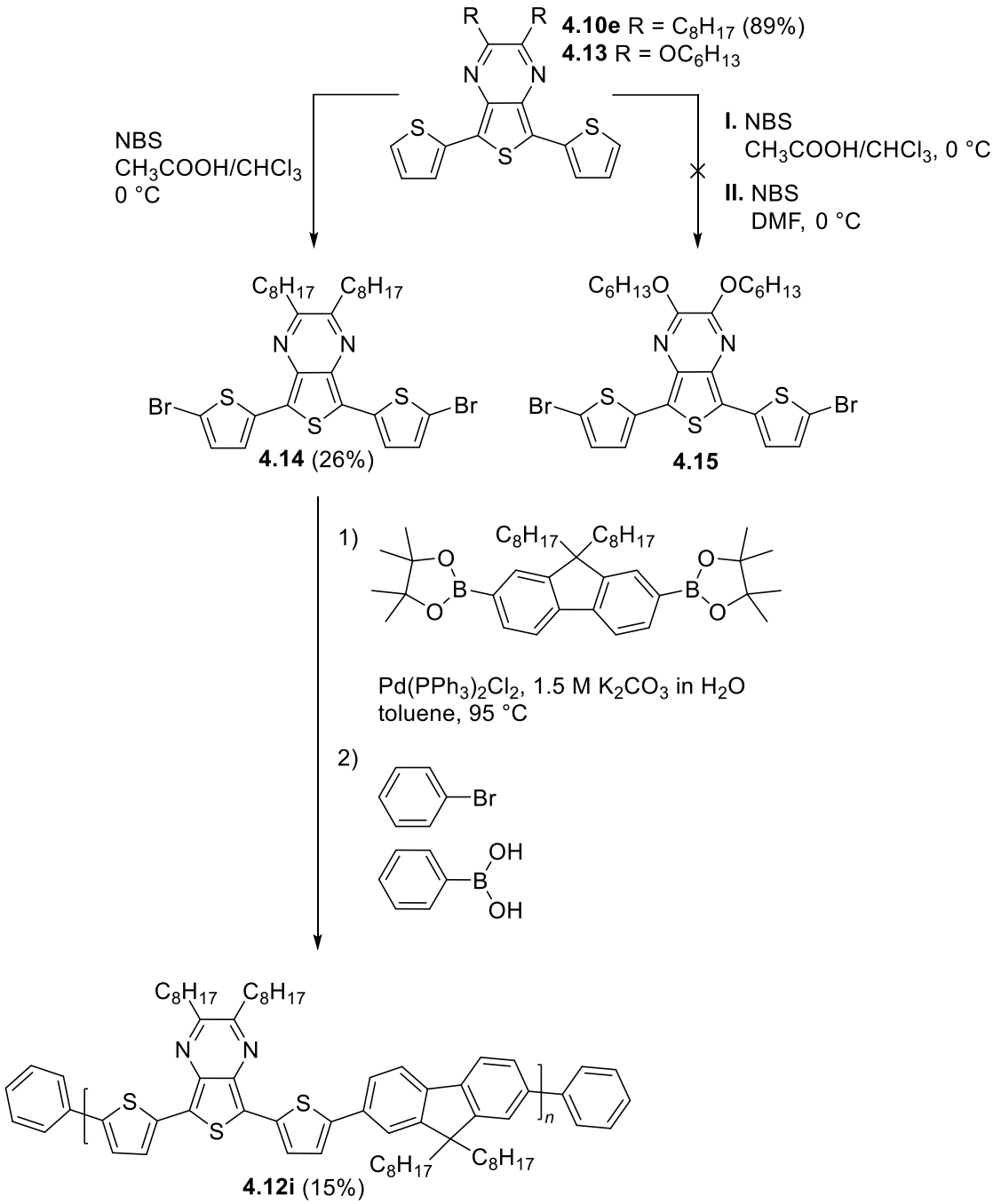

Scheme 4.3. Synthesis of poly(2,3-dioctyl-5,7-bis(2-thienyl)thieno[3,4-*b*]pyrazine-*co*-9,9-dioctyl-9H-fluorene) via Suzuki polymerization

The polymer was end-capped with phenyl groups in order to remove any reactive endgroups (i.e. -Br, -$BO_2C_2(CH_3)_4$) and to provide further chemical stability to the resulting polymer.[77,78] The polymer was isolated in yield of 15% and was readily soluble in $CHCl_3$ and THF. Attempts to brominate terthienyl **4.13** to form the desired dibromide intermediate **4.15** were ultimately unsuccessful, resulting in the production of a unidentified byproduct.[34,43] Instead, the hexyloxy analogue to **4.12i** was formed via Stille cross-coupling by another with the corresponding distannyl intermediate of **4.14** and brominated fluorene.[34]

For the bulk of the material **4.12i**, most of it was low molecular weight. However, a small fraction of the material (~6%) gave good molecular weights (M_n = 54,000), and it is this high weight fraction data that is reported in the following sections. Table 4.1 shows molecular weight and dispersity data for **4.12i** and similar analogous polymers published. It should be noted that many of the previously reported TP-FLO materials were also of low molecular weight, so this is not unexpected.[57-59,61-64] The number average molecular weight (M_n) is the statistical average molecular weight of all the polymer chains in a sample. The weight average molecular weight (M_w) considers the molecular weight of a chain in determining contributions to the molecular weight average, so a larger chain will have a greater contribution to the molecular weight average.

Table 4.1. GPC data for thieno[3,4-*b*]pyrazine-fluorene copolymers[34]

Polymer	R	M_n[a]	M_w[a]	PDI[a]
4.11e	$C_{12}H_{25}$	5500	6700	1.2
4.11f	OC_6H_{13}	4800	6200	1.3
4.12i	C_8H_{17}	54000	78400	1.4
4.12j	OC_6H_{13}	2700	4000	1.5

[a]Determined by gel permeation chromatography (GPC)

The polydispersity index (PDI) is the indication of molecular weight distribution (M_n/M_w), where the PDI of a monodisperse polymer would equal 1.0.

4.3.2. Absorption spectroscopy of TP-FLO copolymer

Absorption data for polymer **4.12i**, along with analogous derivatives from the literature, are given in Table 4.2. In all cases, the materials exhibit a low-energy ICT transition in the visible portion of the spectrum from the thiophene in the conjugated backbone to the pyrazine of the TP units.[32,33,42,43] There is also a second $\pi \rightarrow \pi^*$ transition at higher energy. Overall, TP-based terthienyl polymers (**4.12**) give slightly lower E_g values than the pure TP units (**4.11**). For example, comparing the band gap of **4.12i** to its TP analogue **4.11e** that does not contain thiophene spacer units shows a reduction of 0.3 eV.

Table 4.2. Absorption data for selected thieno[3,4-*b*]pyrazine-fluorene copolymers

Polymer	**R**	**$\lambda_{max, abs}$ (nm, $CHCl_3$)**[a]	**$\lambda_{max, abs}$ (nm, film)**	**E_g (eV)**[b]
4.11b[61]	H	573	590	1.8
4.11d[61]	Ph	628	629	1.7
4.11e	$C_{12}H_{25}$	360, 515	365, 558	1.9
4.11f	OC_6H_{13}	360, 454	338,475	2.0
4.12b[64,69]	CH_3	*nr*	416, 616	1.7
4.12f[57,59]	Ph	*nr*	380, 615	1.6
4.12i	C_8H_{17}	396, 590	398, 606	1.6
4.12j	OC_6H_{13}	343, 451	375, 444	2.1

[a]*nr* = not reported. [b]Determined from absorption onset of thin films.

The absorption spectra of **4.12i** in the solution and solid state are displayed in Figure 4.7. The absorption maxima and E_g values of **4.12i** agree with previously reported trends in side-

chain tuning of the TP unit.[30-33,41-43] As the donor character of the side chain increases, the E_g value also increases (H < alkyl < alkoxy). The phenyl groups (**4.11d, 4.12f**) give the lowest optical E_g values, because of both electronic effects and the increased conjugation.

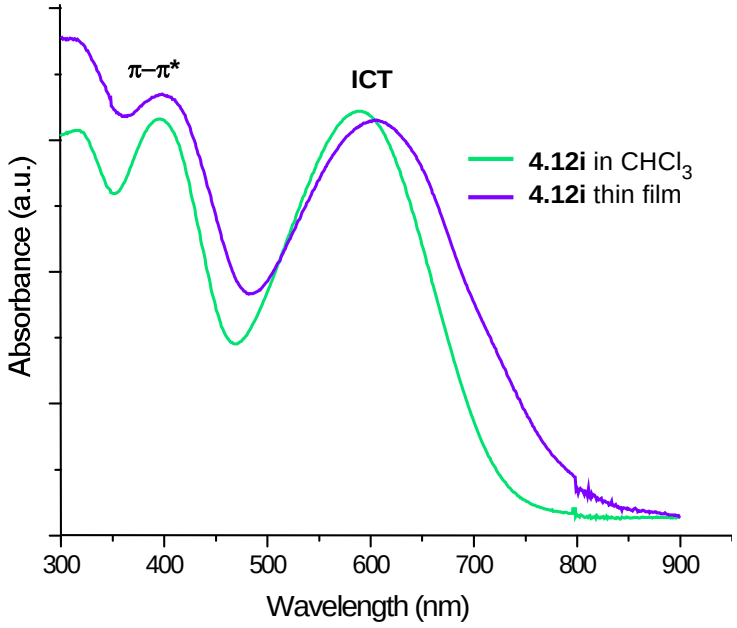

Figure 4.7. Absorption spectra of **4.12i** in solution and thin film

4.3.3. Electrochemistry of TP-FLO copolymer

The cyclic voltammogram of polymer **4.12i** is displayed in Figure 4.8. As typical of most TP-based materials, there is a fairly broad oxidation with a sharper, better-defined reduction (amphoteric redox properties). Table 4.3 summarizes electrochemical data for **4.12i** and analogous polymers from the literature. In general, the polymers without thiophene spacers (**4.11**) undergo oxidation at slightly higher potentials than those with spacers (**4.12**). Also, consistent with previously reported trends for side chain tuning of the TP unit,[30-33,41-43] as the electron donor strength of the side chain increases, the polymer's oxidation potential decreases, and the corresponding polymer's reduction moves to lower negative potentials.

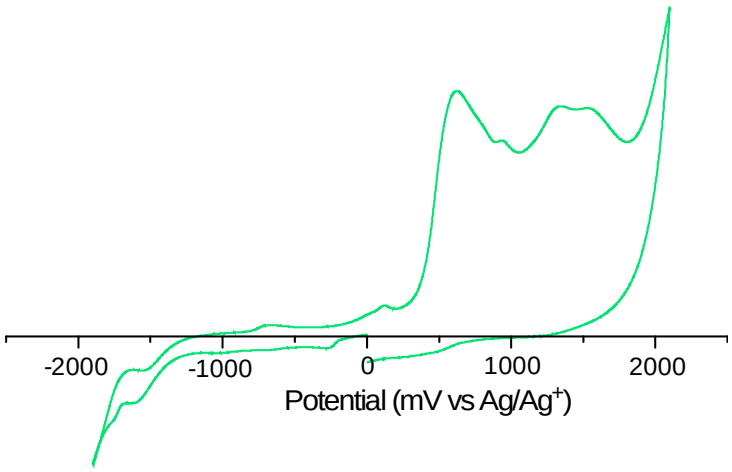

Figure 4.8. Cyclic voltammograms of polymer **4.12i**

As the conceptual model of D-A polymers attributes the bulk of the conjugated backbone as the donor, with the HOMO somewhat delocalized along this conjugated path,[80] then all species that make up the backbone should contribute to the polymer HOMO. This can be observed when comparing TP-FLO copolymers with and without thiophene spacers. Those with thiophene spacers (4.12) exhibit less side-chain tuning of the HOMO levels compared to those without spacers (4.11).As TP makes up only ~1/5 of the thiophene backbone in thiophene-spaced polymers vs ~1/3 of the thiophene backbone in TP-FLO polymers without spacers.

4.3.4. OPV device properties

A BHJ OPV device was fabricated from **4.12i** in a 1:1 polymer blend with [6,6]-phenyl-C_{61} butyric acid methyl ester (PCBM) (by Trent Anderson) as a representative example, although no device optimization was attempted. Exhibiting a quite low PCE of 0.020%, this can mostly be attributed to the short circuit current value (0.041 mA cm^{-2}). The calculation for PCE is given in Equation 4.1, where J_{sc} is the short circuit current, V_{oc} (0.93 V) is the open circuit potential, and FF (42.41%) is the fill factor.

$$\text{PCE} = \frac{Jsc\ x\ Voc\ x\ FF}{Pin} = \frac{Pout}{Pin} \qquad \text{(Equation 4.1)}$$

Additionally, very few reports of OPV devices have been published based on TP-FLO materials, and non-optimized PCBM blends of these materials have generally given poor device results (0.1-0.5%),[61,66,69] with optimized PCE values only as high as 1.37%,[58,67] so the extremely low device results for the TP-FLO polymer synthesized are disappointing but not surprising.

4.3.5. Conclusions to TP-FLO polymers

Overall, it was shown that properties exhibited by the model D-A polymer **4.12i** fit in with the general framework of trends for these TP-FLO materials. The application of electron-donating side chains results in an increase in E_g due to destabilization of the LUMO to a greater extent than analogous effects on the polymer HOMO. The addition of the thiophene spacer units confirms that these units do contribute to the polymer HOMO energy and thus the resultant Eg. The overall effect of the spacer is dependent on the relative electronic differences between the chosen spacer and the corresponding donor and acceptor. Comparing equivalent conjugation lengths, the oxidation potential of thiophene falls between that of TP and fluorene, which means that its addition to the TP-fluorene backbone should reduce the overall fluorene contribution, minimizing fluorene's stabilizing effect, which would result in the destabilization of the HOMO and a decrease in the material E_g.[34] This effect is confirmed with the fact that all the TP-FLO polymers with thiophene spacer units give higher HOMOs than the analogous TP-FLO polymers without spacers (Table 4.2).

4.4. TP-Thiophene Polymers

TP-thiophene conjugated materials are particularly interesting because the thiophene moiety offers judicious opportunities to tune the optical and electronic properties via structural modification. TP-based copolymers generated with thiophene, which is a common strong donor unit, yield low band gap materials (1.07 eV).[81-83] TP would be expected to act as an acceptor-

type unit in the formation of the polymer LUMO. However, as stated before, TP can oftentimes have a HOMO higher than many common donor materials.[84] Attempts were made in a collaborative project to synthesize TP-thiophene polymers for device applications. However, overall these polymers were of too low molecular weights to be ultimately useful.

4.4.1. Synthesis of TP-thiophene polymers

A series of unfunctionalized thiophene-TP polymers were synthesized using Stille cross-coupling methods, which is shown in Scheme 4.4. Each of these coupled the 2,3-dodecylthieno[3,4-*b*]pyrazine moiety with either thiophene (**4.18**), thieno[3,2-*b*]thiophene (**4.20**), or a random polymer of both thiophene and thieno[3,2-*b*]thiophene. These were all relatively soluble, with a chloroform soluble fraction isolated in good yields (57-81%).

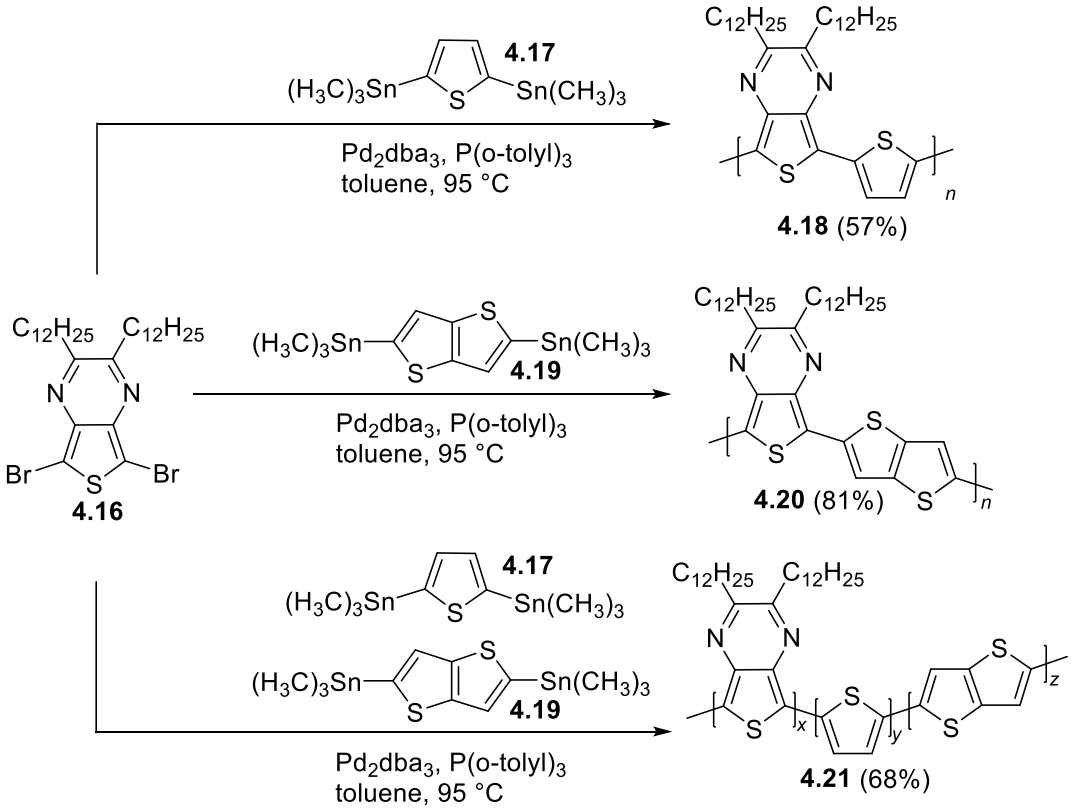

Scheme 4.4. Synthesis of TP-thiophene copolymers

Additionally, for polymer **4.18**, an insoluble fraction (1%) was isolated, which would be assumed to be of higher molecular weight. However, since it was not solution processible, no further analysis could be done. Only very minor analysis was done on these polymers, and GPC data collected showed that they were all of very low molecular weight (<3000), and below the calibration curve of the instrument, which would make them unreliable if reported.

4.4.2. Absorption spectroscopy of TP-thiophene polymers

Solution and solid-state absorption spectroscopy were recorded for the polymers **4.18**, **4.20**, **4.21**, the thin films of which are shown in Figure 4.9. As would be expected for TP materials, there is a low-energy ICT transition and higher-energy $\pi \rightarrow \pi^*$ transitions for each polymer. Spectral data for the polymers is tabulated in Table 4.3, including an estimate of the optical E_g. These band gaps are consistent with others observed for TP-thiophene polymers in the literature, [81-83] but it would be fair to say that these materials are probably more oligomeric than polymeric in character.

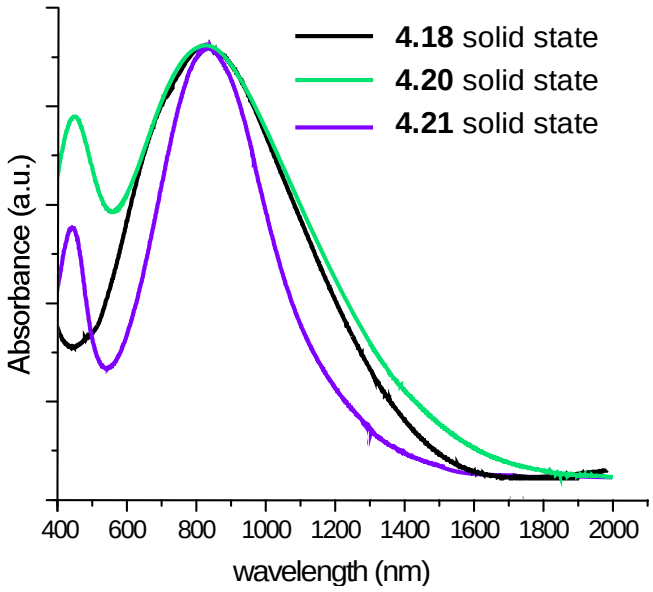

Figure 4.9. Absorption spectra of **4.18**, **4.20**, and **4.21** in thin film

Table 4.3. Absorption data for selected thieno[3,4-*b*]pyrazine-thiophene polymers

Polymer	$\lambda_{max, abs}$ (nm, $CHCl_3$)[a]	$\lambda_{max, abs}$ (nm, film)	E_g, optical (eV)[b]
4.18	nc	918	0.9 eV
4.20	nc	836	0.9 eV
4.21	811	817	1.0 eV

[a]nc, not collected. [b]Estimated from onset of low-energy absorption, 1240 nm = 1 eV conversion.

4.4.3. Conclusions on TP-thiophene polymers

Although a series of TP-thiophene and TP-thieno[3,2-*b*]thiophene were generated via Stille cross-coupling methods, it would be fair to say that the materials properties were disappointing. There are several issues that should be considered for this project, that could be further improved upon to give better material properties. First, co-polymerizations require an absolute 1:1 ratio in monomers for polymerization of high molecular weight materials to be successful. Any inclusion of impurities will disrupt the polymerization prematurely. For example, 0.9 equivalents of 'monomer A' and 1.0 equivalents of 'monomer B' were included in this chain growth polymerization, monomer B unit would end up as the terminal unit for all chains, and polymer growth would be terminated. Issues with weighing out mg scale quantities can affect this, but even more detrimental would be impurity in the starting material. For the polymers shown, the TP unit was ^{1}H NMR pure and the thiophene units were commercially purchased. However, although not discussed above, multiple attempts were made to synthesize a more soluble 2,5-bis(trimethylstannyl)-3-hexylthiophene-containing TP-thiophene polymer, with the stannyl thiophene monomer being synthesized from 2,5-dibromo-3-hexylthiophene. Besides being quite toxic to work with and sensitive to decomposition, these stannyl thiophenes were near impossible to purify completely, containing both tin salts and grease in the final product,

even after multiple washes, filtrations, and columns. The polymers that resulted were low molecular weight and had little to recommend them.

One way to resolve many of these issues would be to completely avoid organometallic cross-coupling altogether. Since the first report of Direct Arylation Polymerization (DArP) as a means of using C-H activation in 2010,[84] a growing number of researchers are using the technique to avoid many of the issues involved in older methods of CP synthesis.[85-87] There are several potential advantages of direct arylation coupling, including less waste (i.e. usually fewer synthetic steps to get to monomers), no toxic byproducts (i.e. organo tin species),[85-87] and lower production costs in theory (i.e. monomer preparation and solvent volume is reduced).[88] The Rasmussen group has even recently reported the use of DArP in the generation of generation of thieno[3,4-*b*]pyrazine copolymers,[36,37] and the advantages therein, although the methodology was not in the purview of this project. This is a very promising future direction, with the generation of high molecular weight materials with good band gaps.

4.5. Extended Fused-Ring TP-based Terthienyls

While most TP-based materials utilize various 2,3-difunctionalized TP monomers, a number of extended fused-ring analogues have also been utilized as potentially improved building blocks in conjugated materials. Figure 4.10 shows examples of such TP-monomers that have been reported in the literature. Such extended fused-ring analogues have included acenaphtho[1,2-*b*]thieno[3,4-*e*]pyrazines (**4.22**),[38,44,89-97] dibenzo[*f,h*]thieno[3,4-*b*]quinoxalines (**4.23**),[38,96-101] thieno[3′,4′:5,6]pyrazino[2,3-*f*][1,10]phenanthroline (**4.24**),[102,103] trithieno[3,4-*b*:3',2'-*f:*2",3"-*h*]quinoxaline (**4.25**),[70,95] and trithieno[3,4-*b*:2',3'-*f*:3",2"-*h*]quinoxaline (**4.26**).[70,95] As discussed earlier, traditional TPs can act as both a donor and an acceptor, and these monomers (**4.22-4.26**) are also ambipolar units.[36,45]

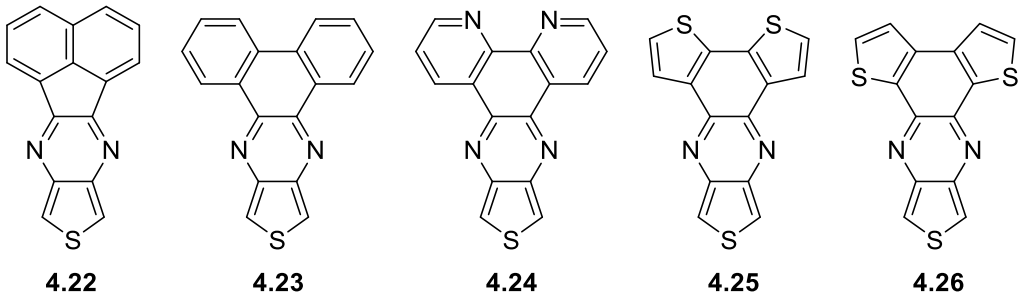

Figure 4.10. Representative fused ring analogues of thieno[3,4-*b*]pyrazine

Of the extended fused-ring units shown in Figure 4.7, only **4.22** is sterically small enough to give homopolymeric materials.[44,89] Thus, nearly all known polymers of **4.22-4.26** consist of D-A copolymers. Oftentimes, the extended fused-ring TP is incorporated into these materials as a TP-based terthienyl, which provides a thiophene 'spacer' unit within the polymer backbone. This is then copolymerized with additional monomeric species (e.g. alkylated-fluorenes and thiophenes). Additionally, there is only one report of a direct polymerization of an extended fused-ring TP based terthienyl in the literature, which was an analogue of **4.23** with dihexylfluorene units functionalizing the benzene rings.[101] The incorporation of the thiophene spacer unit both gives a monomer that is easier to work with and provides a motif that can accommodate the increased size of the extended fused-ring TP. As discussed earlier, although the increased conjugation length of the TP-based terthienyls causes them to undergo oxidation at lower potentials than their analogous TP monomers, the increased size and conjugation length actually results in slower reactivity and thus less production of byproducts via unwanted oxidative coupling or decomposition pathways.[32,43]

Most of the studies involving extended fused-ring TP-based terthienyls have focused on the resulting polymers, with characterization of the TP-based terthienyls seeming to be a lower priority. As such, little effort has been put forth to correlate the effects of changes in chemical structure to the electronic and optical properties. It was determined to be worthwhile to examine

these structure-function relationships with simple extended fused-ring TP-based terthienyls and the properties of their polymer analogues formed through electropolymerization. The bulk of work presented in this section was published in the journal *Materials*.[35]

4.5.1. Synthesis of TP-based terthienyls and homopolymers

A series of extended fused-ring TP-based terthienyls were synthesized using standard conditions, which are the same methods previously reported for traditional TP-based terthienyls[29,43,52] and their extended fused-ring analogues.[29,96,100,102] Scheme 4.5 shows the final step in the production of **4.27**-**4.29**, which is a simple double condensation with 3',4'-diamino-2,2':5',2"-terthiophene (**4.9**) and the appropriate fused-ring α-dione in ethanol.

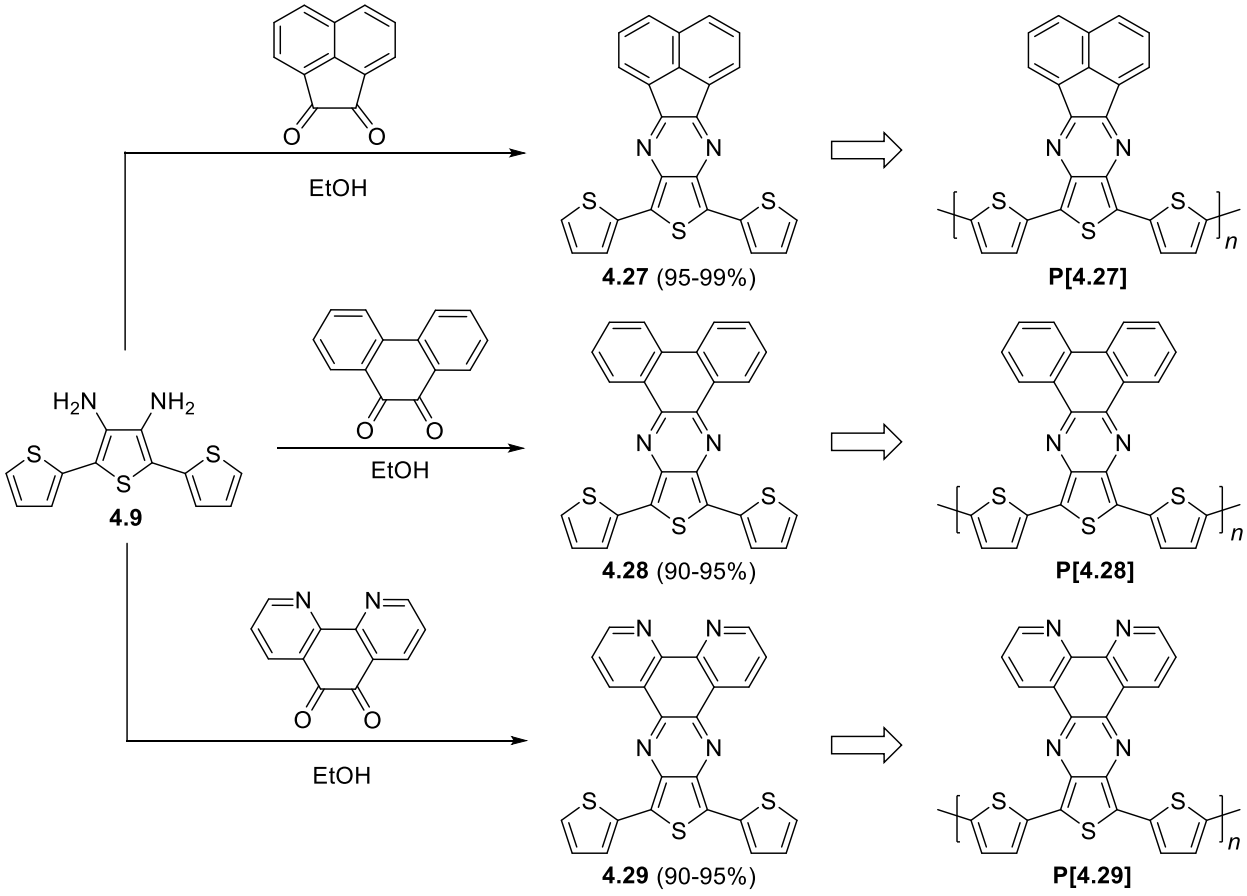

Scheme 4.5. Synthesis of extended fused-ring TP-based terthienyls **4.27-4.29** and corresponding electropolymerized polymeric materials **P[4.27]-P[4.29]**

Due to the low solubility of the products, the product precipitated immediately upon formation in hot ethanol. Nearly quantitative yields (90-99%) of product were isolated, after collection via filtration and purification with simple solvent washes. Previously reported yields of **4.27-4.29** were much lower (62-83%), and it is believed that the isolated difference in the products reported here is the result of a much higher quality of **4.9**, the synthesis of which was discussed earlier in the chapter (section 4.2). Monomers **4.27-4.29** were then electropolymerized to form their corresponding homopolymers **P[4.27]**, **P[4.28]**, and **P[4.29]**, and these corresponding materials are also shown in Scheme 4.5.

4.5.2. Spectroscopy and electrochemistry of extended fused-ring TP-based terthienyls

The absorption spectra of terthienyls **4.27-4.29** are displayed in Figure 4.11 and spectral data for these materials are tabulated in Table 4.4. Also included in the table is the spectral data for thieno[3,4-*b*]pyrazine-based terthienyl analogues **4.10b** (R = CH_3, Scheme 4.2) and **4.10g** (R = Ph, scheme 4.2) to provide a comparison to the non-fused-ring species. As discussed previously, the lowest energy absorption is a broad ICT band resulting from a transition between a predominately thiophene-localized HOMO and a LUMO of greater pyrazine contribution. The addition of the 2-thienyls at the 5- and 7-positions of the TP unit results in a HOMO now delocalized across the entire terthienyl backbone. The extinction coefficients (ε) and oscillator strengths (*f*) of these transitions are also low in comparison to the simpler analogue α-terthiophene ($\varepsilon = 22100\ M^{-1}\ cm^{-1}$, $\lambda_{max} = 354$ nm).[104] This is due to the reduced "allowedness" of the ICT transition in the TP as a result of limited spatial overlap of the molecular orbitals involved in these transitions.[105] As the fused-ring character of the TP-based terthienyls increases (**4.27-4.29** compared to **4.10b, 4.10g**), the molar absorptivities and oscillator strength, a dimensionless quantity that refers to the probability of absorption, decrease, which is to be

expected. These trends also agree closely with those of the analogous monomeric extended fused-ring TPs,[45] although with nearly double the absorption intensities, a result of the increase in cross-sectional area of the terthienyls, and red shifts of 150-200 nm, a result of the extension of the conjugated backbone.

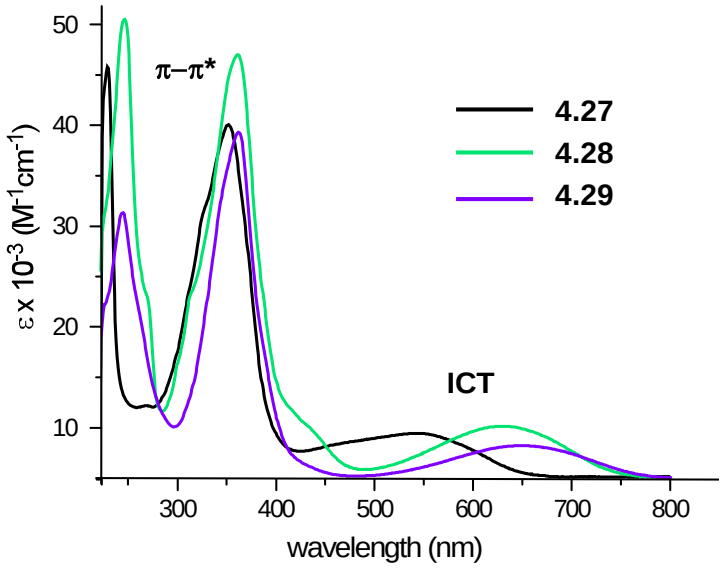

Figure 4.11. UV-visible spectra of TP-based terthienyls **4.27-4.29**

Table 4.4. UV-visible spectral data for thieno[3,4-*b*]pyrazine-based terthienyls[a]

Terthienyl	$S_0 \rightarrow S_1$ (ICT)			$S_0 \rightarrow S_2$ ($\pi \rightarrow \pi^*$)		
	λ_{max} (nm)	ε (M^{-1} cm^{-1})	*f*	λ_{max} (nm)	ε (M^{-1} cm^{-1})	*f*
4.10b[43,b]	492	12100	0.242	339	21000	0.268
4.10g[43,b]	540	7800	0.123	338	45100	0.908
4.27	547	5000	0.139	352	40400	0.822
4.28	629	5800	0.097	361	47500	1.183
4.29	644	3800	0.060	360	39300	0.793

[a]In CH_2Cl_2; S_0 = singlet ground state; S_1 = first singlet excited state; S_2 = second singlet excited state; ICT = intramolecular charge transfer; λ_{max} = wavelength of absorbance maximum; ε = extinction coefficient; *f* = oscillator strength; [b]In CH_3CN.

Besides the ICT band, a stronger set of bands attributed to of π→π* transitions are exhibited in the higher energy region of the spectrum. These absorptions correspond to strongly allowed transitions, with molar absorptivities of 39-48x10^3 M^{-1} cm^{-1} for the extended fused ring analogues, compared to molar absorptivities of 21-45x10^3 M^{-1} cm^{-1} for the traditional TP-based terthienyls.[43] It is quite possible that these are not just simple singular transitions for **4.27-4.29**, but rather the overlap of multiple localized π→π* transitions. This is because the energies of these transitions agree well with the absorption energies reported for α-terthiophene,[104] and also with localized π→π* transitions of acenapthylene,[106] phenanthrene,[107] and 1,10-phenanthroline.[108]

Cyclic voltammograms (CVs) of species **4.27-4.29** are shown in Figure 4.12 and the electrochemical data is tabulated in Table 4.5. Similar to previously reported TP-based terthienyls, there is a well-defined irreversible oxidation assigned to the oxidation of the terthiophene backbone and a quasi-reversible pyrazine-based reduction. Typical for most thiophene species, the irreversible nature of the oxidation is the result of formation of thiophene-based radical cations that undergo rapid coupling to produce higher weight oligomeric and polymeric species.[43] In these terthienyl species, the central TP only makes up one-third of the terthienyl backbone, resulting in quite uniform oxidations across the series. However, as the HOMO is delocalized across the backbone, this results in significant destabilization (700-800 mV) of the HOMO energy in the terthienyls **4.27-4.29** compared to the analogous TP monomers **4.22-4.24** (E_{HOMO} = -6.20 to -6.52 V), and more significant deviations in oxidation potentials of the monomers too.[45] Also, the most easily oxidized terthienyl **4.28** is also the most easily oxidized monomer **4.23** (E_{pa} = 0.98 mV).[45]

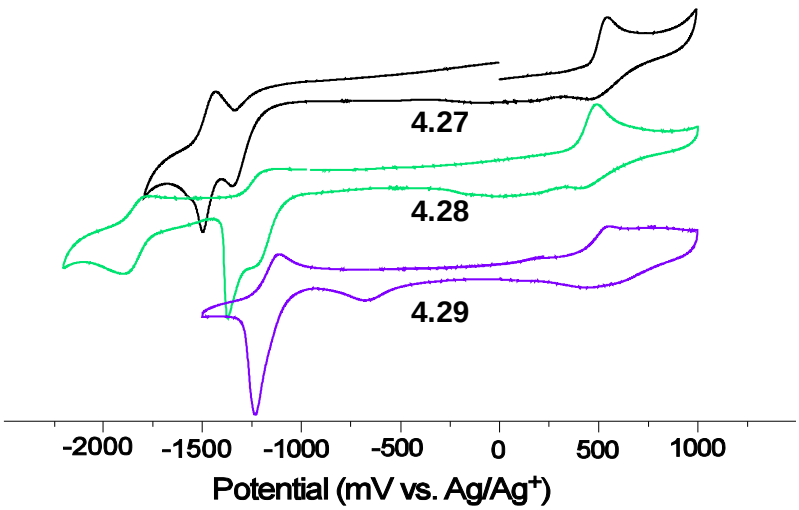

Figure 4.12. Cyclic voltammograms of extended fused-ring thieno[3,4-*b*]pyrazine-based terthienyls **4.27-4.29**

Table 4.5. Electrochemical data for thieno[3,4-*b*]pyrazine-based terthienyls[a]

Terthienyl	Oxidation			Reduction			
	E_{pa} (V)	$E_{1/2}$ (red1, V)	ΔE (mV)	E_{pc} (red2, V)	ΔE (mV)	E_{HOMO} (eV)[b]	E_{LUMO} (eV)[b]
4.10b[43,c]	0.50	-1.68	100	-	-	-5.39	-3.46
4.10g[43,c]	0.54	-1.46	80	-	-	-5.41	-3.80
4.27	0.49	-1.35[d]	-	-2.55	100	-5.37	-3.82
4.28	0.43	-1.28	80	-1.90	120	-5.29	-3.86
4.29	0.51	-1.23	100	-1.82	130	-5.40	-3.91

[a]All potentials vs. Ag/Ag^+. In CH_2Cl_2 containing 0.10 M $TBAPF_6$; E_{pa} = aniodic peak potential; $E_{½}$ = half-wave potential; ΔE = peak separation; E_{pc} = cathodic peak potential; [b]$E_{HOMO} = -(E_{[onset, ox vs Fc+/Fc]} + 5.1)$(eV); $E_{LUMO} = -(E_{[onset, red vs Fc+/Fc]} + 5.1)$(eV).[79] [c]In CH_3CN containing 0.10 M $TBAPF_6$. [d]Irreversible, E_{pc} reported.

The differences in reduction potentials however are greater, as a result of the LUMO being relatively pyrazine-localized and thus all functionalization or ring-fusion that occurs on the pyrazine-ring has a more significant effect on the reduction. The species **4.27-4.29** undergo reduction at lower potentials than the non-extended fused-ring species **4.10b** and **4.10g**,[41,43] a

result of the extended conjugation provided by the fused rings. Two distinct reduction processes are observed for **4.27-4.29** within the solvent window. **4.27** has a slightly destabilized LUMO (E_{pc} = -2.55 V) in comparison to the two other terthienyls, and this is likely because it has two fewer π-electrons. Although **4.28** and **4.29** are isostructural to each other, the additional nitrogens in **4.29** further stabilizes it to give it the lowest reduction potential in the series. Finally, the strong adsorption spikes observed directly following the reductions are the result of analyte strongly adsorbing to the electrode, which is most likely facilitated here by the large planar structures of the extended fused-ring terthienyls.

4.5.3. Electropolymerization of TP-based terthienyls and characterization of polymers

Although most current efforts to produce soluble, processible materials are focused on organometallic cross-coupling methods and the growing field of direct arylation, the ability to produce polymer films onto an electroactive species provides a simple means to electrochemically and optically characterize the resulting materials. A major advantage of electropolymerization is that it allows for the direct comparison of materials while minimizing the effects of differences in solubility or processability.[32,109,110.] Potential cycling through the irreversible oxidation of **4.27-4.29** resulted in the incremental growth of the corresponding conjugated polymer film **P[4.27]-P[4.29]** on the surface of the working electrode. Figure 4.13 shows the growth of the film **P[4.29]** with potential cycling, where the oxidation wave of the initial terthienyl shifts to lower potential with the increase in current, which corresponds to the growth of the polymer film. The lowest potential E_{pa} shifts by *ca*. 360 mV in comparison to the initial terthienyl **4.29**, which is in contrast to the electropolymerization of simple terthienyls like **4.10g**, which although there is a shift in the oxidation onset to lower potential, there is no

significant shift in the polymer E_{pa}. This suggests that the polymer films **P[4.27]-P[4.29]** contain fewer chains of lower conjugation length than the film for **4.10g**.

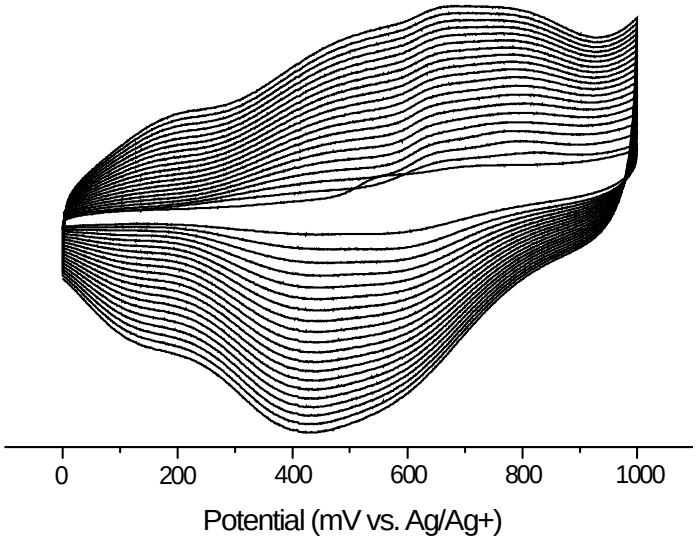

Figure 4.13. Growth of polymer **P[4.29]** with potential cycling

Representative CVs of the electropolymerized polymers **P[4.27]-P[4.29]** are shown in Figure 4.14 and electrochemical data is tabulated in Table 4.6.

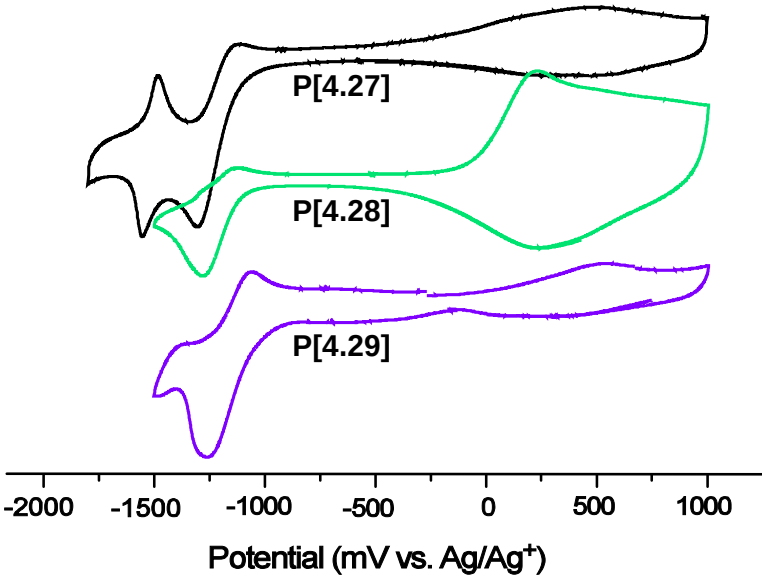

Figure 4.14. Cyclic voltammograms of extended fused-ring TP polymers **P[4.27]-P[4.29]**

As discussed earlier, typical of most TP-based materials, these polymer films exhibit amphoteric redox properties which consist of relatively broad oxidation waves and sharper, more well-defined reductions. The peak potentials for both the oxidation (E_{pa}) and reduction (E_{pc}) processes follow the same general trends seen in both the monomers **4.22-4.24**[45] and terthienyls **4.27-4.29** (Table 4.5).

Table 4.6. Electrochemical data for polymer films **P[4.27]-P[4.29]** and analogues

Polymer	**Oxidation**		**Reduction**				
	E_{pa} (V)	**E_{onset} (V)**	**E_{pc} (V)**	**E_{onset} (V)**	**E_{HOMO} (eV)**[b]	**E_{LUMO} (eV)**[b]	**E_g^{elec} (eV)**
P[4.10b][32,c]	0.54, 0.85	0.32	-1.48,-1.82	-1.24	-5.37	-3.81	1.56
P[4.10g][32,c]	0.58	0.33	-1.39	-1.00	-5.38	-4.05	1.33
P[4.27]	0.45	-0.25	-1.37,-1.63	-1.05	-4.80	-4.00	0.80
P[4.28]	0.24	-0.07	-1.28	-0.95	-4.98	-4.10	0.88
P[4.29]	0.51	0.00	-1.25	-0.90	-5.05	-4.15	0.90

[a]All potentials vs. Ag/Ag^+. In CH_2Cl_2 containing 0.10 M $TBAPF_6$; E_{pa} = aniodic peak potential; E_{onset} = onset potential; E_{pc} = cathodic peak potential; E_g^{elec} = electrochemical band gap; [b]$E_{HOMO} = -(E_{[onset, ox vs Fc+/Fc]} + 5.1)(eV)$; $E_{LUMO} = -(E_{[onset, red vs Fc+/Fc]} + 5.1)(eV)$.[79] [c]In CH_3CN containing 0.10 M $TBAPF_6$.

In contrast to the other polymer films, the onset of oxidation for **P[4.28]** is quite sharp, resulting in a HOMO energy level that is deeper than anticipated. This sharper onset and more defined oxidation could be the result of reduced polydispersity, with fewer segments of higher conjugation lengths in the polymer films formed. Otherwise, all the HOMO and LUMO energy levels for the polymers **P[4.27]-P[4.29]** in Table 4.6 follow expected trends, resulting in low band gaps between 0.80-.90 eV for the extended fused-ring terthienyl TP polymers. These E_g values are lower than that of any TP-based terthienyl copolymers,[29,38,70,91-98,101,103] and only two homopolymers of the non-terthienyl acenaphtho[1,2-*b*]thieno[3,4-*e*]pyrazine moiety have been

reported in the literature to give lower band gaps.[29,44,89] This is consistent with previous reports that TP and its terthienyl analogues are stronger donors than nearly all other commonly applied building blocks,[31,34,36,37,42] and therefore the inclusion of additional monomeric units stabilizes the polymer HOMO which leads to an increase in E_g. As **P[4.27]-P[4.29]** are limited to only the 2-thienyl groups as additional monomeric units, the overall TP content in the backbone is high in comparison which gives higher HOMO levels and lower E_g values.

Terthienyls **4.27-4.29** were then electropolymerized onto indium tin oxide (ITO) plates, which allowed for the measurement of the absorption spectra of the corresponding thin films **P[4.27]-P[4.29].** The collected data is tabulated in Table 4.7. In concurrence with the monomers, the polymers exhibit a low energy ICT transition in the visible-NIR (near infrared) region and a $\pi \rightarrow \pi^*$ transition at higher energy. The trends in these optical data (λ_{max} = 750, 880, and 1060 for **P[4.27]-P[4.29]**, respectively) agree well with the trends observed in the optical characterization of the terthienyl precursors (Table 4.4, λ_{max} = 547, 627, 644 for **4.27-4.29**, respectively). The more significant differences in absorption properties of the polymer films observed for **P[4.28]** and **P[4.29]** in comparison to **P[4.27]** could at least partially be to **P[4.28]** potentially containing segments of lower conjugation lengths (as proposed earlier). The optical band gaps (E_g^{opt}) determined from absorption onsets (0.82-.0.99 eV, Table 4.7) agree well with the trends observed for the electrochemical measurements of the polymer films (0.80-0.90 eV, Table 4.6). Finally, comparison of **P[4.28]** to its previously reported dihexylfluorene-functionalized analogue reveals a significant difference in E_g (0.89 eV vs. 1.21 eV).[101] This could either be the result of the analogue being of limited molecular weight, or the two dihexylfluorene groups attached to the central TP impart significant steric hinderance which reduces planarity and limits conjugation.

Table 4.7. Absorption data for polymer films **P[4.27]-P[4.29]**[a]

Polymer	λ_{max} (nm)	λ_{onset} (nm)	E_g^{opt} (eV)
P[4.10b][32]	626	850	1.46
P[4.10g][32]	712	1230	1.01
P[4.27]	750	1250	0.99
P[4.28]	880	1400	0.89
P[4.29]	1060	1510	0.82

[a]Measured as films electropolymerized onto ITO slides; λ_{max} = wavelength of absorbance maximum; λ_{onset} = wavelength of absorbance onset; E_g^{opt} = optical band gap.

4.5.4. Conclusions to extended fused-ring TP-based terthienyl polymers

TP-based terthienyls containing extended fused-ring units (**4.27-4.29**) have been optically and electrochemically characterized, to reveal that these species follow the same trends in properties as their respective monomeric units (**4.22-4.24**). Electropolymerization of terthienyls **4.27-4.29** afforded low band gap materials (E_g = 0.80-1.00 eV) **P[4.27]-P[4.29]** whose polymer films match the trends of both the terthienyls (**4.27-4.29**) and the initial monomeric TP analogues (**4.22-4.24**). The fact that these trends hold consistent from monomer to terthienyl to polymer strengthens the claim that the ambipolar nature of TPs and their extended terthienyl analogues contributes completely to both the HOMO and LUMO of any resulting TP-based material. Resultingly, the electronic nature of the ambipolar TP unit has the greatest impact on the determination of the HOMO and LUMO levels and the band gap of TP-based materials.

4.6. Conclusions

A series of investigations have been performed in which fused-ring thieno[3,4-*b*]pyrazines and TP-based terthienyls have been both chemically and electrochemically polymerized to observe how structural changes affect the material properties. Although not all of

these investigations were successfully concluded (i.e. TP-thiophene polymerizations), the results obtained provided continued support that the TP moiety is an ambipolar unit, that when incorporated into conjugated materials, holds consistent trends between the TP monomer, TP-based terthienyl monomer, and resulting polymers. Additionally, this highlights the importance of structure-function relationships and provides further data to support the design of new CP materials that can be tuned for advantageous material properties.

4.7. Experimental Methods

4.7.1. General

Unless noted, all materials were reagent grade and used without further purification. Dry THF and toluene were obtained via distillation over sodium benzophenone. CH_3CN were dried over CaH_2 and distilled prior to use. DMF and CH_2Cl_2 were dried over $MgSO_4$, filtered through silica gel, degassed with N_2, and stored over molecular sieves (size 4A) for at most 3 days. All glassware was oven-dried, assembled hot, and cooled under a dry N_2 stream before use. Transfer of liquids was carried out using standard syringe techniques and all reactions were performed under a dry N_2 stream. Chromatographic separations were performed using standard column chromatography methods with silica gel (230– 400 mesh). Melting points were determined using a digital thermal couple with a 0.1 °C resolution. ^{1}H and ^{13}C NMR spectra were obtained in $CDCl_3$ on a 400 MHz spectrometer (Bruker Corporation, Pittsburgh, PA, USA) and referenced to the $CHCl_3$ signal. Peak multiplicity is reported as follows: s = singlet, d = doublet, dd = doublet of doublets, dt = doublet of triplets, t = triplet, p = pentet, m = multiplet and br = broad. Coupling constants *J* are given in Hertz. High resolution mass spectrometry (HRMS) was obtained on a mass spectrometer (Waters, Boston, MA, USA) with electrospray ionization and quantitative

time of flight. The following was synthesized as previously reported: 9,9-diocyl-2,7-bis(4,4',5,5'-tetramethyl-1,3,2-dioxaborolan-2-yl)-9*H*-fluorene.[111]

4.7.2. Synthesis

3',4'-diamino-2,2':5',2"-terthiophene (4.9). The following is a modification of previously reported methods.[32] Precursor **4.8** (11.4 g, 33.7 mmol) and $SnCl_2$ (57.5 g, 303 mmol) were added to a flask equipped with a condenser, followed by ethanol (150 mL) and HCl (150 mL). The flask was evacuated and backfilled with N_2, after which the suspension was heated at reflux with stirring overnight. The solution was cooled to 0 °C, filtered, and washed with diethyl ether to give a tan-green solid. This salt was then added to 100 mL H_2O at 0 °C and 1 M KOH solution added dropwise until the solution turned basic (pH 7-8). The product was extracted from the basic solution with CH_2Cl_2, and the combined organic extracts were washed with H_2O, dried over $MgSO_4$, and the solvent was removed via rotatory evaporation to yield a golden yellow solid (80%–85%) (Note: If stored in the dark at reduced temperature, **4.9** is stable for a period of several months). mp 97.5–98.6 °C (lit. mp 96.0–96.5 °C)[41]; ^{1}H NMR ($CDCl_3$) δ 7.27 (dd, *J* = 1.4, 4.8 Hz, 2H), 7.10 (dd, *J* = 1.4, 3.7 Hz, 2H), 7.08 (dd, *J* = 3.7, 4.8 Hz, 2H), 3.67 (br s, 4H); ^{13}C NMR ($CDCl_3$) δ 136.0, 133.6, 127.8, 124.0, 123.9, 110.2.

2,3-Dioctyl-5,7-bis(2-thienyl)thieno[3,4-*b*]pyrazine (4.10e) The following is similar to previously reported methods.[52] **4.9** (0.10 g, 0.36 mmol) and octadecane-9,10-dione (0.16 g, 0.58 mmol) were added to methanol (15 mL). The mixture was heated to reflux for 1.5 h under an N_2 atmosphere, and then cooled to room temperature where a dark-red precipitate formed. The product was then concentrated under vacuum, and purified by silica chromatography (hexanes) and recrystallized in absolute EtOH to give 0.17 g (89 %) of a dark red solid; mp 97–98 °C; ^{1}H NMR ($CDCl_3$) 7.63 (dd, *J* = 1.2, 3.7, 2H), 7.37 (dd, *J* = 1.2, 5.1, 2H), 7.11 (dd, *J* = 3.7, 5.1, 2H),

2.93 (t, *J* = 7.6, 4H), 1.98 (p, *J* = 7.3, 4H), 1.53 (m, 4H), 1.49–1.27 (m, 16H), 0.91 (t, *J* = 6.8, 6H). ^{13}C NMR ($CDCl_3$) δ 156.4, 137.7, 135.0, 127.1, 126.1, 123.9, 123.6, 35.0, 32.0, 29.7, 29.5, 29.3, 26.9, 22.7, 14.1.

5,7-Bis(5-bromo-2-thienyl)-2,3-dioctylthieno[3,4-*b*] pyrazine (4.14). Terthienyl **4.10e** (0.17 g, 0.32 mmol) was added to a 250-mL round-bottom flask while N-bromosuccinimide (NBS) (0.13 g, 0.71 mmol) was added to an attached addition funnel. A 50 : 50 mixture of AcOH /$CHCl_3$ (100 mL) was added to the flask, with another 50 mL added to the addition funnel. The NBS solution was added dropwise over 1 h under N_2 at -5 °C. The reaction was then stirred 3 h at room temperature in the dark, poured into H_2O, extracted with $CHCl_3$ (3x50 mL), and the combined organic phases were then washed with 1 M KOH, H_2O, and then dried over $MgSO_4$. The product was then concentrated under vacuum and purified by silica chromatography (1 % CH_2Cl_2 in petroleum spirits) to give 0.056 g (26 %) of a dark red solid; mp 139–141 °C; ^{1}H NMR ($CDCl_3$) δ 7.22 (d, *J* = 3.9, 2H), 7.03 (d, *J* = 3.9, 2H), 2.90 (t, *J* = 7.4, 4H), 1.96 (p, *J* = 7.3, 4H), 1.53 (m, 4H), 1.47–1.29 (m, 16H), 0.92 (t, *J* = 6.8, 6H). ^{13}C NMR 156.9, 137.6, 136.3, 129.5, 123.2, 123.0, 114.1, 35.0, 32.0, 29.7, 29.4, 29.3, 26.8, 22.7, 14.2.

Poly(2,3-dioctyl-5,7-bis(2-thienyl)thieno[3,4-b]pyrazineco-9,9-dioctyl-9H-fluorene) (4.12i). To a 50-mL Schlenk tube was added **4.14** (0.047 g, 0.069 mmol), 9,9-diocyl-2,7-bis(4,4',5,5'-tetramethyl-1,3,2-dioxaborolan-2-yl)-9*H*-fluorene (0.047 g, 0.072 mmol), and $Pd(PPh_3)_2Cl_2$. The tube was then evacuated and backfilled five times with N_2, and then N_2-purged 1.5 M K_2CO_3 (1.0 mL) and toluene (10 mL) were added and the reaction was heated to 90 °C for 3 days. Bromobenzene (1.0 mL of 0.0035 mL per 5 mL solution in toluene, 0.0069 mmol) was then added and the solution stirred for 2 h, after which phenylboronic acid (1.0 mL of 0.0040 g per 5 mL solution in toluene, 0.0069 mmol) was added and the reaction stirred

overnight. The reaction was then cooled to room temperature, and the product concentrated under vacuum and precipitated in MeOH (100 mL). The crude polymer was purified by Soxhlet extraction with MeOH, acetone, and hexanes and then collected with $CHCl_3$. The polymer was concentrated via rotary evaporation to produce a dark-blue solid (15 %). ^{1}H NMR ($CDCl_3$) δ 7.71, 7.56, 7.43, 7.25, 7.06, 2.96, 2.08, 1.70–0.62. GPC: M_n, 54000; M_w, 78400; PDI, 1.4.

2,3-Didodecylthieno[3,4-*b*]pyrazine (4.7i). The following is a modification of previously reported methods.[49] Hexacosane-13,14-dione (1.97 g, 5.00 mmol) was added to 500 mL 3-neck rbf, followed by absolute ethanol (300 mL). After all the dione was dissolved with the help of heat gun, 3,4-diaminothiophene (0.571 g, 5.00 mmol) was added. Solution was evacuated/backfilled 3x with N_2 and stirred at rt for 4 h. Solution was quenched with H_2O (100 mL), extracted with DCM, and then washed with brine. Organic extracts were dried over Na_2SO_4, and solvent was removed via rotatory evaporation. Product was purified via silica gel column chromatography (~2% EtOAC/hexanes) and further recrystallized in hexanes to yield tan solid, 60-70% yield.

5,7-Dibromo-2,3-didodecylthieno[3,4-*b*]pyrazine (4.16). The following is a modification of previously reported methods.[112] A solution of recrystallized NBS (2.22 g, 12.5 mmol) in N_2-purged, dry DMF (10 mL) was added dropwise to -78°C (dry ice/acetone) solution of 2,3-didodecylthieno[3,4-b]pyrazine **4.7i** (2.36 g, 5.00 mmol) in DMF (100 mL) that was under N_2. The mixture was then stirred at 0°C for ~5 h under N_2, until TLC shows complete conversion of product (blue spot to yellow). Poured solution onto ice and extracted with Et_2O, washed with 5 x 100 mL NH_4Cl, and then dried over $MgSO_4$ and removed solvent via rotatory evaporation. Purify product by silica gel column chromatography with 2% Et_2O in hexanes. Recrystallized in hexanes for further purification, 60-70% yield.

Poly(2,3-didodecylthieno[3,4-*b*]pyrazine-*alt*-thiophene) (4.18). 5,7-dibromo-2,3-didodecylthieno[3,4-*b*]pyrazine (0.250 g, 0.396 mmol), 2,5-bis(trimethylstannyl) thiophene [**4.17**, commercially purchased] (0.162 g, 0.396 mmol), tris(dibenzylideneacetone)-dipalladium(0) (0.0091 g, 0.0091 mmol), and tri(o-tolyl)phosphine (0.0120 g, 0.036 mmol) were added to a 50 mL Schlenk tube and then evacuated/backfilled with N_2 5x. N_2 bubbled toluene (10 mL) was then added and the reaction was evacuated/backfilled with N_2 5x. The reaction was then heated and stirred at 90-95 °C for 5 days (5 x 24 h). Reaction was cooled and transferred to flask with MeOH (100 mL) and precipitated. Collected solid was then cleaned via soxhlet extraction with methanol, acetone, hexanes, and then chloroform to yield a chloroform-soluble product (0.125 g, 57 %) and insoluble product (0.074 g, 1 %).

Poly(2,3-didodecylthieno[3,4-*b*]pyrazine-*alt*-thieno[3,2-*b*]thiophene) (4.20). 5,7-dibromo-2,3-didodecylthieno[3,4-*b*]pyrazine **4.16** (0.250 g, 0.396 mmol), 2,5-bis(trimethylstannyl)-thieno[3,2-*b*]thiophene [**4.19**, commercially purchased] (0.184 g, 0.396 mmol), tris(dibenzylideneacetone)dipalladium(0) (0.0091 g, 0.0091 mmol), and tri(o-tolyl)phosphine (0.0120 g, 0.036 mmol) were added to a 50 mL Schlenk tube and then evacuated/backfilled with N_2 5x. N_2 bubbled toluene (10 mL) was then added and the reaction was evacuated/backfilled with N_2 5x. The reaction was then heated and stirred at 90-95 °C for 5 days (5 x 24 h). Reaction was cooled and transferred to flask with MeOH (100 mL) and precipitated. Collected solid was then cleaned via soxhlet extraction with methanol, acetone, hexanes, and then chloroform to yield a chloroform-soluble product (0.195 g, 81 %).

Poly(2,3-didodecylthieno[3,4-*b*]pyrazine-*ran*-thieno[3,2-*b*]thiophene -*ran*-thiophene) (4.21). 5,7-dibromo-2,3-didodecylthieno[3,4-*b*]pyrazine **4.16** (0.150 g, 0.238 mmol), 2,5-bis(trimethylstannyl) thiophene **4.17** (0.0487 g, 0.119 mmol), 2,5-bis(trimethylstannyl)-

thieno[3,2-*b*]thiophene **4.19** (0.0554 g, 0.119 mmol), tris(dibenzylideneacetone)dipalladium(0) (0.0054 g, 0.0060 mmol), and tri(o-tolyl)phosphine (0.0072 g, 0.024 mmol) were added to a 50 mL Schlenk tube and then evacuated/backfilled with N_2 5x. N_2 bubbled toluene (10 mL) was then added and the reaction was evacuated/backfilled with N_2 5x. The reaction was then heated and stirred at 90-95 °C for 4 days (4 x 24 h). Reaction was cooled and transferred to flask with MeOH (100 mL) and precipitated. Collected solid was then cleaned via soxhlet extraction with methanol, acetone, hexanes, and then chloroform to yield a chloroform-soluble product (0.094 g, 68 %).

8,10-Bis(2-thienyl)acenaphtho[1,2-*b*]thieno[3,4-*e*]pyrazine (4.27). Diamine **4.9** (278 mg, 1.00 mmol) and 1,2-acenaphthylenedione (1.20 mmol) were added to a 100 mL 3-neck flask equipped with a condenser, which was then evacuated and backfilled with N_2 three times. Absolute EtOH (50 mL) was then added and the mixture heated to reflux overnight with stirring until a colored precipitate formed. The reaction was then cooled to room temperature and filtered. The collected precipitate was washed well with first ethanol and then hexanes to yield a dark purple solid (95%–99% yield). mp ~330 °C (dec); ^{1}H NMR ($CDCl_3$, 50 °C) δ 8.37 (d, J = 7.1 Hz, 2H), 8.08 (d, J = 8.3 Hz, 2H), 7.83 (dd, J = 7.1, 8.3 Hz, 2H), 7.78 (dd, J = 1.2, 3.6 Hz, 2H), 7.44 (dd, J = 1.2, 5.1 Hz, 2H), 7.17 (dd, J = 3.6, 5.1 Hz, 2H). The ^{1}H NMR spectrum data agree well with previously reported values;[96] ^{13}C NMR not obtained due to low solubility; HRMS m/z 424.0189 [M+] (calcd for $C_{24}H_{12}N_2S_3$ 424.0163).

10,12-Bis(2-thienyl)dibenzo[*f*,*h*]thieno[3,4-*b*]quinoxaline (4.28). Diamine **4.9** (278 mg, 1.00 mmol) and 9,10-phenanthrenedione (1.20 mmol) were added to a 100 mL 3-neck flask equipped with a condenser, which was then evacuated and backfilled with N_2 three times. Absolute EtOH (50 mL) was then added and the mixture heated to reflux overnight with stirring

until a colored precipitate formed. The reaction was then cooled to room temperature and filtered. The collected precipitate was washed well with first ethanol and then hexanes to yield a dark green solid (90%–95% yield). mp ~290 °C (dec); ^{1}H NMR ($CDCl_3$, 50 °C) δ 9.32 (dd, *J* = 2.0, 7.8 Hz, 2H), 8.45 (dd, *J* = 1.4, 7.8 Hz, 2H), 7.77 (dd, *J* = 1.0, 3.7 Hz, 2H), 7.75 (dt, *J* = 2.0, 7.8 Hz, 2H), 7.71 (dt, *J* = 1.4, 7.8 Hz, 2H), 7.49 (dd, *J* = 1.0, 5.2 Hz, 2H), 7.19 (dd, *J* = 3.7, 5.2 Hz, 2H). ^{13}C NMR not obtained due to low solubility; HRMS m/z 450.0320 [M+] (calcd for $C_{26}H_{14}N_2S_3$ 450.0319).

10,12-Bis(2-thienyl)thieno[3',4':5,6]pyrazino[2,3-*f*][1,10]phenanthroline (4.29). Diamine **4.9** (278 mg, 1.00 mmol) and 1,10-Phenanthroline-5,6-dione (1.20 mmol) were added to a 100 mL 3-neck flask equipped with a condenser, which was then evacuated and backfilled with N_2 three times. Absolute EtOH (50 mL) was then added and the mixture heated to reflux overnight with stirring until a colored precipitate formed. The reaction was then cooled to room temperature and filtered. The collected precipitate was washed well with first ethanol and then hexanes to yield a dark turquoise solid (90%–95% yield). mp ~360 °C (dec); ^{1}H NMR ($CDCl_3$, 50 °C) δ 9.15 (dd, *J* = 2.0, 8.0 Hz, 2H), 9.10 (dd, *J* = 2.0, 4.3 Hz, 2H), 7.55 (dd, *J* = 4.3, 8.0 Hz, 2H), 7.47 (dd, *J* = 1.1, 3.7 Hz, 2H), 7.40 (dd, *J* = 1.1, 5.1 Hz, 2H), 7.08 (dd, *J* = 3.7, 5.1 Hz, 2H). ^{13}C NMR not obtained due to low solubility; HRMS m/z 453.0316 [M + H]+ (calcd for $C_{24}H_{12}N_4S_3H$ 453.0302).

4.7.3 Absorption Spectroscopy

UV-visible spectra were measured on a dual beam scanning spectrophotometer (Varian, Mulgrave, Australia) using samples prepared as dilute CH_2Cl_2, $CHCl_3$, or CH_3CN solutions in 1 cm quartz cuvettes or polymer films cast onto glass slides. Oscillator strengths were determined from the visible spectra via spectral fitting to accurately quantify the area of each transition and

then calculated using literature methods.[113] Visible-NIR spectra of the polymeric materials were measured as polymer films on ITO-coated glass plates. Optical band gaps were determined from the absorption onset of the lowest-energy transition as previously described.[28]

4.7.4. Electrochemistry

All electrochemical methods were performed on a BAS Potentiostat utilizing a three-electrode cell consisting of platinum disc working electrode, a platinum wire auxiliary electrode, and a Ag/Ag^+ reference electrode (0.251 V vs. saturated calomel electrode (SCE)).[113] Supporting electrolyte consisted of 0.10 M $TBAPF_6$ in dry CH_3CN or CH_2Cl_2. Solutions were deoxygenated by sparging with argon prior to each scan and blanketed with argon during the measurements. All measurements were collected at a scan rate of 100 mV/s. Solutions of polymers in $CHCl_3$ were drop-cast on the working electrode and dried to form a solid film. E_{HOMO} and E_{LUMO} values were estimated from the onset of oxidation and reduction in relation to ferrocene (50 mV versus Ag/Ag^+), using the value of 5.1 eV versus vacuum for ferrocene.[79]

4.7.5. Electropolymerizations

Electropolymerizations of **4.27-4.29** were carried out in a three-electrode cell consisting of a platinum disc working electrode, a platinum wire auxiliary electrode, and Ag/Ag^+ reference electrode. Solutions consisted of oligomer dissolved in anhydrous CH_3CN or CH_2Cl_2 containing 0.10 M tetrabutylammonium hexafluorophosphate ($TBAPF_6$). The solutions were deoxygenated by sparging with argon prior to each scan and blanketed with argon during the polymerizations. The platinum disc working electrode was polished with 0.05 mm alumina and washed well with deionized water and dry solvent prior to each film growth. The films were grown by cyclic voltammetry scanning through the E_{pa} region for each oligomer. Electropolymerizations for optical experiments were carried out in the same manner as discussed above except an ITO-

coated glass plate was used as the working electrode. Polymer films were grown by continuous repeated potential cycling around the E_{pa} for each monomer until a suitable film was obtained and then held at a fixed potential corresponding to the neutral form of the polymer under investigation

4.7.6. OPV Device Fabrication

Organic solar cells were fabricated by Trent Anderson on patterned indium tin oxide (ITO) glasses with a sheet resistance of 20 Ω per square. The ITO was cleaned by ultrasonic treatment in detergent, deionized water, acetone, and isopropanol, and then treated in a bench-top plasma cleaner for 2 min. Poly(3,4-ethylenedioxythiophene):poly(styrenesulfonate) (PEDOT:PSS, Clevious P VP AI 4083, H. C. Stark, Germany) solution was filtered through a 0.45-mm filter and then spin-coated at 4000 rpm for 60 s on the ITO electrode, and then heated at 100 °C for 40 min. The PEDOT:PSS-coated substrates were transferred to an N_2-filled glovebox. The polymer and PCBM solutions were prepared in 0.3 mL of o-dichlorobenzene (7 mg for **4.12i**) before spin-coating onto the PEDOT:PSS layer at 400 rpm for 45 s. After 1 h of aging, blend films were thermally annealed at 105 °C for 5 min. The cells were completed with a cathode consisting of LiF (~1 nm) and Al (~100 nm), which were thermally evaporated on the active layer under a shadow mask in a base pressure of $1x10^{-4}$ Pa. The device active area was ~7.9 mm^2 for all the solar cells and J-V measurement of the devices was conducted on a computer-controlled Keithley 2400 source meter. The J-V measurement system uses a solar simulator with a Class-A match to the AM1.5 Global Reference Spectrum. It is calibrated with KG5-filtered silicon reference cell with calibration traceable to the National Renewable Energy Laboratory (NREL) and National Institute of Standards and Technology (NIST).

4.7.7. Modeling of 2nd Order Effects in the 1H NMR

The enhanced purity of **4.9** reported is also supported by the ability to fully resolve the ^{1}H NMR signals at *ca.* 7.1 ppm, which have previously always been reported as a generic multiplet. To verify the assignment of peaks in the NMR as two strongly coupled doublet of doublets, the experimentally determined coupling constants and chemical shifts were used to simulate the NMR spectrum. This was accomplished using a freely available NMR simulator[114] which could accurately model the 2nd order effects inherent from the close spacing of the coupled multiplets.[115] The values for the modeling are as follows: Spin system (ABC), delta 1 (7.1018 ppm), delta 2 (7.0848 ppm, J1-2 3.65 Hz), delta 3 (7.2714 ppm, J1-3 = 1.44 Hz, J2-3 = 4.84 Hz), From (7.0-7.3 ppm), Field strength (400 MHz), Line width (0.5 Hz). Figure 4.15 shows a comparison between the modeled spectrum and the experimental data observed in the ^{1}H NMR, which visually confirms these 2nd order effects.

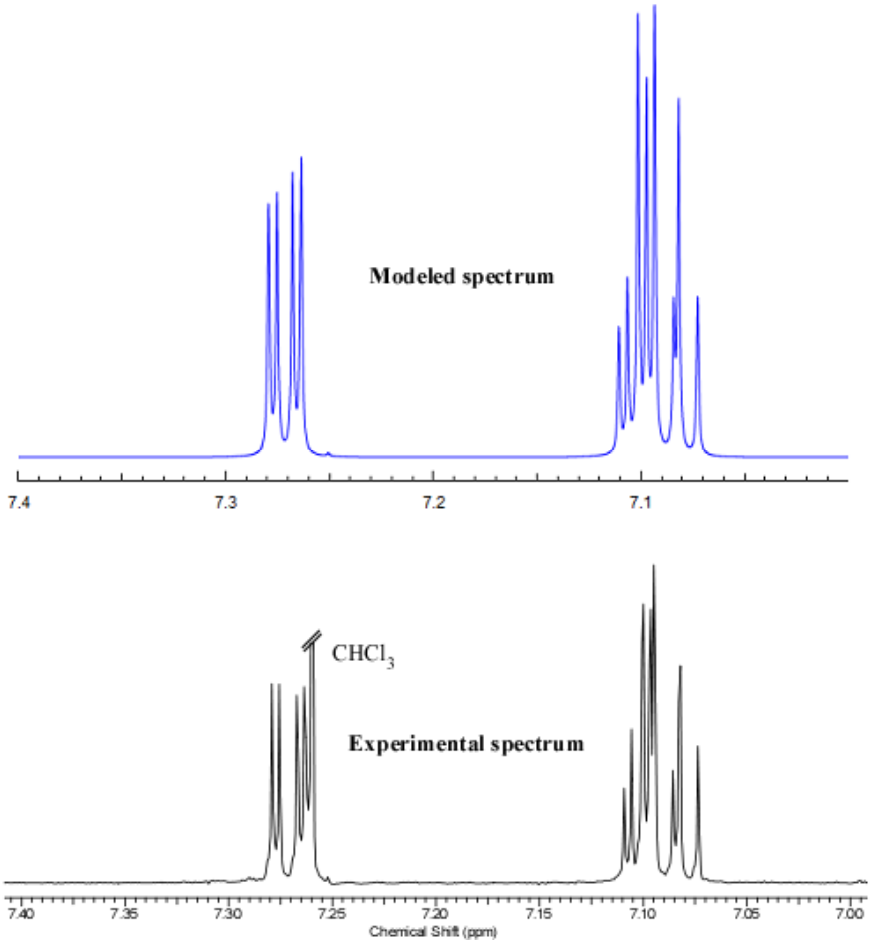

Figure 4.15. Comparison of results from modeling 2nd order effects in the ^{1}H NMR spectrum of **2.9**

4.8. References

1. Mishra, A.; Ma, C.-Q.; Segura, J. L.; Bauerle, P. In *Handbook of Thiophene-Based Materials: Applications in Organic Electronics and Photonics*; Perepichika, I. F., Perepichka, D. F., Eds.; Wiley: West Sussex, U.K., 2009; Vol 1, pp 1-157.

2. Rasmussen, S. C.; Pomerantz, M. In *Handbook of Conducting Polymers: Theory, Synthesis, Properties, and Characterization*, 3rd ed.; Skotheim, T. A.; Reynolds, J. R., Eds.; CRC Press: Boca Raton, FL, 2007, Chapter 12.

3. Rasmussen, S. C. Low Bandgap Polymers. In *Encyclopedia of Polymeric Nanomaterials*; Mullen, K., Ed.; Springer: Berlin, 2013; pp 1-13.
4. Rasmussen, S. C. In *Handbook of Conducting Polymers*, 4th ed.; Reynolds, J. R., Thompson, B. C., Skotheim, T. A., Eds.; CRC Press: Boca Raton, FL, 2019, Chapter 1.
5. Perepichka, I. F.; Perepichka, D. F.; Meng, H.; Wudl, F. *Adv. Mater.* **2005**, *17*, 2281-2305.
6. Günes, S.; Neugebauer, H.; Sariciftci, N. S. *Chem. Rev.* **2007**, *107*, 1324-1338.
7. Grimsdale, A. C.; Chan, K. L.; Martin, R. E.; Jokisz, P. G.; Holmes, A. B. *Chem. Rev.* **2009**, *109*, 897-1091.
8. Scharber, M. C.; Sariciftci, N. S. *Prog. Polym. Sci.* **2013**, *38*, 1929-1940.
9. Nielsen, C. B.; McCulloch, I. *Prog. Polym. Sci.* **2013**, *38*, 2053-2069.
10. Rasmussen, S. C.; Evenson, S. J.; McCausland, C. B. *Chem. Commun.* **2015**, *51*, 4528-4543.
11. de Leeuw, D. M.; Cantatore, E. *Mater. Sci. Semicond. Process.* **2008**, *11* (5-6), 199-204.
12. Logothetidis, S.; Laskarakis, A. *Eur. Phys. J. Appl. Phys.* **2009**, *46* (1), 12502/p1-p9.
13. Sekitani, T.; Someya, T. *Adv. Mater.* **2010**, *22* (10), 2228-2246.
14. Kaltenbrunner, M.; Sekitani, T.; Reeder, J.; Yokota, T.; Kuribara, K.; Tokuhara, T.; Drack, M.; Schwoediauer, R.; Graz, I.; Bauer-Gogonea, S.; Bauer, S.; Someya, T. *Nature* **2013**, *499* (7459), 458-463.
15. Thompson, B. C.; Frechet, J. M. J. *Angew. Chem., Int. Ed.* **2008**, *47* (1), 58-77.
16. Dennler, G.; Scharber, M. C.; Brabec, C. J. *Adv. Mater.* **2009**, *21* (13), 1323-1338.
17. Zhou, H.; Y.; L.; You, W. *Macromolecules* **2012**, *45* (2), 607-632.
18. Cao, W.; Xue, J. *Energy Environ. Sci.* **2014**, *7*, 2123-2144.

19. Zhang, G.; Zhao, J.; Chow, P. C. Y.; Jiang, K.; Zhang, J.; Zhu, Z.; Zhang, J.; Huang, F.; Yan, H. *Chem. Rev.* **2018**, *118*, 3447-3507.

20. Wang, G.; Melkonyan, F. S.; Facchetti, A.; Marks, T. J. *Angew. Chem., Int. Ed.* **2019**, *58* (13), 4129-4142.

21. Chapin, M.; Fuller, C. S.; Pearson, G. L. *J. Appl. Phys.* **1954**, *25*, 676-677.

22. Yu, G.; Gao, J.; Hummelen, J. C.; Wudl, F.; Heeger, A. J. *Science* **1995**, *270* (52493), 1789-1791.

23. Borchert, H. *Energy Environ. Sci.* **2010**, *3*, 1682-1694.

24. Meng, L.; Zhang, Y.; Wan, X.; Li, C.; Zhang, X.; Wang, Y.; Ke, X.; Xiao, Z.; Ding, L. *Science* **2018**, *361* (6407), 1094-1098.

25. Bourzac, K. Organic solar cell smashes performance record. *Chem. Eng. News* **2018**, *96* (33).

26. Roncali, J. *Chem. Rev.* **1997,** *97* (1), 173-206.

27. Roncali, J. Macromol. Rapid Commun. **2007**, *28* (17), 1761-1775.

28. Rasmussen, S. C.; Ogawa, K.; Rothstein, S. D. In *Handbook of Organic Electronics and Photonics: Electronic Materials and Devices*; Nalwa, H. S., Ed.; American Scientific Publishers: Stevenson Ranch, CA, 2008; pp 1-50.

29. Rasmussen, S. C.; Schwiderski, R. L.; Mulholland, M. E. *Chem. Commun.* **2011**, *47*, 11394-11410.

30. Mulholland, M. E.; Schwiderski, R. L.; Rasmussen, S. C. *Polym. Bull.* **2012**, *69*, 291-301.

31. Mulholland, M. E.; Schwiderski, R. L.; Evenson, S. J.; Rasmussen, S. C. *Polym. Mater. Sci. Eng.* **2012**, *107*, 36-37.

32. Schwiderski, R. L.; Rasmussen, S. C. *Synth. Met.* **2014**, *193*, 58-63.

33. Mulholland, M. E.; Wen, L.; Rasmussen, S. C. *Topol. Supramol. Polym. Sci.* **2015**, *2*, 18-29.

34. Mulholland, M. E.; Konkol, K. L.; Anderson, T. E.; Schwiderski, R. L.; Rasmussen, S.C. *Aust. J. Chem.* **2015**, *68*, 1759-1766.

35. Konkol, K. L.; Schwiderski, R. L.; Rasmussen, S. C. *Materials* **2016**, *9* (6), 404/1-16.

36. Culver, E. W.; Anderson, T. E.; Lopez Navarrete, J. T.; Ruiz Delgado, M. C.; Rasmussen, S. C. *ACS Macro Lett.* **2018**, *7* (10), 1215-1219.

37. Anderson, T. E.; Culver, E. W.; Almyahi, F.; Dastoor, P. C.; Rasmussen, S. C. *Synlett* **2018**, *29* (19), 2542-2546.

38. Mondal, R.; Ko, S.; Bao, Z. *J. Mater. Chem.* **2010**, *20* (47), 10568-10576.

39. Rasmussen, S. C.; Mulholland, M. E.; Schwiderski, R. L.; Larsen, C. A. *J. Heterocyclic Chem.* **2012**, *49* (3), 479-493.

40. Rasmussen, S. C.; Sattler, D. J.; Mitchell, K. A.; Maxwell, J. *J. Lumin.* **2004**, *190*, 111-119.

41. Wen, L.; Nietfeld, J. P.; Amb, C. M.; Rasmussen, S. C. *J. Org. Chem.* **2008**, *73*, 8529-8536.

42. Wen, L.; Heth, C. L.; Rasmussen, S. C. *Phys. Chem. Chem. Phys.* **2014**, *16*, 7231-7240.

43. Schwiderski, R. L.; Rasmussen, S. C. *J. Org. Chem.* **2013**, *78*, 5453-5462.

44. Wen, L.; Nietfeld, J. P.; Amb, C. M.; Rasmussen, S. C. *Synth. Met.* **2009**, *159*, 2299-2301.

45. Nietfeld, J. P.; Schwiderski, R. L.; Gonnella, T. P.; Rasmussen, S. C. *J. Org. Chem.* **2011**, *76*, 6383-6388.

46. Motoyama, R.; Sato, D.; Imoto, E. *Nippon Kagaku Zassi* **1957**, *78* (64), 793-794.

47. Outurquin, F.; Paulmier, C. *Bull. Soc. Chim. Fr.* **1983**, (5-6, Pt. 2), 153-158.

48. Outurquin, F.; Paulmier, C. *Bull. Soc. Chim. Fr.* **1983**, (5-6, Pt. 2), 159-163.

49. Kenning, D. D.; Mitchell, K. A.; Calhoun, T. R.; Funfar, M. R.; Sattler , D. J.; Rasmussen, S. C. *J. Org. Chem.* **2002**, *67* (25), 9073-9076.

50. Wen, L.; Rasmussen, S. C. *J. Chem. Crystallogr.* **2007**, *37* (6), 387-398.

51. Kitamura, C.; Tanaka, S.; Yamashita, Y. *J. Chem. Soc., Chem. Commun.* **1994**, (13), 1585-1586.

52. Kitamura, C.; Tanaka, S.; Yamashita, Y. *Chem. Mater.* **1996**, *8* (2), 570-578.

53. Scherf, U.; List, E. J. W. *Adv. Mater.* **2002**, *14*, 477-487.

54. Chen, P.; Yang, G.; Liu, T.; Li, T.; Wang, M.; Huang, W. *Poly. Int.* **2006**, *55*, 473-490.

55. Bundgaard, E.; Krebs, F. C. *Sol. Energy Mater. Sol. Cells* 2007, *91* (11), 954-985.

56. Cheng, Y.-J.; Yang, S.-H.; Hsu, C.-S. *Chem. Rev.* **2009**, *109* (11), 5868-5923.

57. Perzon, E.; Wang, X.; Zhang, F.; Mammo, W.; Delgado, J. L.; de la Cruz, P.; Inganas, O.; Langa, F.; Andersson, M. R. *Synth. Met.* **2005**, *154* (1-3), 53-56.

58. Zhang, F.; Perzon, E.; Wang, X.; Mammo, W.; Andersson, M. R.; Inganas, O. *Adv. Funct. Mater.* **2005**, *15* (5), 745-750.

59. Admassie, S.; Inganas, O.; Mammo, W.; Perzon, E.; Andersson, M. R. *Synth. Met.* **2006**, *156* (7-8), 614-623.

60. Zhu, Y.; Champion, R. D.; Jenekhe, S. A. *Macromolecules* **2006**, *39* (25), 8712-8719.

61. Ashraf, R. S.; Hoppe, H.; Shahid, M.; Gobsch, G.; S. Sensfuss, S.; Klemm, E. *J. Polym. Sci. Part A: Polym. Chem.* **2006**, *44* (24), 6952-6961.

62. Wu, W.-C.; Liu, C.-L.; Chen, W.-C. *Polymer* **2006**, *47* (2), 527-538.

63. Kuo, C.-C.; Lin, C.-H.; Chen, W.-C. *Macromolecules* **2007**, *40* (19), 6959-6966.

64. Lee, W.-Y.; Cheng, K.-F.; Wang, T.-F.; Chueh, C.-C.; Chen, W.-C.; Tuan, C.-S.; Lin, J.-L. *Macromol. Chem. Phys.* **2007**, *208* (17), 1919-1927.

65. Bull, T. A.; Pingree, L. S. C.; Jenekhe, S. A.; Ginger, D. S.; Luscombe, C. K. *ACS Nano* **2009**, *3* (3), 627-636.

66. Helgesen, M.; Krebs, F. C. *Macromolecules* **2010**, *43* (3), 1253-1260.

67. Zhou, E.; Cong, J; Yamakawa, S.; Wei, Q.; Nakamura, M.; Tajima, K.; Yang, C.; Hashimoto, K. *Macromolecules* **2010**, *43* (6), 2873-2879.

68. Chao, C.-Y.; Lim, H.; Chao, C.-H. *Polym. Prepr.* **2010**, *51* (1), 715-716.

69. Lee, W.-Y.; Cheng, K.-F.; Wang, T.-F.; Chen, W.-C.; Tsai, F.-Y. *Thin Solid Films* **2010**, *518* (8), 2119-2123.

70. Mondal, R.; Becerril. H. A.; Verploegen, E.; Kim, D.; Norton, J. E.; Ko, S.; Miyaki, N.; Lee, S.; Toney, M. F.; Brédas, J.-L.; McGhee, M. D.; Bao, Z. *J. Mater. Chem.* **2010**, *20* (28), 5823-5834.

71. Aoki, H.; Kakuta, J.; Yamaguchi, T.; Nitahara, S.; Ito, S. *Polym. J.* **2011**, *43* (11), 937-940.

72. Xia, Y.; Tong, J.; Li, B.; Wang, C.; Liu, H. *J. Polym. Sci. Part A: Polym. Chem.* **2011**, *49* (13), 2969-2979.

73. Huber, J.; Jung, C.; Mecking, S. *Macromolecules* **2012**, *45* (19), 7799-7805.

74. Lai, Y.Y.; Cheng, Y.-J.; Chen, C.-H.; Cheng, S.-W.; Cao, F.-Y.; Hsu, C.-S. *Polym. Chem.* **2013**, *4* (11), 3333-3344.

75. Miyaura, N.; Sukuki, A.; *Chem. Rev.* **1995**, *95* (7), 2457-2483.

76. Cheng, Y.-J.; Luh, T.-Y. *J. Organomet. Chem.* **2004**, *689* (24), 4137-4148.

77. Blouin, N.; Michaud, A.; Leclerc, M. *Adv. Mater.* **2007**, *19* (17), 2295-2300.

78. Zou, Y.; Gendron, D.; Badrou-Aïch, R.; Najari, A.; Tao, Y.; Leclerc, M. *Macromolecules* **2009**, *42* (8), 2891-2894.

79. Cardona, C. M.; Li, W.; Kaifer, A. E.; Stockdale, D.; Bazan, G. C. *Adv. Mater.* **2011**, *23* (30), 2367-2371.

80. Pandey, L.; Risko, C.; Norton, J. E.; Brédas, J.-L. *Macromolecules* **2012**, *45* (16), 6405-6414.

81. Cheng, K.-F.; Liu, C.-L.; Chen, W.-C. *J. Polym. Sci., Part A Polym. Chem.* **2007**, *45* (24), 5872-5883.

82. Lee, W.-Y.; Cheng, K.-F. Liu, C.-L.; Lin, S.-T.; Chueh, C.-C.; Tsai, F.-Y.; Chen, W.-C. *J. Polym. Res.* **2009**, *16* (3), 239-244.

83. Howard, J. B.; Ekiz, S.; Cuellar de Lucio, A. J.; Thompson, B. C. *Macromolecules* **2016**, *48* (17), 6360-6367.

84. Wang, Q.; Takita, R.; Kikuzaki, Y.; Ozawa, F. *J. Am. Chem. Soc.* **2010**, *132* (33), 11420-11421.

85. Mercier, L. G.; Leclerc, M. *Acc. Chem. Res.* **2013**, *46* (7), 1597-1605.

86. Segawa, Y.; Maekawa, T.; Itami, K. *Anew. Chem., Int. Ed.* **2015**, *54* (1), 66-81.

87. Bohra, H.; Wang, M. *J. Mater. Chem. A* **2017**, *5*, 11550-11571.

88. Matsidik, R.; Komber, H.; Luzio, A.; Caironi, M.; Sommer, M. *J. Am. Chem. Soc.* **2015**, *137* (20), 6705-6711.

89. Nietfeld, J. P.; Heth, C. L.; Rasmussen, S. C. *Chem. Commun.* **2008**, (8), 981-983.

90. . Karsten, B. P.; Bijleveld, J. C.; Viani, L.; Cornil, J.; Gierschner, J.; Janssen, R. A. J. *J. Mater. Chem.* **2009**, *19*, 5343-5350.

91. Becerril, H. A.; Miyaki, N.; Tang, M. L.; Mondal, R.; Sun, Y.-S.; Mayer, A. C.; Parmer, J. E.; McGehee, M. D.; Bao, Z. *J. Mater. Chem.* **2009**, *19*, 591-593.

92. Mondal, R.; Ko, S.; Norton, J. E.; Miyaki, N.; Becerril, H. A.; Verploegen, E.; Toney, M. F.; Brédas, J.-L.; McGehee, M. D.; Bao, Z. *J. Mater. Chem.* **2009**, **19**, 7195-7197.

93. Keshtov, M. L.; Godovsky, D .Y.; Khokhlov, A. R.; Mizobe, T.; Fujita, H.; Goto, E.; Hiyoshi, J.; Nakamura, S.; Kawauchi, S.; Higashihara, T.; et al. *J. Polym. Sci. A Polym. Chem.* **2015**, *53*, 1067-1075.

94. Keshtov, M. L.; Marochkina, D. V.; Kochurov, V. S.; Komarov, P. V.; Parashchuk, D. Y.; Trukhanov, V. A.; Khokhlov, A. R. *Polym. Sci. Ser. B* **2014**, 56 (1), 89-108.

95. Pu, K.; Shuhendler, A. J.; Jokerst, J. V.; Mei, J.; Gambhir, S. S.; Bao, Z.; Rao, J. *Nat. Nanotech.* **2014**, *9*, 233-239.

96. Petersen, M. H.; Hagemann, O.; Nielsen, K. T.; Jørgensen, M.; Krebs, F. C. *Solar Energy Mater. Sol. Cells* **2007**, *91*, 996-1009.

97. Mondal, R.; Miyaki, N.; Becerril, H. A.; Norton, J. E.; Parmer, J.; Mayer, A. C.; Tang, M. L.; Brédas, J.-L.; McGehee, M. D.; Bao, Z. *Chem. Mater.* **2009**, *21*, 3618-3628.

98. Mondal, R.; Ko, S.; Verploegen, E.; Becerril, H. A.; Toney, M. F.; Bao, Z. *J. Mater. Chem.* **2011**, *21*, 1537-1543.

99. Velusamy, M.; Huang, J.-H.; Hsu, Y.-C.; Chou, H.-H.; Ho, K.-C.; Wu, P.-L.; Chang, W.-H.; Lin, J.T.; Chu, C.-W. *Org. Lett.* **2009**, *11*, 4898-4901.

100. Mak, C. S. K.; Leung, Q. Y.; Chan, W. K.; Djurisic, A. B. *Nanotechnology* **2008**, *19* (42), 424008/1-424008/8.

101. Wang, Z.; Gao, Z.; Feng, Y.; Liu, Y.; Yang, B.; Liu, D.; Lv, Y.; Lu, P.; Ma, Y. *Polymer* **2013**, *54*, 6191-6199.

102. Nishida, J.; Murakami, S.; Tada, H.; Yamashita, Y. *Chem. Lett.* **2006**, *35*, 1236-1237.

103. Čík, G.; Krajčovič, J.; Veis, P.; Végh, D.; Šeršen, F. *Synth. Met.* **2001**, *118* (1-3), 111-119.

104. Mo, H.; Radke, K. R.; Ogawa, K.; Heth, C. L.; Erpelding, B. T.; Rasmussen, S. C. *Phys. Chem. Chem. Phys.* **2010**, *12*, 14585-14595.

105. Turro, N. J.; Ramamurthy, V.; Scaiano, J. C. *Modern Molecular Photochemistry of Organic Molecules*; University Science Books: Sausalito, CA; 2010; pp 195-200.

106. Birer, Ö.; Moreschini, P.; Lehmann, K.K.; Scoles, G. *J. Phys. Chem. A* **2007**, *111*, 12200-12209.

107. Zhou, W.-Q.; Peng, H.-P.; Xu, J.-K.; Xia, H.-Y.; Pu, S.-Z. *Polym. Int.* **2008**, *57*, 92-98.

108. Han, Z.-B.; Cheng, X.-N.; Chen, X.-M. *Cryst. Growth Des.* **2005**, *5*, 695-700.

109. Waltman, R. J.; Bargon, J. *Can. J. Chem.* **1986**, *64*, 76-95.

110. Gurunathan, K.; Murugan, A. V.; Marimuthu, R.; Mulik, U. P.; Amalnerkar, D. P. *Mater. Chem. Phys.* **1999**, *61*, 173-191.

111. Cho, S. Y.; Grimsdale, A. C.; Jones, D. J.; Watkins, S. E.; Holmes, A. B. *J. Am. Chem. Soc.* **2007**, *129* (39), 11910-11911.

112. Wen, L.; Duck, B. C.; Dastoor, P. C.; Rasmussen, S. C. *Macromolecules* **2008**, *41* (13), 4576-4578.

113. Larson, R. C.; Iwamoto, R. T.; Adams, R. N. *Anal. Chim. Acta* **1961**, *25*, 371-374.

114. Institute of Chemical Sciences and Engineering. Tools for NMR Spectroscopists. Available online: http://www.nmrdb.org/simulator/index.shtml?v=v2.34.1 (accessed on April 22, 2016).

115. Castillo, A. M.; Patiny, L.; Wist, J. *J. Mag. Res.* 2011, *209*, 123-130.

CHAPTER 5. SYNTHESIS OF THIENO[3,4-b]PYRAZINE-BASED BRIDGING LIGANDS FOR INCORPORATION IN SUPRAMOLECULAR ASSEMBLIES

5.1. Introduction

Transition metal complexes containing bridging ligands have been widely studied in the last several decades because of their unique photophysical, photochemical, and electrochemical properties.[1-3] The combination of multiple metal centers into a supramolecular assembly allows for the production of complex multi-metallic systems capable of a variety of useful light- and/or redox-induced functions.[2-6] Applications of such functions include light harvesting, conversion of light into chemical or electrical energy, sensing, and photocatalysis.[4] One of the primary advantages of this approach is that careful selection of the molecular components can allow for fine-tuning and production of specific desired properties for the particular application.[2] Additionally, the suitable choice of metal-based components and bridging ligands and an appropriate design of the supramolecular structure can in fact allow for the occurrence of very interesting and potentially useful multi-component processes such as energy transfer along predetermined pathways, photoinduced charge separation, and multielectron exchange at a predetermined potential.[4]

A supramolecular species can be defined as a complex system made of molecular components with definite individual properties.[4] These organizations can be attained by either linking together molecular components through covalent bonds, electrostatic forces, or weak van der Waals interactions.[2,5] From a photo- and electrochemical viewpoint, the difference between a large molecule and a supramolecular species can be based on the degree of interaction between the electronic subsystems of the component units.[2,4] Light excitation in a supramolecular species leads to excited states that are substantially localized on components of the assembly, whereas large

molecules have substantially delocalized excited states.[2,4] When localized redox and excitation processes cannot be performed, a complex should be considered a large molecule and not a supramolecular organization.[4] The general scheme of these supramolecular organizations in which energy is transferred is shown in Figure 5.1. The first step in this process is that a photon of light is absorbed by an antenna complex (M_1). This then undergoes energy transfer (ET) through the conjugation pathway of a bridging ligand (BL). After electron transport through the ligand, a chemical reaction occurs at the reactive complex (M_2) in the supramolecular organization.

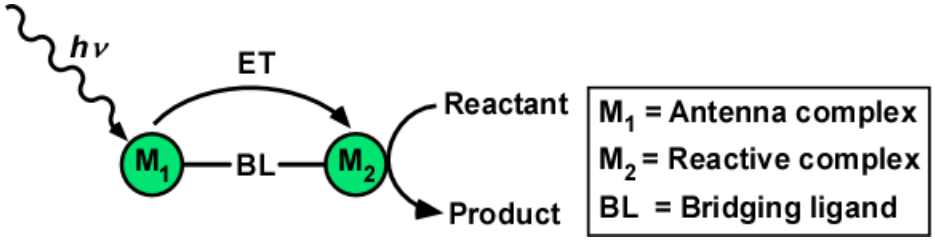

Figure 5.1. General scheme for absorption of light in supramolecular assembly

A seemingly infinite number of possibilities for supramolecular organizations arises from the large variety of known chemical species, however supramolecular assemblies based on coordination compounds provide a rather attractive approach.[5] Metals can be incorporated into assemblies in a variety of arrangements, both varying the number and type of metal complexes, defined as mononuclear (M = 1), polynuclear (M = 2+), homometallic ($M_1 = M_2$, etc.), and heterometallic ($M_1 = M_2$, etc.) arrangements.[2-6] A variety of metals have been incorporated into supramolecular assemblies, mostly limited to transition metals, and some of the common ones incorporated into polypyridyl-type assemblies include Re(I), Cu(I), Ru(II), Fe(II), Os(II), Rh(III), Ir(III), and Cr(III), although Ru(II) remains one of the most popular due to its chemical stability and favorable photophysical and redox characteristics.[1-9]

The choice of bridging ligand that is employed to connect the various individual metal-based components is a critical component of these supramolecular assemblies.[4,8] Although

technically any moiety capable of donating two pairs of electrons to two separate metal centers can serve as a bridging ligand, bridging ligands capable of multidentate coordination provide greater stability of the multi-metallic species during excitation. In addition, ligands that provide a conjugated path between metals can promote electronic coupling. Furthermore, some bridging ligands contain either conjugated or non-conjugated spacer units between the coordination sites, which can have structural and electronic effects.[4,8] By promoting electronic communication between the metal-based units, the electronic properties of the bridged polynuclear systems are changed in comparison to mononuclear single metal systems.[4,8] Additionally, such π-conjugated bridging ligands are also often redox and spectroscopically active, oftentimes possessing empty low-lying π*-orbitals and high-energy filled π-orbitals that serve to mediate electron and energy transfer between bridged metals.[8] The nature of the bridging ligands dictates the energy and occupation of these π- and π*-orbitals, for example bridging ligands with extended aromatic systems typically display lower energy π*-orbitals, which often function as the site of localization of the LUMO in complexes constructed with these ligands. Therefore, this makes the nature of the bridging ligand vital to the redox, spectroscopic, and photochemical properties of these multi-metallic complexes.[8]

Various polypyridyl-type bridging ligands utilized in supramolecular organizations are shown in Figure 5.2.[4,8] Of the ligands shown, the multidentate 2,2'-bipyridine (**bpy**),[3,6,7,10-12] 1,10-phenanthroline (**phen**),[3,6,7,10,11,13] 2,2':6',2''-terpyridine (**tpy**),[2,7,14-17] and dipyrido[3,2-*a*:2',3'-*c*]phenazine (**dppz**)[3,6,18] are not capable of multi-metallic coordination because they have only one coordination site on the ligand. However, 2,2'-bipyrimidine (**bpm**),[6,13,19-21] 2,3-di-2-pyridinylpyrazine (**dpp**),[3,6,22-24] pyrazino[2,3-*f*][4,7]phenanthroline (**dpp'**),[3,25-27] 2,3-di-2-pyridinylquinoxaline (**dpq**),[3,22,28,29] dipyrido[2,3-*a*:3',2'-*c*]phenazine (**dpq'**),[3,6,30-32] 2,3-di-2-

pyridinylbenzo[*g*]quinoxaline (**dpb**),[22,26,30,33] benzo[*i*]dipyrido[2,3-*a*:3',2'-*c*]phenazine (**dpb'**),[26,30,33] and 2,3,5,6-tetra-2-pyridinylpyrazine (**tpp**)[34,35] can coordinate multiple metals, and thus can be utilized in supramolecular assemblies as good bridging ligands. Generally, the more rigid structures (**dpp'**, **dpq'**, **dpb'**) have less steric requirements than their non-rigid analogues (**dpp**, **dpq**, **dpb**),[30] and the forced-planarity should provide better metal-metal communication because of enhanced electron delocalization. Additionally, extension of the aromatic π-system of **dpp**, to **dpq** and **dpb**, leads to increased conjugation and stabilized π*-orbitals, which leads to interesting modulation of the spectroscopic and electrochemical properties.[8]

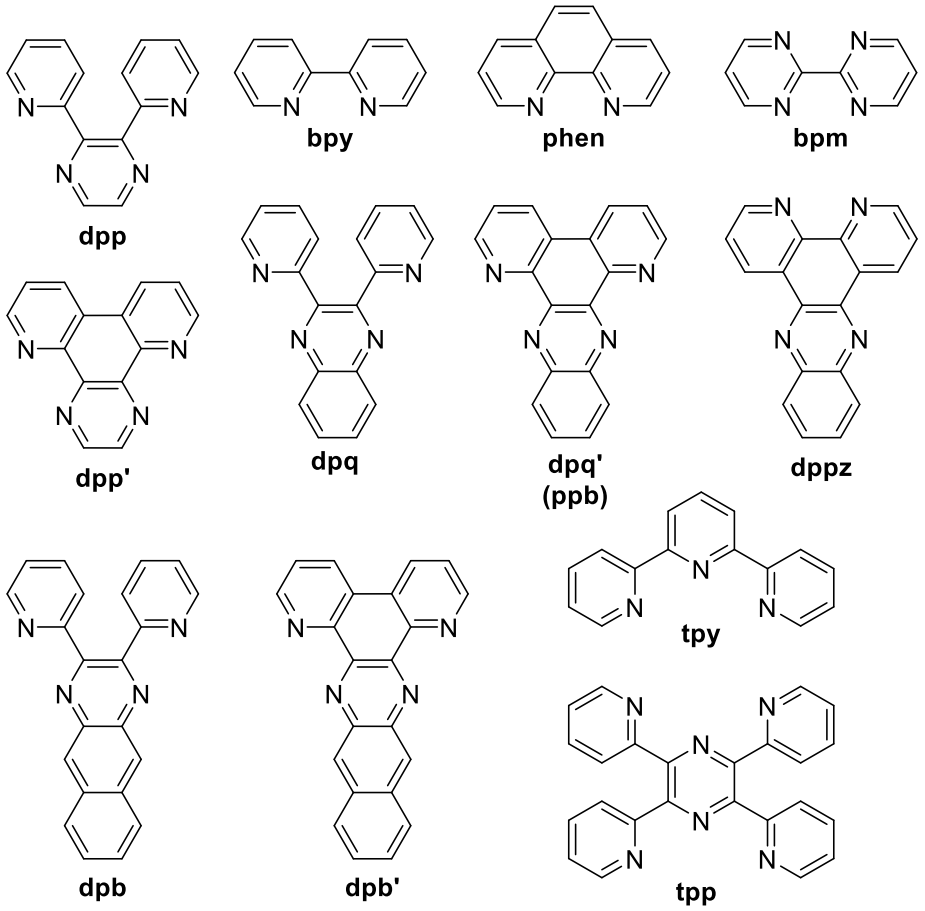

Figure 5.2. Representative examples of polypyridyl bridging ligands capable of metallic coordination

The fused-ring heterocycle thieno[3,4-*b*]pyrazine (TP) is a common monomeric unit used in the generation of low band gap materials.[36-38] Over the last two decades, the Rasmussen research group has applied TP monomers to various homopolymeric and copolymeric conjugated materials,[37-51] in the process fully optimizing the synthesis of this heterocycle and it's 2,3-disubstituted derivatives.[39-42] To review, the fusion of the electron-rich thiophene with the electron-poor pyrazine results in partially localized frontier orbitals, in which the HOMO is largely localized on the thiophene and the LUMO is shared across both rings, but with greater pyrazine contribution.[40,42,52] Figure 5.3 shows the density functional theory (DFT) calculated molecular orbitals for TP.[52] Consequently, the HOMO and LUMO can be to some extent independently tuned by the addition of substituents on either the thiophene (to tune the HOMO) or the pyrazine (to tune the LUMO). Moreover, the lowest energy absorption in TP consists of an ICT band resulting from a transition between the predominately thiophene-localized HOMO and the LUMO of greater pyrazine contribution.

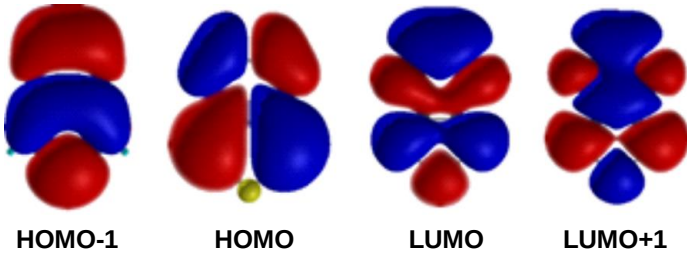

Figure 5.3. DFT calculated molecular orbitals of thieno[3,4-*b*]pyrazine

Typically, pyrazines and their derivatives are relatively weak bases. For example, the first protonation of pyrazine occurs with pK_a of 0.57, while the much more basic pyridine occurs at pK_a of 5.23.[39] Figure 5.4 shows the structures and basicity of several nitrogen-containing aromatics. This difference in basicity can be attributed to the strong inductive and mesomeric effects of the sp^2 nitrogen para to N(1). Additionally, the fusion of benzene or thiophene rings to these aromatic bases only causes a minor change in basicity, where the pK_a of quinoxaline and thieno[3,4-*b*]pyrazine

being essentially identical to pyrazine.[39] Furthermore, the increased basicity with added methyl groups is typical for pyrazines, and is due to the electron donating effect of the methyl group. It is expected that since the basicity for the TP, quinoxaline, and pyrazine is essentially identical, they should have similar metal coordinating ability. However, the application of this basicity to the generation of dedicated ligands has remained largely unexplored.

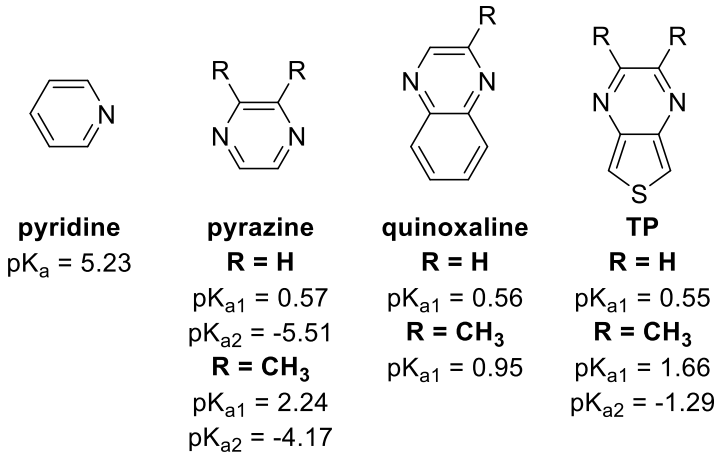

Figure 5.4. Structures and pK$_a$ values for selected heteroaromatic species

Currently, there are only three TP-based species reported in the literature that are capable of acting as multidentate ligands (Figure 5.5). [41,49,53-55] Of these, only metal complexes of **5.1** have been reported.[18,56-58] Additionally, none of these species (**5.1-5.3**) can bridge multiple metals.

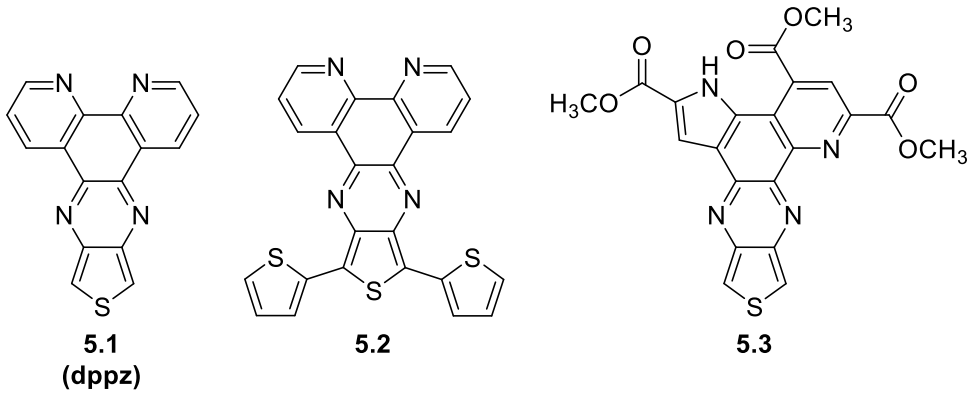

Figure 5.5. Known thieno[3,4-*b*]pyrazine species capable of metal chelation

Structurally, TP is quite similar to the bridging ligand **dpq**, which has proven multi-metallic chelation abilities. [3,22,28,29] Recognizing this, it was considered a valuable new avenue of research to use our expertise and familiarity with the synthesis of the thieno[3,4-*b*]pyrazine heterocycle and apply it to a new family of bridging ligands. Furthermore, to confirm that this new family of bridging ligands is capable of good metal-metal communication, the mono- and bimetallic ruthenium(II) species were fully characterized. For proof-of-concept, the following research will focus solely on TPs functionalized with 2-pyridyl coordinating groups, for comparison with the well-studied ligands discussed earlier (Figure 5.2), but if successful, the synthetic methodologies of TP units could be easily expanded to other heterocycles such as 2-thiazolyl or 2-imidazolyl.

5.2. Synthesis

5.2.1. Synthesis of bridging ligands

The extended fused-ring species 2,3-di-2-pyridinylthieno[3,4-*b*]pyrazine (**5.6**) was synthesized under fairy standard conditions as illustrated in Scheme 5.1. These are the same methods as previously reported for various TPs (Chapter 4), where the final step of the production of **5.6** is the simple double condensation of 3,4-diaminothiophene (**5.4**) with 1,2-bis(2-pyridyl)-1,2-ethanedione (**5.5**, often referred to by the common name 2,2'-pyridil) in yields of 80-88% as a bright yellow solid. Lindsley and co-workers previously reported the synthesis of **5.6** via microwave heating in 2004,[59] claiming analytically pure **5.6** as a brown solid in a yield of 77%. However, the methods given in Scheme 5.1 are simpler and produce **5.6** in higher yields. Additionally, comparison of the bright yellow material isolated by these methods to the characterization data reported by Lindsley and coworkers confirms that the previously reported material was certainly not a pure material.

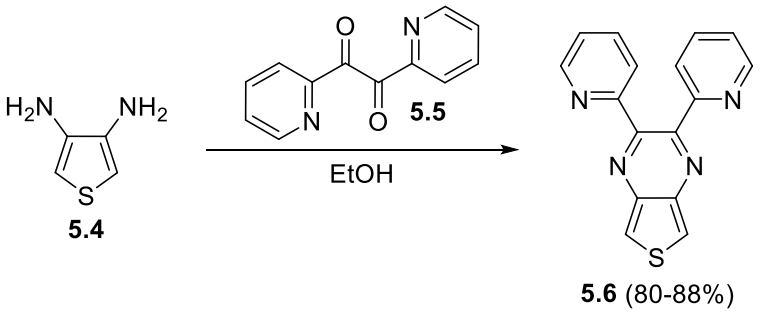

Scheme 5.1. Synthesis of 2,3-di-2-pyridinylthieno[3,4-*b*]pyrazine (**5.6**)

After successfully synthesizing the 2,3-dipyridinyl-functionalized TP **5.6**, attempts were made to synthesize a TP with 2-pyridyl groups affixed to the thiophene at the 5- and 7-positions of the TP unit (**5.10**, Scheme 5.2), which would be analogous to fused-ring TP-based terthienyls. To simplify the synthesis, it would be efficient to synthesize a stockpile of diaminothiophene (**5.9**). Then the appropriate dione could just be added to form the TP (**5.10**), which is the same synthetic methodology of TP-based terthienyls.[44] However, this synthesis had issues, as the first step involves the attachment of the 2-pyridinyl groups to 2,5-dibromo-3,4-dinitrothiophene (**5.7**) to form **5.8**.

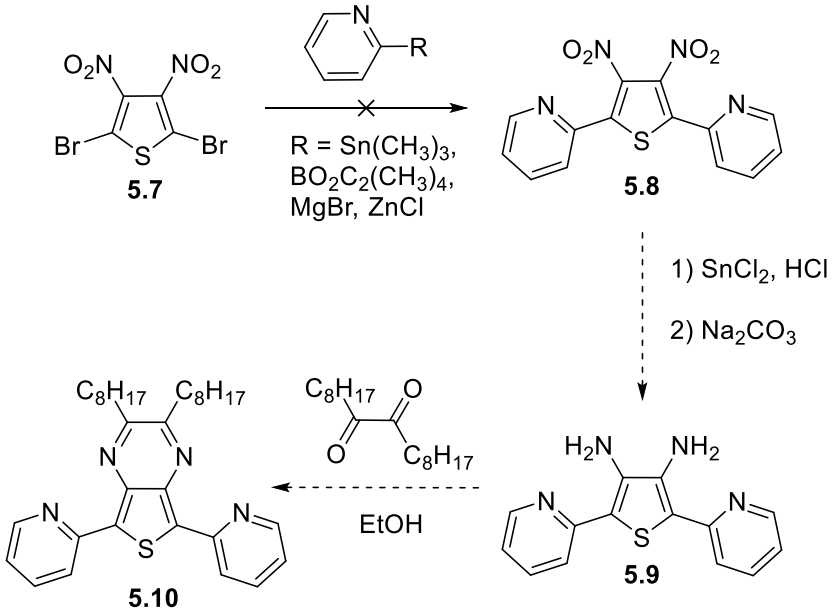

Scheme 5.2. Attempted synthesis of 3,4-dinitro-2,5-di-2-pyridinylthiophene (**5.8**)

Extensive attempts were made to synthesize **5.8**, but none were ultimately able to form it in more than trace yields. This included Stille, Suzuki, Kumada, and Negishi cross-coupling methodologies. Table 5.1 lists the reaction conditions utilized in attempts to synthesize and isolate **5.8**. At best, the monosubstituted product was sometimes formed. Issues with this synthesis could be attributed to the increased basicity of the pyridine ring, which inhibited the cross-coupling to the thiophene ring, as the analogous 2-thienyl[44] and phenyl[60] substituted forms of **5.8** have been successfully synthesized through similar cross coupling methodologies.

Once it was realized that the more step-efficient methodology to form **5.10** was not going to be successful, efforts moved toward forming the TP via Stille cross-coupling of the brominated TP. This synthesis is illustrated in Scheme 5.3. Octyl chains were chosen to functionalize the 2-and 3-positions of the TP, but this could easily be expanded to other R-groups with selection of the appropriate dione. After the five-step process to form the TP **5.11** (this synthesis was discussed extensively in Chapter 4), the TP is brominated with *N*-bromosuccinimide in DMF at -78 °C to form **5.12** in good yield (75-85%) using previously reported methodologies.[61] This was then followed by Stille cross-coupling of **5.12** and **5.13** using a Pd/CuI co-catalyst system to form **5.10** in yield of 65%. The 2-trimethylstannylpyridine **5.13** was synthesized from 2-bromopyidine (79% yield) using literature conditions.[62] This reaction also works well using the tributylstannyl analogue of **5.13**, with little difference in yield.

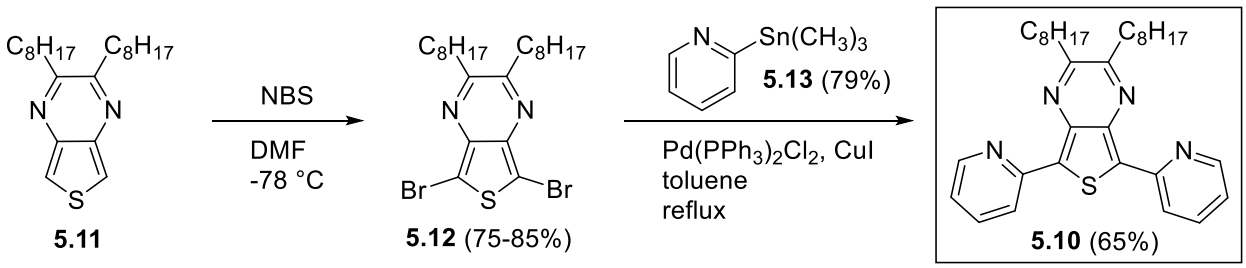

Scheme 5.3. Synthesis of 2,3-dioctyl-5,7-di-2-pyridinylthieno[3,4-*b*]pyrazine (**5.10**)

Table 5.1. Reaction conditions utilized in an attempt to synthesize **5.8**

Entry	Rxn Type	Ratio RX:5.7	RX	Reagents	Notes	Catalyst	Solvent	Temp	Time
1	Suzuki	2.2:1	$RBO_2C_2(CH_3)_4$	K_2CO_3		$Pd(PPh_2)_2Cl_2$ (5 mol%)	toluene	reflux	18 h
2	Stille	2.2:1	$RSnMe_3$			$Pd(PPh_2)_2Cl_2$ (1 mol%)	THF	reflux	18 h
3	Stille	2.2:1	$RSnMe_3$			$Pd(PPh_2)_2Cl_2$ (2.5 mol%)	THF	reflux	18 h
4	Stille	2.2:1	$RSnMe_3$		workup: 10% HCl, neutralize salt	$Pd(dppf)Cl_2$ (2.5 mol%)	THF	reflux	18 h
5	Stille	2.5:1	$RSnMe_3$	CuI (5 mol%)		Pd(dppe) Cl_2 (5 mol%)	THF	reflux	18 h
6	Kumada	2.5:1	RBr	Mg	initiate $C_2H_4Br_2$	$Ni(dppp)Cl_2$ (5 mol%)	THF	reflux	18 h
7	Kumada	5:1	RBr	Mg	initiate I_2	$Ni(dppp)Cl_2$ (5 mol%)	THF	reflux	18 h
8	Kumada	2.5:1	RBr	Mg	initiate $C_2H_4Br_2$	$Pd(PPh_3)_4$ (5 mol%)	THF	reflux	18 h
9	Kumada	2.5:1	RBr	iPrMgCl (2.0 M)		$Ni(dppp)Cl_2$ (5 mol%)	THF	reflux	18 h
10	Kumada	2.5:1	RBr	MeMgBr (3.0 M)		$Ni(dppp)Cl_2$ (5 mol%)	THF	reflux	18 h
11	Kumada	2.5:1	RBr	1)BuLi 2) MgBr $\bullet Et_2O$	workup: extract w/EtOAc	$Ni(dppp)Cl_2$ (5 mol%)	THF	0 °C → rt	18 h
12	Kumada	2.5:1	RBr	1)BuLi 2) MgBr $\bullet Et_2O$	workup: ppt w/hexanes	$Ni(dppp)Cl_2$ (5 mol%)	THF	rt	18 h
13	Negishi	2.5:1	RBr	1)BuLi 2)$ZnCl_2$		$Pd(PPh_3)_4$ (5 mol%)	THF	reflux	18 h
14	Negishi	2.5:1	RBr	1)BuLi 2)$ZnCl_2$		$Pd(PPh_3)_4$ (5 mol%)	THF	rt	18 h

A third potential bridging ligand was hypothesized that would combine the methodologies of the first two synthesized, whereby 2-pyridyl groups would be affixed to the 2-, 3-, 5-, and 7-positions of the TP (**5.15**, Scheme 5.4). This would provide two tridentate chelation sites for cross-ring communication. One limitation of most current tridentate BLs is that they are based upon the 2,2';5',2''-terpyridine (**tpy**) core (Figure 5.2, see **tpp**), which is known to result in an unfavorable bite angle (< 160 °) upon coordination of the metal. This limits the photophysical properties of these complexes.[8,63] Structure **5.15** would afford a larger bite angle (>160 °) because of the inclusion of an additional pyridine-pyrazine coordination mode in the larger 5,6-membered chelate.[1]

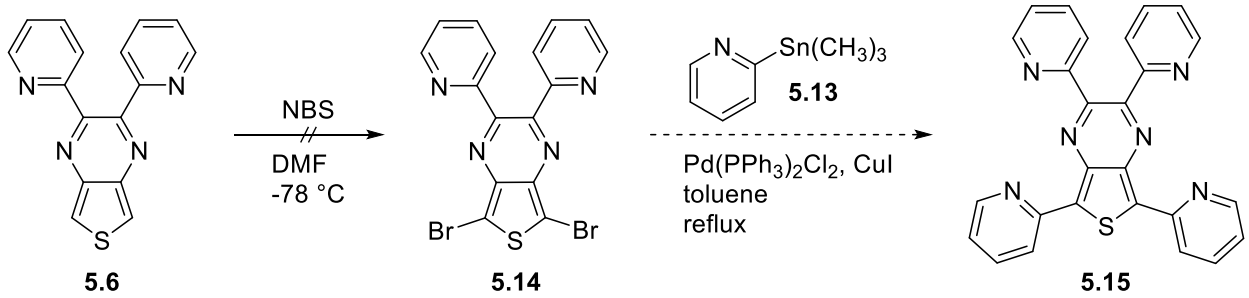

Scheme 5.4. Attempted synthesis of 5,7-dibromo-2,3-di-2-pyridinylthieno[3,4-*b*]pyrazine (**5.14**)

Using normal TP-bromination methodologies,[61] **5.6** is dibrominated to form **5.14**. Although the ^{1}H NMR showed the presence of the product of **5.14**, a significant portion of the monobrominated species was also present. This could be attributed to the electron-withdrawing nature of the pyridyl groups, which reduces the reactivity of **5.6** to electrophilic aromatic substitution. Additionally, the mono- and dibrominated species are extremely difficult to separate by either column chromatography or recrystallization techniques, and as of this time, none of the purification methods attempted have successfully isolated pure **5.14**. However, if this issue can be overcome in the future, **5.15** should be easily produced through Stille cross-coupling of **5.14**

and **5.13**. Cleanliness of each monomer is key for both reproducibility of the synthesis and properties of the final materials.

Furthermore, if the monobrominated species of **5.6** could be synthesized, this would provide an attractive mixed-denticity bridging ligand that possesses both a tridentate and bidentate chelation site. Most current BLs reported in the literature capable of simultaneous bidentate and tridentate coordination utilize a spacer between chelation sites, which can limit the effectiveness of the metal-metal communication.[6,8]

5.2.2. Synthesis of metal complexes

In order to evaluate the effectiveness of this new family of bridging ligands for multi-metallic complexes, attempts were made to generate the mono- and bimetallic ruthenium(II) complexes. For the first BL discussed (**5.6**), this involved reaction with 1.1 equivalents of *cis*-$[Ru(bpy)_2Cl_2]$ to form the monometallic complex **5.16** ($[(bpy)_2Ru(\mathbf{5.6})](PF_6)_2$) as a magenta solid in 68% yield. To form the corresponding bimetallic species **5.17** ($[(bpy)_2Ru(\mathbf{5.6})Ru(bpy)_2](PF_6)_4$), 2.5 equivalents of *cis*-$[Ru(bpy)_2Cl_2]$were reacted with **5.6** to form a dark green solid in 64% yield. These species were also easily purified by alumina column chromatography. This synthesis is illustrated in Scheme 5.5. ^{1}H NMR spectra were collected for both **5.16** and **5.17**, to see if any additional structural information could be elucidated. Because of the large number of unique aromatic protons in these complexes, it is difficult to say much about the splitting. The ^{1}H NMR spectrum of **5.16** is shown in Figure 5.6. The two inequivalent protons of the thiophene (*a*, *b*) are distinguishable as the doublets at 8.5 and 7.2 ppm, respectively. The proton in close proximity to the bipyridine ligands (*b*) is shielded in comparison to the other proton (*a*), which could be attributed to anisotropic effects of the nearby bipyridyl ligands. The spectrum for **5.17** was more complex and is not shown.

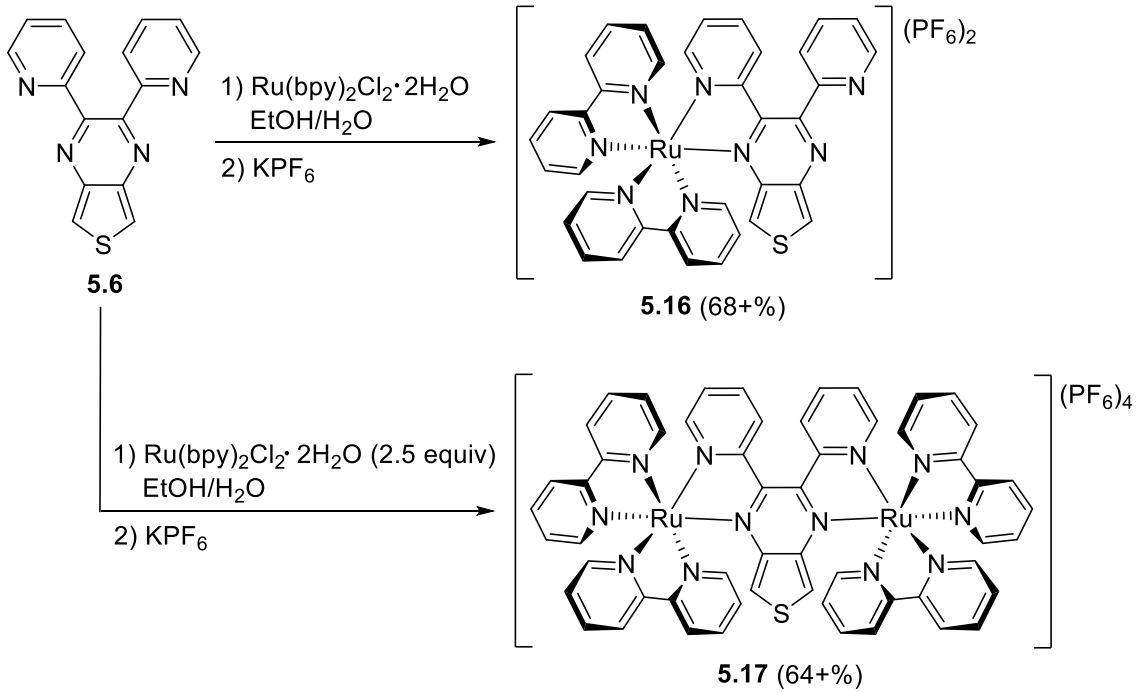

Scheme 5.5. Synthesis of mono- and bi-metallic ruthenium(II) coordination complexes of **5.6**

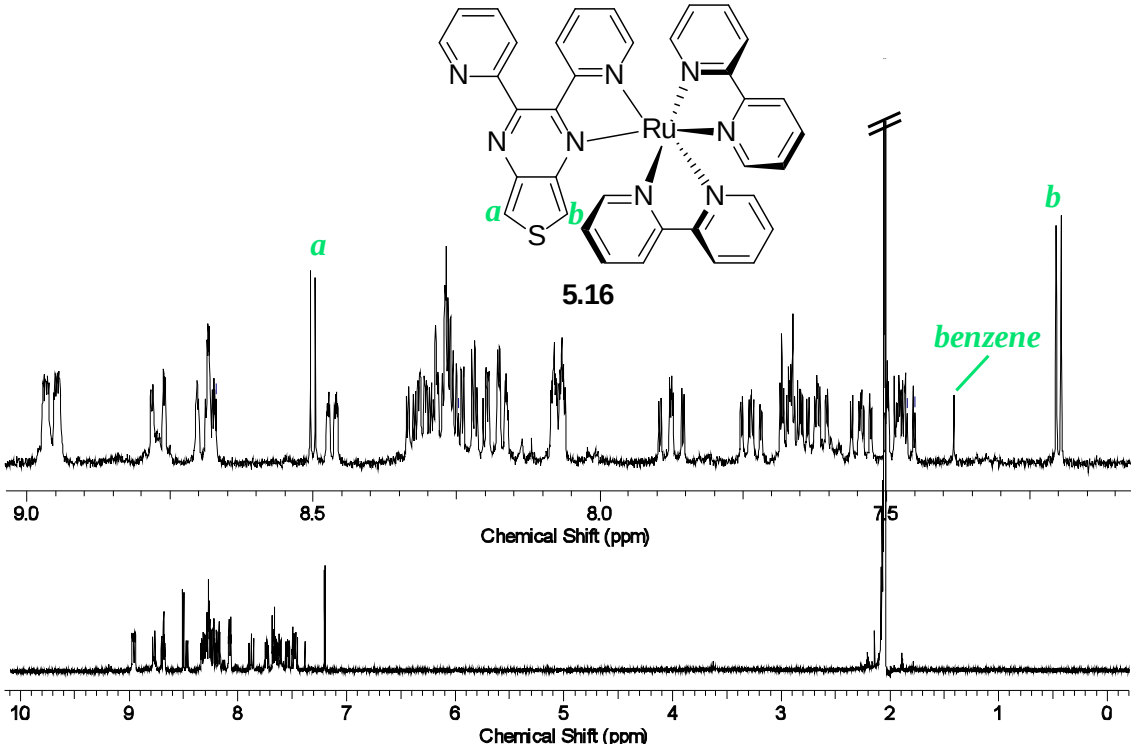

Figure 5.6. ^{1}H NMR spectra of complex [(bpy)$_2$Ru(**5.6**)](PF$_6$)$_2$ (**5.16**) in d6-acetone

For the second BL discussed (**5.10**), attempts were also made to generate ruthenium(II) complexes, which are illustrated in Scheme 5.6. The monometallic species **5.18** ($[(bpy)_2Ru(\mathbf{5.10})](PF_6)_2$) was synthesized using the same methods as previous, 1.1 equivalents of *cis*-$[Ru(bpy)_2Cl_2]$ in EtOH at reflux 3-24 hours, however low yields of 10-15% were obtained. This could be because the BL **5.18** will form a less stable 6-membered chelate with the metal, whereas the 5-membered chelate formed with the BL **5.6** is easier to make. To clarify, **5.18** has two bonds locked in position, and **5.16** only has one, therefore the greater bond angle of **5.18** is not as favorable for metal binding. Also, all attempts to synthesize the bimetallic species using the *cis*-$[Ru(bpy)_2Cl_2]$ were unsuccessful, which is not surprising given the low yields of the monometallic species. Thereafter, we reconsidered the synthetic conditions. The largest change was using $Ru(bpy)_2(OTf)_2$ as the ruthenium source, as triflate is an excellent leaving group (better than chloride), which should hopefully ease coordination. Additionally, the solvent was switched from aqueous ethanol to absolute ethanol, as there were concerns that maybe water was too strong of a coordinating solvent. Modifying the ruthenium source and solvent was able to produce **5.18** as a dark purple solid in an improved 29% yield.

Finally, even increasing the mole ratio of $Ru(bpy)_2(OTf)_2$ to 3.0 equivalents in an attempt to form even a small amount of bimetallic **5.19** proved unsuccessful. Typically, 5-membered chelate rings, such as that formed by BL **5.6**, promote selectivity for larger metal ions (i.e. Ru(II)).[7] However, because of steric constraints, 6-membered chelate rings prefer smaller ions to coordinate (e.g. Na^+ or Ca^{2+}).[7] Thus, the reason the bimetallic species **5.19** was not able to be isolated, and the monometallic **5.18** was isolated in low yields, could be due to a combination of factors. This includes the stability of the ring formed (5-membered rings are more stable than 6-, and both are

much more stable than 4- or 7-) and the limited space with the Ru(II), the two bipyridine ligands, and the BL surrounding each chelation site.

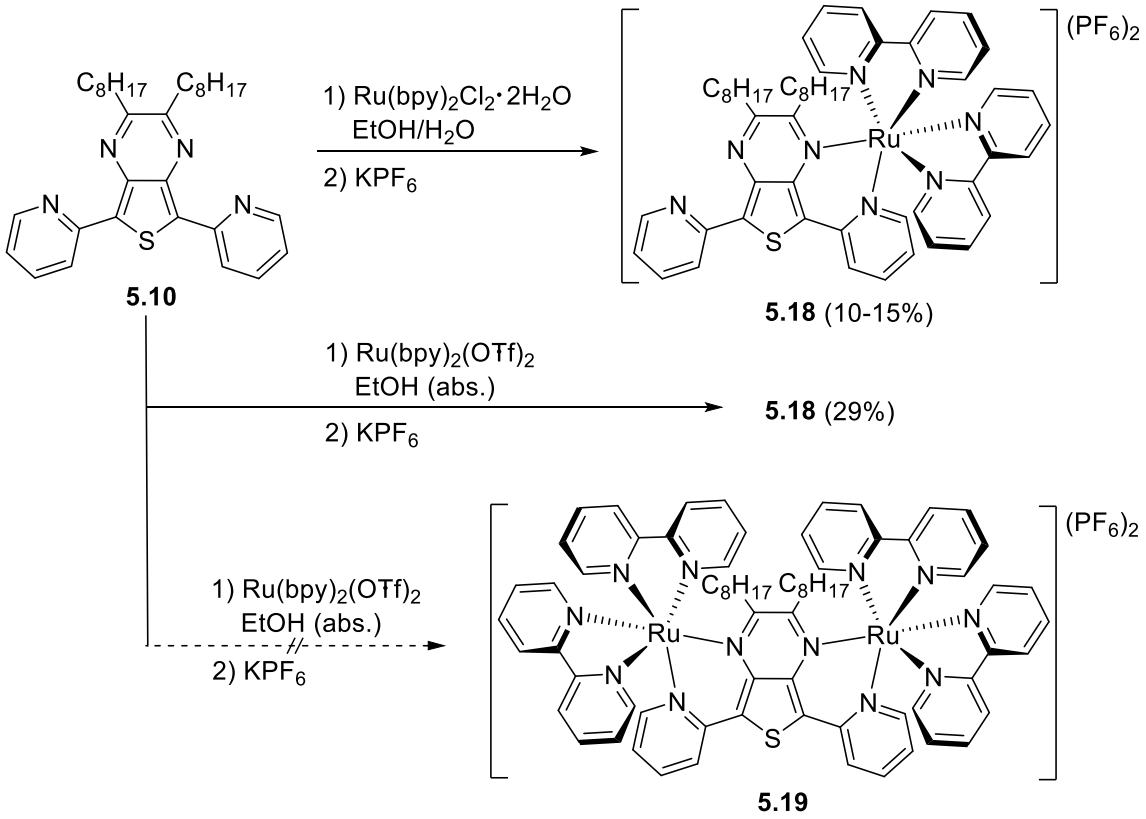

Scheme 5.6. Synthesis of monometallic ruthenium(II) coordination complexes of **5.10**

5.3. Spectroscopy

The acquired photophysical data for all BLs and Ru(II) complexes is presented in Table 5.2. The bridging ligand **5.6**, the spectrum of which is illustrated in Figure 5.7, shows the presence of a low energy charge-transfer (CT) band, along with a higher energy π-π* transition, which is typical for TPs (Chapter 4). This additional CT band, which is the result of a transition between the primarily thiophene-localized HOMO and the LUMO of greater pyrazine contribution, provides interesting possibilities for the complexity of the photophysics in the resulting complexes. The room temperature fluorescence singlet emission (370 nm) and quantum yield (1.8×10^{-3}) were determined for BL **5.6**. The low quantum yield for the TP seems

reasonable, as this compares well to the analogous 2,3-diphenylthieno[3,4-b]pyrazine (**2,3-PhTP**).[52] However, the difference in emission (ca. 108 nm) between the two species is wide, and the shift from absorption to emission for **5.6** is only ~40 nm.

Table 5.2. Photophysical data for BLs and Ru(II) complexes[a]

BL	λ_{max}^{abs} (nm)	ε (M^{-1} cm^{-1})	λ_{max}^{em} (nm)	Φ^{em}
2,3-PhTP[58]	252	26000	478	0.0033
	340	10500		
5.6	255	28600	370[b]	0.0018[c]
	332	12700		
5.10	278	29600	545[d]	0.82[e]
	323	20300		
	443	13500		
complex				
$[(bpy)_2Ru(\mathbf{dpq})]^{2+}$ [28]	284	680000		
	515	8100		
$[[(bpy)_2Ru]_2\mathbf{dpq}]^{4+}$ [28]	283	120000		
	399	12000		
	605	9800		
5.16	284	70100		
	535	10200		
5.17	284	105000		
	400	21500		
	628	20500		
5.18	289	55100		
	443	10300		
	532	7700		

[a]Measured in CH_3CN. [b]Measured in cyclohexane. [c]With reference to 9,10-diphenylanthracene std. [dd]Measured in ethanol. [e]With reference to Rhodamine 6G std.

While the excitation spectrum shows contribution mainly from the transition at 332 nm, lesser contributions from the transition centered at 255 nm are possible. Lesser contributions of the higher energy band could potentially provide additional pathways back to the ground state. Such pathways would most likely involve intersystem crossing which would then diminish the fluorescence efficiency upon excitation from these bands.[52] The BL **5.10** demonstrates a red-shift (*ca.* 111 nm) in the CT band of **5.6**, which is the result of increased conjugation in the pyridyl-thiophene-pyridyl backbone. The room temperature fluorescence singlet emission (545 nm) is also shifted in comparison to that of **2,3-PhTP**, but this could also be attributed to increase in conjugation. Additionally, **5.10** is a quite strong emitter, with a quantum yield of 0.82, significantly stronger than that of conventional TPs. This could be attributed to the increase in conjugation along the backbone.

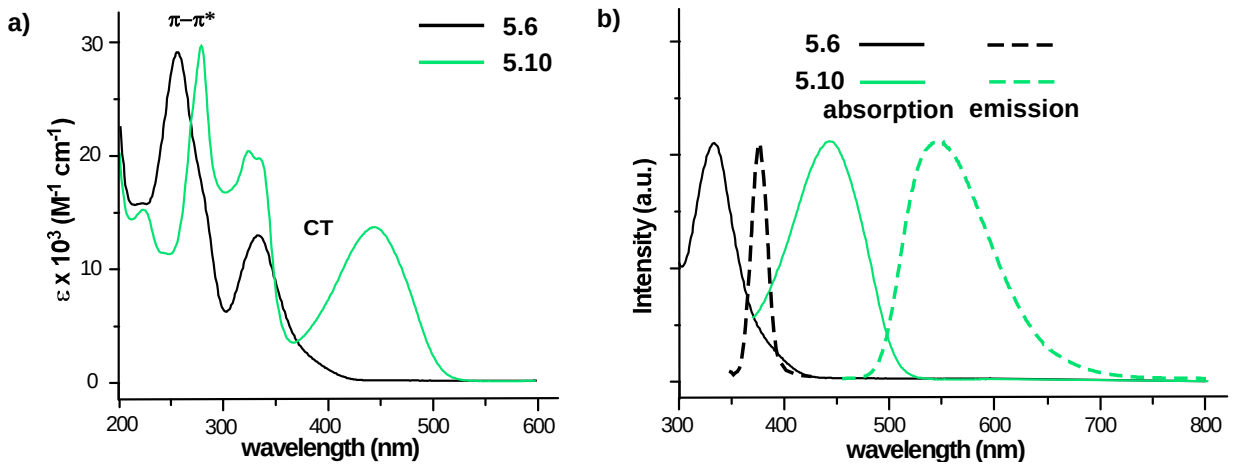

Figure 5.7. Spectra for BLs **5.6** and **5.10** including a) UV-vis and b) absorption and emission

The optical properties of the resulting Ru(II) complexes were also investigated, with both complexes red-shifted in comparison to the analogous monometallic and bimetallic **dpq** complexes. The complex $[(bpy)_2Ru(\mathbf{5.6})]^{2+}$ (**5.16**) exhibits a low energy MLCT transition at 535 nm, followed by a lower energy shoulder extending out to 700 nm. The absorption spectra for **5.16-5.18** are illustrated in Figure 5.8. The corresponding bimetallic complex (**5.17**) exhibits a

similar low energy profile, but with its absorbance shifted even further into the red. In this case the low energy transition (λ_{max} at 628) is followed by a lower energy shoulder extending out to *ca.* 825 nm. The monometallic complex **5.18** shows similar features to the other monometallic complex **5.16**, with a low energy MLCT transition at 532 nm, followed by a low energy shoulder extending out to *ca.* 675 nm. At this point, it is unclear if these two low energy features correspond to separate transitions or are just vibrational components of the same electronic transition. Also, the distinct increase in the molar absorptivity (ε) of the bimetallic species in comparison to the monometallic can be attributed to the larger chromophore size of the complex.

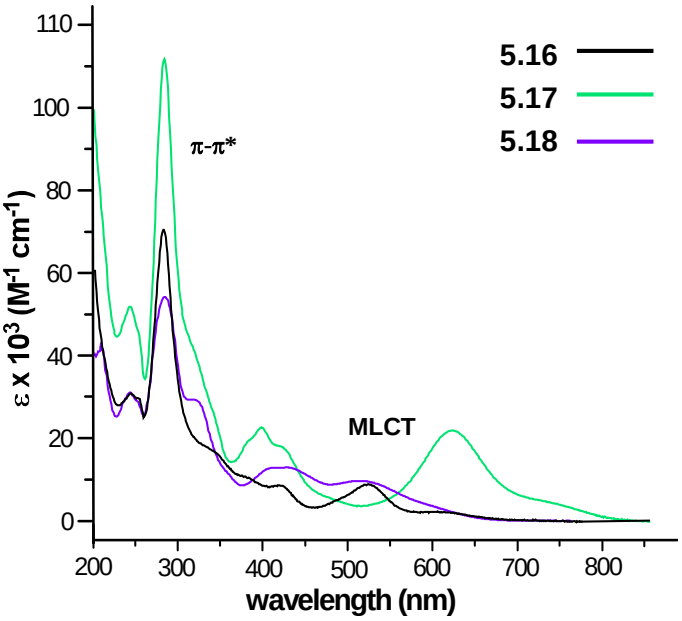

Figure 5.8. UV-vis absorption spectra for Ru(II) complexes **5.16**- **5.18**

5.4. Electrochemistry

The BLs **5.6** and **5.10** were characterized electrochemically and that data is presented in Table 5.3. The reduction potentials are typically the best indication of a species' ability to act as a bridging ligand, since the excitation involves the empty π* orbital (LUMO). Characterization of **5.6** via cyclic voltammetry (CV) reveals that its reduction falls between that of **dpp** and **dpq**. This

is to be expected as **5.6** is more conjugated than **dpp**, thus lowering the LUMO energy, but the electron-rich nature of the thiophene counteracts this stabilization such that the LUMO of **5.6** is higher in energy than that of **dpq**. However, the electron-rich nature of the thiophene also results in a much higher HOMO for **5.6** in comparison to the traditional polypyridyl ligands. As such, a distinct oxidation can be measured for **5.6** (E_p^{ox} = 2.15 V), something that is not possible for the traditional ligands.

Table 5.3. Electrochemical data for various bridging ligands[a]

Ligand	E_p^{ox} (V)	$E_{1/2}^{red}$ (V)
dpp[64]		-1.85[b]
dpq[65]		-1.30[b]
dpb[65]		-1.01[b]
th-MeTP-th[44]	0.50	-1.68
5.6[c]	2.15	-1.70
5.10[c]	0.98	-1.61

[a]All potentials vs. Ag/Ag^+. In CH_3CN containing 0.10 M $TBAPF_6$. [b]Literature values converted to Ag/Ag^+. [c]Glossy carbon working electrode was used in place of Pt disc.

The reduction of BL **5.10** falls between that of **5.6** and **dpq**. Compared to its thiophene-substituted analogue 2,3-dimethyl-5,7-bis(2-thienyl)thieno[3,4-*b*]pyrazine (**th-MeTP-th**),[44] the more electron donating character of the chain (C_8 vs. methyl) causes the LUMO of **5.10** to be slightly lower in energy than ***tert*-thTPCH$_3$** and higher in energy than that of **dpq**. Significant tuning of the LUMO can be achieved by functionalization of the 5- and 7-positons of TP.[44] The addition of terminal thiophene units on TP-based terthienyls is found to have essentially no effect on the LUMO.[44] Also, these terminal thiophene units have been found to reduce the effect of the functional groups on the HOMO by approximately one-third. In terms of oxidation, the BL **5.10** is

the easier to oxidize than **5.6** because there is an extension of conjugation along the thiophene backbone, of which the HOMO is predominantly localized upon in TPs. However, the HOMO of **5.10** is still harder to oxidize than ***tert*-thTPCH$_3$** because of the electron-poor nature of the pyridine rings.

The electrochemical data for the synthesized ruthenium complexes is presented in Table 5.4. The monometallic complex **5.16** exhibits a single oxidation of the $Ru^{II/III}$ metal center at 1.07 V (Figure 5.9). The weak oxidation for the **5.6** ligand is not visible in this complex, most likely hidden beneath that of the metal. A single distinct reduction for the **5.6** ligand (-1.01 V) and two reductions for the pendant bipyridine ligands are observed at lower potential (-1.72, -1.96 V). This shift in the reduction of **5.16** to higher potential from the uncoordinated ligand **5.6** (*ca.* 690 mV), making it easier to reduce, is most likely the result of loss of electron density because of coupling to the metal.

Table 5.4. Electrochemical data for various Ru(II) complexes[a]

complex	Oxidation			Reduction		
	E_{ox2} (V)	E_{ox1} (V)	ΔE_{ox} (mV)	E_{red1} (V)	E_{red2} (V)	E_{red3} (V)
$[(bpy)_2Ru]_2$**dpp**$^{4+}$ [28]	1.63	1.43	200	-1.67	-1.17	
$[(bpy)_2Ru]_2$**dpq**$^{4+}$ [28]	1.70	1.52	180	-0.35	-1.13	
$[(bpy)_2Ru]_2$**dpb**$^{4+}$ [66]	1.83	1.65	180	-0.07	-0.71	
5.16	-	1.07	-	-1.01	-1.72	-1.96
5.17	1.34	1.12	220	-0.65	-1.34	-1.83
5.18	-	0.99	-	-1.10	-1.67	-1.92

[a]All potentials vs. Ag/Ag^+. In CH_3CN containing 0.10 M $TBAPF_6$. [b]Literature values converted to Ag/Ag^+.

Similar trends were observed for the other monometallic complex **5.18**, which is marked by a single oxidation of the $Ru^{II/III}$ at 0.99 V, a reduction of the ligand **5.10** at -1.10 V, and two reductions for the pendant bipyridine ligands at lower potential. The shift in reduction of **5.18** from the uncoordinated ligand **5.10** ligand is *ca.* 510 mV. Comparatively, **5.18** is slightly easier to oxidize than **5.16**, and slightly more difficult to reduce, possibly because of the reduced electron density of the pyridyl rings in the backbone.

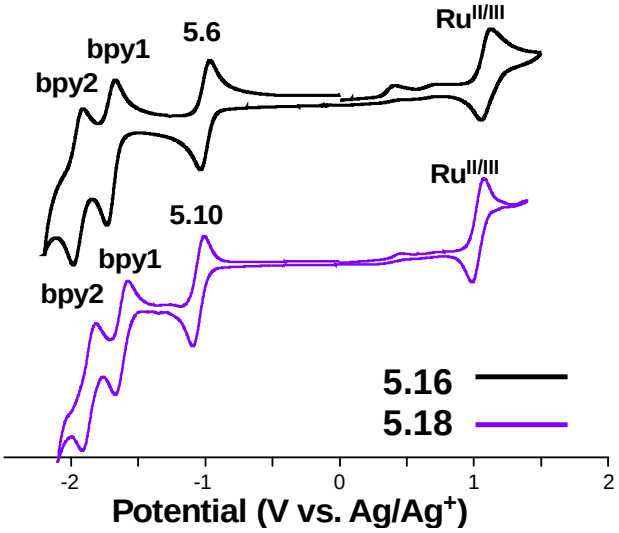

Figure 5.9. Cyclic voltammograms of monometallic complexes **5.16** and **5.18**

The electrochemical potentials of the bimetallic complex are the gauge of effectiveness for metal-metal communication. If zero communication exists between the coordinated metals, the metals would act as independent species and undergo oxidation at the same potential. If the metals are communicating through the electron-delocalized bridging ligand, there should be a separation in the oxidation potentials of the metal centers. The further this separation in oxidation, the better the communication.

Comparison of the CV of the bimetallic complex **5.17** (Figure 5.10) to its analogous bimetallic complexes (Table 5.4) shows that the first reduction of the bridged **5.17** complex agrees well with the trend for the free ligands above, with the bridging-ligand-based reductions falling

between that of the analogous **dpp** and **dpq** complexes. In addition, the electron-rich nature of the **5.6** thiophene allows the donation of greater electron density to the metals and thus the metal oxidations occur at significantly lower potentials (>300 mV) than the corresponding complexes of the traditional bridging ligands, as exhibited in Table 5.4. In addition to the metal oxidations occurring at lower potentials, the two oxidations are well separated with the two $E_{1/2}$ values differing by 220 mV. This observed separation in the oxidations of the two bridged metal centers is indicative of the stability of the mixed-valence intermediate,[67] and has been ascribed to the electrostatic and electronic effects brought about by the proximity of the two metals and the shared π-system between them.[28] As can been seen in Table 5.4, this separation in complex **5.17** (220 mV) is greater than that for any of the traditional bridging ligand complexes, indicative of stronger coupling between the two metals, thus improved metal-metal communication. This separation has been previously related to the structural and electronic properties of the bridging ligand,[64] and the slightly greater separation observed for the **5.17** could be a result of the reduced aromaticity of thiophene, which allows greater delocalization through the organic ligand.

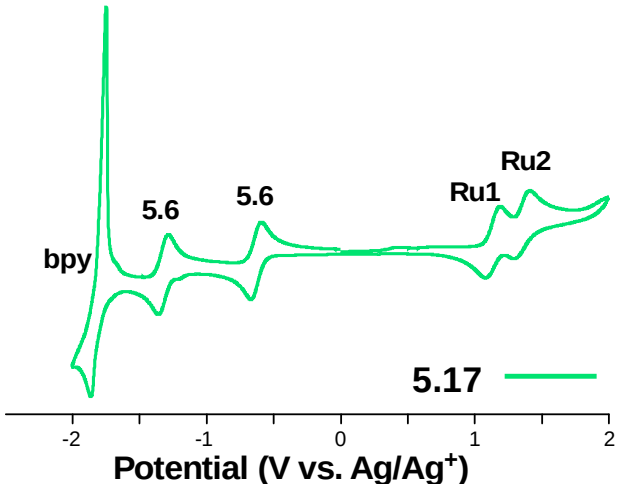

Figure 5.10. Cyclic voltammogram of bimetallic complexes **5.17**

5.5. X-Ray Crystallography

Crystals were able to be grown and the crystal structures were elucidated for bridging ligands **5.6** and **5.10**, and the bimetallic complex **5.17**. Bridging ligand **5.6** (Figure 5.11) was relatively planar, however there was a 4° deviation from planarity, due to the slight twist within the pyrazine ring. The crystal structure of BL **5.10** was also obtained (Figure 5.12).

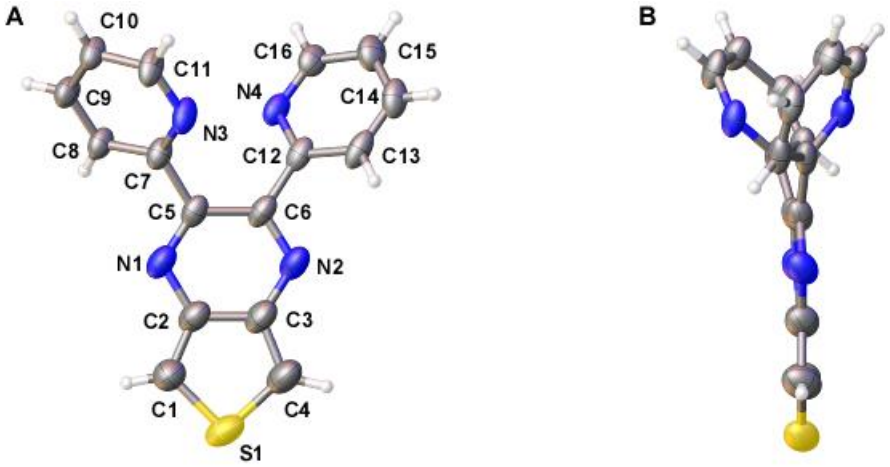

Figure 5.11. Crystal structure of **5.6** showing (a) front-facing and (b) planar views with ellipsoids set at 50% probability

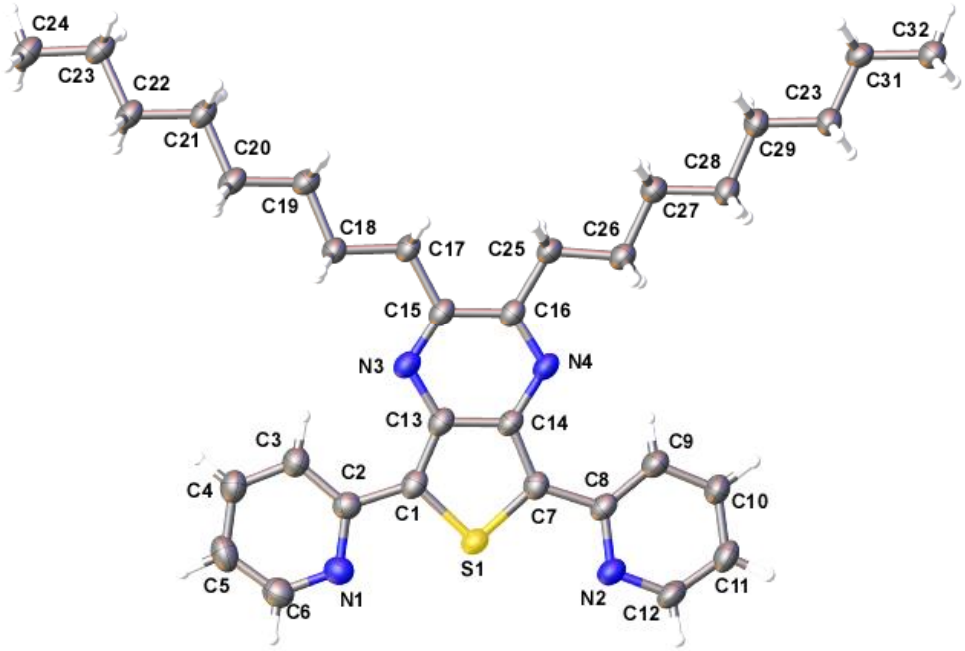

Figure 5.12. Crystal structure of **5.10** showing front facing view with ellipsoids set at 50% probability

The most interesting crystal structure obtained was that of **5.17**, which crystallized as racemic pairs of the chiral enantiomers. The Λ,Λ-configuration is shown in Figure 5.13. Usually complexes like this crystallize in the Λ,Δ-configuration.

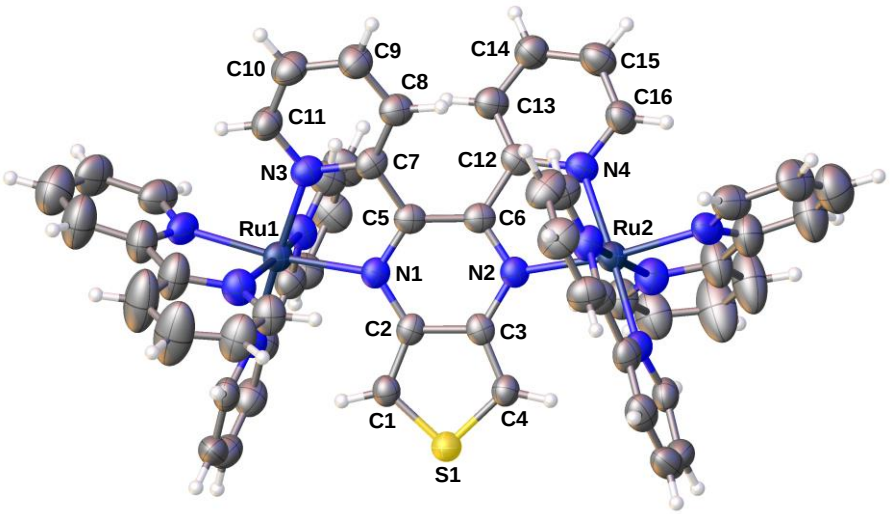

Figure 5.13. Crystal structure of Λ,Λ-configuration of multi-metallic complex **5.17** showing front facing view with ellipsoids set at 50% probability

5.6. Conclusions

The organic unit thieno[3,4-*b*]pyrazine has been successfully employed as a bridging ligand in multi-metallic coordination complexes, showing that this species has great potential as a bridging ligand in supramolecular organization applications. This is also a completely new application for the TP species, which is mostly utilized in organic conjugate materials applications. The advantage with TPs is that the electronics can be effectively tuned by functionalization of the 2,3-positions, or in this case functionalization of the pyridyls attached to the pyrazine could potentially provide further tuning of the electronics.

One improvement that could be made to get even better communication would be to fuse the pendent 2-pyridyl groups of bridging ligand **5.6** into a 4,7-phenanthroline unit. The forced planarity in this ligand would enhance electron delocalization and afford an increased metal-metal

communication. This would require synthesis of the 4,7-phenanthroline-5,6-dione,[68] as it is not commercially available at reasonable cost.

If the issue of the isolation of the brominated TP **5.14** can be resolved, the tridentate TP-based ligand **5.15** would provide a BL with three coordination sites on each side of the ligand, providing stereochemical control of complexes and eliminating the Δ and Λ isomeric mix, and further stabilizing the corresponding metal complexes.

5.7. Experimental Methods

Unless otherwise specified, all reactions were carried out under nitrogen atmosphere with reagent grade materials. DMF was dried over $MgSO_4$/silica gel and stored with molecular sieves under N_2 and bubbled with N_2 before use. THF was distilled over sodium with a benzophenone indicator. All glassware was oven-dried, assembled hot, and cooled under a dry nitrogen stream before use. Chromatographic separations were performed using standard column methods with silica gel (230-400 mesh) or alumina (neutral). The ^{1}H and ^{13}C NMR were completed on a 400 MHz spectrometer. All NMR data was referenced to residual solvent peaks and peak multiplicity reported as follows: s = singlet, d = doublet, dd = doublet of doublets, dt = doublet of triplets, td = triplet of doublets, ddd = doublet of doublet of doublets, m = multiplet. HRMS (ESI-TOF) was performed. UV-vis spectra were measured on a dual beam scanning spectrophotometer using samples prepared as CH_3CN solutions in 1-cm quartz cuvettes. Emission measurements were taken on a Horiba NanoLog Spectrofluorometer. Electrochemical measurements were carried out in a three-electrode cell using a platinum disc working electrode (or glossy carbon working electrode), platinum wire auxiliary electrode, and Ag/Ag^+ reference referenced to the Fc/Fc^+ couple. Solutions consisted of sample dissolved in 0.1M $TBAPF_6$ (tetrabutylammonium hexafluorophosphate) in anhydrous CH_3CN and were sparged with argon prior to each scan and

blanketed with argon during the experiment. Crystals were grown in EtOH solutions with slow evaporation.

2,3-di-2-pyridinylthieno[3,4-*b*]pyrazine (5.6). To a 250 mL 3-neck rbf with attached condenser was added 3,4-diaminothiophene **5.4** (1.14 g, 10.0 mmol) and 2,2'-pyridil **5.5** (2.33 g, 11.0 mmol), which was evacuated/backfilled three times with N_2. Absolute EtOH (100 mL) was then added and the solution was heated to reflux and stirred under N_2 for 3 h. The reaction was then cooled to rt, and poured into sep. funnel with water, organic layer was extracted with EtOAc, and washed with brine, then water and dried over Na_2SO_4. Organic layer was concentrated via rotatory evaporation, and solid was purified via silica gel column chromatography (50:50 hexanes:EtOAc → EtOAc) to yield bright yellow solid (80-88%). mp = 165 °C (decomp.) HRMS = ($M+H^+$): calc. 291.0704, expt. 291.0694; (M+Na): calc. 313.0524, expt. 313.0540; ε = 28,600 (λ_{max} = 255 nm), 12,700 ((λ_{max} = 332 nm) L mol^{-1} cm^{-1}. ^{1}H NMR (400 MHz, $CDCl_3$) δ 8.32 (ddd, *J = 4.88, 1.96, 1.12 Hz*, 2H), 8.14 (s, 2H), 7.92 (dt, *J = 7.84, 1.24 Hz*, 2H), 7.80 (td, *J = 7.84, 1.96 Hz*, 2H), 7.22 (ddd, *J = 7.60, 4.88, 1.24 Hz*, 2H). ^{1}H NMR (400 MHz, d6-acetone) δ 8.29 (s, 2H), 8.19 (ddd, *J = 4.88, 1.72, 1.00 Hz*, 2H), 8.00 (dt, *J = 7.80, 1.24 Hz*, 2H), 7.91 (td, *J = 7.80, 1.72 Hz*, 2H), 7.28 (ddd, *J = 7.56, 4.88, 1.24 Hz*, 2H). ^{13}C NMR (400 MHz, d6-acetone) δ 159.3, 153.8, 148.9, 142.3, 137.5, 124.6, 123.9, 119.7.

5,7-dibromo-2,3-dioctylthieno[3,4-*b*]pyrazine (5.12). The following is a modification of previously reported conditions.[61] In a 500 mL 3-neck rbf under N_2 add 5.08 g 2,3-dioctylthieno[3,4-*b*]pyrazine and 100 mL DMF and in a separate rbf add 6.72 g *N*-bromosuccinimide (37.7 mmol) and 50 mL of DMF, warm solutions slightly to dissolve solids. Cool TP solution to -78 °C then add NBS solution dropwise via cannula, stir green solution at 0 °C for 4 h, then add ice to form a yellow precipitate. Add 50 mL of H2O, extract with Et2O,

wash with brine, H_2O (5x 50 mL), NH_4Cl. Dry over $MgSO_4$ and remove solvent via rotatory evaporation. Purify via silica gel column chromatography (hexanes → 1% EtOAc/hexanes) followed by recrystallization in hexanes to give red solid (75-85%). ^{1}H NMR (400 MHz, $CDCl_3$) δ 2.90 (t, *J = 7.68 Hz*, 4H), 1.80 (p, *J = 7.24*, 4H), 1.50-1.25 (m, 20H), 0.89 (t, *J = 7.00 Hz*, 6H). ^{1}H NMR shifts agree well with previously reported values.

2-(trimethylstannyl)pyridine (5.13). The following is a modification of previously reported conditions.[62] All care taken to perform reaction and purification in the absence of light and heat. In a 250 mL 3-neck rbf with attached addition funnel, evacuate/backfill with N_2 3x, and then add 100 mL THF to rbf, cool solvent to -78 °C, then add 2.42 mL 2-bromopyridine (25 mmol), followed by 11.0 mL BuLi (2.5 M in hexanes, 27.5 mmol) dropwise and stir 1 h. Then add 27.5 mL trimethylstannyl chloride (1.0M in THF, 27.5 mmol) over the course of 10 min, and stir for an additional 30 min at -78 °C. The green solution turns yellow upon warming to rt. Pour the solution through a silica frit (silica gel previously washed with 3% solution of triethylamine in hexanes, followed by 100 mL pure hexanes) and rinse the frit with hexanes to collect all product. Solvent was removed by rotatory evaporation without heating, and a short plug (3% triethylamine-treated silica gel) column chromatography was done to purify with hexanes, to give a 4.75 g bright yellow oil (79% yield). ^{1}H NMR (400 MHz, $CDCl_3$) δ 8.75 (ddd, J =1.00, 1.68, 4.88 Hz, 1H), 7.52 (td, J = 1.80, 7.48 Hz, 1H), 7.45 (dt, J = 1.20, 7.40 Hz, 1H), 7.14 (ddd, J = 1.52, 4.84, 7.56 Hz, 1H), 0.35 (s, 9H). ^{1}H NMR shifts agree well with previously reported values.

2,3-dioctyl-5,7-di-2-pyridinylthieno[3,4-*b*]pyrazine (5.10). In the absence of light, add 2.49 g 5,7-dibromo-2,3-dioctylthieno[3,4-*b*]pyrazine **5.12** (4.80 mmol), 2.90 g 2-(trimethylstannyl)pyridine **5.13** (12.0 mmol), 0.337 g $Pd(PPh_3)_2Cl_2$ (0.480 mmol), 0.0914 g CuI

(0.480 mmol) to 250 mL rbf. Evacuate/backfill with N2 3x, add 100 mL toluene and stir at reflux overnight. Pour solution into H2O, extract with DCM, wash with brine, dry over MgSO4, and remove solvent by rotatory evaporation. Purify via silica gel column chromatography (10% EtOAc/hexanes) and recrystallize in hexanes to give 1.60 g green solid (65 % yield). mp = 93.2-94.7 °C. ε = 29,600 (λ_{max} = 278 nm), 20,300 ((λ_{max} = 323 nm), 13,500 ((λ_{max} = 443 nm) L mol^{-1} cm^{-1}. ^{1}H NMR (400 MHz, $CDCl_3$) δ 8.99 (dt, *J = 1.00, 8.04 Hz,* 2 H), 8.61 (ddd, *J = 1.00, 1.72, 4.64 Hz,* 2H), 7.76 (td, *J = 1.96, 7.60* Hz, 2H), 7.17 (ddd, *J = 1.00, 4.88, 7.32 Hz*, 2H), 2.96 (t, *J = 7.36 Hz*, 4H), 1.94 (p, *J = 7.32 Hz,* 4H), 1.56-1.28 (m, 20H), 0.89 (t, *J = 6.60 Hz*, 6H). ^{13}C NMR (400 MHz, $CDCl_3$) δ 155.7, 152.4, 149.3, 139.8, 136.3, 133.8, 122.3, 121.9, 35.1, 32.0, 29.7, 29.5, 29.3, 27.1, 22.7, 14.1.

***cis*-Ru(bpy)$_2$Cl$_2$.2H$_2$O** The following is a modification of previously reported conditions.[69] To a 100 mL 3-neck rbf with attached condenser was added ruthenium(III) chloride hydrate (2.61 g, 10.0 mmol), 2,2'-bipyridine (3.14 g, 20.1 mmol), and lithium chloride (2.54 g, 60.0 mmol). Flask was evacuated and backfilled three times with N_2, and then 25 mL of N_2-bubbled DMF was added. The dark brown solution was heated at reflux and stirred for 4 h. Solution was cooled to rt, and 50 mL of acetone was added. Solution was further cooled to 0 °C and stirred for 30 min. Purple solution was filtered through glass frit via vacuum filtration, and precipitate was washed with H_2O, then Et_2O. Violet-black crystalline powder was yielded (3.39 g, 65-70%).

Ru(bpy)$_2$(OTf)$_2$ The following is a modification of previously reported conditions.[70] To a 250 mL 3-neck rbf add 150 mL 1,2-dichlorobenzene and bubble with N_2 for 30 min. To this add 1.62 g *cis*-Ru(bpy)$_2$Cl$_2$.2H$_2$O (3.2 mmol), to this suspension add 1.00 mL trifluoromethane

sulfonic acid (11.3 mmol) and stir red solution under N_2 for 1.5 h. Filter to collect solid and wash with Et_2O to give 2.15 g (90%) of dark red solid. Store under argon in freezer.

[(bpy)$_2$Ru(5.6)](PF$_6$)$_2$ (5.16). To a 100 mL 3-neck rbf with attached condenser was added *cis*-Ru(bpy)$_2$Cl$_2$.2H$_2$O (0.242 g, 0.500 mmol) and **5.6** (0.218 g, 0.750 mmol), which was evacuated/backfilled three times with N_2. EtOH/H_2O (25 mL/25 mL) was then added and the solution was heated to reflux and stirred under N_2 3 h. The reaction was then cooled to rt, and poured into a concentrated aqueous solution of KPF_6, whereby a precipitate instantaneously formed, and solution was stirred for 10 min. Precipitate was collected via vacuum filtration, and washed with H_2O (~500 mL) until filtrate ran clear, followed by Et_2O. Crude solid was purified on alumina column chromatography (50:50 toluene:acetone → acetone) to yield magenta solid (68%). mp = 195 °C (decomp.) HRMS = (M^{2+}): calc. 352.0527, expt. 352.0523; ε = 70,100 (λ_{max} = 284 nm), 10,200 (λ_{max} = 535nm) L mol^{-1} cm^{-1}. ^{1}H NMR (400 MHz, d6-acetone) δ See Figure 5.6.

[(bpy)$_2$Ru(5.6)Ru(bpy)$_2$](PF$_6$)$_4$ (5.17). To a 250 mL 3-neck rbf with attached condenser was added *cis*-Ru(bpy)$_2$Cl$_2$.2H$_2$O (1.30 g, 2.50 mmol) and **5.6** (0.290 g, 1.00 mmol), which was evacuated/backfilled three times with N_2. EtOH/H_2O (50 mL/50 mL) was then added and the solution was heated to reflux and stirred under N_2 3 h. The reaction was then cooled to rt, and poured into a concentrated aqueous solution of KPF_6, whereby a precipitate instantaneously formed, and solution was stirred for 10 min. Precipitate was collected via vacuum filtration, and washed with H_2O (~500 mL) until filtrate ran clear, followed by Et_2O. Crude solid was purified on alumina column chromatography (50:50 toluene:acetone → acetone) to yield green solid (64%). mp = 210 °C (decomp.) HRMS = (M^{4+}): calc. 279.5372, expt. 279.5371; ε = 105,000 (λ_{max} = 284 nm), 21,500 (λ_{max} = 400 nm), 20,500 (λ_{max} = 628 nm) L mol^{-1} cm^{-1}.

[(bpy)$_2$Ru(5.10)](PF$_6$)$_2$ (5.18). To a 100 mL 3-neck rbf with attached condenser was added 0.16 g Ru(bpy)$_2$(OTf)$_2$ (0.21 mmol) and 0.10 g 2,3-dioctyl-5,7-di-2-pyridinylthieno[3,4-*b*] pyrazine **5.10** (0.19 mmol), which was evacuated/backfilled three times with N_2. Absolute EtOH (50 mL) was then added and the solution was heated to reflux and stirred under N_2 18 h. The brown-red solution was then cooled to rt, and poured into a concentrated aqueous solution of KPF_6, remove EtOH via rotatory evaporation, add Et_2O to precipitate. Precipitate was collected via vacuum filtration, and washed with H_2O (~500 mL) until filtrate ran clear, followed by Et_2O. Crude solid was purified on alumina column chromatography (50:50 toluene:acetone → acetone), solvent was removed, and solid was precipitated from Et_2O to yield 0.059 g purple solid (26%). mp = 130 °C (decomp.) ε = 55,100 (λ_{max} = 289 nm), 10,300 (λ_{max} = 443 nm), 7,700 (λ_{max} = 532 nm) L mol^{-1} cm^{-1}.

5.8. References

1. (a) Juris, A.; Balzani, V.; Barigelletti, F. C.; Campagna, S.; Belser, P.; on Zalawsky, A. *Coord. Chem. Rev.* **1988**, *84*, 85-277. (b) Floris, B.; Donzello, M. P.; Ercolani, C.; Viola, E. *Coord. Chem. Rev.* **2017**, *347*, 115-140.
2. Sauvage, J.-P.; Collin, J.-P.; Chambron, J.-C.; Guillerez, S.; Coudret, C. *Chem. Rev.***1994**, *94*, 993-1019.
3. Arias, M.; Concepción, J.; Crivelli, I.; Delgadillo, A.; Díaz, R.; Francois, A.; Gajardo, F.; López, R.; Leiva, A. M.; Loeb, B. *Chem. Phys.* **2006**, *326*, 54-70.
4. Balzani, V.; Juris, A.; Venturi, M.; Campagna, S.; Serroni, S. *Chem. Rev.***1996**, *96* (2), 759-833.
5. Toma, H. E.; Araki, K. *Coord. Chem. Rev*. **2000**, *196*, 307-329.
6. Ward, M. D. *Coord. Chem. Rev.* **2006**, *250*, 3128-3141.

7. Hancock, R. D. *Chem. Soc. Rev.* **2013**, *42*, 1500-1524.

8. Rogers, H. M.; Arachchige, S. M.; Brewer, K. J.; Swavey, S. Polyatomic Bridging Ligands. In: *Elsevier Reference Module in Chemistry, Molecular Sciences and Chemical Engineering*; Reedijk, J., Ed.; Elsevier: Waltham, MA, 2014; pp 1-21.

9. Therrien, B. Arene Ruthenium Complexes in Supramolecular Chemistry. In *Advances in Inorganic Chemistry*; van Eldki, R., Puchta, R., Eds.; Elsevier: Cambridge, MA, 2018; pp 379-402.

10. Bignozzi, C. A.; Chiorbloi, C.; Indelli, M. T.; Scandola, M. A. R.; Varani, G.; Scandola, F. *J. Am. Chem. Soc.* **1986**, *108* (24), 7872-7873.

11. Kovacs, M.; Horvath, A. *Inorg. Chim. Acta* **2002**, *335*, 69-76.

12. Fodor, L.; Ulvecki, A.; Horvath, A.; Steiner, U. E. *Inorg. Chim. Acta* **2002**, *338*, 133-141.

13. Adams, H.; Alsindi, W. Z.; Davies, G. M.; Duriska, M. B.; Easun, T. L.; Fenton, H. E.; Herrera, J.-M.; George, M. W.; Ronayne, K. L.; Sun, X.-Z.; et. al *Dalton Trans.* **2006**, (1), 39-50.

14. Schubert, U. S.; Eschbaumer, C.; Andres, P.; Hofmeier, H.; Weidl, C. H.; Herdtweck, E.; Dulkeith, E.; Morteani, A.; Hecker, N. E.; Feldmann, J. *Synth. Met.* **2001**, *121*, 1249-1252.

15. Hofmeier, H.; Schubert, U. S. *Chem. Soc. Rev.* **2004**, *33* (6), 373-399.

16. Constable, E. C. Chem. Soc. Rev. 2007, 36 (2), 246-253.

17. Wild, A.; Winter, A.; Schluetter, F.; Schubert, U. S. Chem. Soc. Rev. 2011, 40 (3), 1459-1511.

18. Keller, C. E.; Pollard, C.; Yeung, L. K.; Drane-Plessinger, W.; Murphy, C. J. *Inorg. Chim. Acta* **2000**, *298* (2), 209-215.

19. Samuels, A. C.; DeArmond, M. K. Inorg. Chem. 1995, 34 (22), 5548-5551.

20. Herrera, J.-M.; Baca, S. G.; Adams, H.; Ward, M. D. *Polyhedron* **2006**, *25* (4), 869-875.

21. Swavey, S.; Fang, Z.; Brewer, K. J. *Inorg. Chem.* **2002**, *41* (9), 2598-2607.

22. Rasmussen, S. C.; Richter, M. M.; Yi, E.; Place, H.; Brewer, K. J. *Inorg. Chem.* **1990**, *29*, 3926-3932.

23. Garcia Posse, M. E.; Fagalde, F.; Vergara, M. M.; Katz, N. E. *Polyhedron* **1998**, *17* (16), 2733-2738.

24. Xiang, J.; Cheng, S.-C.; Jin, X.-X.; Su, Q.-Q.; Zhou, X.; Chu, W.-K.; Leung, C.-F.; Ko, C.-C. *Dalton Trans.* **2019**, *48* (2), 741-750.

25. Morgan, O.; Wang, S.; Bae, S.-A.; Morgan, R. J.; Baker, A. D.; Strekas, T. C.; Engel, R. *J. Chem. Soc., Dalton Trans.* **1997**, (20), 3773-3776.

26. D'Alessandro, D. M.; Dinolfo, P. H.; Davies, M. S.; Hupp, J. T.; Keene, F. R. *Inorg. Chem.* **2006**, *45* (8), 3261-3274.

27. Cho, Y.-J.; Kim, S.-Y.; Cha, H. Y.; Seo, B. S.; Kim, C. H.; Son, H.-J.; Kang, S. O. *J. Phys. Chem. C.* **2018**, *122* (41), 23288-23298.

28. Rillema, D. P.; Mack, K. B. *Inorg. Chem.* **1982**, *21*, 3849-3854.

29. White, J. K.; Brewer, K. J. *Chem. Commun.* **2015**, *51* (89), 16123-16126.

30. Polson, M. I. J.; Howell, S. L.; Flood, A. H.; Burrell, A. K.; Blackman, A. G.; Gordon, K. C. *Polyhedron* **2004**, *23*, 1427-1439.

31. Howell, S. L.; Gordon, K. C.; McGarvey, J. J. *J. Phys. Chem. A* **2005**, *109*, 2948-2956.

32. Polson, M. I. J.; Blackman, A. G.; Gordon, K. C. *Polyhedron* **2007**, *26* (2), 266-274.

33. D'Alessandro, D. M.; Keene, F. R. *Aust. J. Chem.* **2005**, *58* (11), 767-777.

34. Brewer, R. G.; Jensen, G. E.; Brewer, K. J. *Inorg. Chem.* **1994**, *33* (1), 124-129.

35. Zare, D.; Doistau, B.; Nozary, H.; Besnard, C.; Guenee, L.; Suffren, Y.; Pele, A.-L.; Hauser, A.; Piguet, C. *Dalton Trans*. **2017**, *46* (28), 8992-9009.

36. Hou, J.; Park, M.-H.; Zhang, S.; Yao, Y.; Chen, L.-M.; Li, J.-H.; Yang, Y. *Macromolecules* **2008**, *41* (16), 6012-6018.

37. Rasmussen, S. C.; Schwiderski, R. L.; Mulholland, M. E. *Chem. Commun.* **2011**, *47*, 11394-11410.

38. Wen, L.; Duck, B. C.; Dastoor, P. C.; Rasmussen, S. C. *Macromolecules* **2008**, *41* (13), 4576-4578.

39. Kenning, D. D.; Mitchell, K. A.; Calhoun, T. R.; Funfar, M. R.; Sattler , D. J.; Rasmussen, S. C. *J. Org. Chem.* **2002**, *67* (25), 9073-9076.

40. Wen, L.; Nietfeld, J. P.; Amb, C. M.; Rasmussen, S. C. *J. Org. Chem.* **2008**, *73*, 8529-8536.

41. Nietfeld, J. P.; Schwiderski, R. L.; Gonnella, T. P.; Rasmussen, S. C. *J. Org. Chem.* **2011**, *76*, 6383-6388.

42. Rasmussen, S. C.; Mulholland, M. E.; Schwiderski, R. L.; Larsen, C. A. *J. Heterocyclic Chem.* **2012**, *49* (3), 479-493.

43. Mulholland, M. E.; Schwiderski, R. L.; Rasmussen, S. C. *Polym. Bull.* **2012**, *69*, 291-301.

44. Schwiderski, R. L.; Rasmussen, S. C. *J. Org. Chem.* **2013**, *78*, 5453-5462.

45. Schwiderski, R. L.; Rasmussen, S. C. *Synth. Met.* **2014**, *193*, 58-63.

46. Wen, L.; Heth, C. L.; Rasmussen, S. C. *Phys. Chem. Chem. Phys.* **2014**, *16*, 7231-7240.

47. Mulholland, M. E.; Konkol, K. L.; Anderson, T. E.; Schwiderski, R. L.; Rasmussen, S.C. *Aust. J. Chem.* **2015**, *68*, 1759-1766.

48. Mulholland, M. E.; Wen, L.; Rasmussen, S. C. *Topol. Supramol. Polym. Sci.* **2015**, *2*, 18-29.

49. Konkol, K. L.; Schwiderski, R. L.; Rasmussen, S. C. *Materials* **2016**, *9* (6), 404/1-16.

50. Culver, E. W.; Anderson, T. E.; Lopez Navarrete, J. T.; Ruiz Delgado, M. C.; Rasmussen, S. C. *ACS Macro Lett.* **2018**, *7* (10), 1215-1219.

51. Anderson, T. E.; Culver, E. W.; Almyahi, F.; Dastoor, P. C.; Rasmussen, S. C. *Synlett* **2018**, *29* (19), 2542-2546.

52. Rasmussen, S. C.; Sattler, D. J.; Mitchell, K. A.; Maxwell, J. *J. Lumin.* **2004**, *190*, 111-119.

53. Čík, G.; Krajčovič, J.; Veis, P.; Végh, D.; Šeršen, F. *Synth. Met.* **2001**, *118* (1-3), 111-119.

54. Nishida, J.; Murakami, S.; Tada, H.; Yamashita, Y. *Chem. Lett.* **2006**, *35*, 1236-1237.

55. Paz, M. A.; Martin, P.; Fluckiger, R.; Mah, J.; Gallop, P. M. *Anal. Biochem.* **1996**, *138* (2), 145-149.

56. Peng, B.; Chao, H.; Sun, B.; Li, H.; Gao, F.; Ji, L.-N. *J. Inorg. Biochem.* **2007**, *101* (3), 404-411.

57. Peng, B.; Chao, H.; Sun, B.; Gao, F.; Ji, L.-N.; Zhang, J. *Transit. Metal Chem.* **2007**, *32* (2), 271-277.

58. Liu, X.; Li, L.; Sun, J.; Yan, Y.; Shu, X.; Liu, B.; Sha, W.; Feng, H.; Sun, S.; Zhu, J. *Inorg. Chem.* **2012**, *51* (1), 188-192.

59. Zhao, Z.; Wisnoski, D. D.; Wolkenberg, S. E.; Leister, W. H.; Wang, Y.; Lindsley, C. W. *Tetrahedron Lett.* **2004**, *45*, 4873-4876.

60. Li, Q.; Li, J.; Deng, L.; Wang, Q.; Gao, Z.; Liu, D. *Chem. Lett.* **2011**, *40* (4), 417-419.

61. Casado, J.; Ortiz, R. P.; Ruiz Delgado, M. C.; Hernandez, V.; Lopez Navarrete, J. T.; Raimundo, J.-M.; Blanchard, P.; Allain, M.; Roncali, J. *J. Phys. Chem. B* **2005**, *109* (35), 16616-16627.

62. Brotschi, C.; Mathis, G.; Leumann, C. J. *Chem. Eur. J.* **2005**, *11*, 1911-1923.

63. Kirchhoff, J. R.; McMillin, D. R.; Marnot, P. A.; Sauvage, J.-P. *J. Am. Chem. S.* **1985**, *107*, 1138-1141,

64. Cai, X.; Donzello, M. P.; Viola, E.; Rizzoli, C.; Ercolani, C.; Kadish, K. M. *Inorg. Chem.* **2009**, *48*, 7086-7098.

65. Polson, M. I. J.; Howell, S. L.; Flood, A. H.; Burrell, A. K.; Blackman, A. G.; Gordon, K. C. *Polyhedron* **2004**, *23* 1427-1439.

66. Cooper, J. B.; MacQueen, D. B.; Petersen, J. D.; Wertz, D. W. *Inorg. Chem.* **1990**, *29*, 3701-3705.

67. Richter, M. M.; Brewer, K. J. *Inorg. Chem.* **1993**, *32*, 2827-2834.

68. D'Alessandro, D. M.; Keene, F. R. *Dalton Trans.* **2006**, (8), 1060-1072.

69. Marmion, M. E.; Takeuchi, K. J. *J. Am. Chem. Soc.* **1988**, *110* (5), 1472-1480.

70. Hoertz, P. G.; Staniszewski, A.; Marton, A.; Higgins, G. T.; Incarvito, C. D.; Rheingold, A. L.; Meyer, G. J. *J. Am. Chem. Soc.* **2006**, *128*, 8234-8245.

CHAPTER 6. FINAL WORDS

Design plays a vital role in the synthesis of these conjugated thiophene-based materials., which all comes back to structure-function relationships. In Chapter 2, a catalytic hydrodebromination of 2,3,5-tribromothiophene was reconsidered in terms of sterics and electronics. It was demonstrated that both the catalytic reaction and the extremely facile background reaction were competing in solution. Thus, it was concluded that this reaction could only really be successful in the absence of any significant background reaction. This reaction played a role in the synthesis of metal thiophenedithiolenes, which were presented in Chapter 3. The optical, electronic and solubility properties can be tuned by thoughtful consideration of molecular design. Because of their unique low-energy IVCT transition, these materials are quite attractive for NIR photodetector applications. Chapter 4 focused on chemically and electrochemically polymerizing the fused-ring thieno[3,4-*b*]pyrazine unit and TP-based terthienyls to observe how structural modifications affected material properties. The optical and electrochemical trends hold consistent between the TP monomer, the TP-based terthienyl monomer, and the resulting polymers. Finally, in Chapter 5, the TP unit was incorporated into a supramolecular architecture which demonstrated good metal-metal communication, an improvement over the communication observed for its classical analogues (dpp, dpq, and dpb). Additionally, there is still room for improvement and optimization of the incorporation of the TP unit as a bridging ligand. Overall, the properties of these fused-ring and metal-coordinated materials can be tuned with careful thought of molecular design.